REMOVAL OF ORGANIC POLLUTANTS FROM WATER USING CARBON NANOTUBES FUNCTIONALIZED WITH DEEP EUTECTIC SOLVENTS

RUSUL KHALEEL IBRAHIM

FACULTY OF ENGINEERING
UNIVERSITY OF MALAYA
KUALA LUMPUR

2018

REMOVAL OF ORGANIC POLLUTANTS FROM WATER USING CARBON NANOTUBES FUNCTIONALIZED WITH DEEP EUTECTIC SOLVENTS

RUSUL KHALEEL IBRAHIM

THESIS SUBMITTED IN FULFILMENT OF THE REQUIREMENTS FOR THE DEGREE OF DOCTOR OF PHILOSOPHY

FACULTY OF ENGINEERING
UNIVERSITY OF MALAYA
KUALA LUMPUR

2018

UNIVERSITY OF MALAYA

ORIGINAL LITERARY WORK DECLARATION

Name of Candidate: Rusul Khaleel Ibrahim

Matric No: KHA140031

Name of Degree: Doctor of Philosophy (Ph.D.)

Title of Project Paper/Research Report/Dissertation/Thesis ("this Work"):

REMOVAL OF ORGANIC POLLUTANTS FROM WATER USING CARBON NANOTUBES FUNCTIONALIZED WITH DEEP EUTECTIC SOLVENTS

Field of Study: Environmental engineering

I do solemnly and sincerely declare that:

(1) I am the sole author/writer of this Work;
(2) This Work is original;
(3) Any use of any work in which copyright exists was done by way of fair dealing and for permitted purposes and any excerpt or extract from, or reference to or reproduction of any copyright work has been disclosed expressly and sufficiently and the title of the Work and its authorship have been acknowledged in this Work;
(4) I do not have any actual knowledge nor do I ought reasonably to know that the making of this work constitutes an infringement of any copyright work;
(5) I hereby assign all and every right in the copyright to this Work to the University of Malaya ("UM"), who henceforth shall be owner of the copyright in this Work and that any reproduction or use in any form or by any means whatsoever is prohibited without the written consent of UM having been first had and obtained;
(6) I am fully aware that if in the course of making this Work I have infringed any copyright whether intentionally or otherwise, I may be subject to legal action or any other action as may be determined by UM.

Candidate's Signature **Date:**

Subscribed and solemnly declared before,

Witness's Signature **Date:**

Name:

REMOVAL OF ORGANIC POLLUTANTS FROM WATER USING CARBON NANOTUBES FUNCTIONALIZED WITH DEEP EUTECTIC SOLVENTS

ABSTRACT

Many industries discharge large amount of wastewater that constitute the attention of many environmental concerns because it contains toxic and persistent organic pollutants that pollute the nature and threaten the human health. Although, carbon nanotubes (CNTs) have a high adsorption capacity for the removal of various kinds of organic pollutants from water, many flaws are hindering their adsorption performance. Functionalization of CNTs is a decisive process to overcome all the restrictions of CNTs application and to increase their removal efficiency. Therefore, this research has been carried out to investigate the potential of deep eutectic solvents (DESs) as novel functionalization agents for carbon nanotubes (CNTs) which can open a new window of opportunity in the area of wastewater treatment. In this regard, ten DESs were synthesized using five different salts and two hydrogen bond donors (HBDs) (i.e. ethylene glycol and di-ethylene glycol). Various molar ratios of HBD to salts were prepared to determine the optimum molar ratio by which the DES is homogeneous and stable. The DESs freezing points and functional groups were investigated, in addition to their physical properties of viscosity, density, conductivity and surface tension were determined as function of temperature in the particular temperature range of 293.15- 353.15 K. It is worth mentioning that all examined DESs were stable and in liquid phase at room temperature which emphasize their promising potential to be utilized as inexpensive environment-friendlier solvents. Owing to their low recorded freezing points and viscosities, DESs can be effortlessly processed without any further heating required. Subsequently, the prepared DESs were used to functionalize CNTs and produce novel adsorbents for the removal of 2,4-dichlorophenol (2,4-DCP) and methylene orange (MO) from water. A primary screening of adsorption process was conducted, and the chemical, physical and

morphological properties of the adsorbents with the highest removal efficiencies were investigated using RAMAN, FTIR, FESEM, zeta potential, TGA and BET surface area. The effect of DES was obvious by increasing the purity and the surface area of CNTs resulting in increasing the maximum adsorption capacity of CNTs for 2,4-DCP and MO removal to reach 290 mg/g and 224 mg/g, respectively. Adsorption studies were carried out to evaluate the optimum conditions, kinetics and isotherms for 2,4-DCP adsorption process. RSM-CCD experimental design was used to conduct the optimization studies and to determine the optimum conditions for 2,4-DCP and MO removal by each selected adsorbent individually. Furthermore, all experimental data fitted well the pseudo-second order kinetic model and the equilibrium data for all DES-functionalized adsorbents was well fitted by both Langmuir and Freundlich isotherm models.

Keywords: 2,4-dichlorophenol, methyl orange, deep eutectic solvents, carbon nanotubes, functionalization.

REMOVAL OF ORGANIC POLLUTANTS FROM WATER USING CARBON NANOTUBES FUNCTIONALIZED WITH DEEP EUTECTIC SOLVENTS

ABSTRAK

Kebanyakan industri telah membuang sejumlah besar sisa-sisa air yang telah mencemarkan alam sekitar kerana sisa-sisa air ini mengandungi toksik dan bahan cemar organik yang kekal, di mana ia boleh menyebabkan pencemaran alam dan mengancam kesihatan manusia. Namun begitu, tiub-tiub karbon nano (CNTs) mempunyai daya penjerapan yang tinggi bagi menyingkirkan pelbagai sisa cemar organik daripada air. Walaubagaimanapun masih terdapat beberapa kekurangan yang merencatkan kebolehan proses penjerapan ini. Proses penambahan kumpulan berfungi terhadap CNTs merupakan satu proses yang sesuai untuk mengatasi segala kekurangan terhadap pengaplikasian CNTs dan meningkatkan kecekapan penyingkirannya. Justeru itu, kajian ini telah dijalankan untuk mengkaji kebolehan pelarut-pelarut eutektik dalaman (DESs) sebagai agen kebolehfungsian yang baru untuk tiub-tiub karbon nano (CNTs) di mana ia boleh membuka peluang yang baru dalam rawatan sisa-sisa air. Dalam kajian ini, sepuluh DESs telah disintesiskan dengan menggunakan lima garam yang berbeza dan dua jenis penderma ikatan hydrogen yang berbeza (HBDs) (iaitu ethylene glycol dan di-ethylene glycol). Pelbagai nisbah molar HBD terhadap garam telah disediakan untuk menentukan nisbah molar yang optimum di mana DES adalah homogen dan stabil. Takat beku DESs dan kumpulan-kumpulan berfungsi telah dikaji menerusi kajian ini dalam menentukan ciri-ciri fizikal mereka seperti kelikatan, ketumpatan, kekonduksian dan ketegangan permukaan, terhadap pelbagai suhu, iaitu di antara 293.15- 353.15 K. Kajian ini dapat membuktikanbahawa kesemua DESs yang telah dikaji adalah stabil dan wujud dalam bentuk cecair dalam suhu bilik dan menunjukkan potensi yang baik untuk digunakan sebagai pelarut yang murah dan mesra alam. Disebabkan oleh rekod sejukbeku dan kelikatan yang rendah, DESs mudah diproses tanpa sebarang proses pemanasan.

Seterusnya, DESs yang telah disediakan digunakan untuk menambah kumpulan berfungsi di CNTs dan menghasilkan penjerap baru yang boleh mengasingkan 2,4-dichlorophenol (2,4-DCP) and methyl oren (MO) daripada air. Satu ujikaji yang penting terhadap proses penjerapan telah dijalankan, dan ciri-ciri kimia, fizikal dan morfologi penjerap dengan kecekapan penyingkiran paling tinggi telah diuji menggunakan RAMAN, FTIR, FESEM, potensi zeta, TGA dan luas permukaan BET. Kesan DES jelas terlihat dengan meningkatkan ketulenan dan luas permukaan CNTs, di mana menghasilkan kapasiti penjerapan maksimum CNTs untuk 2,4-DCP dan penyingkiran MO, masing-masing untuk mencapai 290 mg/g dan 224 mg/g. Kajian-kajian proses penjerapan juga telah dijalankan untuk menilai keadaan optimum, kinetik dan isotherm untuk proses penjerapan 2,4-DCP. Rekabentuk eksperimen menggunakan RSM-CCD telah dijalankan untuk kajian optimum dan untuk menentukan kondisi yang sesuai untuk 2,4-DCP dan penyingkiran MO bagi setiap penjerap yang telah dipilih. Disamping itu juga, kesemua data eksperimen bersesuaian dengan pseudo-kedua model kinetic dan keseimbangan data untuk kesemua DES dengan fungsi penjerap masing-masing bersesuaian dengan model isotherm Langmuir dan Freundlich.

Kata kunci: 2,4-dichlorophenol, metil oren, pelarut eutektik yang mendalam, nanotube karbon, fungsian.

ACKNOWLEDGEMENTS

In the name of Allah, the Most Gracious and the Most Merciful.

All the praises and thanks are to Allah Almighty for granting us success in this work. Praise to Allah Almighty for giving us patience and strength to overcome all the difficulties and the obstacles we faced to finish this study successfully.

I would like to extend my sincere appreciation and gratitude to my supervisors Prof. Dr. Shaliza Binti Ibrahim and Dr. Mohammed Abdulhakim AlSaadi for their continued support, supervision, encouragement and valuable guidance throughout the duration of this research study, without them it could not have been possible to finish this work. I also would like to express my warmest gratitude to my research colleagues and my friends who have always encouraged me and believed in me.

My profound and warmest appreciation goes to my parents, my brother and my sisters who have always been there for me, holding my hands throughout my desperate moments and showing their endless love and faith to help me reach the top at everything. Finally, I would like to dedicate this achievement to the moon of my life, my heaven, my beloved mother to fulfill part of her dream.

TABLE OF CONTENTS

LIST OF FIGURES

LIST OF TABLES

LIST OF SYMBOLS AND ABBREVIATIONS

EG	:	Ethylene glycol
DEG	:	Diethylene glycol
GLY	:	Glycerol
MA	:	Malonic acid
U	:	Urea
ChCl	:	Choline chloride
MTPB	:	Methyl triphenyl phosphonium bromide
BTPC	:	Benzyl triphenyl phosphonium chloride
DAC	:	N, N-diethyl ethanol ammonium chloride
TBAB	:	Tetra-n-butyl ammonium bromide
CNTs	:	Carbon nanotubes
SWCNTs	:	Single-wall carbon nanotubes
NPs		Nanoparticles
2,4-DCP	:	2,4-dichlorophenol
MO	:	Methyl orange
DES	:	Deep eutectic solvents
HBD	:	Hydrogen bond donor
ILs	:	Ionic liquids
SEM	:	Scanning electron microscope
FESEM	:	Field emission scanning electron microscope
TGA	:	Thermo gravimetric
BET	:	Brunauer–Emmet–Teller
FTIR	:	Fourier transforms infrared
CCD	:	Central composite design

DOE	:	Design of expert
RSM	:	Response surface methodology
ANOVA	:	Analysis of variance
VOC	:	Volatile organic compound
COC	:	Chlorinated organic compound
RO	:	Reverse osmosis
FO	:	Forward osmosis
UF	:	Ultrafiltration
MF	:	Microfilteration
TFC	:	Thin film composite
QD	:	Quantum dot
AOP	:	Advanced oxygen process
DBP	:	Disinfection by product
REOS	:	Reactive oxygen species
UPLC	:	Ultra-performance liquid chromotography
ID	:	Intraparticle diffusion
q_e	:	Equilibrium adsorption capacity
q_t	:	Adsorption capacity at time t
q_m	:	Maximum adsorption capacity
m	:	Weight of adsorbent
V	:	Volume of solution
C_0	:	Initial concentration
C_t	:	Concentration at time t
R^2	:	Correlation coefficient
K_L	:	Langmuir adsorption constant
K_F	:	Freundlich isotherm constant

1/n	:	The intensity parameter in Freundlich isotherm
S	:	Conductivity
K_1	:	Rate constant of pseudo-first-order
K_2	:	Rate constant of Pseudo-second-order
K_d	:	Rate constant of intraparticle diffusion
B_1	:	Constant of Temkin isotherm model
K_t	:	Temkin isotherm equilibrium binding constant

LIST OF APPENDICES

CHAPTER 1: INTRODUCTION

1.1 Overview

1.1.1 Environmental issues and nanotechnology

The ongoing propagation of industrialization and urbanization processes involving transportation, manufacturing, construction, petroleum refining, mining etc., deplete the natural resources as well as produce large amounts of hazardous wastes which cause air, water and soil pollution, and consequently threaten human public health and the environmental security. The generated wastes are released to the environment in different forms, for example atmospheric pollutants include toxic gases (nitrogen oxides, sulfur oxides, carbon oxides, ozone etc), suspended airborne particles and volatile organic compounds (VOCs); while soil and water pollutants may comprise of organic substances (pesticides, insecticides, phenols, hydrocarbons etc.), heavy metals (lead, cadmium, arsenic, mercury, etc.), as well as microbial pathogens. These environmental pollutants have a great potential to adversely influence the human health, since they can find their way into human body either through inhalation, ingestion or absorption. In addition to that, some of these toxicants tend to accumulate in food chains, such as the bioaccumulation of heavy metals (Smical et al., 2008) and persistent organic pollutants (POPs) (Houde et al., 2008) in biota and fishes, which poses major risks to human and wildlife. Therefore, there is an exigent demand for the improvement of sustainable, efficient and low-cost technologies to monitor and properly treat toxic environmental pollutants.

One of the most promising approaches to revolutionize the environmental remediation techniques is 'Nanotechnology' which can be defined as a group of emerging technologies that work on nanometer scale (i.e. between 1 to 100 nm range) to produce materials, devices and systems with fundamentally new properties and functions by controlling the size and the shape of matters (Ramsden, 2009). The global momentum of

nanotechnology due to its potential applications, that are covering many fields (e.g., medicine (Müller et al., 2015), food industry (Duncan, 2011), Energy (Zang, 2011), pollution treatment (Karn, Kuiken, & Otto, 2009)), is offering leapfrogging prospects in the improvement and transformation of conventional remediation technologies.

Different processes, (including: photocatalytic deposition (PD) deposition−precipitation (DP), chemical vapor decomposition (CVD), chemical solution decomposition (CSD), wet chemical method, sol-gel, ultrasonic irradiation, thermal and hydrothermal processes, *etc.*), have been used to synthesize various types of nanomaterials that exhibit unique merits differ from that of their bulk counterparts. The extraordinary properties such as, thermal, optical, mechanical, electromagnetic, structural and morphological properties provide the nanomaterials with advantageous features for many applications where they can be utilized as nanoadsorbents, nanosensors, nanomembrane and disinfectants. Furthermore, many attempts were reported to synthesize more sophisticated nanostructure (e.g., nanorods, nanobelts, nanowires, nanofibers, *etc*.) in order to increase the versatility of nanomaterials and to overcome all the challenges that hinder their applications. In view of the remarkable advances in nanotechnology and the urgent need to develop green, robust and economic approaches for environmental remediation, this research highlights an auspicious method to functionalize carbon nanotubes (CNTs) and investigate their applicability for water remediation.

1.1.2 Deep eutectic solvents (DESs)

Regarding to their significant physiochemical properties, ionic liquids (ILs) have served various purposes and have gained a considerable attention in different academic and industrial researches. For instance, ILs have been used in metal extraction, in Polymeric Electrolyte Membrane Fuels Cells (PEMFC), in Solar Cells and in biological

applications such as drug delivery and activation of enzymes, as well as they have been applied as electrolytes in batteries and as reaction media for organics synthesis and biochemical reactions (Patel & Lee, 2012). However, many studies have underlined the limitations of ILs, which restrain their applications on large scale in commerce, including their poor sustainability and biodegradability (Paiva et al., 2014), their high toxicity to human and environment and the high required cost for their complicated synthesizing process (Dai et al., 2013). Therefore, the emergence of deep eutectic solvents (DESs) as inexpensive solvents with easier preparation and better biodegradability has enlightened the opportunities of their exploitations as appealing alternatives to maintain the useful characteristics of ILs and to overcome the challenges that hinder ILs applications (Tang & Row, 2013). Generally, the formation of DES can be easily obtained by mixing two or more of cheap and biodegradable components, namely, hydrogen bond acceptor (HBA) and hydrogen bond donor (HBD), which are connected with each other by hydrogen bond interactions (Pena-Pereira & Namieśnik, 2014). DES is well characterized by its freezing point which is usually lower than that of its individual components. The main reason behind the depression of the eutectic mixture freezing point, is the delocalization of the charge occurring through hydrogen bonding between the halide anion and the HBD (Hayyan, Hashim, Al-Saadi, et al., 2013a).

Besides of having low production cost and having a good biocompatibility (Hayyan, Hashim, Hayyan, et al., 2013), DESs have been reported to own remarkable properties such as high viscosity, high thermal stability and low vapor pressure (Maugeri & Dominguez de Maria, 2012). Therefore, many studies have been widely investigating the possibility of employing DESs in different applications (Hayyan, Looi, et al., 2015). For instance, DESs have shown interesting potentials in the electrochemistry technology, such as surface cleaning and metallurgy, due to their capability of donating or accepting electrons or protons to form hydrogen bonds which makes them of a great interest for

dissolution of metal oxides (Abbott, Frisch, et al., 2011). Abbott et al. (2004) studied the solubility of CuO in a choline chloride (ChCl) –urea (U) DES for the first time (Abbott, Boothby, et al., 2004). Another example, DESs have been used to remove air pollutants from gas emissions, due to their physiochemical properties which make them great substitutes for volatile organic compounds. Yang et al. (2013) explored the removal of Sulfuric dioxide (SO_2) by (ChCl)-glycerol (Gl) DESs (Yang, Hou, et al., 2013b). The results showed the high absorption efficiency of SO_2 by the eutectic mixture which was increased by decreasing the temperature. Moreover, the absorbed SO_2 could be easily stripped out from the DES by bubbling nitrogen through the eutectic mixture (Yang, Hou, et al., 2013b). In addition, the effect of different temperatures and different DES molar ratio on the solubility of Carbon dioxide (CO_2) was investigated by Han and co-workers using [ChCl:U] DES (Li, Hou, et al., 2008b). In like manner, Wong and co-workers explored the effect of water content on the absorption of CO_2 by using ChCl-U-H_2O (Su, Wong, & Li, 2009). These studies are considered of great concern for the development the separation and gas purification technology using DESs. Furthermore, Morison et al (Morrison, Sun, & Neervannan, 2009) examined the potentials of ChCl-U and ChCl-malonic acid DESs for the drug solubilization, Hayyan et al (Hayyan et al., 2010b) studied the application of ChCl-glycerol based DESs in fuel purification by extracting glycerol from palm oil-derived biodiesel, and Abbott et al. (2012)used ChCl-Ethylene glycol (EG) as dispersant for electrodeposition of Ag and formation of Ag/ SiC/Al2O3 nanocomposite film (Abbott et al., 2012).

DESs have been reported to have a promising industrial application (Guo, Hou, Wu, et al., 2013). Therefore, to suggest further application and design green technologies involving DESs, many studies have extensively been attempting to cover and understand the unique and common properties of DESs followed by applying them in different chemical researches. For example, Shahbaz et al. (2011) and (2012) had successfully

predicted the density and the surface tension of different DESs, and the effect of salt to HBD molar ratio on the predicted DESs densities was investigated (Shahbaz, Mjalli, et al., 2012). Also, Yadav et al. (2014) investigated the densities and the dynamic viscosities of (ChCl:Gl) DES at a temperature range of (283.15–363.15 K) (Yadav et al., 2014).

1.2 Problem statement

One of the major problem in the global environment is the scarcity of safe drinking water sources due to all kinds of pollution that cause the death to different water systems. Industrial, agricultural and residential wastes are highlighted to be the main sources of water pollution. It is well known that these kinds of wastes involve different types of toxic and extremely hazardous pollutants that can cause a severe damage to the ecological dynamics leading to a serious disruption in the natural food chains (Afroz et al., 2014). Chlorophenols is a common group of organic pollutants and they are considered as industrial wastes. They are relatively soluble in water and can easily be detected in different water bodies as they are discharged from various kinds of industries, such as the iron-steel, coke, petroleum, pesticide, paint, solvent, pharmaceutics, wood preserving chemicals, and paper and pulp industries (Aksu & Yener, 2001; Calace et al., 2002). The presence of chlorophenols in water even at low concentrations is of a great risk since the human consumption of phenol-polluted water can lead to fatal damage to human health. Another example of organic based industrial pollutants is Azo dyes, which are known to be very stable, difficult to biodegraded and widely disposed to the environment through the effluents of different industries, such as textile, paper, ink, plastic, rubber, cosmetic, drugs, paint and printing industries (Shu & Huang, 1995). The improper disposal of industrial effluents containing large amount of azo dyes significantly causes serious problems to the photosynthetic activity in aquatic life as well as some of azo dyes and their dye precursors are poisonous and carcinogenic to human (Shu & Huang, 1995).

Therefore, there is an utmost need to treat the industrial wastewater that contains as dangerous pollutants as phenolic compounds and azo dyes, to protect and preserve the natural water systems.

The most promising treatment method for all non-biodegradable organic pollutants is "adsorption" and many studies were conducted to find efficient materials with high adsorption capacities (Aksu, 2005b). Thus, attention has been focused on carbon nanotubes (CNTs) since their discovery by Iijima in 1991, due to their exceptional characteristics including large surface area, hollow and layered structures, as well as due to their significant thermal and chemical stability (Gong et al., 2009; Smart et al., 2006; Yang, Wu, et al., 2010a). Accordingly, CNTs have shown great potential as competent adsorbents for removal of wide range of organic and inorganic pollutants (Ren et al., 2011), such as, fluoride (Yan et al., 2006), lead (Li et al., 2002), nickel (Chen & Wang, 2006), cadmium (Luo, Wei, et al., 2013), zinc (Lu & Chiu, 2006) 1,2-dichlorobenzene (Peng et al., 2003b), 2,4,6-trichlorophenol (Chen, Shan, et al., 2009), pentachlorophenol (Abdel Salam & Burk, 2008), reactive dyes(Wu, 2007), etc. Despite of the high adsorption capacity of CNTs on the removal of various of toxic organic contaminants from water, insignificant information is reported about their adsorption capacity on the removal of 2,4-DCP (Xu et al., 2012). Not to mention, some shortcomings hinder the application of CNTs such as agglomeration and their poor dispersion in aqueous solutions which results in decreasing the surface area of CNTs and lowering their ability to remove certain compounds (Ibrahim et al., 2016)**.** Consequently, functionalization of CNTs has gained lots of interest as an attempt to remove CNTs impurities and introduce different functional groups, which subsequently enhance CNTs solubility, graphitic networks and improving their process-ability (Datsyuk et al., 2008; Yu et al., 2006). Modification of CNTs can be achieved either by physical absorption method, which is efficient but conducted by weak hydrophobic interactions, or chemical bonding method which is on

the other hand leads to damage on the structure of CNTs which reducing their efficiency (Hu et al., 2010; Jung et al., 2008). Thus, seeking for versatile, effective and low-cost functionalization agents to manipulate the application of CNTs for highly selective removal of pollutants.

Recently, deep eutectic solvents (DESs) have been highlighted as outstanding low-cost alternatives for ionic liquids (ILs) due to their high biodegradability and easy preparation process (Durand, Lecomte, & Villeneuve, 2013; Tang & Row, 2013). Basically, DES is a mixture of two or more of inexpensive and biodegradable components, specifically, Salt and hydrogen bond donors (HBDs). It was suggested that DESs possess the potential to be exploited in different fields of chemistry and electrochemistry (de María & Maugeri, 2011). As well as, the possibility of using DESs in nanotechnology have been investigated, including their use for nanomaterials production or as functionalization agents to overcome the challenges restraining the application of nanomaterials (AlOmar, Alsaadi, Hayyan, Akib, & Hashim, 2016; AlOmar, Alsaadi, Hayyan, Akib, Ibrahim, et al., 2016; Hayyan, Abo-Hamad, et al., 2015a).

Eventually, the scope of this account is established to investigate the potential of DESs as functionalization agents for multi-wall carbon nanotubes (CNTs), and to compare the removal efficiency and adsorption capacity of pristine and functionalized CNTs adsorbents for 2,4-dichlorophenol (2,4-DCP) and methyl orange (MO) removal from water. RAMAN, FTIR, BET surface area, FESEM, TGA and zeta potential have been employed to comprehensively study the chemical, physical and morphologic characteristics of all examined adsorbents. Optimization, kinetics and isotherms studies were conducted to describe the optimum adsorption conditions and to illustrate the adsorption mechanism of 2,4-DCP and MO on DES-functionalized CNTs, which can be a significant contribution for CNTs application in wastewater treatment.

1.3 Objectives of study

1. To synthesize and study the physiochemical properties of new types of deep eutectic solvents (DESs).
2. To prepare and characterize DESs-functionalized multi-walled carbon nanotubes (CNTs).
3. To investigate the capability of using DESs-functionalized CNTs as new adsorbents for the removal of 2,4-dichlorophenol and methyl orange from water.
4. To determine the optimum conditions for the adsorption of organic pollutants such as (adsorbent dose, contact time, pH and initial concentration) by obtaining empirical models.
5. To investigate the adsorption kinetics as well as the isothermal adsorption behavior and determine all related coefficients and parameters.

1.4 Research philosophy

The main reason behind the selection of this research area is to open a new window of opportunity in remediation of contaminated water, by introducing a new qualified treatment method to remove toxic organic pollutants from water. The key aspect of this research is to employ DESs as green and efficient novel functionalization agents for carbon nanotubes. DESs have significant physiochemical properties and they are easy to synthesize, biodegradable and cost-efficient solvents. Therefore, DESs could be remarkable substitutes to acids and other chemicals since they have the potential to modify the surface of CNTs and to improve their adsorption capacity without the need of expensive and complex processes.

1.5 Research methodology

The methodology of this research can be summarized by the following steps:

- Preparation of two DESs systems by mixing two different HBDs and five different salts.
- Selection of the most homogeneous and stable DESs of each prepared system by conducting a primary screening of various molar ratios.
- Characterization of the selected DESs comprehensively, including freezing point, FTIR, density, viscosity, conductivity and surface tension.
- Investigation the capability of DESs as CNTs functionalization agents.
- Studying the characteristics of DES-CNTs combination such as, RAMAN, FTIR, FESEM, BET surface area, TGA and zeta potential.
- Application of DESs functionalized CNTs as new adsorbents for organic pollutants removal from water.
- Applying Response Surface Methodology (RSM) to develop an estimated regression and to optimize the experimental conditions for organic pollutants adsorption from water.
- Determination of the adsorption kinetics and isotherms along with their perspective coefficients and parameters.

1.6 Outline of the thesis

There is a total of five chapters in this thesis, as follows:

- Chapter One (Introduction): This chapter gives a brief introduction on the presence of organic contaminants in water and problems encountered during the application of carbon nanotubes as adsorbents. Moreover, the research objectives and methodology are illustrated.

- Chapter Two (Literature Review): This chapter discusses the environmental application of nanotechnology in air, soil and water and it contains a simple survey of previous works in relation to the nanotechnology employments in different field. In addition, this chapter discusses the history and application of DESs, as well as the most common methods used to remove organic compounds from water.
- Chapter Three (Materials and Methods): This chapter deals with experimental set up for synthesizing, characterizing of DESs and DESs functionalized CNTs. Moreover, it explains the detailed research methodology including, functionalization, batch adsorption and response surface methodology (RSM). All chemicals, materials, equipment and analytical instruments involved in this research are described in this chapter.
- Chapter Four (Results and Discussion): Presents results and discussion obtained from characterization of DESs, functionalization of CNTs and results obtained from RSM, ANOVA analysis and regression models for each adsorbate adsorbent system.
- Chapter Five (Conclusion): Comprises the overall findings of this research and summarizes the achievement extents of this research objectives. The last section of this chapter involves some recommendations for future work.

CHAPTER 2: LITERATURE REVIEW

2.1 Water pollution

One of the major challenges that is facing the globe is providing a convenient access to clean and affordable water that can keep up with rapid growing demands. Population growth, global climate change, and water pollution are the highest challenges that increasing the struggles faced by water supply systems, where around 780 million people still lack access to reliable drinking water sources worldwide (WHO, 2012). In both developing and industrialized countries, water scarcity is exacerbated by human activities that play the greatest role in contaminating the natural water resources by releasing energy, chemicals and other pollutants that deteriorate the water quality for other users. In addition, nature itself can be one of the contamination sources such as water storm runoff, animal wastes, etc. The United States Environmental Protection Agency (EPA) classifies water pollution into the following six categories: (1) Plant nutrients; (2) Biodegradable waste; (3) Heat; (4) Sediment; (5) Hazardous and toxic chemicals; (6) Radioactive pollutants. Thus, water pollutants such as organic pollutants, pathogens, heavy metals and different anions, that are added to the water and cannot be naturally broken down and tend to change the properties of the water body.

2.1.1 2,4-DCP in water

One of the most common chloroorganic pollutant in water is 2,4-DCP with pKa of 7.4 and water solubility of 4.5 g/L at 25 °C (Bilgin Simsek et al., 2016). The main source of water contamination with such hazardous chlorinated organic compounds is the wastewater discharged from industries of steel, plastic, rubbers, wood-preserving, pharmaceuticals and petroleum refineries (Li, Li, et al., 2009). Moreover, 2,4-DCP is utilized widely in the manufacture of herbicide and pesticides, therefore, the municipal and agricultural wastewater is considered an additional important source of water

pollution (Jin, Zhang, & Jian, 2007; Kuśmierek, Szala, & Świątkowski, 2016a). The presence of 2,4-DCP in environment poses a serious risk due to its high persistency, toxicity, and its organoleptic and carcinogenic effects (Bhattacharya & Banerjee, 2008; Igbinosa et al., 2013). As a result, Environmental Protection Agency (EPA) listed 2,4-DCP as dangerous contaminant to be removed from water system. Many photochemical, biochemical and electrochemical techniques have been proposed for the removal of chlorophenols from water, such as oxidation, precipitation, ion-exchange and solvent extraction (Bilgin Simsek et al., 2016; Liu et al., 2010). Nevertheless, Adsorption is proved to be the most effective and economic process due to its ability to purify and separate pollutants from wastewater without disturbing water quality or generating toxic secondary pollutants (Bailey et al., 1999; Gupta & Imran, 2004). Various adsorbents have been reported for 2,4-DCP elimination from water, for example, carbon fibers (Liu et al., 2010), carbon nanotubes (Kusmierek, Sankowska, & Swiatkowski, 2013) and most of all, activated carbons (Hamdaoui & Naffrechoux, 2007a).

2.1.2 MO in water

Today, many industries such as paper, printing, textiles, cosmetics and pharmaceutical manufacturing discharge large amounts of wastewaters that contain variety of synthetic dyes (Chen et al., 2010). The intricate chemical structure of dyes contributes in their resistance to light and oxidation and reinforces their non-biodegradability nature (Aksu, 2005a; Ofomaja & Ho, 2008). Therefore, the presence of dyes in water bodies, even in simple traces, imposes an objectional threat to the environment. One of the prevalent ecological risks that are caused by the improper discharge of toxic dyes into open water is reducing the oxygen and sunlight penetration and consequently affecting the photosynthesis activity in aquatic planktons (Mittal et al., 2007). Furthermore, dyes are commonly known carcinogenic and mutagenic organic substances (Chen et al., 2010)

and inadvertent ingestion of toxic dyes may lead to sever health problems to mankind including dysfunction of liver, brain, kidney, nervous system and reproductive system (Ajji & Ali, 2007). Consequently, environmental concerns have focused on finding a proper treatment method to control the coloured materials and toxic dyes in the industrial effluent prior to its discharge into receiving water bodies. Methyl orange (MO) is an example of toxic azo dyes, it is known to be water-soluble dye and its aqueous solution functions as weak acid with an approximate pH value of 6.5 (5 g/l, H_2O, 20 ◦C) (Küçükosmanoğlu, Gezici, & Ayar, 2006). Several treatment methods have been reported for azo dyes removal such as photochemical method (Guettai & Amar, 2005), biodegradation (Chang et al., 2001), electrochemical treatment (Fan et al., 2008), chemical coagulation (Vandevivere, Bianchi, & Verstraete, 1998), reverse osmosis (Al-Bastaki, 2004) and adsorption (Mittal & Gupta, 2010; Mittal, Thakur, & Gajbe, 2013). Owing to its high effectiveness, low cost, low energy requirements and its simple operational design (Jalil et al., 2010; Tan, Ahmad, & Hameed, 2008), adsorption technique has proved to more efficient and advantageous over other reported physio-chemical techniques (Başar, 2006; Srivastava, Mall, & Mishra, 2006).

2.2 Nanotechnology applications in water treatment.

Essentially, the wastewater treatment involves physical, chemical and biological technologies and it usually occurs in four stages: (1) preliminary; (2) primary; (3) secondary; and (4) tertiary advanced treatment. The technologies that are generally used for water purification are coagulation and flocculation; sedimentation; dissolved air flotation; filtration; steam distillation; ion exchange; deionization; reverse osmosis; and disinfection. Materials usually used in these technologies are sediment filters, activated carbon, Coagulants, ion exchangers, ceramics, activated alumina, organic polymers and many hybrid materials (Hotze & Lowry, 2011). However, the conventional water

treatment procedures might be costly and could release secondary toxic contaminants into the environment (Gaya & Abdullah, 2008b).

Nanotechnology enables extremely efficient, flexible and multifunctional processes that can provide a promising route, in order to retrofit aging infrastructure and to develop high performance, inexpensive treatment solutions which less depend on large infrastructures (Qu et al., 2013). The current advancements in nanotechnology spot the light on great opportunities to develop the next-generation of water supply systems and expose the possibilities to expand the water supplies by affording new and cost-effective treatment capabilities that can overcome the major challenges faced by the current treatment technologies (Qu, Alvarez, & Li, 2013). This section mainly focuses on the role of nanomaterials in the adsorption technique, later the nanomaterial applications in some other water treatment techniques are discussed.

2.2.1 Adsorption

Compared to the limited active sites surface area and low efficiency of the conventional adsorbents, the nano-adsorbents offer a considerable development with their high adsorption kinetics as demonstrated by their extremely high specific surface area and associated adsorption sites, short intraparticle diffusion distance, tunable pore size and surface chemistry (Qu, Alvarez, & Li, 2013), that provides useful features for effective adsorption process. Their great adsorption capacity is mainly because of their high specific area and the highly active adsorption sites that are created by high surface energy and size dependent surface structure at the nanoscale (Auffan et al., 2008). The nano-adsorbents are effectively used in the removal of organic compounds and metal ions and their selectivity toward specific pollutants can be increased by functionalization.

2.2.1.1 Nanoscale metal oxides as adsorbents

Nanoscale metal oxides such as titanium dioxides, iron oxides, zinc oxides, alumina, etc., have been explored as low cost, effective adsorbent for water treatment offering a more cost-efficient remediation technology due to their size and adsorption efficiency (Engates & Shipley, 2011). The adsorption is chiefly controlled by forming a complex with the surface of nanoscale metal oxides and undergoing one electron oxidation reaction under visible irradiation (Peng, Feng, et al., 2012). Among the nanoscale metal oxides, the magnetic nanoparticles have drawn a considerable concern because of their potential application (Xin et al., 2012) and their exhibition of interesting magnetic properties (e.g., super paramagnetism, strong magnetic response under low applied magnetic fields (Figure 2.1)) (Kilianová et al., 2013). Table 2.1 shows the applications of nanoscale metal oxides as adsorbents.

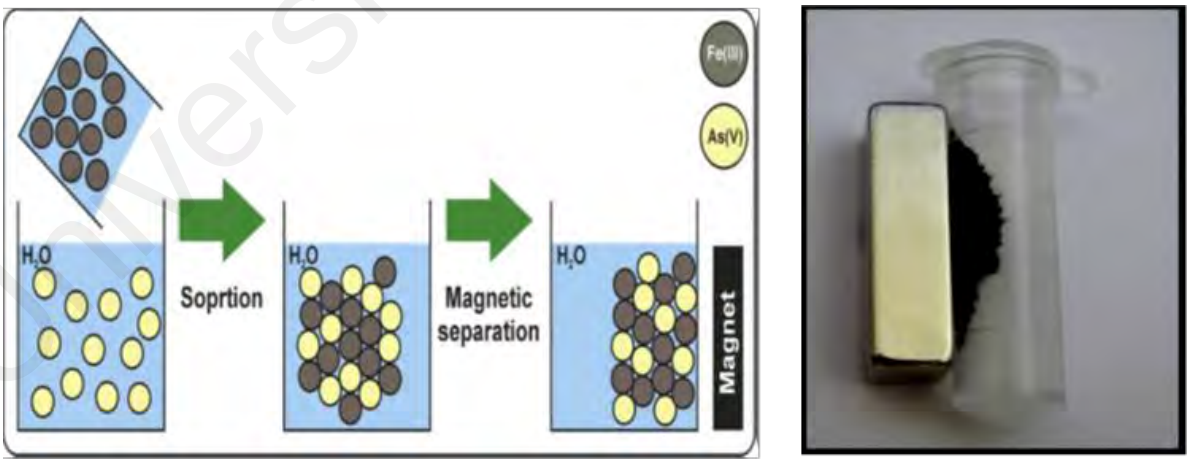

Figure 2.1: Illustrative photo of magnetic nanoparticles of iron oxide nature interacting with a simple hand magnet (Kilianová et al., 2013).

Table 2.1: Nano-scale metal oxides as adsorbents.

Adsorbents	Modification/ Synthesis	Target pollutants	Performance	Adsorption isotherm	Remarks	REF
Magnetite Fe_3O_4	zirconium (IV)-metalloporphyrin	Fluoride	The percentage of the extracted fluoride ions was 92.0 ±1.7%. (contact time: 20 min; pH: 5.5)	_____	These modified nanoparticles were separated by an external magnetic field	(Poursaberi et al., 2012)
Magnetite Fe_3O_4	amino-functionalized (1,6-Hexadiamine)	Cu (II)	The maximum adsorption capacities was 25.77mgg^{-1} at pH 6, and 298 K.	Langmuir	adsorption process was spontaneous, endothermic and chemical in nature coexisted ions, Ca^{2+} and $Mg2^{+}$, have no influence on the removal efficiency of Cu^{2+} with MNP-NH_2	(Hao, Man, & Hu, 2010)
Magnetite Fe_3O_4	Polymer modified nanoparticles (3-aminopropyltriethoxysilane (APS) and copolymers of acrylic acid (AA) and crotonic acid (CA)).	Cd(II) Zn(II) Pb(II) Cu(II)	95% of the metal ions were adsorbed at about 30 min. pH 5.5	Langmuir	The adsorption capacity remained almost constant for the 4 cycles the adsorption capacity of Cu^{2+} decreased with increasing coexisting ions(Na^{+}, K^{+}, or Mg^{2+})	(Ge et al., 2012)

Table 2.1 (continued)

Titanate nanotube (TNTs)	hydrothermal method from TiO_2 nanoparticles	Pb(II) Cd(II) Cu(II) Cr(II)	TNTs followed the sequence of Pb^{2+} (2.64 mmol g−1) ≫ Cd^{2+} (2.13 mmol g−1) > Cu^{2+} (1.92 mmol g−1) ≫ Cr^{3+} (1.37 mmol g−1).	_____	TNTs can be considered as good adsorbents for heavy metals as the can effectively adsorb cations via ion-exchange due to their low point of zero charge (pHPZC) and abundant hydroxyl groups (OH) on the surface.	(Liu, Wang, et al., 2013)
Titanate nanoflowers (TNF)	_____	Cd(II) Ni(II) Zn(II) Pb(II)	The maximum adsorption capacity for Pb(II), Cd(II), Ni(II), and Zn(II) ions were were 1.47 mmol/g, 0.73 mmol/g, 0.33 mmol/g, and 0.44 mmol/g respectively	Langmuir	high selectivity in the removal of Cd(II) than less toxic ions (Zn(II) and Ni(II)).	(Huang, Cao, et al., 2012)
Iron oxide–alumina Fe_2O_3–Al_2O_3		Cu(II) Pb(II) Ni(II) Hg(II)	Maximum sorption capacities were found to be 4.98 mg/g for Cu^{2+}, 32.36 mg/g for Ni^{2+}, 23.75 mg/g for Pb^{2+} and 63.69 mg/g for Hg^{2+} ions.	Langmuir	The removal percentage was in the order of Cu^{2+} < Pb^{2+} < Ni^{2+} < Hg^{2+}.	(Mahapatra, Mishra, & Hota, 2013)

Table 2.1 (continued)

Titanium dioxide	_____	Pb(II), Cu(II) Zn (II)	Largest adsorption capacity (2312.18 μmol/g) with Pb, while the smallest adsorption capacity (40.10 μmol/g) with Cu.	Freundlich	desorption was pH dependent and that more than 98% of all metals desorbed at pH 2 adsorption affinity to be Pb > Zn > Cu	(Hu & Shipley, 2012)
Titanium dioxide	_____	Pb, Cd, Cu, Ni, Zn	TiO_2 nanoparticles removed Pb, Cd, and Ni from solution with similar adsorption at 0.1 and 0.5 g/L.	Langmuir	The high surface area of TiO_2 nanoparticles results in their large adsorption capacities making them better sorbents when compared to bulk particles.	(Engates & Shipley, 2011)
Hydrous cerium oxide (SCO)	(SCO) was synthesized by integrating CeO2 nanoparticles into silica monoliths.	As	Treatment met the maximum contaminant level of arsenic at 10 _g/L for drinking water	_____	The silica monoliths substrate was used to enhance the stability of SCO during the water treatment and preventing the leakage of CeO_2 nanoparticles into the treated water.	(Sun, Li, et al., 2012)

Table 2.1 (continued)

Magnetite Fe_3O_4	Synthesized with high specific area by the aerosol assisted chemical vapour deposition method	As	100% removal efficiency before one minute of contact.	_____	The fast removal of arsenic means that the affinity of arsenic by the iron is very strong.	(Monárrez-Cordero et al., 2014)
Magnetite Fe_3O_4	Amine-functionalized	Pb(II), Cd(II), Cu(II)	Equilibrium within 120 min at pH 7.0. AF-Fe3O4 was able to remove over 98% of Pb(II), Cd(II), and Cu(II)	Langmuir	Affinity Pb > Cu > Cd, separation by magnetic field.	(Xin et al., 2012)
NiO nanoparticles	_____	Cd(II) and Pb(II)	The maximum adsorption capacity for Cd(II) and Pb(II) ions were are 909 and 625 mg/g, respectively	Langmuir	the adsorption was endothermic and spontaneous in nature and followed boundary layer diffusion or external mass transfer effects	(Sheela & Nayaka, 2012)

Table 2.1 (continued)

Mixed maghemite-magnetite nanoparticles **γ-Fe_2O_3- Fe_3O_4**	_____	Cd(II)	About 40% of total Cd(II) was removed within 5 min. Thereafter, the adsorption capacity remained constant after the contact time of 2 h.	Langmuir	Upon exposure to mixed maghemite-magnetite, Cd^{2+} ions may go through oxidation-reduction reactions, or may become fixed by complexation with oxygen atoms in the oxy-hydroxy groups at the shell surface of the iron oxide nanoparticles.	(Chowdhury & Yanful, 2013)
Iron oxide nanoparticls (magnetite and maghemite)	Iron oxides nanoparticles was produced by employing Electrical wire explosion (EWE)	As(III) and As(V)	qmax, for As(III) and As(V) was 2.90 and 3.05 mg/g respectively	Langmuir	The sorption capacity values are lower than those of the commercial ones	(Song et al., 2013)
Magnetic iron oxide nanoparticles (MION-Tea) Fe_3O_4	Synthesized using tea waste	As(III) and As(V)	High adsorption capacity of 188.69 mg/g for arsenic (III), and 153.8 mg/g for arsenic (V).	Langmuir	Thermodynamics revealed the endothermic nature of adsorption MION-Tea can be reused up to 5 adsorption cycles and recycled using NaOH.	(Lunge, Singh, & Sinha, 2014)

Table 2.1 (continued)

Graphene oxide-hydrated zirconium nanocomposite GO–ZrO(OH)$_2$	Prepared by hydro-thermal co-precipitation method.	As(III) and As(V)	Adsorption capacity of 95.15 and 84.89 mg/g for As(III) and As(V)	Langmuir	GO–ZrO(OH)2 was successfully regenerated with a stable adsorption capacity for 5 cycles.	(Luo, Wang, et al., 2013)
Magnetite Fe_3O_4	_____	Pb(II)	Equilibrium was achieved in less than 30 min. . Maximum removal was observed at pH 5.5	Freundlich	Pb(II) removal efficiency was not affected by the add addition coexisting cations such as $Ca^{2+,}$ Ni^{2+}, CO^{2+}, and Cd^{2+} .	(Nassar, 2010)
Iron(III) oxide γ-Fe_2O_3	Wet chemical Method.	As(V)	100% removal of As(V) is achieved at pH from 5 to 7.6 with Fe/As = 20/1.	Freundlich	The strong magnetic interactions they developed between nanoparticles develop a mesoporous nature of nanoparticle arrangement which is responsible for enhancement of adsorption capacity.	(Kilianová et al., 2013)

Table 2.1 (continued)

Magnetic Nanoparticle (Fe_3O_4) Impregnated onto Activated Maize Cob Powder (Fe_3O_4-MCP)	_____	methylene blue (MB)	The highest percentage for dye concentration removal was 93.11% at pH 6.0	_____	The electrostatic attraction between the negatively charged Fe_3O_4-MCP surface and the positively charged cationic dyes is the key mechanism of the adsorption process.	(Tan et al., 2012)
Guar gum–nano zinc oxide (GG/nZnO)	_____	Cr(VI)	98.63% Cr(VI) was removed with a contact time of 50 min, pH 7, and an adsorbent dose 1.0 g/L.	Langmuir and Freundlich	Both liquid-film and intra-particle diffusions dominated the overall kinetics of the adsorption process	(Khan et al.)
Hydrous aluminum oxide embedded with Fe_3O_4 nanoparticle (Fe_3O_4@$Al(OH)_3$ NPs)	_____	Fluoride		_____	The advantages of this adsorbent is a combination from magnetic nanoparticle and hydrous aluminum oxide floc, with magnetic separability and high affinity toward fluoride.	(Zhao et al., 2010)

Table 2.1 (continued)

Nano-sized superparamagnetic zirconia ($ZrO_2/SiO_2/Fe_3O_4$, SPMZ)		Fluoride	The sorption capacity amounts was14.7 mg/g at pH=4	Langmuir and Freundlich	SPMZ possesses a considerable selectivity for fluoride which allows its preferred sorption from multicomponent systems	(Chang, Chang, & Hsu, 2011)
Magnetite nanoparticles Fe_3O_4	direct attachment of reactive blue-19 onto the surface of magnetite nanoparticles	Pb(II)	adsorption of Pb^{2+} takes place at 3.0 < pH < 5.5 range with a maximum capacity factor for Pb^{2+} ion on the RB-MNPs was 79.3 mg g^{-1}.	Langmuir	Ion exchange mechanism is mainly responsible for the removal of lead whie the electrostatic attraction force probably has slight influence on the removal process.	(Madrakian, Afkhami, & Ahmadi, 2013)
PVA/TiO_2/APTES nanohybrid	functionalized with amine groups	Cd(II), Ni(II) and U(VI)	The maximum sorption capacities were 49.0, 13.1 and 36.1 mg g_1 for Cd(II), Ni(II) and U(VI) ions with pH of 5.5, 5 and 4.5, respectively	Freundlich	The sorption process was ideal at higher temperature with affinity order for heavy metal ions is as follows: Cd(II) > U(VI) > Ni(II).	(Abbasizadeh , Keshtkar, & Mousavian, 2014)
Amorphous zirconium oxide (am-ZrO_2)	_____	As(III) and As(V)	The adsorption capacities of am-ZrO2 nanoparticles on As(III) and As(V) at pH 7 are _83.2 mg/g and 32.5 mg/g, respectively	_____	Am-ZrO2 nanoparticles immobilized on glass fiber cloth showed an even better removal effect than am-ZrO2 nanoparticles dispersed in water.	(Cui, Li, et al., 2012)

Table 2.1 (continued)

Amorphous zirconium oxide (am-ZrO_2)	_____	phosphate	adsorption capacity was about 99.01 mg/g at pH 6.2	Langmuir	Hydroxyl groups on the surface played a main role in the phosphate adsorption. am-ZrO_2 nanoparticles. am-ZrO_2 nanoparticles could be easily regenerated using a 0.1 M NaOH	(Su et al., 2013)
Fe_3O_4 nanoparticles	Coated with ascorbic acid	As	maximum adsorption capacity of 16.56 mg/g for arsenic (V), and 46.06 mg/g for arsenic (III).	Langmuir	The use of the ascorbic acid enhanced the suspension of Fe_3O_4 nanoparticles and effectively inhibited the leaching of Fe into the solution.	(Feng et al., 2012)
Single-phase α-MnO_2 nanorodsand δ-MnO_2	_____	As(V)	α-MnO_2, pH 6.5, Maximum removal capacity 19.41(mg g^{-1}) δ-MnO_2, pH6.5, Maximum removal capacity 15.33 (mg g^{-1})	Langmuir	Electrostatic force and the ligand exchange (ligand exchange with –OH) phenomenon are the two factors that play an important role in the adsorption of arsenate species onto Mn-oxides surface.	(Singh et al., 2010)

Table 2.1 (continued)

CeO_2, TiO_2 and Fe_3O_4	_____	Pb(II)	The adsorption capacity obtained for the NPs was: 189 mg Pb/g NPs CeO_2, 83 mg Pb/g NPs Fe_3O_4 and 159 mg Pb/g NPs TiO_2.	_____	The toxicity issue of thee NPs is also assessed in this study and the result showed that the CeO_2 NPs had high phytotoxicity whileTiO_2 and Fe_3O_4 NPs did not exhibit any toxicity.	(Recillas et al., 2011)
Magnesium and zinc oxide MgO and ZnO	_____	Cu(II)	The maximum adsorption capacities obtained for ZnO and MgO are 226 and 593 mg/g, respectively at initial pH of 3–4	Freundlich	MgO has better adsorption potential as compared to ZnO	(Rafiq et al., 2014)
Nano ZnO	gel combustion	Pb(II)	nano ZnO shows almost complete Pb adsorption at lower initial.	Langmuir and Freundlich	The surface area of the powder was 80.425 m2 g-1, has large surface area compared to normal zinc oxide.	(Venkatesham et al., 2013)

2.2.1.2 CNTs as adsorbent

Carbon nanotubes (CNTs), including single-walled CNTs and multi-walled CNTs (CNTs), have lately drawn significant attention because of their mechanical, electrical, optical, physical, and chemical properties (Koziol et al., 2007). Since CNTs discovery by Iijima in 1991 (Iijima, 1991), they have been recognized as alternates for activated carbon as they exhibit remarkable adsorption competency for gas and liquid phases, such as organic vapors, inorganic pollutants and several heavy metal ions(Luo, Wei, et al., 2013) due to their binding sites that are more available than those on activated carbon(Ji et al., 2009).

In comparison to other carbon-based adsorbents, CNTs is the super organic adsorbent for environmental remediation; they behave as flexible porous materials towards the organic pollutants. CNTs have shown remarkable adsorption capability and high removal efficiency for various organic pollutants (Table 2.2), including, organic dyes (e.g., Catoinic, azoic, reactive, basic and acid dyes etc.)(Gao et al., 2013; Geyikçi, 2013; Gupta et al., 2013; Madrakian et al., 2011; Moradi, 2013) pharmaceuticals (e.g., Cephalexin, Tetracycline (TC), Olaquindox, carbamazepine, etc.)(Cai & Larese-Casanova, 2014; Jafari & Aghamiri, 2011; Zhang, Song, et al., 2011; Zhang, Xu, et al., 2011), pesticides (Deng et al., 2012), phenolic compounds (Abdel-Ghani, El-Chaghaby, & Helal, 2014; Pacholczyk et al., 2011; Sheng, Shao, et al., 2010) and other toxic organics. Yu and Apul (2015) reported the adsorption of many different types of organic compounds on Carbon nanotubes (Apul & Karanfil, 2015; Yu et al., 2014). The dominate adsorption mechanisms by which CNTs adsorb organic compounds consist mainly of physical processes and are affected by the properties of the compound of interest (Pan & Xing, 2008). Other studies stated that the aromatic compounds have relatively higher sorption affinity toward CNTs than non-aromatics (Lin & Xing, 2008). Furthermore, organic compounds which have -COOH, -OH, $-NH_2$ functional groups could also form hydrogen

bond with the graphitic surface of CNTs (Yang et al., 2008). In short during organic compound–CNT interactions, different mechanisms may take place simultaneously such as hydrophobic interactions, π_π bonding, electrostatic interactions, covalent and hydrogen bonding (Pan & Xing, 2008; Yang & Xing, 2010).

On the other hand CNTs have shown great capabilities for the adsorption of heavy metals from natural waters and wastewater streams and that is of great environmental relevance due to the high toxicity, non-biodegradability of compounds which are generally considered as carcinogenic(Luo, Wei, et al., 2013). Many researches have investigated the mechanisms of heavy metal ions adsorption on CNTs which appear to be very complicated and attributable to physical adsorption, electrostatic attraction, precipitation and chemical interaction between the heavy metal ions and the surface functional groups of CNTs (e.g., carboxyl, hydroxyl, lactones and phenol)(Ren et al., 2011). Whereas, the chemical interaction between the heavy metal ions and the surface functional groups of CNTs is the main adsorption mechanism and that reflects that the sorption of metal ions onto CNTs is chemisorption process rather than physisorption process and strongly depends upon CNTs surface total acidity (Lu, Chiu, & Liu, 2006; Rao, Lu, & Su, 2007). The adsorption of the heavy metals might be influenced by the presence of some organic compounds for instance, the adsorption of copper (II) is significantly influenced by humic acid (HA), fulvic acid (FA) Hydroxylated and Carboxylated Fullerenes (Sheng, Li, et al., 2010; Wang, Li, et al., 2013).The order of binding of heavy metal ions by CNTs is widely studied, Stafiej (Stafiej & Pyrzynska, 2007) reported the adsorption characteristics of certain divalent metal ions (i.e., Cu, Co, Cd, Zn, Mn, and Pb) by CNTs and found that the affinity of metal ions for CNTs followed the order Cu(II) > Pb(II) > Co(II) > Zn(II) > Mn(II). Meanwhile, the competitive adsorption of Pb(II), Cu(II) and Cd(II) ions by oxidized CNTs was studied and found that the adsorption capacities of CNTs for the three metal ions were in the following sequence:

Pb(II) > Cu(II) > Cd(II) (Li, Ding, et al., 2003). Table 2.3 represents carbon nanotube as heavy metals adsorbent.

The main drawback of CNTs is the poor dispersion in the aqueous phase that significantly hinders the application of CNTs because of the hydrophobicity of their graphitic surface, the strong intermolecular van der Waals interaction between tubes, which can lead to the formation of loose bundles/ aggregates (Figure 2.2) that contain interstitial spaces and grooves which are reported to be high adsorption energy sites for organic molecules(Pan et al., 2008) and despite of that, it was suggested that those aggregated reduce the effective surface area of CNTs (Vuković, Marinković, et al., 2010). To overcome this drawback and enhance the CNTs performance, it can be functionalized in different ways, for example formation of chemical bonds between the modifier and CNTs surfaces or physical adsorption of the modifying species to the surface of CNTs and all the ways lead to the addition of functional groups on the surface of the CNTs improving their efficiency, selectivity, and sensitivity (Ghaedi & Kokhdan, 2012; Han et al., 2006; Liu, Su, & Schlögl, 2008; Perez-Aguilar, Diaz-Flores, & Rangel-Mendez, 2011; Tasis et al., 2006; Wildgoose et al., 2006). The acid treatment produce carboxylic and hydroxylic group (COOH, OH, C=O and OSO_3H) on the external surface of the CNTs (Vuković, Marinković, et al., 2010) as shown in Figure 2.3. The hydrophilic groups (i.e. carboxylic groups) can be introduced onto the sidewall of CNTs, as a result improving the solubility and dispersion of CNTs in aqueous solutions (J. Liu, 1998). Functionalization of CNTs via oxidizing and reducing chemicals such as HNO_3, $KMnO_4$, H_2O_2, NaClO, H_2SO_4, KOH, NaOH and have been widely reported (Li, Hong, et al., 2010; Li, Wang, et al., 2003; Raymundo-Piñero et al., 2005).

Another essential point is the separation of CNTs from the treated medium that may cause considerable inconvenience in their practical application. To cope with this problem, magnetic CNTs have been prepared by association of CNTs with magnetic

nanoparticles and they can be well dispersed in the water as well as can be simply manipulated by external weak magnetic field that permits their easy separation from water (Peng et al., 2005; Qu et al., 2008). Thus, it was demonstrated that combining the magnetic properties of the iron oxides with the adsorption properties of CNTs is an effective, rapid method for the separation of the magnetic adsorbents from aqueous solutions (Gong et al., 2009; Gupta, Agarwal, & Saleh, 2011). Despite that, the magnetic phase can be leached out in acidic mediums because they are placed within the pores which does not protect them from contact with solution, Bystrzejewski and Pyrzyńska (2011) pointed out that carbon-encapsulated magnetic nanoparticles (CEMNPs) are free of this disadvantage, because they comprise of uniform spherical nano-crystallites firmly covered by tight carbon coatings (Bystrzejewski & Pyrzyńska, 2011). The role of the coatings is to protect the encapsulated nanoparticles from agglomeration, corrosion and to provide a scaffold for introducing surface acidic groups that are important to bind the metal ions (Bystrzejewski et al., 2009; Pyrzyńska & Bystrzejewski, 2010).

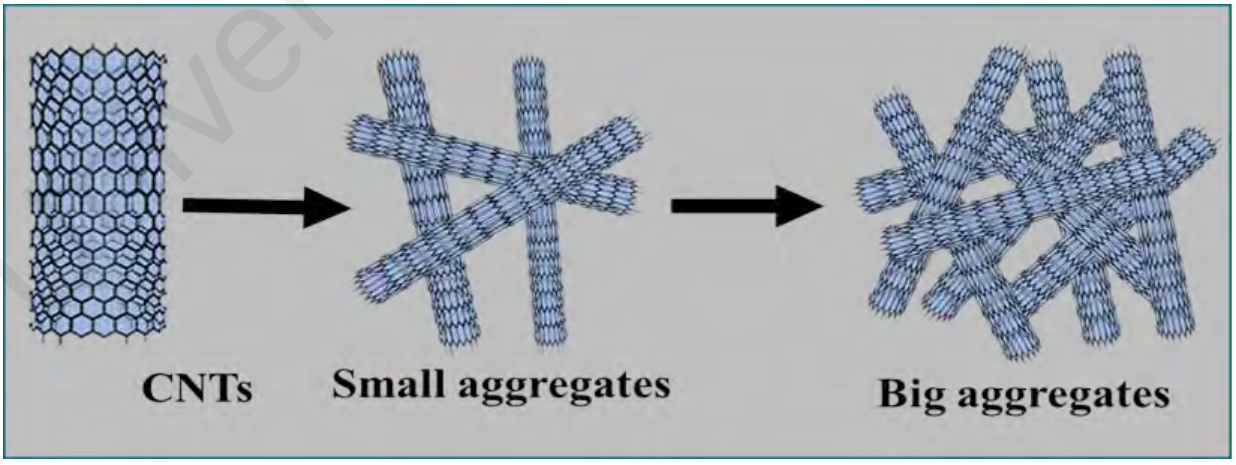

Figure 2.2: Schematic aggregation of Carbon nanotubes which monomers form small aggregates first and then big aggregates (Yang & Xing, 2010).

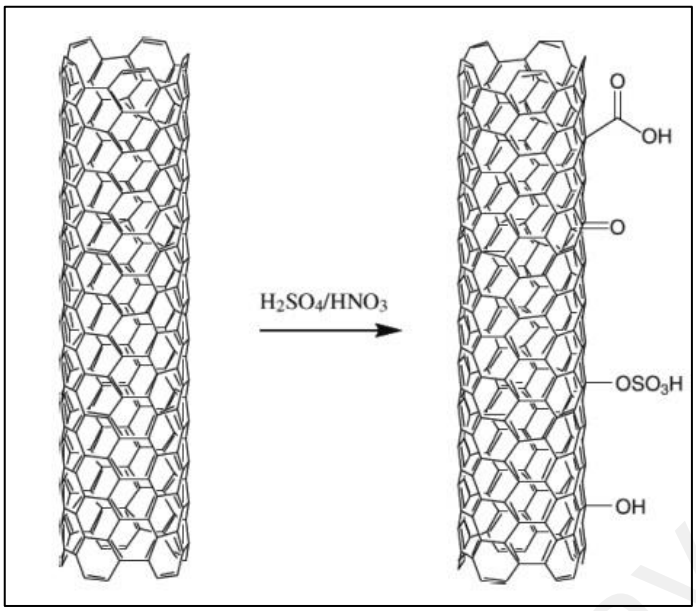

Figure 2.3: Schematic presentation of functional groups of H_2So4/HNO_3 Oxidized CNTs surface (Vuković, Tomić, et al., 2010).

Table 2.2: CNTs as organic pollutants adsorbents.

Organic pollutants type	Examples	CNTs modification	Adsorption isotherm	Remarks	Ref
Pharmaceuticals	Epirubicin (EPI)	Carboxylized with HNO_3	Freundilich	CNTs were able to form supramolecular complexes with EPI via π–π stacking and possessed favorable loading properties as drug carriers	(Chen, Pierre, et al., 2011)
	Ciprofloxacin (CPI)	Graphitized (MG), carboxylized (MC), and hydroxylized (MH).	Freundlich and Dubinin–Ashtakhov (DA).	The π–π electron donor–acceptor interactions were the reason for higher sorption on MH than MC	(Li, Zhang, et al., 2014)
	Tetracycline (TC)	Treated by heating and trace metals by sodium hypochlorite.	Freundilich	The aqueous solution chemistry played a significant role in tetracycline adsorption on carbon nanotubes	(Ji et al., 2010)
	Sulfamethoxazole (SMX)	Graphitized (MG), carboxylized (MC), and hydroxylized (MH).	Dubinin-Ashtakhov	The π-π electron donor-acceptor interactions is responsible for high SMX adsorption at low pHs and resulting in the following adsorption sequence: MH > MG > MC	(Zhang, Pan, et al., 2010)
	Norfloxacin (NOR)	Graphitized (MG), carboxylized (MC), and hydroxylized (MH).	Freundilich	The sorption process is affected by the properties of CNTs surface; therefore the functionalized carbon nanotubes show great sorption affinity and capacity for NOR	(Wang, Yu, et al., 2010)
	Ofloxacin (OFL)	Graphitized (MG), carboxylized (MC), and hydroxylized (MH).	Freundlich	The high sorption of OFL was through several mechanisms including electrostatic interactions, cationic exchange, and hydrogen bond	(Peng, Pan, et al., 2012)

Table 2.2 (continued)

Organic Dyes	Methylene blue (MB)	Loaded with magnetite (M-CNTs)	Langmuir	The electrostatic attraction and π–π stacking interactions between (M-CNTs) and (MB) was responsible for the high adsorption capacity.	(Ai et al., 2011)
	Methyl orange (MO)	Purified with acids washing and oxidation in diluted air	Langmuir	Dyes molecules diffusion to the surface of CNTs was inhibited by the increased viscosity as the CNTs dosage was increased.	(Yao et al., 2011)
	Alizarin red S (ARS) and Morin	_____	Langmuir	The adsorption capacity of both of the dyes was increased at low pH due to the electrostatic interaction between negatively charged adsorbents surface and these charged dye cations.	(Ghaedi, Hassanzadeh , & Kokhdan, 2011)
	Reactive red M-2BE (RRM)	_____	Liu isotherm	The maximum adsorption capacities were 335.7 mg/g, and the loaded CNTs with RRM dye can be efficiently regenerated using a mixture of methanol + 4 mol L^{-1} NaOH	(Machado et al., 2011b)
	Reactive blue 4 (RB4)	_____	Liu isotherm	At high temperature, CNTs adsorption capacity increased because of enhancing the rate of intra-particle diffusion.	(Machado et al., 2012)

Table 2.2 (continued)

	C.I. Direct Yellow 86 (DY86) and C.I. Direct Red 224 (DR224)	_____	Freundlich (DY86); D–R isotherm (DR224)	The affinity between DY86 and CNTs was less than that between DR224 and CNTs; and the adsorption process was physiosorption and can be characterized as ion exchange process.	(Kuo, Wu, & Wu, 2008)
Pesticides	Diuron and dichlobenil	_____	Polanyi–Manes	The main adsorption mechanism was hydrogen bonding and the adsorption was diminished by increasing the oxygen containing groups.	(Chen, Shan, et al., 2011)
	Atrazine	_____	Polanyi–Manes	Hence the adsorption of atrazine was at external surface of CNTs and no closed interstitial spaces in CNTs aggregates were formed; reversible adsorption of atrazine was observed.	(Yan et al., 2008)
	diuron, fluridone and norflurazon	Purified by a mixed HNO_3 and H_2SO_4	Freundlich model and Dubinin Ashtakhov (DA)	The adsorption mechanism was mainly controlled by hydrogen bonding and hydrophobic interactions.	(Sun, Zhang, et al., 2012)
Phenolic compounds; benzene	1,2-dichlorobenzene (1,2 DCP)	Graphitized (MG)	Freundlich	At pH above 10, the adsorption capacity of CNT decreased because of the formation of water clusters on the oxygen groups.	(Peng et al., 2003a)
	2,4,6-trichlorophenol (TCP)	Treated with HNO_3	Polanyi–Manes	Oxidation treatment of CNTs increased the adsorption capacity for TCP due to the increased surface area and hydrophilic carboxylic groups.	(Chen, Shan, et al., 2009)
	benzene, toluene, ethylbenzene and *p*-xylene	Oxidized by sodium hypochlorite (NaOCl)	Langmuir and Freundlich	The adsorption performance was enhanced by oxidation due to the increased of purity, carboxylic groups, negative surface charge and carbon containing defects.	(Su, Lu, & Hu, 2010)

Table 2.2 (continued)

	Pentachlorophenol (PCP)	Oxidized by HNO_3, H_2O_2 and $KMnO_4$	Langmuir, and Freundlich models, Radke–Prausnitz model and Fritz–Schlünder model.	The more oxygen containing groups were introduced (carboxylic, phenolic and lactonic), the lower the adsorption of PCP to CNTs became.	(Abdel Salam & Burk, 2008)
	Naphthalene with 2,4-Dichlorophenol and 4-Chloroaniline	_____	Dubinin Ashtakhov (DA)	The adsorption of 2,4-Dichlorophenol and 4-Chloroaniline was suppressed by added naphthalene.	(Yang, Wu, et al., 2010b)
Natural organic maters (NOMs)	Fulvic acid (FA)	purified by mixed HNO_3 and H_2SO_4 solutions	Freundlich	As the pH increased the adsorption of fulvic acids was decreased due to because of increasing repulsive interaction.	(Yang & Xing, 2009)
	Humic acid (HA)	Purified by mixed HNO_3 and H_2SO_4solutions.	Langmuir	Adsorption of HA with high polarity could efficiently stabilize CNTs in water.	Lin et al. 2012)

Table 2.3. Carbon nanotube as heavy metals adsorbent

Modification	Target pollutants	Adsorption isotherm	Remarks	Ref
Oxidized with H_2O_2, $KMnO_4$ and HNO_3.	Cadmium(II)	_____	Many functional groups have been introduced to the surface of the CNTs, which are responsible for the increasing of Cadmium(II) adsorption capacities	(Li, Wang, et al., 2003)
Manganese dioxide MnO_2	Cadmium(II)	Langmuir	The mechanism of cadmium adsorption onto the MnO_2/O-CNTs may include both physical and chemical adsorptions and appeared to be influenced by external mass transfer, intraparticle diffusion, and chemical adsorption	(Luo, Wei, et al., 2013)
Iron oxide magnetic	Nickle Ni(II) and strontium Sr(II)	Langmuir	Both adsorption capacity of CNTs and iron oxides are much less that of the magnetic composites. The separation of the composites from the treated solution can be achieved by a magnetic process.	(Chen, Hu, et al., 2009)
Acidified by concentrated nitric acid	Lead Pb(II)	Langmuir	Salt or complex deposited on the surface of CNTs due to reaction between Pb (II) and the oxygenous functional groups formed on the surface of acidified CNTs and increased adsorption capacity.	(Wang, Zhou, Peng, Yu, & Chen, 2007)
Alumina	Lead Pb(II)		The coated nanotubes demonstrated better removal ability over uncoated where the removal ratio of lead increased from 20% to around 99%.	(Liu & Zhao, 2013)

Table 2.3 (continued)

$KMnO_4$ (98% concentration) and 0.4 M HNO_3 (68% concentration)	Zinc Zn(II)	Langmuir and Freundlich	The removal percentage of $Zn2^+$ was more than 99%.	(Mubarak et al., 2013)
Silver nanoparticles	Copper Cu(II) and cadmium Cd(II)	Langmuir	The adsorption process was spontaneous and exothermic.	(Venkata Ramana, Yu, & Seshaiah, 2013)
Sodium hypochlorite NaClO	Zinc Zn(II)	Langmuir	CNTs could be efficiently regenerated by a 0.1 mol/L HNO_3 solution and the sorption capacity was maintained after 10 cycles of the sorption/desorption process.	(Lu, Chiu, & Liu, 2006)
Manganese oxide MnO_2	Lead Pb(II)	_____	The mechanism of adsorption mainly controlled by a liquid film diffusion and the results showed that most of the lead could be removed from a solution at a pH between 7.0 and 9.0, and within a few min	(Salam, 2013)
Sodium hypochlorite NaClO	Nickel Ni(II)	_____	The oxidation process significantly improved the hydrophilicity of CNTs and as a result more Ni(II) was adsorbed.	(Lu & Liu, 2006)
Manganese oxide (MnO_2)	Lead Pb(II)	Langmuir	After the loading of MnO_2, smaller pore width (2.6 nm) and larger surface area (275m2/g) were observed.	(Wang, Gong, et al., 2007)
Amino modified (ethylenediamine, diethylenetriamine and triethylenetetramine)	Lead Pb(II) and Cadmium Cd(II)	Langmuir	The surface basicity of treated CNTS was increased offering numerous adsorption sites and thus enhancing the adsorption capacity. The adsorption affinity of the heavy metals to CNTs followed the sequence $Pb^{2+} > Cd^{2+}$.	(Vuković et al., 2011)

Table 2.3 (continued)

8-hydroxyquinoline C_9H_7NO	Copper Cu(II), lead Pb(II), cadmium Cd(II) and zinc Zn(II)		The competition between the target heavy metals was in the order of Cu (II) > Pb(II)≈ Zn(II) > Cd(II) for % adsorption.	(Kosa, Al-Zhrani, & Abdel Salam, 2012)
Oxidation (O-CNT)	Anionic chromate (CrO_4^{-2})		Excellent adsorption was attributed to interaction of the CrO_4^{-2} with the surface oxygen-containing functional groups on the modified CNTs.	(Xu et al., 2011)
Ethylenediamine	Cadmium (Cd^{+2})	Langmuir	The mechanism of which may include both of physisorption and chemisorption mechanisms	(Vuković, Marinković, et al., 2010)
Nitric acid HNO_3	Lead Pb(II)	_____	The main adsorption mechanism was Chemisorption and/or chemical complexation	(Xu et al., 2008)
nitric acid (HNO_3)	Lead Pb(II)	_____	The maximum adsorption capacity of 6-h-acidified CNTs for Pb(II) is 91 mg/g, which is more than 10 times greater than that of untreated CNTs for Pb(II) (7.2 mg/g).	(Wang, Zhou, Peng, Yu, & Yang, 2007)
Poly(vinylpyridine) and ferroferric oxide	divalent metal ion (M^{2+}) (such as Zn^{2+}, Cu^{2+} and Pb^{2+})	_____	Formation of insoluble bundles in which the divalent metals remain trapped through pyridyl–M^{2+}–pyridyl interactions. Adsorbate loaded CNTs can be separated using magnetic filtration and recycled by acid treatment	(Maggini et al., 2013)

Table 2.3 (continued)

Ammonium iron(II) sulfate and Ammonium iron(III) sulfate	copper Cu (II)	Langmuir	The main adsorption mechanism of Cu (II) was by physical force while the chemisorption played a small role due to a few oxygen-containing functional groups on CNTS.	(Tang et al., 2012)
Nanoscale zero-valent iron (nZVI)	Chromium Cr(VI)	_____	The adsorption process, stimulated by electrostatic, hydrophobic and hydrogen-bond interactions, depends strongly on pH value.	(Lv et al., 2011)
Diamine modified mesoporous silica	Copper Cu(II), lead Pb(II), zinc Zn(II) And nickel Ni(II)	Langmuir	The order of removal percentage for metal ions is Pb(II) > Cu(II) > Zn(II) > Ni(II).	(Yang, Ding, et al., 2013)
Chitosan (polysaccharide biopolymer)	copper, zinc, cadmium, and nickel ions	_____	The order of metal ion removal from aqueous solution was Cu(II) > Cd(II)≈Zn(II) > Ni(II) due to the competition for the binding sites at the surface of CNTs/CS nanocomposite	(Salam, Makki, & Abdelaal, 2011)
Mercapto-propyl triethoxysilane, Thiol-functionalized (MPTS-CNTs/Fe_3O_4)	Mercury (Hg^{2+}) and lead (Pb^{2+})	Langmuir	The maximum adsorption capacities for Hg^{2+} is 65.52 and for Pb^{2+} is 65.40 mg/g.	(Zhang, Sui, et al., 2012)

2.2.2 Photocatalysis

The main problems that are affecting the water treatment competence are removing of non-biodegradable organic pollutants which are resistant to conventional treatment methods, as well as killing waterborne pathogens without the formation of harmful disinfectants by products (DBPs) from disinfection process. Addressing these problems calls for an imperative need to develop an innovative, low- cost and eco-friendly technology that can destroy these pollutants with less energy consumption and less chemical utilization. Therefore, research activities have focused on advanced oxidation processes (AOPs) as alternative robust methods that are capable of oxidizing and mineralizing wide range of organic chemicals due to their highly potent and strongly oxidizing radicals (Gaya & Abdullah, 2008a).

Photocatalysis, is a well-known AOP, has been established as an efficient method to enhance the biodegradability of persistent organic contaminants and to remove the current and emerging microbial pathogens. Photocatalytic oxidation comprises a class of reactions which use a catalyst activated by solar, chemical or other forms of energy (Augugliaro et al., 2006) and relies on generation of strong reactive radical species such as H_2O_2, $O_2^{\bullet-}$, O_3 (Pera-Titus et al., 2004) and mostly hydroxyl radical ($OH^{\bullet}$) (Huang et al., 2000), which is a strong oxidizing agent that non-selectively destroy all organic molecules in water (Wang & Xu, 2012).

The main source for the generation of ($OH^{\bullet}$) is the conventional oxidants H_2O_2 and O_3 (Karci, 2014). Different methods have been reported to photolysis these oxidants, facilitating compliance with the specific treatment requirements and improve the versatility of AOPs (Malato et al., 2009). Methods based on UV (Goi & Trapido, 2002) and combination of UV light and oxidants (H_2O_2, $O_2^{\bullet-}$, O_3 etc.)(Karci, 2014; Malato et al., 2009). In addition to that methods that involve catalysts, such as homogeneous photocatalysis method which is based on the addition of H_2O_2 to dissolved iron salts and

can be classified into two types of reaction: Fenton reaction, that does not involve any light irradiation and photo-Fenton reaction that reacts up to a light wavelength of 600 nm (Chong et al., 2010). Moreover, heterogeneous photocatalysis methods that uses a wide-band gap semiconductors in contact with water (e.g., titanium dioxide (TiO_2) (Wang & Jing, 2014) , tungsten trioxide (WO_3) (Liu, Han, et al., 2013), zinc oxide (ZnO) (Kaur & Singhal, 2014), tin dioxide (SnO_2) (Al-Hamdi, Sillanpää, & Dutta, 2015) cadmium sulfide (CdS)(Chronopoulos et al., 2014), etc.) and they are photoexcited by light in the presence of oxygen (Malato et al., 2013). Table 2.4 shows different methods that are used to produce hydroxyl radicals**.**

Both homogeneous (photo-Fenton) and heterogeneous photocatalysis methods are considered of great interests because they can either use UV light (Pera-Titus et al., 2004) or solar light (Malato et al., 2013) for irradiation. Although photo-Fenton photocatalysis has higher reactivity than heterogeneous photocatalysis but its operation is complex and expensive due to pH rectification that is required to control the formation of photoactive iron complexes (De Laat, Le, & Legube, 2004). Accordingly, heterogeneous photocatalysis proved to be a promising water treatment technology for elimination of persistent organic pollutants as well as for water sterilization.

Among the above mentioned semiconductors, titanium dioxide (TiO_2) has drawn a special attention in the water treatment research including photo-degradation of numerous organic pollutants, photo-reduction of inorganic contaminants and inactivation of microorganisms.(Kurniawan TA, 2011), due to its environmentally benign merits such as low toxicity, high photoconductivity, chemical stability as well as its low cost and commercial availability (Choi et al., 2014; Xiao, Xie, & Cao, 2015). The photocatalysis mechanism of (TiO_2) relies on the formation of active oxygen species such as hydroxyl radicals, superoxide, hydrogen peroxide, singlet oxygen, etc., may participate in organic pollutants photo-degradation or disinfection process (Fujishima, Zhang, & Tryk, 2008).

The mechanism consists of several steps (Berger et al., 2006; Chong MN, 2010; Fujishima, Zhang, & Tryk, 2008; Gaya & Abdullah, 2008a; Mayer, Daugherty, & Abbaszadegan, 2014) starting with Photoexcitation to induce series of reductive and oxidative reaction on the surface of (TiO_2) photocatalyst through irradiation by an adequate wavelength (usually with photon energy (*hv*) greater than or equal to the band gap energy). Since the band gap of (TiO_2) is about 3.0 eV, wavelengths shorter than ~400 nm can excite the lone electron from the valance band to the empty conduction band in femtoseconds resulting in the generation of electron-hole pair. Super oxide radical anions ($^{\bullet}O_2^-$) and hydroxyl radicals ($OH^{\bullet}$) are then generated through reaction between (photogenerated electrons and molecular oxygen) and between (photogenerated holes and water) respectively. Hydroxyl radicals are considered the major species responsible for decomposition of organic pollutants (Zhang, Qiu, et al., 2009) into water and carbon dioxide. Figure 2.4 represents the mechanism steps of TiO_2 photocatalysis.

However, several disadvantages of nanocrystalline TiO_2 powders in water system have been identified, such as agglomeration, difficult recovery and short activity which could restrain its application in wastewater treatment (Baolong et al., 2003). For the purpose of overcoming the mentioned drawbacks and developing highly active catalyst to be exploited for large scale applications, the morphological, crystallographic, and electronic properties of TiO_2 material should be controlled through alternative synthesis procedures (Choi et al., 2010). The most common investigated methods to prepare TiO_2 are sol-gel method (Caratto et al., 2012),which is used to fabricate highly pure with a relatively low temperature nanosized titanium dioxide , and hydrothermal method (Jing et al., 2011), that works in synthesizing high crystalline titanium dioxide with controlled size and shape. Thereupon, three main approaches that are aimed to modify titanium dioxide (Xiao, Xie, & Cao, 2015) have been highlighted in Table 2.5. Development of TiO_2 composites codoped with two or more of nonmetals such as, S, N,F and C (Banerjee et

al., 2014; Fagan et al., 2016; Likodimos et al., 2013) is considered one of the promising strategies that have been suggested to reduce the band gap and improve the visible light (VIS) responsive photocatalytic activity. For instance, N-F codoped TiO_2 under VIS has successfully been used for photocatalytic degradation of bisphenol-A- (BPA) due to its high surface area to volume ratio, enrichment of surface oxygen vacancies by F- and N-doping, improved surface acidity by F-doping as well as enhancement of VIS absorption by N-doping (He et al., 2016). Moreover, carbon doped TiO_2 composites under VIS has been used for the degradation of some occurring algal toxins in water (e.g cyanotoxins, microcystin-LR (MC-LR) and cylindrospermopsin (CYN)) and the resulted intermediate products from the toxins degradation process were attributed to a Peroxide that was formed through the action of $O_2^{\bullet-}$ (Fotiou et al., 2016). In short, photocatalytic process of nonmetal doped TiO_2 has shown large potential as a renewable water treatment process and it is considered a more eco-friendly approach comparing to the photocatalytic process of metal-doped TiO_2, for the latter is vulnerable to photocorrosion and potential metal problems (Zhang et al., 2014).

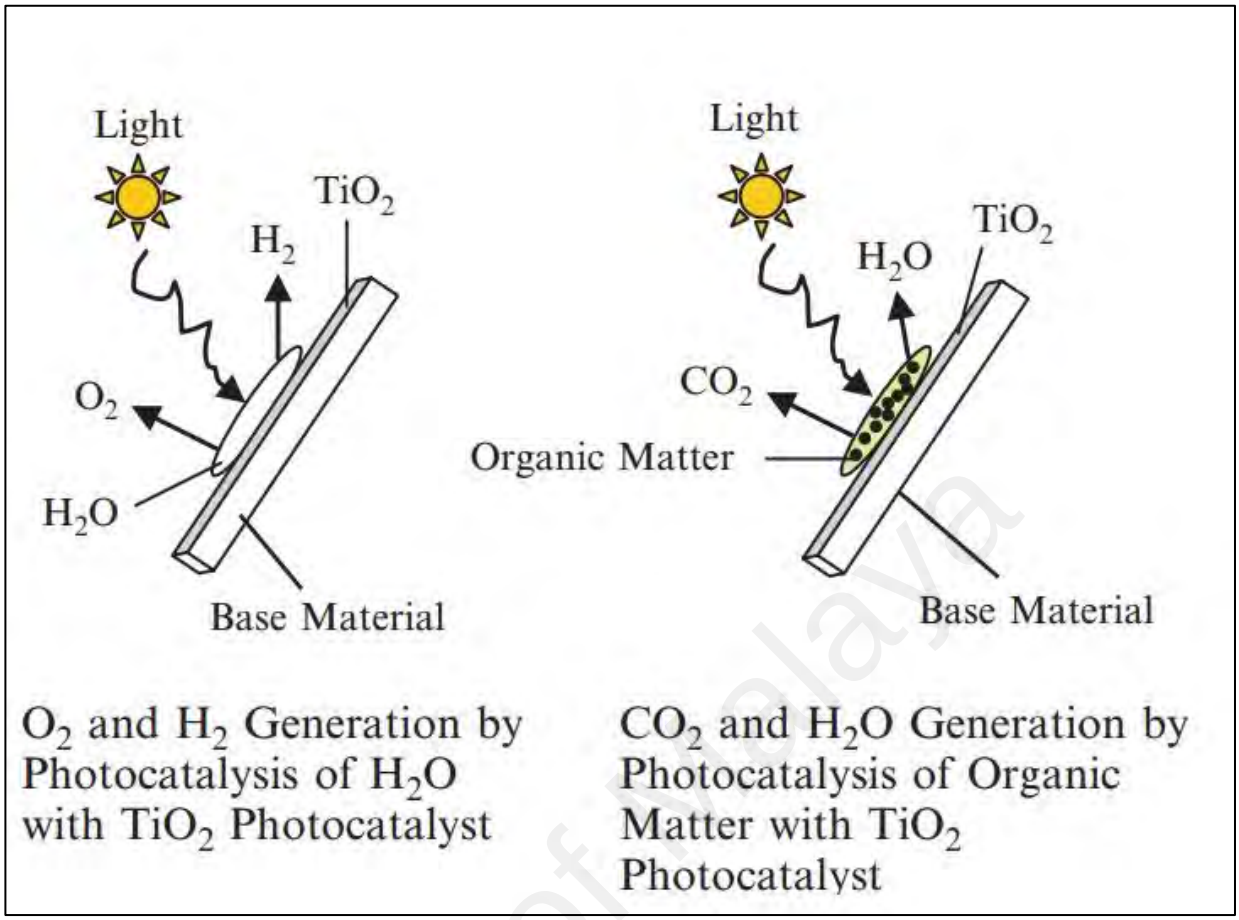

Figure 2.4: Light Absorption by TiO_2 Photocatalyst (Ohama & Van Gemert, 2011).

Table 2.4: AOPs Using Radiation for the Generation of Hydroxyl Radicals (Malato et al., 2013).

AOP	Key Reaction	Wavelength
UV/H_2O_2	$H_2O_2(aq) + h\nu \rightarrow 2HO^{\bullet}$	$\lambda < 300$ nm
UV/O_3	$O_3(aq) + h\nu \rightarrow O_2(aq) + O(^1D)O(^1D) + H_2O \rightarrow 2HO^{\bullet}$	$\lambda < 310$ nm
UV/H_2O_2/O_3	$O_3(aq) + H_2O_2 + h\nu \rightarrow O_2(aq) + HO^{\bullet} + HO^{\bullet}{}_2$	$\lambda < 310$ nm
	$TiO_2(s)+h\nu \rightarrow TiO_2(e^- + h^+)$	
UV/TiO_2	$TiO_2(h^+)+HO^-_{ad} \rightarrow TiO_2(s)+HO^{\bullet}_{ad}$	
Fenton	$Fe^{2+}(aq) + H_2O_2(aq) \rightarrow Fe^{3+}(aq) + HO^{\bullet} + HO^-$	$\lambda < 390$ nm
Photo-Fenton	$Fe^{3+}(aq) + H_2O + h\nu \rightarrow Fe^{2+}(aq) + H^+ + HO^{\bullet}$	$\lambda < 580$ nm

Table 2.5: Common strategies to modify titanium dioxide (TiO_2).

Approach	Remark	Examples	REF
Control the size and morphology of titanium dioxide (TiO_2)	Increase the exposed photo reactive sites.	TiO_2 quantum dots (QDs)	(Pan et al., 2014)
		TiO_2 nanotubes	(Xing et al., 2014)
		TiO_2 nanosheets	(Pan et al., 2013)
		TiO_2 nanowires	(Pu et al., 2014)
		TiO_2 mesoporous hollow shells	(Joo et al., 2013; Moon et al., 2014)
Doping (TiO_2) with metal or non-metals/ compounding (TiO_2) with charge transfer materials	Improve charge separation or boarding the absorption spectrum	Metal-doped TiO_2	(Suri, Thornton, & Muruganandham, 2012; Wang & Jing, 2014)
		Non-metal- doped TiO_2	(Dong, Zhao, & Wu, 2008; Lin, Tseng, & Chu, 2014; Sathish, Viswanath, & Gopinath, 2009)
		Deposited TiO_2 (e.g TiO_2-carbon nanotubes and TiO_2 – grapheme composites)	(Saleh & Gupta, 2012; Wang, Serp, et al., 2008; Yang, Liu, et al., 2013)
mixed-phase samples of Anatase and Rutile TiO_2	Enhance the quantum yield and photocatlytic reactivity	Build Anatase–Rutile (A–R) phase junction of TiO_2	(Liu et al., 2014; Scanlon et al., 2013)

2.2.3 Membrane processes

Membrane process has proven to be an effective way for water remediation because of its high separation efficiency, easy operation where no chemical addition or thermal input is required, and it does not lead to secondary pollution as well as no regeneration of spent media is required. (Balamurugan, Sundarrajan, & Ramakrishna, 2011; Buonomenna, 2013). The performance of the membrane system basically influenced by the membrane material, which afford an inherent trade-off between membrane selectivity and permeability. The common membrane materials applied for water treatment are polymers, for instance cellulose acetate (CA), polyacrylonitrile (PAN), polyamide (PA)(Yang, Lin, & Huang, 2009). Based on the pore size and filtration application the

membrane process can be classified as microfiltration (MF) for suspended solids, protozoa, and bacteria removal, ultrafiltration (UF) for virus and colloid removal, nanofiltration (NF) for hardness, heavy metals, and dissolved organic matter removal, and for desalination, water reuse, and ultrapure water production (reverse osmosis (RO), and forward osmosis (FO)) (Balamurugan, Sundarrajan, & Ramakrishna, 2011; Bernardo, Drioli, & Golemme, 2009).

Over the past decade nanotechnology have led to new water treatment membranes by incorporation of nanomaterials into membranes either by blending or surface grafting for producing membranes with desirable structure and new functionality such as high permeability, catalytic reactivity, contaminant degradation and self-cleaning (Pendergast & Hoek, 2011), moreover, controlling membrane fouling due to nanoparticles functional groups and their hydrophilic properties(Vatanpour et al., 2012).

2.2.3.1 Nanofibrous membranes

Polymer or composite nanofibrous membranes can be generated using electrospinning method which is versatile and efficient technique to compose ultra-fine fibers using various materials (e.g., polymers, ceramics, or even metals) with diameters in the range of 20–2000 nm (Cloete, 2010; Li et al., 2013; Yang, Lin, & Huang, 2009). Electrospun nanofibrous membranes have large specific surface area (Balamurugan, Sundarrajan, & Ramakrishna, 2011), fine tunable pore size (Ramakrishna et al., 2006), as well as high water flux that attracted both industry and academic researchers to study their application for microfiltration (MF) and ultrafiltration (UF) (Gopal et al., 2007; Gopal et al., 2006). The researches revealed that nanofiber membranes can sufficiently remove micron size particles from aqueous solutions at high rejection rate and without a significant fouling therefore the membrane could be successfully recovered upon cleaning (Ramakrishna et al., 2006).

The electro-spun nanofibers can be simply manipulated for particular application and used as affinity membrane to remove heavy metals and organic pollutants during filtration by the introduction of certain functional groups (Li et al., 2013; Qu, Alvarez, & Li, 2013). The nanofibers are functionalized by covalently attaching ligands onto the surface, for example, using cibacron blue to functionalize cellulose nanofiber membranes for albumin purification (Ma, Kotaki, & Ramakrishna, 2005), functionalization of polymer nanofibers membranes with a ceramic nanomaterials such as hydrated alumina/alumina hydroxide and iron oxide for removal of heavy metals ions by adsorption/chemisorption and electrostatic attraction mechanisms (Ramakrishna et al., 2006) and introducing of cyclodextrin into a poly(methyl methacrylate) nanofiber membrane to enhance their affinity for organic waste removal (KAUR et al., 2006).

2.2.3.2 Nanocomposite membranes

Although the membrane separation technology plays a remarkable role in water and wastewater treatment, membrane fouling is still the main shortcoming that reduces the lifetime of the membrane and limits its application due to the increasing of energy consumption, operating costs and difficulty of process operation (Balta et al., 2012). The membrane fouling can be classified into organic fouling and biological fouling and both are responsible for the flux decline in the membrane processes (Meng et al., 2009). The main reason of membrane organic fouling is the abundance of natural organic matters (NOM) in water that are adsorbed and deposited on the surface of the membrane lead to the blockage of the pores forming a cake layer on the surface (Meng et al., 2009). Next, the leading causes of the biological fouling is the adhesion of bacteria to the membrane surface producing a sticky biofilm composed of polysaccharide, organic chemicals and a complex community of microbial cells resulting in biofouling which is considered a serious problem due to the ability of bacteria to reproduce at the surface of the membrane, forming biofilms and producing an additional fouling which is difficult to be removed

(Bjørkøy & Fiksdal, 2009; Ciston, Lueptow, & Gray, 2009; Herzberg & Elimelech, 2007; Sawada et al., 2012). With regards to the causes of both organic and biological membrane fouling and their severe consequences, it is important to improve the antifouling and antibacterial properties of the membranes.

The fouling of the membranes is affected by their morphology, charge as well as the hydrophobicity of the membranes (Gray et al., 2008; Sun et al., 2009). Many studies have proven that the membrane shows stronger resistance to substances adsorption when increasing its surface hydrophilicity, therefore modifying the membrane hydrophobicity can be an effective technique to improve its organic antifouling (Arahman et al., 2009; Rahimpour & Madaeni, 2007).

Many efforts have been devoted to study number of modification methods in order to improve the hydrophilicity and reduce membrane fouling, involving coating (Razmjou et al., 2011), grafting (Rahimpour, 2011) and blending with hydrophilic metal oxide nanoparticles which is proved to be an effective method to obtain nanocomposite membranes without complicated operation process (Yu et al., 2013). The blending of metal oxide nanoparticles including alumina.(Maximous et al., 2010), zirconium dioxide (Pang et al., 2014), Silica (Jin et al., 2012; Yu et al., 2013), zeolites (Pendergast et al., 2010) and titanium dioxide (Razmjou, Mansouri, & Chen, 2011; Razmjou et al., 2012). It was highlighted that the addition of metal oxides nanoparticles does not affect the membrane structure while it obviously enhances the performance of the membrane (Shen et al., 2011) as well as its thermal stability (Pendergast et al., 2010). Additionally, functionalized multi wall carbon nanotubes (CNTs) was successfully blended with polymer membranes. The membrane, permeability, hydrophilicity and fouling resistance were significantly improved by the functional groups on CNTs which embedded in membrane nanocomposite (Choi, Jegal, & Kim, 2006; Daraei et al., 2013).

Another prerequisite argument is preventing the development of biofilms on membrane surface; thus many antimicrobial nanoparticles have been studied to endow the membrane with a self-antimicrobial property. For example, silver nanoparticles (Nano-Ag) have been exploited to inactivate viruses(De Gusseme et al., 2011), mitigate the bacterial growth and inhibit biofilms formation (Mauter et al., 2011; Zodrow et al., 2009) not only by being coated or grafted on the surface of the membranes but also by being blended in the membrane fabrication process (Zodrow et al., 2009). Ag-nanocomposite membranes showed a significant antibacterial property towards Escherichia coli (E. coli) (Zodrow et al., 2009) (Obalová et al., 2013), with antibacterial efficiency about 99.999% (Sawada et al., 2012). Another nanomaterial integrated into membranes as antimicrobial agent is single wall carbon nanotubes (SWCNTs). The antibacterial activity of SWCNTs-nanocomposites was investigated and the results exposed that high bacterial inactivation (>90%) was attained by the SWCNTs-nanocomposites reducing the growth of biofilms on the surface of the membranes (Ahmed et al., 2011).

It is important to point out that photo-catalytic nanoparticles, namely titanium dioxide (TiO_2) which has drawn a significant attention due to its stability and promising applications as photocatalysis (Cao et al., 2006) , have been used to develop photocatalytic nanocomposites membranes (reactive membranes) with higher hydrophilicity(Li, Fang, et al., 2014), improved fouling resistance and thermal stability (Wu et al., 2008) coupled with their ability to combine their function of physical separation and the reactivity of a catalyst toward pollutants degradation (Bae & Tak, 2005; Choi, Stathatos, & Dionysiou, 2006). In addition to that, metallic/bi-metallic nanoparticles precisely nano zero-valent iron (nZVI) which serves as electron donor and catalyst (Qu, Alvarez, & Li, 2013; Wang, Yang, et al., 2013), have also been integrated into membranes for reductive dechlorination of contaminants mainly chlorinated organic

compounds (COCs) (Wu & Ritchie, 2008; Wu, Shamsuzzoha, & Ritchie, 2005). Finally, although nanoparticles are very effective for environmental remediation and enhancement of the performance of membrane process, they tend to leach out and aggregate especially if they were grafted on the membrane without surface protection and that might complicate the operation and decrease the contaminants degradation. Consequently, many studies have investigated the possibilities to employ a mediation (Li, Fang, et al., 2014) or solid supports (Wang, Chen, et al., 2008) for immobilization of the nanoparticles in order to overcome the aforementioned shortcomings.

2.2.3.3 Osmatic membranes

Both reverse osmosis (RO) and forward osmosis (FO) exploit semi permeable membrane for water purification and desalination processes and their performances are defined by their salt rejection, energy consumption not to mention their antifouling property. Reverse osmosis membranes (RO) are easy to be designed and operated as well as they can produce high quality clean water (Greenlee et al., 2009; Tarboush et al., 2008) by employing a high hydraulic pressure to force the water through the semi permeable membrane (Liu et al., 2011). RO membranes with an active layer on the top are called thin film composite (TFC) (Fathizadeh, Aroujalian, & Raisi, 2011). The standard material for this active layer is polyamide (Tiraferri, Vecitis, & Elimelech, 2011) and it employs the diffusion mechanism to separate the water from the pollutants (Paul, 2004).

The primary disadvantages of RO membranes are high energy consumption (Liu et al., 2011), irreversible membrane fouling (Chung et al., 2012) in addition to that, the polyamide tends to degrade in the presence of the chemical oxidants that are used for mitigation of the microbial growth (Tiraferri, Vecitis, & Elimelech, 2011). Consequently, many attempts have been proposed utilizing nanoparticles to functionalize the active layer to improve TFC membranes application. Modification methods include incorporation of nanomaterial into the active layer of TFC (Lee, Arnot, & Mattia, 2011) to evolve new

polyamide-NPs membranes which are called thin film nanocomposite (TFN) membranes with increased fouling resistance, higher permeability and improved salt rejection (Fathizadeh, Aroujalian, & Raisi, 2011). Figure 2.5 Shows the difference between TFC and TFN. The most prominent nanoparticles being researched for integration into the active layer are nano-zeolites that proved to maintain the solute rejection and resulted in thicker, more permeable and hydrophilic negatively charged active layer (Jeong et al., 2007; Lind et al., 2009). Also, titanium dioxide (TiO_2) which increased the water flux and led to organic degradation and microbial inactivation upon ultra-violet (UV) irradiation due to its photocatalytic attributes (Chin, Chiang, & Fane, 2006). Finally, silver nanoparticle-TFN membranes exhibited an obvious antibiofouling influence on Pseudomonas (Lee et al., 2007), while unaligned single wall carbon nanotube (SWCNTs) were covalently bound to the TFC membrane surface and inactivated 60 % of E. Coli bacteria attached to the membrane within 1 hour of contact time resulting in moderate biological antifouling membrane (Tiraferri, Vecitis, & Elimelech, 2011).

Comparing to conventional reverse osmosis (RO) membrane, forward osmosis (FO) membrane is considered less prone to fouling (Ge et al., 2010; Holloway et al., 2007; Niksefat, Jahanshahi, & Rahimpour, 2014) and does not consume energy (Cornelissen et al., 2008) for it is exploiting the osmotic pressure gradient as the driving force for the separation process and draws water from a low osmotic pressure solution, referred to as "feed" to a high osmotic pressure one, often referred to as "draw solute" (Buonomenna, 2013; Liu et al., 2011). However the product of FO membranes (the diluted draw solution) usually requires a second separation step (Chung et al., 2012) to generate pure water either by applying RO or thermal treatment and both are high cost, intensive energy operations. To address this challenge, it is recommended to have a high osmolality draw solution that can be separated easily from water (Ge et al., 2010) as well as applying a low cost separation technology. Recently, nanoparticles have been discovered as a new

draw solution and used to develop a novel draw solution recovery system. For instance, hydrophilic coated magnetic nanoparticles have been explored as new, easily separable and reusable draw solution with high osmotic pressure that improved FO membrane performance (Ge et al., 2010). Moreover, magnetic nanoparticles have been applied to recover draw solutes without any intensive energy input where their negatively charged surface facilitated the recovery process through coagulation (Liu et al., 2011).

In the light of FO process disadvantages, it is important to mention that the main obstacle of FO application is the accumulation of the rejected feed solutes in the support layer resulting in what is known as internal concentration polarization (ICP) (Tang et al., 2010). This phenomenon causes an intense loss in the osmotic driving force (McCutcheon & Elimelech, 2008) and since it occurs in the support layer, it cannot be removed by increasing the flow rate turbulence (Zhao et al., 2012). With the intention to minimize the ICP problem, it was suggested that the fabrication of appropriate FO membranes with small structure parameter for the support layer had improved the membrane behavior (Liu et al., 2011). In recent times, developments of nanotechnology have led to fabrication of novel groups of FO membranes inspired by the thin film nanocomposite reverse osmosis (TFN-RO) membranes. The nanostructured FO membranes, synthesized with metal oxides nanoparticles or carbon nanotubes, demonstrated considerably enhanced membrane properties like selectivity, permeability and stability in different separation processes (Amini, Jahanshahi, & Rahimpour, 2013). After all, nanotechnology have contributed in eco-sustainable membrane processes for wastewater treatment, producing pure drinking water without any wastes.

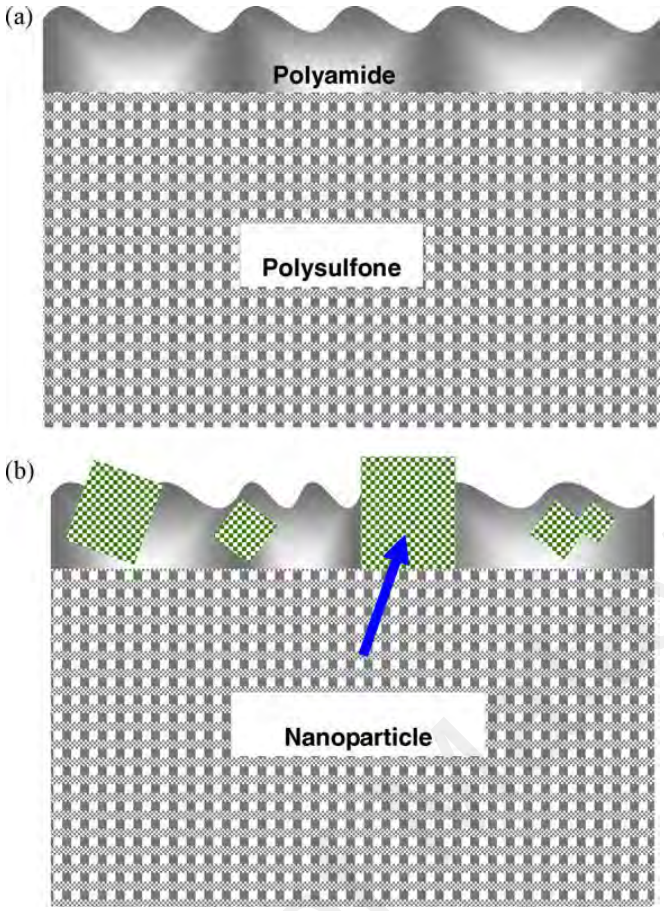

Figure 2.5: Conceptual illustration of (a) TFC and (b) TFN membrane structures (Jeong et al., 2007).

2.2.4 Disinfection and pathogens control

Disinfection process is applied to inactivate various types of microbial pathogens including viruses, bacteria, protozoa and other microorganisms that often found in water from sewage discharges or runoff from animal feedlots into the water bodies. Although the current conventional disinfectants such as chlorine, chloramines, ozone, chlorine dioxide and chlorine gas (Savage & Diallo, 2005) can effectively control the microbial growth, they have short-lived reactivity and can be problematic due to formation of toxic disinfection byproducts (DBPs) (Li, Mahendra, et al., 2008). These DBPs are formed by the reaction between the aforesaid conventional oxidizing disinfectants with various constituents (e.g natural organic matters (NOMs)) in water (Hossain et al., 2014). More than 600 DBPs have been acknowledged all over the world (Richardson et al., 2007) and

most of which are considered carcinogenic. This dilemma is aggravated when high dosages of the oxidizing disinfectant are required to kill highly resistant pathogens such as *Cryptosporidium* and *Giardia* (Li, Mahendra, et al., 2008). These limitations provoke an urgent need to balance the risks of microbial pathogens and formation of toxic DBPs. Therefore it is important to provide an innovative alternative technique that can effectively prevent DBPs formation and improve the reliability of disinfection by using harmless, non-corrosive, water soluble disinfectants (Rutala, Weber, & Control, 2008).

The rapid development of nanotechnology has encouraged a significant concern in studying the antimicrobial characteristics of several nanomaterials (NMs) and applying them for water disinfection processes. These NMs have shown a promising approach to be utilized as alternatives for conventional disinfectants (Li, Mahendra, et al., 2008) as well as to be associated with other existing technologies to enhance the disinfection efficacy such as photo-excitation due to the ability of the NMs to be excited under solar light illumination (Hossain et al., 2014). Accordingly many nanoparticles (NPs) have suggested to control the microbial growth and inactivate different types of microorganisms in water, such as metal and metal oxides nanoparticles (Dizaj, Lotfipour, et al., 2014; Vargas-Reus et al., 2012) (e.g titanium dioxide (TiO_2) (Mayer, Daugherty, & Abbaszadegan, 2014), magnesium oxide (MgO) (Jin & He, 2011), zinc oxide (ZnO) (Gordon et al., 2011), nanosilver (nAg) (Kaegi et al., 2011), nano zero valent iron (nZVI) (Crane & Scott, 2012)) and carbon nanotubes (Ahmed et al., 2013), chitosan (Kong et al., 2010) and fullerene NPs (nC_{60}) (Aquino et al., 2010; Dizaj, Mennati, et al., 2014).

The above-mentioned nanoparticles have shown good antimicrobial properties without strong oxidation, employing diverse mechanisms to disinfect water. Several antimicrobial mechanisms have been proposed for various nanoscale metal oxides, for instance, it was confirmed that the surface of zero valent iron nanoparticles (ZVIn) corrode and create more metal oxides that could inactivate waterborne viruses by carrying

out two critical mechanisms: irreversible adsorption and inactivation of viruses by direct contact (You et al., 2005). Another example on naoscale metal oxides is zinc oxides (ZnO) that demonstrated as a strong antibacterial on different types of bacteria (Adams, Lyon, & Alvarez, 2006; Aruoja et al., 2009). The main antibacterial mechanism of ZnO is the photoctlytic generation of hydrogen peroxide H_2O_2 from ZnO surface (Sawai & Yoshikawa, 2004; Yamamoto, 2001) followed by cell envelop penetration and accumulation of ZnO nanoparticles in membranes and cytoplasm of bacteria leading to bactericidal cells damage and inactivation or inhabitation of bacterial growth (Huang, Zheng, et al., 2008; Jones et al., 2008). Additionally, it was verified that due to the photoreactivity and visible light response of titanium dioxide (TiO_2), it can inactivate microorganisms under UV/ solar irradiation by generating hydroxyl radical ($OH^{\bullet}$), superoxide radical ($O^{2\bullet-}$) and hydrogen peroxide H_2O_2 as reactive oxygen species (ROS) (Li, Mahendra, et al., 2008). Besides, it was concluded that the photocatalytic inactivation of bacteria (Page et al., 2007; Pratap Reddy, Venugopal, & Subrahmanyam, 2007) and viruses (Kim et al., 2006) was improved by doping TiO_2 with silver, thus (Ag/TiO_2) shows a great potential as a photocatalytic material. By the same token, the antimicrobial mechanism of the widely used silver nanoparticles stems from the release of silver ions (Ag+) which accounts for the biological response even at low concentration (Xiu et al., 2012) . Silver ions inactivate the respiratory enzymes of bacteria by binding to thiol group in proteins (Liau et al., 1997) and result in production of reactive oxygen species (ROS). In addition to that Ag+ interacts with DNA preventing its replication and forming structural changes in the cell envelope (Qu, Alvarez, & Li, 2013).

On the other hand, the cytotoxicity of Carbon based nanomaterials (CBNs) (e.g, CNTs, fullerene etc) to bacteria in aqueous solution is a complex function of solution chemistry, transport behavior and physiochemical properties of the nanomaterials (Kang, Mauter, & Elimelech, 2009). The antibacterial activity of CNTs starts with an initial contact between

the bacteria and CNTs followed either by physical perturbation of cell membrane or by disruption of particular microbial process through oxidizing of vital cellular structure/component (Vecitis et al., 2010) and both cases lead to bacterial cells death. One of the main factor governing the antibacterial activity of CNTs is their size (diameter) (Liu et al., 2009). Therefore, the small diameter, short length SWCNTs with surface groups of -OH and -COOH demonstrating the strongest antibacterial activity (Arias & Yang, 2009; Yang, Mamouni, et al., 2010). Figure 2.6 shows the antibacterial effects of SWCNTs on E-Coli bacteria. Another illustration for CNMs antibacterial mechanism is fullerene NPs (nC_{60}) mechanism to kill bacteria which is mostly assigned to its ability to produce reactive oxygen species (ROS) resulting in various types of cell damage including DNA damage, lipid peroxidation, protein oxidation as well as interruption of cellular respiration (Fang et al., 2007; Lyon & Alvarez, 2008). Fullerene mechanism requires a direct contact between the nanoparticles and bacteria cells which makes it different from previously reported mechanisms of nanomaterial the involve ROS generation (metal oxides) or releasing of toxic elements (silver nanoparticles). Finally, Chitosan, derived from shells of shrimp and other sea crustaceans (Shahidi & Synowiecki, 1991), at its nanoscale has long been noted for its antimicrobial activity. The main proposed antimicrobial mechanism for chitosan is that the positively charged chitosan particles interact with negatively charged bacteria increasing the permeability of cell membranes and eventually leak the cell substances (Holappa et al., 2006; Qi et al., 2004). In short, nanomaterial had proven to be good disinfecting agents for water treatment systems by employing diverse antibacterial mechanisms (Figure 2.7) as well as they successfully overcome the limitations that hindered the viability of conventional disinfection (Mahendra et al., 2014).

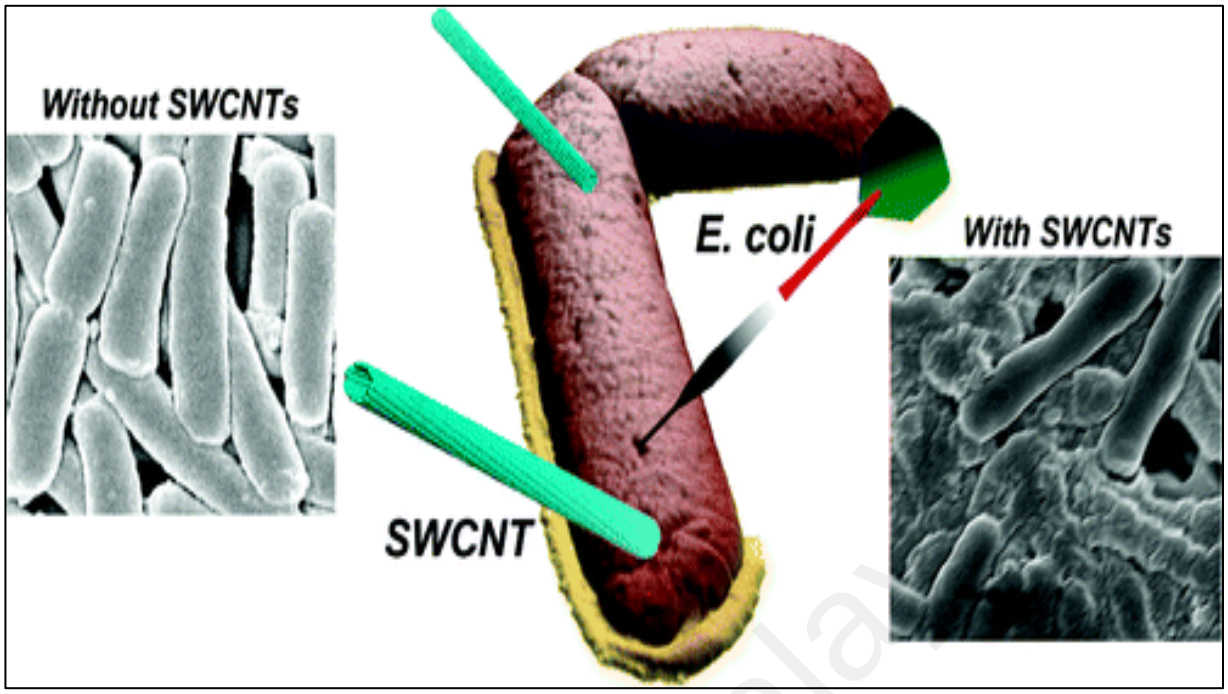

Figure 2.6: SEM images of *E. coli* after incubation with saline solution for 2 h without SWCNTs and after incubation with SWCNTs dispersed in the Tween-20 saline solution (0.1 wt % Tween-20 and 0.9 wt % NaCl) for 2 h (Liu et al., 2009).

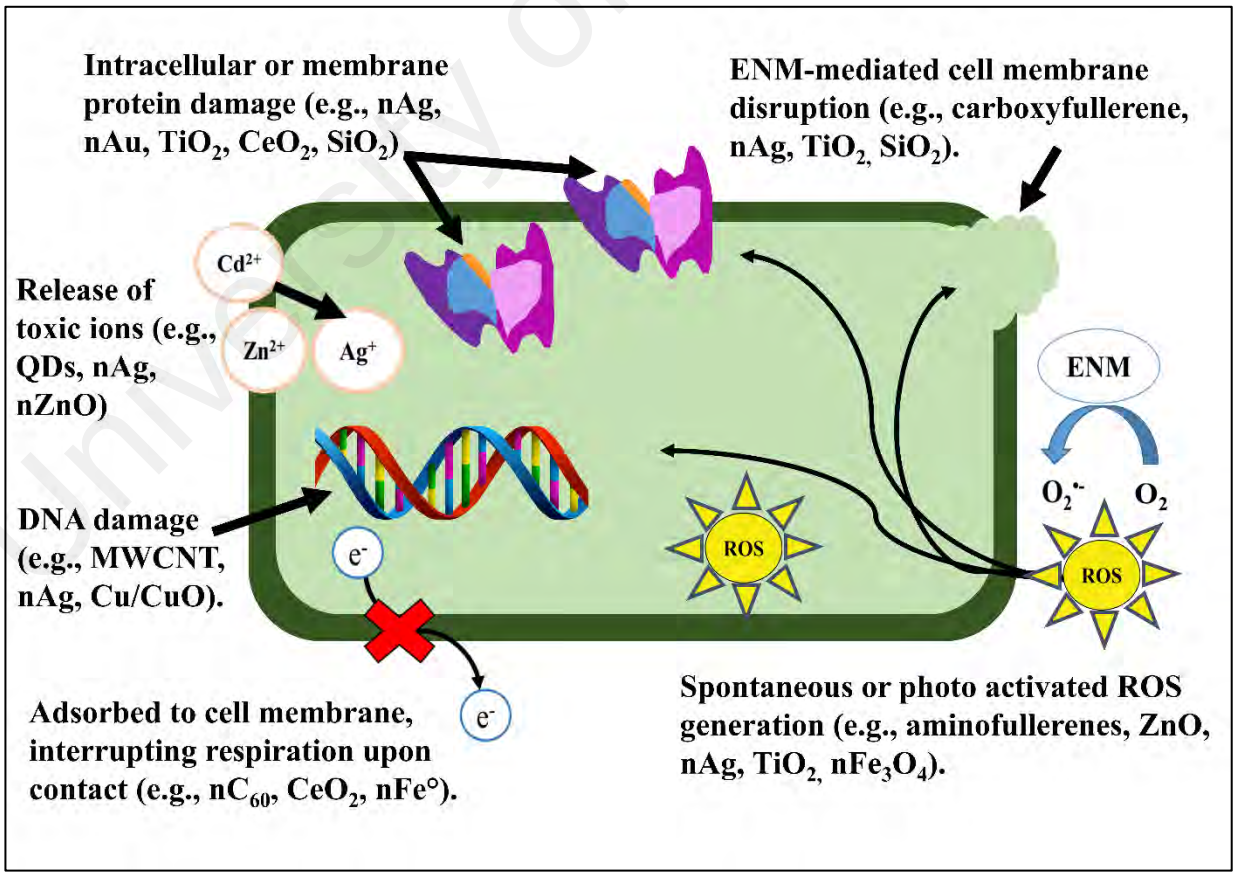

Figure 2.7: Various mechanisms of antimicrobial activities exerted by nanomaterials (Li, Mahendra, et al., 2008).

2.2.5 Sensing and monitoring systems

A major challenge for environmental remediation management is monitoring the emission of toxic substance (i.e. organic and inorganic pollutants, pathogens and hazardous atmospheric pollutants), coupled with accurately assessing the extent and composition of these contaminants. Therefore, various analytical techniques have been employed in environmental pollution detection and monitoring, for instance surface plasmon resonance (SPR) (Salah, Jenkins, & Handy, 2014; Shankaran, Gobi, & Miura, 2007), high-performance liquid chromatography (HPLC) (Shintani, 2014), gas chromatography-mass spectrometry (GC-MS) (Tranchida et al., 2014), supercritical fluid chromatography (SFC) (Bamba, 2014), capillary electrophoresis (CE) (Sánchez-Hernández et al., 2014), flow injection analysis (FIA) (Gerez, Rondano, & Pasquali, 2014). Nevertheless, these techniques are inappropriate for routine environmental detection because of their high cost, time consumption in addition to their complicated requirements (Su et al., 2012).

The growing advances in nanoscience and nanotechnology are having a remarkable influence on the field of environmental monitoring and sensing, where large number of nanoparticles have been introduced for detection and remediation of wide range of contaminants (Andreescu et al., 2009; Theron, Eugene Cloete, & de Kwaadsteniet, 2010) in both gaseous and aqueous mediums. Many investigations have been carried out to develop high selectivity and sensitivity nanosensors for water quality monitoring by detection of organisms fecal pollution (Savichtcheva & Okabe, 2006) such as fecal coliforms, total coliforms, E. coli, enterococci bacteriophages and disease causing viruses and parasites (Theron, Eugene Cloete, & de Kwaadsteniet, 2010), furthermore, detection of different types of trace contaminants (such as, pesticides, phenolic compounds, inorganic anions, heavy metals) (Govindhan, Adhikari, & Chen, 2014).

As any other chemical sensors, Nanoparticles based sensors, are usually consist of two components: the receptor, which enhances the detection sensitivity, and the transducer, a chemical or physical sense component (nanomaterial), that works with electrochemical, thermal, optical and other detection principles (Su et al., 2012). The operating mechanism involves a charge transfer that occurs between pollutants molecules and the receptors, resulting in an electrical and/or optical signal that is related to the molecules type and number (Di Francia, Alfano, & La Ferrara, 2009). Not to mention that in the case of bio-nanosensors, recognitions agents (e.g antibodies (Volkert & Haes, 2014), carbohydrates (Chen, Vedala, et al., 2011), aptamers (Li, Shi, et al., 2009), and antimicrobial peptidesis (AMPs) (Cui, Kim, et al., 2012)) are presented as a third components, specifically provide the selectivity by interacting with antigens or other epitopes on the pathogens surface (Vikesland & Wigginton, 2010). Moreover, to obtain nanosensors with high sensitivity and fast response time, nanostructers such as nanorods, nanobelts, nanowires were functionalized (Kanade et al., 2007). For instance tungsten oxide nanowires (WO_3-NWs) were functionalized with palladium for hydrogen gas detection (Chávez et al., 2013) and with copper oxide for high performance hydrogen sulfide sensor (Park et al., 2014).

As a matter of fact, Nanomaterial-based sensors have shown great potential in the chemical and biological detection researches due to their physical, chemical, optical, catalytic, magnetic and electronic properties as well as their high selectivity and sensitivity (Qu, Alvarez, & Li, 2013; Wang, Ma, et al., 2010). Some examples of widely used nanomaterials in sensors technology include quantum dots (QDs) which can be benefited from their fluorescence properties to detect heavy metals, toxic gases, cyanotoxins and pathogens (Feng et al., 2014; Hahn, Tabb, & Krauss, 2005; Koneswaran & Narayanaswamy, 2009; Ma, Cui, & Su, 2009; Wu, Khaing Oo, & Fan, 2010). Metal nanoparticles such as silver and gold nanoparticles relies on the changes in their color for

pollutants detection (Saha et al., 2012). Furthermore, carbon based nanomaterials (CNMs), including single wall carbon nanotube (SWCNTs), multi wall carbon nanotube and graphene, are used to facilitate the electron transfer between electrodes and electro active species (Su et al., 2012).

2.3 Deep Eutectic Solvents

In the last two decades, the focus on the application if ionic liquids (ILs) has increased, notably with respect to catalysts, electrochemistry process technology and analytics, biotechnology and functional liquids. It is well known that ILs are solvents which merely compose of ions. Generally, the synthesis of ILs can be classifies into two definite categories: (1) ILs prepared from eutectic mixtures of metal halides and organic salts, and (2) ILs consist of discrete anions (Smith, Abbott, & Ryder, 2014a). The physical and chemical properties of ILs play a key role in determining the type of application that ILs can be involved in (Zhang, Zhang, & Deng, 2011). However, ILs have many restraints due to their relatively high cost of ILs as well as their complicated synthesizing process which is usually associated with discharging of undesirable wastes (Phadtare & Shankarling, 2010). As a result, many attempts have been carried out to reduce the cost of ILs and to find alternative solvents with affordable prices, easy to prepare and eco-friendlier. Thus, Abbot et al. (2003) presented for the first time the so-called deep eutectic solvent (DES) as a substitute or improvement of ILs (Abbott et al., 2003).

DESs are a developing type of solvents that are acknowledged as ILs analogues (Abbott et al., 2001). Fundamentally, DES is a mixture of two or more compounds and it is distinguished with its low melting point which is lower that of its individual constituents (Hayyan et al., 2010a). Moreover, the preparation of DES can be achieved by mixing a salt and a hydrogen bond donor (HBD) at specific molar ratio, hence the anion of the salt bonds with the hydrogen from HBD. Knowing that, various kinds of salts

(organic and inorganic) with different kinds of HBDs can be used to prepare numerous mixtures of DESs (Zhang, De Oliveira Vigier, et al., 2012b). Mainly, three types of DESs can be recognized. Class (A) includes DESs that are basically comprised of an ionize salt and a HBD, such as choline chloride and urea DES (Figure 2.8), and this class is considered the most studied DES class. Class (B) involves DESs that are composed of an ionize salt and a metal salt such as choline chloride and zinc chloride (Abbott, Capper, et al., 2004b). The last class (C) contains more complex DESs compare to the other two classes. This type of DESs can be attained from the mixture of a carbohydrate, urea, and an ammonium salt in different ratios, for instance choline chloride : D-fructoseis DES (Hayyan et al., 2012b).

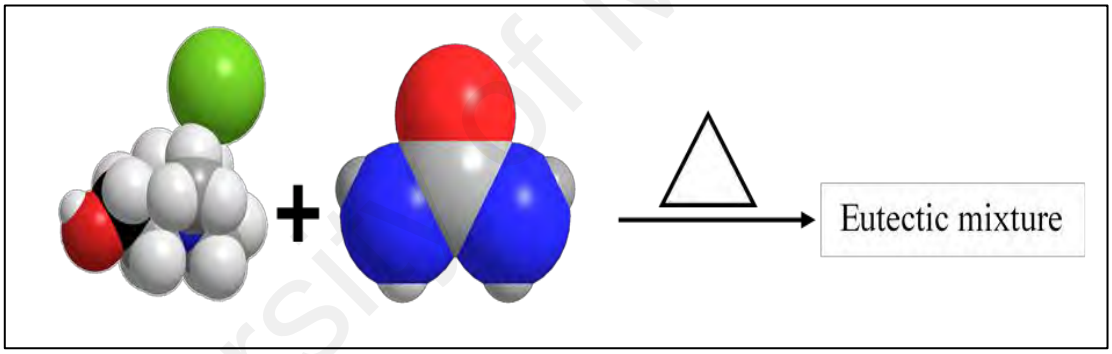

Figure 2.8: Choline chloride: urea eutectic mixture.

The conventional ILs and DESs share some of physiochemical properties (Hayyan, Hashim, Al-Saadi, et al., 2013b), such as non-flammability, non-volatility, high viscosity as well as they share the same stating constituents. Taking that into account, DESs can be considered as the fourth generation of ILs (Cvjetko Bubalo et al., 2015). However, DESs have many advantageous properties over conventional ILs and which can be defined by their low toxicity profiles, their environmental and economic benefits (Hayyan, Hashim, Al-Saadi, et al., 2013b), and finally their simple, economic and ecological synthesizing process which mainly depends on mixing DES's components without any unfavorable waste disposal (Zhang, De Oliveira Vigier, et al., 2012b).

2.3.1 Synthesis of DESs

The first combination of DES was prepared by mixing urea and choline chloride at 80 ˚C until the mixture turned into homogenous liquid (Abbott et al., 2003), later, different types of DESs were reported using various kinds of salts and HBDs. Figure 2.9 depicts some of the starting salts and HBDs for the preparation of DESs. Freeze drying method was also reported for the synthesis of DESs. This method is conducted by mixing a concentrated aqueous solution of the two DESs compounds and freeze dry the combination in order to obtain the DES mixture (Gutiérrez et al., 2009). Hayyan et, al. (2012 and 2013) prepared the fruit sugar and the glucose based DESs (Hayyan, Mjalli, et al., 2013). In addition, phenols based DESs was synthesized based on phenol, o-cresol, and 2,3-xylenol, and ChCl at different molar ratios (Guo, Hou, Ren, et al., 2013). All the studies were focusing on the deepest eutectic point can be formed from mixing molar ration, until Hayyan et, al. (2015) examined the stability of the TEG based DESs by observing it for eight weeks to acquire the first eutectic molar ration without any precipitate (Hayyan, Aissaoui, et al., 2015).

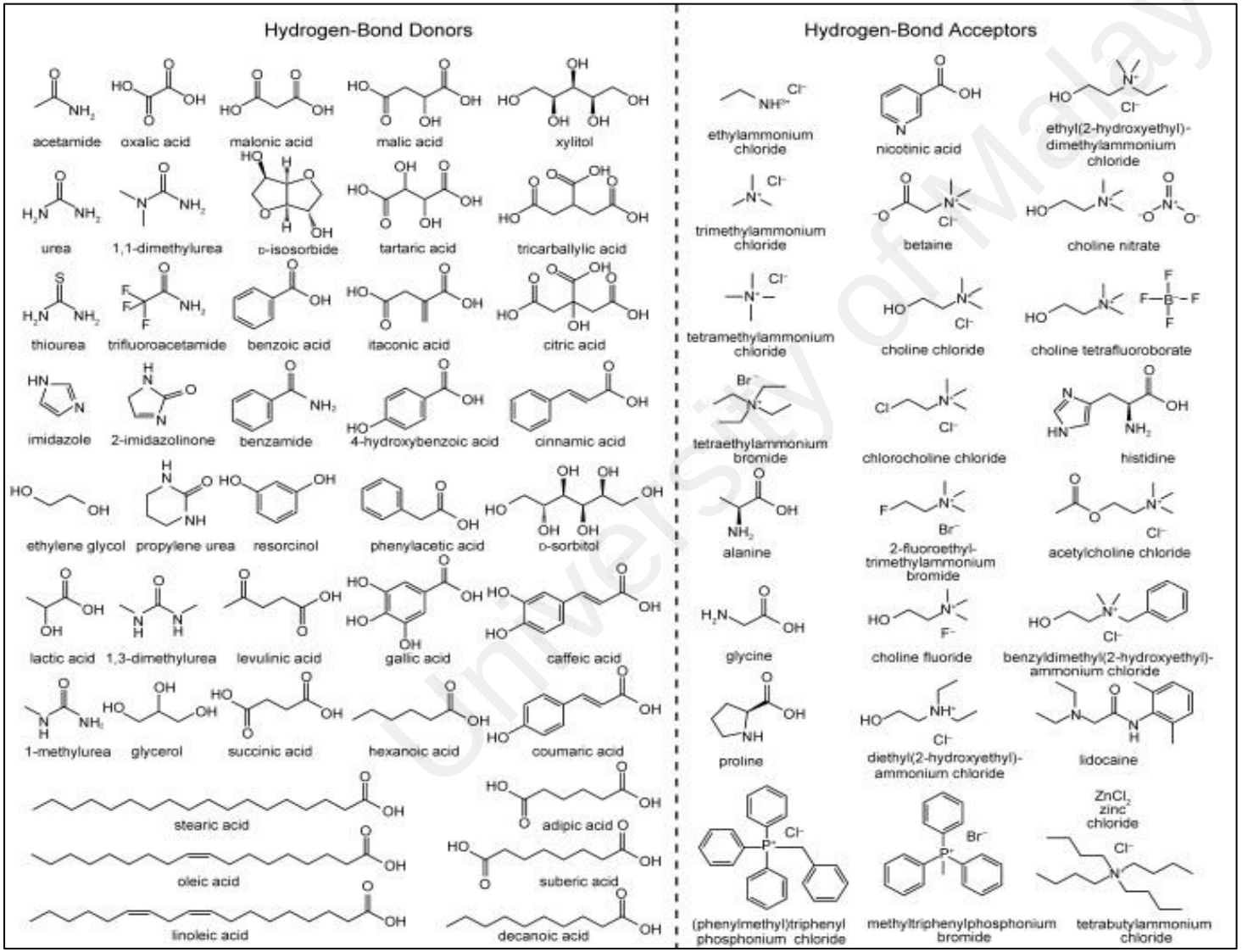

Figure 2.9: DESs starting materials (salts and HBDs) (Francisco, van den Bruinhorst, & Kroon, 2013).

2.3.2 physical properties of DESs

Many studies investigated and record the physical and chemical properties of different combinations of DESs. The impact of temperature and the component's molar ratio on the physiochemical properties of DESs was also studied. This can help in boosting the possibilities of DESs to replace ILs as novel solvents and to be employed in interdisciplinary domains.

2.3.2.1 Freezing point

The relatively low freezing point is the unique property of DESs which distinguish them from other solvents. The molar ratio and structure of the salts and HBDs remarkably affect the low freezing point of the DESs (Hayyan et al., 2010a). Abbott et, al. (2003) synthesized the first DES combination which comprised of ChCl and Urea and the freezing point of this DES was determined. Subsequently, many studies were carried out to investigate the freezing points of different types of DESs. Kareem et, al. (2010) used different types of DESs based on different types of phosphonuim based salts and different HBDs (Kareem et al., 2010a). Later, Hayyan et, al. (2012) examined the effect of molar ration on the Chcl: fruit sugar DES (Hayyan et al., 2012b), and the same team investigated the role of molar ration on the freezing points for the glucose based DES (Hayyan, Mjalli, et al., 2013). Table 2.6 shows the freezing points of some of the reported DES.

2.3.2.2 Density

Density is one of the important properties that should be studied for any new solvents to ease their application in many industrial fields. The densities value for different types of DESs were reported along with effect of different temperature on their values. Hence, the temperature significantly reduced the densities values due to increased molecular

mobility which causes an increase in the molar volume (Hayyan et al., 2012b). Generally, the trend of density-temperature of most DESs followed the general rule of most liquidous materials i.e. the density decreased linearly with the increase of temperature. Abbot et, al. (2007) examined the effect of some HBDs, i.e. ethylene glycol, glycerol and 1,4Butanediol weight percentage with ChCl. They found that by adding 5 % ChCl to 1,4Butanediol, the resulted density was the lowest compare to other ratios and other HBDs, also it was the closest value to the density of water (Abbott, Harris, & Ryder, 2007b). In 2010, a group of researchers investigated some physical properties on phosphonium based DESs, the densities of all DESs were fitted linearly. Later, Abbott et,al. (2011) also examined the effect of salts concentration on the density of some DESs formed from ChCl and glycerol, it was noticed that the density was decreasing by increasing the salt concentration until it reached 1.18 g cm^{-3} at 33% salt concentration (Abbott, Harris, et al., 2011a). Table 2.6 shows some reported DESs densities.

2.3.2.3 Viscosity

Generally, the viscosity of a liquid can be defined as its resistance to flow. It was found that most of the DESs showed a relatively high viscosity values (> 100 cp) which are similar to most of ILs (Zhang, De Oliveira Vigier, et al., 2012b). The viscosity of most known DESs are listed in Table 2.6. Basically, DESs with strong hydrogen bonding own high viscosity values due to the restricted mobility of DESs molecules (D'Agostino et al., 2011; Ru & Konig, 2012). Moreover, some factors including temperature, molar ration, atomic structure of the components, the interaction forces including van der Waals and electrostatic forces, and void volume also have a noteworthy influence on the viscosity of DESs. Bien that, DES is considered as a designer solvent and this an important advantage over other solvents in industrial applications. It was proven that the amount of salt in DES composition has a direct impact on DES viscosity value. As the salt amount increases the viscosity of DES increases which is caused by the ratio of the

ion radius to the hole size within the liquid. Finally, the hole theory suggests that the viscosity of ILs and DESs is controlled by the cation size of the salt. As the salt ratio increase the viscosity of ChCl: glycerol DES decreased which can be ascribed to the three OH groups in the glycerol molecular which have extensive hydrogen bonding. The presence of the cation contributes into braking the hydrogen bond between the glycerol molecules to form new weak hydrogen bonds with cation of the salt (AlOmar, Hayyan, et al., 2016a).

2.3.2.4 Conductivity

The conductivity of a material is defined as its ability to conduct an electrical current. In another word, conductivity can be considered as an indication of the presence of chemicals dissolved in the solution (i.e. the higher the conductivity is, the more dissolved ionic species are existing and moving freely within the solution). It is a very important parameter for various range of industries including semiconductors, electroplating, petroleum, iron and steel industries. Hence, most of DESs show low ionic conductivity and high viscosity (Zhang, De Oliveira Vigier, et al., 2012b). The low conductivity values of DESs can be ascribed to the mobility of pore ion which is caused by the large size of ions, pairing or agglomeration which leads to the availability of a smaller size of charge carriers. Table 2.6 shows the most known DESs recorded conductivities.

2.3.2.5 Surface tension

Surface tension phenomenon is measured as the necessary energy to increase the liquid surface area by a unit of area. This phenomenon is resulted from the reduction in the surface area of the liquid's interface with other phases in contact with the liquid due to the cohesive tension which is resulted from the intermolecular attractive forces in the liquid. The proper prediction of surface tension value considerably influences a number of reservoir engineering calculations in oil-gas systems, also influences the relative

gas/liquid phase permeability and helps in estimation of capillary pressure of the oil in a porous solid (Pedersen, Lund, & Fredenslund). Moreover, surface tension plays a major role in the design of thermal systems and heat exchangers and it is considered a significant parameter in design formulas for systems include mass and momentum transfer, such as falling films and drops and bubbles formation (Bird, Stewart, & Lightfoot). The surface tension-temperature trend usually fitted by Arrhenius like model. However, the effect of temperature on the surface tension of ILs and DESs can be describe by a linear fitting model (Abbott, Harris, et al., 2011a; Zhang, De Oliveira Vigier, et al., 2012b). Table 2.6 presents some DESs reported surface tension values.

Table 2.6: physical properties of some reported DESs

DES (Salt:HBD)	Molar ratio (salt:HBD)	Freezing point ˚C	μ (cP)	ρ (g cm^{-3})	S (mS/cm)	σ (mN/m)	Ref.
ChCl:Urea	1:2	12	750 (25 ˚C)	1.25	0.199 (40 C)	52	(Abbott et al., 2007b; D'Agostino et al., 2011)
ChCl:EG	1:2	-66	37 (25 ˚C)	1.12	7.61 (20 ˚C)	48.91	(Abbott, Harris, et al., 2011a; Shahbaz, Baroutian, et al., 2012b)
ChCl:Gly	1:2	-34	350 (25 ˚C)	1.15	985 (25 ˚C)	57.93	(AlOmar, Hayyan, et al., 2016a)
ChCl:TEG	1:3	-19	110 (80 ˚C)	1.13	1.41 (25 ˚C)	-	(Hayyan, Aissaoui, et al., 2015)
ChCl:TFA	1:3	Liquid	77 (40 ˚C)	1.342	-	35.9	(Abbott, Capper, & Gray, 2006b)
ChCl:D-F	2:1	10	280.6 (40 ˚C)	1.25	-	74	(Hayyan et al., 2012b)
MTPB:Gly	1:3	-24.33	2775.9 (25 ˚C)	1.29	0.054 (25 ˚C)	54.74	(AlOmar, Hayyan, et al., 2016a)
BTPC:Gly	1:16	-21.99	1353 (25 ˚C)	1.24	0.694 (75 ˚C)	53.14	(AlOmar, Hayyan, et al., 2016a)
ATPB:Gly	1:14	-23	1029 (25 ˚C)	1.26	0.68 (75 ˚C)	41	(AlOmar, Hayyan, et al., 2016a)
DAC:Gly	1:2	-24	433.10 (25 ˚C)	1.17	3.4 (75 ˚C)	55.23	(AlOmar, Hayyan, et al., 2016a)
TBAB:Gly	1:4	-24	885.80 (25 ˚C)	1.15	1.2 (75 ˚C)	36	(AlOmar, Hayyan, et al., 2016a)

Table 2.6 (continued)

BTPC:Gly	1:5	50.36	553.7 (55 ˚C)	-	0.162 (55 ˚C)	-	(Kareem et al., 2010a)
MTPB:EG	1:4	-49.34	109.8 (25 ˚C)	1.23	2.85 (75 ˚C)	-	(Kareem et al., 2010a)
BTPC:TEG	1:8	-19.49	116.7 (80 ˚C)	1.1	2.46 (80 ˚C)	-	(Hayyan, Aissaoui, et al., 2015)
ATPB:TEG	1:10	-19.52	84.6 (80 ˚C)	1.145	4.0 (80 ˚C)	-	(Hayyan, Aissaoui, et al., 2015)
TBAC:Gly	1:5	-42.78	1110 (25 ˚C)	1.143	2.2 (80 ˚C)	47	(Mjalli et al., 2014a)
TBAC:EG	1:3	-30.88	110 (25 ˚C)	1.03	6.0 (80 ˚C)	40	(Mjalli et al., 2014a)
TBAC:TEG	3:1	-12.69	-	0.99	0.25 (80 ˚C)	40	(Mjalli et al., 2014a)
TPAB:EG	1:4	-23.4	55 (25 ˚C)	1.138	11.0 (80 ˚C)	47	(Jibril et al., 2014)
TPAB:TEG	1:3	-19.2	120 (25 ˚C)	1.148	4.0 (80 ˚C)	46.2	(Jibril et al., 2014)
TPAB:Gly	1:3	-16.1	900 (25 ˚C)	1.21	2.5 (80 ˚C)	53	(Jibril et al., 2014)

2.3.3 DES applications

Recently, research papers and patents have showed an excessive interest in DESs synthesis and application which sheds the light of the substantial role of DESs as promising economic solvents of the future. In this section, a brief review is presented to highlight some of the main application of DESs.

Electrodeposition and electroplating application is the first domain that employed DESs as new solvents (Abbott & McKenzie, 2006). Then, the progress of using DESs as media for electroplating by different metals have gained a great concern and endless efforts from many researchers worldwide (Smith, Abbott, & Ryder, 2014a). For Biodiesel production and purification field, a new technique using DESs was introduced by Hayyan et al. in 2010 by extracting glycerol from biodiesel (Hayyan et al., 2010a).

DESs showed a promising potential in the control and elimination of greenhouse gases which are considered the main contributors to the global warming. It was found that the capability of DESs to dissolve CO_2 is similar to that of ILs (Zhang, De Oliveira Vigier, et al., 2012b). Li et, al. (2008) examined the effects of different conditions such as temperature, pressure, and molar ratio on the ability of [ChCl:urea] DES to dissolve CO_2 (Li, Hou, et al., 2008a). Salas et, al. (2014) prepared two DESs-based hierarchical carbon monoliths and studied the effect of DESs on the composition of the pore structure of carbon which played a noteworthy part in the adsorption of CO_2. It was found that both DESs based carbon exhibited superior adsorption capacity and selectivity toward CO_2 (López-Salas et al., 2014). In addition, a study was carried out by Yang et al. (2013) to investigate the ability of [ChCl: Glycerol] DES to adsorb SO_2 with respect to temperature, pressure and molar ratio (Yang, Hou, et al., 2013a). Not to mention that DESs can be significantly used to improve the gas storage capacity through providing a unique route by creating porosity and coordinative unsaturated metal centers (Ferey, 2008; Zhang, Wu, et al., 2009).

The enzymatic field has witnessed numerous emerging publications which focus on the possibility of using DESs as new solvents in biotransformation. The first involvement of DESs in biotransformation was reported by Gorke et, al. 2008, by which the catalytic activity of hydrolases in DES was studied (Gorke, Srienc, & Kazlauskas, 2008). Later, the reaction involving lipase-catalyzed processes have been broadly investigated (Singh, Lobo, & Shankarling, 2011; Zhao, Baker, & Holmes, 2011).

2.3.4 DESs and Nanotechnology

The first attempt to apply ILs in nanotechnology filed was achieved by Deshmukh et al. (2001), who used IL at room temperature as media to synthesize Pd–biscarbene complexes and stabilized clusters of zero-valent Pd nanoparticles (Deshmukh, Rajagopal, & Srinivasan, 2001). Later, different research papers and patents investigated the prospects of applying ILs in different applications of nanotechnology area. It is well knows that DESs are recently being used as simple and cost-effective replacement of ILs (Cvjetko Bubalo et al., 2015), consequently they have been replacing ILs in nanotechnology applications. However, the number of research publications involving ILs in nanotechnology domain is much more than that of DESs. Figure 2.10 shows the number of publications of both ILs and DESs in nanotechnology field. Moreover, this section briefly reviews the current reported fields that involve DESs and nanotechnology.

Despite of their exquisite characteristics, nanomaterials have a well-known drawback which is their tendency of agglomeration. Thus, it is crucial to provide a synthesizing media that can ensure a good dispersion and can reduce or cope with the common shortcomings of nanomaterials. DESs were firstly used as dispersants media for nanomaterial synthesis just like some reported ILs. Oh and Lee (2014) prepared gold nanoparticles using [ChCl: malonic acid] DES as a reaction media and structure directing agents (Oh & Lee, 2014). Mota-Morales et al. (2013) synthesized macroporous poly

(acrylic acid)–carbon nanotube composites by using [Acrylic Acid:ChCl] DESs as synthesizing solvent and they stated that this method can be used to produce nanocomposites for bio and environmental applications (Mota-Morales et al., 2013).

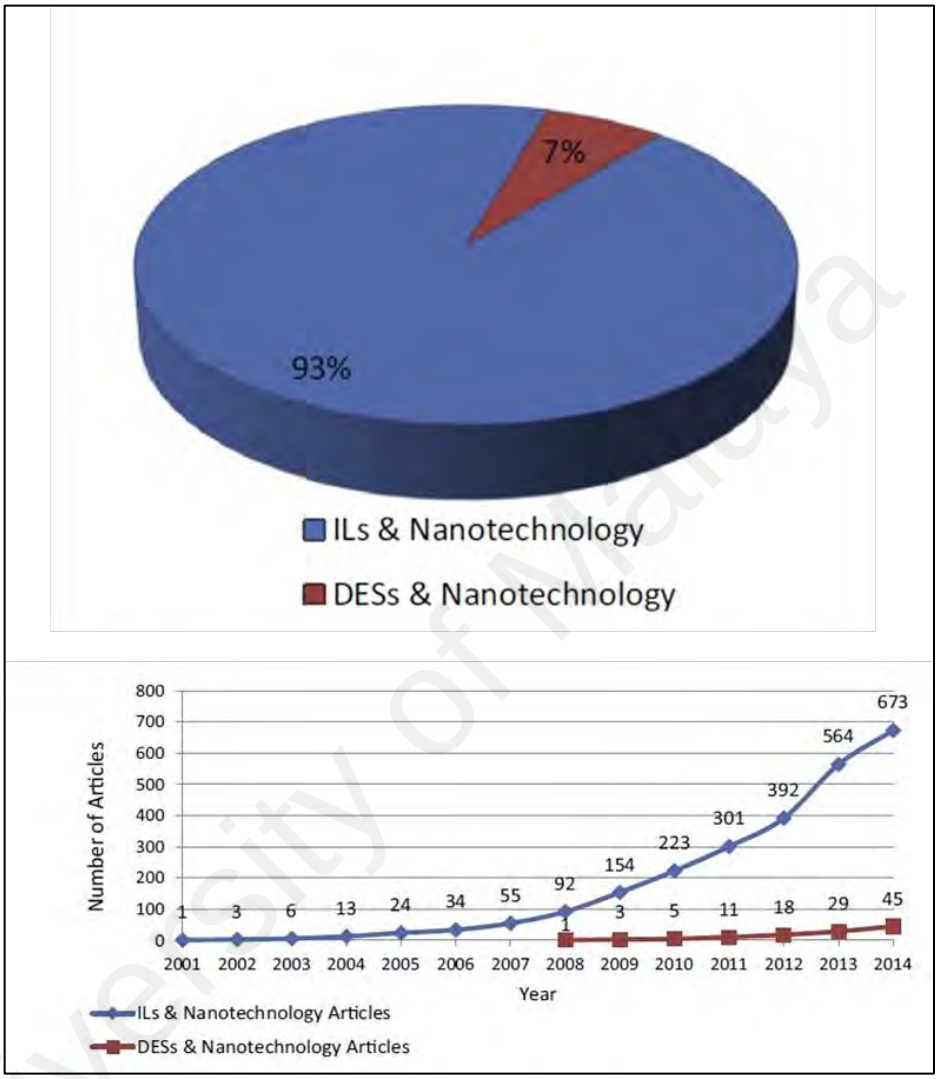

Figure 2.10: ILs and DESs in nanotechnology related publications (Abo Hamed et al. 2015)

DESs were also used as epoxy resin curing agents as reported by Mąka et al. (2014) who have used [ChCl: Tris(hydroxymethyl)propane] DES to produce GNP/DES/ epoxy resin. It was found that the use of DESs improved the electrical volume resistivity of epoxy composites (Mąka, Spychaj, & Kowalczyk, 2014).

Another reported application of DESs is being utilized as exfoliation agent of nanomaterials. Boulos et al. (2013) transformed the human hair into functional nanoparticles by utilizing [ChCl:Urea] DESs as an exfoliation media. Figure 2.11 represents the SEM results which revealed the cuticle cells that was completely exfoliated from the hair after the treatment of DES (Boulos et al., 2013).

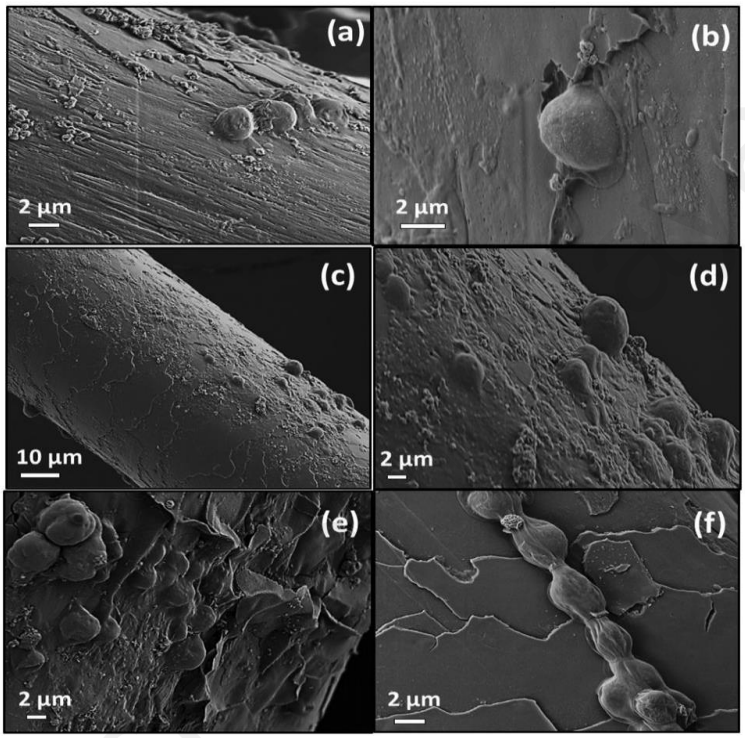

Figure 2.11: images of immobilized microalgae cells on the surface of hairmicrofibers without treatment with the IL composite (a) and (b); hair microfiber after treatment with the IL composite, (c) and (d); hair microfibers after IL composite and liquid N2 treatment, (e) and (f). Note that individual C. vulgaris cellshave a slightly variable size diameter between 2 to 4 µm.(Boulos et al., 2013)

The role of DESs and nanomaterials was remarkable in electrochemistry field. Easier and more expedient method was introduced for quercetin sensors by using CNTs electrode and [ChCl:urea] DES as electrolyte (Zheng et al., 2014). Wei et al. (2012) used DESs in electrochemically shaped control methods to synthesize the uniform Pt nanoflowers which have a higher electro-catalytic activity and stability (Wei et al., 2012).

A study was carried out by Chen et al. (2009) to encapsulate [ChCl:Zinc Chloride] DES in SWCNT (Figure 2.12). SWCNTs were thermally treated to remove the ending cups. Different methods was used to characterize the resulted product. The morphology study revealed that the DES was encapsulated as single-chain, double-helix, and zigzag tubes (Chen, Kobayashi, et al., 2009).

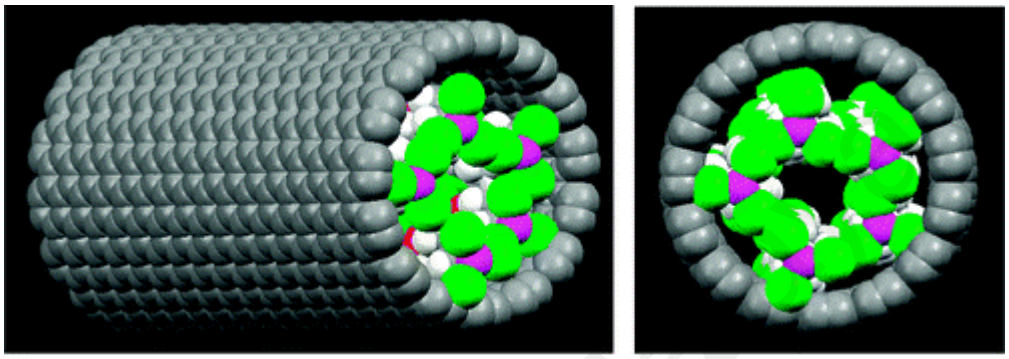

Figure 2.12: DES encapsulated SWCNT (Chen, Kobayashi, et al., 2009)

Moreover, a new method to dissolve metal complexes and to enable thermochromism was introduced by Gu and Tu (2011). Two types of ChCl based DESs i.e. [ChCl:U] DES and [ChCl:EG] DES were involved in this method to dissolve several transition metal chlorides. $NiCl_2$-$6H_2O$ displayed a stable and prominent thermochromic behavior within a wide temperature range started from room temperature to about 150 °C. It was claimed that this method can develop high performance thermochromic materials for the simple fabrications (Gu & Tu, 2011). Table 2.7 shows some of the reported applications of DESs in nanotechnology related field.

Finally, DESs were used as a functionalization agent of graphene. The effect of various types of DESs on the graphene surface was investigated. The result exposed that the graphene-functionalized DES has a great potential to be employed in many applications due to the new functional groups introduced to the surface of graphene after treatment with DESs (Hayyan, Abo-Hamad, et al., 2015b).

Table 2.7: Nanotechnology applications involving DESs

DES salt	HBD	Molar ratio	Nano application	Remark	Ref.
ChCl	EG	1:2	SnO_2 nanocrystalline	room temperature Homogeneous precipitation of SnO_2 nanocrystalline	(GU et al., 2011)
ChCl	Urea	1:2	Spherical Fe_3O_4 magnetic nanoparticles	Co-precipitation of Spherical Fe_3O_4 magnetic nanoparticles using 2.164 g (8 mmol) of $FeCl_3.6H_2O$ and 1.194 g (6 mmol) of ground $FeCl_2.4H_2O$ were added to 15.585 g of DES, or adding 2.613 g (46.7 mmol) of KOH to the mixture	(Chen et al., 2013)
ChCl	Urea	1:2	Used as a dispersant of Pristine MWCNTs / oxidized MWCNTs	The dispersion of oxidized CNT was much highier that that with the pristine CNT	(Martis et al., 2010)
ChCl	Urea	1:2	Production of CuCl nanoparticles	The rule of DES was in the oxidation-reduction reaction. The reaction time was 1 h in the presence of polyvinylpyrrolidone in the DES	(Huang, Li, et al., 2012)
ChCl	Gallic acid: glycerol	1:0.25:0.25	Cold gold nanoparticles coated gum Arabic	The rule of DES was Reduction of $HAuC_{l4}$	(Shahidi et al., 2015)

Table 2.7 (continued)

ChCl	EG	1:2	codeposition f SiO_2 nanoparticles in Ni matrix	The new composite showed excellent corrosion resistance compare to Ni coating alone	(Li, Hou, & Liang, 2016)
ChCl	$FeCl_3$	1:2	Fe_3O_4/Fe doped graphene nanosheets	The DES play a significant rule as catalysts based on the complexation of ChCl–$FeCl_3$	(Mondal et al., 2016)
ChCl	EG	1:2	magnetic graphene oxide (Fe_3O_4–NH_2@GO) nanoparticles in core-shape structure	This study demonstrates the use of (Fe_3O_4–NH_2@GO) coated with DES for protein extraction	(Xu, Wang, et al., 2016)
ChCl	Gly	1:1			
ChCl	D-glucose	2:1			
ChCl	D-sorbitol solution	1:1			
ChCl	Urea	1:2	silver nanoparticles	Synthesis of silver nanoparticles by laser ablation in DES. The rule of DES was controlling the formation of uniform nanoparticles.	(Oseguera-Galindo et al., 2016)
ChCl	EG	1:2	DNA–N-doped graphene hybrid	The DES was used as a dissolution media of DNA. Also it was used as a dispersion media of Fe_3O_4.	(Bhatt et al., 2016)
ChCl	Urea	1:2	Copper–zinc–tin chalcogenide (CZTS) nanoparticles	The DES was used as green solvent, thiourea as sulfur source and metal chloride reagents.	(Karimi, Eshraghi, & Jahangir, 2016)
ChCl	succinic acid	1:1	TiO_2 Nanobamboos	The high conductivity and viscosity might be the main reason for the self-organization of NBs	(Chen et al., 2015)

Table 2.7 (continued)

ChCl	EG	1:2	Ni matrix coatings micro or nano-sized SiC particles	The DES was used as electrolyte. The Ni–SiC composite coatings exhibits very good water resistance.	(Li, Chu, & Liang, 2015)
ChCl	Urea	1:2	Nanoporous copper films	An in situ electrochemical process involving alloying/dealloying of Cu–Zn surface alloys from DES containing ZnO at elevated temperatures from 353 to 393 K	(Zhang, Abbott, & Yang, 2015)
ChCl	gallic acid/Gly	1 : 0.25 : 0.25	Ultra-thin and large gold nanosheets	The DES was used as directing and reduction agent. Along with the Arabic gum which acted as stabilizer and shape-controlling agent	(Tohidi, Mahyari, & Safavi, 2015)

2.3.5 Summary

A detailed overview was displayed in this chapter covering the challenges caused by the water pollution and all the risks raised from the discharge of different hazardous and non-biodegradable organic pollutants. The presence of 2,4-DCP and MO was discussed along with their threatening effect on human health and the environment. Furthermore, some of the available techniques and recent attempts to remediate the polluted water from both 2,4-DCP and MO were also reported in this section. This section also highlighted the hurdles that limit the applications of nanomaterials and suppress the advantages of their unrivaled merits; such hurdles include conditions of surrounding environment (e.g., humidity, temperature, acidity, etc.), particle agglomeration, and separation difficulties. It has been shown that nanotechnology exhibits remarkable features for advanced, robust, and multifunctional treatment processes that can enhance pollution monitoring, treatment performance, as well as overcome all the mentioned barriers. Carbon nanotubes were one of the discussed nanomaterials involving their historical background, their unique characteristics as well as the significance of their functionalization techniques. Based on all the information and all published treatment techniques, the experimental work in this thesis was constructed, including functionalization process, characterization techniques, and adsorption procedures.

Th final part of this chapter reviewed the history of DESs as well as their physical and chemical properties. Moreover, the application of DESs in wide ranges of scientific fields and their contribution in nanotechnology domain was comprehensively discussed. The knowledge from this part was used as platform to design the experimental procedures which were adopted for the synthesis of DESs and for the measurement of their physical properties. Taking in mind the detailed survey displayed in this chapter, the use of DESs as functionalization agents to be applied as adsorbents for organic pollutants was proposed.

CHAPTER 3: MATERIALS AND METHODS

3.1 Materials

3.1.1 Chemicals

All the chemicals and reagents used to carry out this research are listed in Table 3.1 along with their corresponding suppliers, purity grade and applications. Figure 3.1 display the chemical structures of the used salts, HBDs and organic pollutants. The Material Safety Data sheet (MSDS) for each material used in this study was examined and understood.

Table 3.1: Chemical utilized in this research.

Material name	Supplier	Purity grade	Application in this research
Ethylene glycol	Merck	≥ 98.0 %	Used as HBD to prepare DES
Diethylene glycol	Merck	≥ 98.0 %	Used as HBD to prepare DES
Choline Chloride	Sigma Aldrich	≥ 99.0 %	Used as salt to prepare DES
N,N-diethylethanolammonium chloride	Merck	≥ 98.0 %	Used as salt to prepare DES
Tetra-n-butylammonium bromide	Merck	≥ 99.0 %	Used as salt to prepare DES
Methyltriphenylphosphonium bromide	Merck	≥ 98.0 %	Used as salt to prepare DES
Benzyltriphenylphosphonium chloride	Merck	≥ 98.0 %	Used as salt to prepare DES
Carbon nanotubes	Sigma Aldrich	≥ 95.0 %	Used as adsorbent
2,4-dichlorphenol	Merck		Used as adsorbate
Methyl orange	Sigma Aldrich		Used as adsorbate
Sodium hydroxide	Sigma Aldrich	98-99%	Used to adjust solution pH
Hydrochloric acid	Sigma Aldrich	36.5–38%	Used to adjust solution pH
Potassium permanganate	Sigma Aldrich		Used to functionalize CNTs
Nitric acid	Sigma Aldrich	65 %	Used to functionalize CNTs
Sulfuric acid	Sigma Aldrich	95–97%	Used to functionalize CNTs
Methanol	Merck	Analytical reagent	Used to determine 2,4-DCP concentration using UPLC
Acetonitrile	Merck	Analytical reagent	Used to determine 2,4-DCP concentration using UPLC

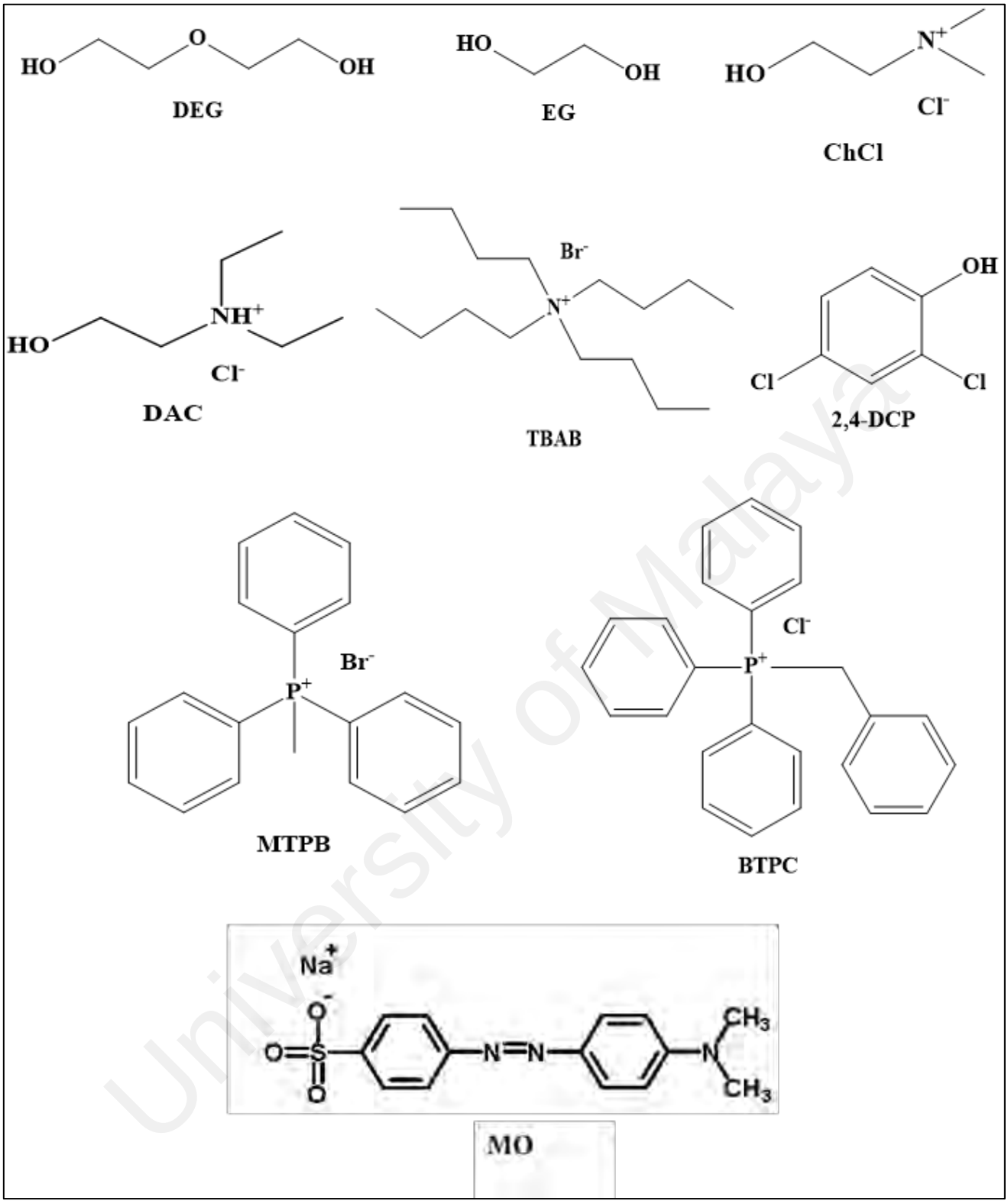

Figure 3.1: Molecular structure of some used chemicals in this research.

3.1.2 Equipment

3.1.2.1 DESs synthesizing and characterization

1. Hotplates from Fisher Scientific (SASTEC and WiseStire)
2. Digital balance (Mettler Toledo AG204)
3. Vacuum oven (memmert VO500)
4. External water circulator (Techne-Tempette TE-8A)
5. Spectrum 400-fourier transform infrared (FTIR) spectrometer.
6. Differential scanning calorimetry (DSC) (METTLER TOLEDO)
7. Density meter (DM 40) (METTLER TOLEDO)
8. Brookfield R/S Rheometer
9. Automated tensiometer Krüs K10ST classification B with Du Noüy ring method
10. Eutech Cyberscan Con 11 hand-held meter.

3.1.2.2 CNTs functionalization and characterization

1. Digital balance (Mettler Toledo AG204)
2. Vacuum oven (memmert VO500)
3. Hotplates from Fisher Scientific (SASTEC and WiseStire)
4. Reflux system
5. Ultrasonic bath from (JAC, Korea, model JAC 2010P)
6. Vacuum pump station of (model DAA-P601-LD, Germany)
7. membrane 0.45 μm in size (Sartorius stedim biotech GmbH 37070 Goettingen Germany)
8. pH//Ion Benchtop meter (Mettler Toledo S220 SevenCompact).
9. Fourier transform infrared (FTIR) spectroscopy (PerkinElmer® FTIR spectrometer)
10. Raman spectroscopy (Renishaw System 2000 Raman Spectrometer)

11. Zetasizer (Malvern, UK)
12. Thermogravimetric analysis (TGA) (STA-6000, PerkinElmer®)
13. FieldEmission Scanning Electron Microscope (SEM) (JEOL Ltd., Japan. JSM-6700F)
14. Brunauer-Emmett-Teller (BET) surface area (micromeritics, TriStar II 3020, USA)
15. Transmittance Electron Microscopy (TEM) (LEO-Libra 120)

3.1.2.3 Adsorption experiments and water analysis

1. Digital balance (Mettler Toledo AG204)
2. Orbital laboratory shaker.
3. Refrigerator (TOCHIBA GR-R72MD)
4. ultra-high-performance chromatography (Waters ACQUITY UPLC System)
5. UV/vis spectrophotometer (PerkinElmer-Lambda 35)

3.2 Methods

Figure 3.2 demonstrates the experimental steps followed to achieve the objectives of this research. More details of each step are additionally explained in this section.

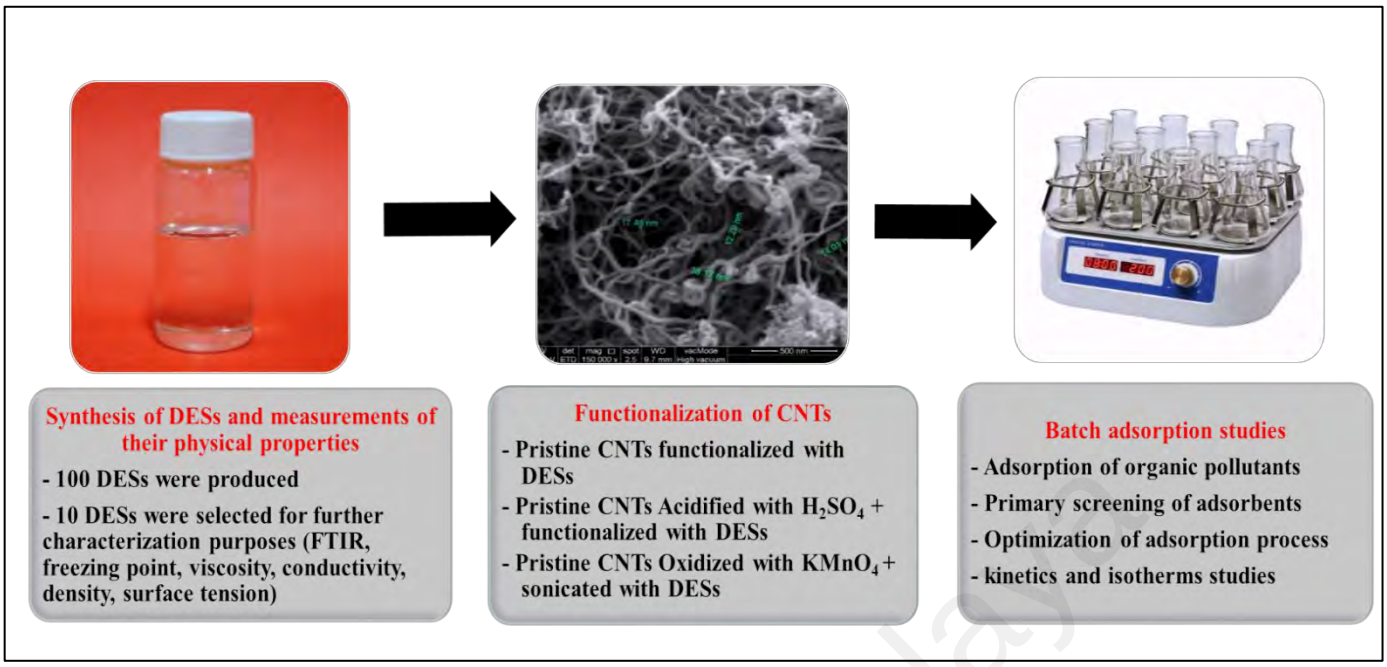

Figure 3.2: The experimental steps of this research.

3.2.1 Synthesis of DESs and measurements of their physical properties

3.2.1.1 DES Preparation

All the chemicals used to prepare DESs were dried in a vacuum oven for 3 hours before conducting any experiments to prevent the effect of moisture content on the physical properties measurements. Two DESs systems were prepared by using two HBDs (i.e., EG and DEG), and five different salts (i.e., ChCl, TBAB, BTPC, MTPB and DAC). Each salt was mixed with one of the HBDs at 180 rpm and 343.15 K for 120 min using magnetic stirring. The synthesis of DESs was carried out under atmospheric pressure and in a high moisture-controlled environment.

3.2.1.2 DES screening

A primary screening was conducted to determine the optimum DES composition ratio, at which DES is homogeneous and stable. As can be noticed from Figure 3.3 different molar ratios in the range of 1:1-1:10 were prepared for each salt and HBD combination. 100 DESs was prepared based on [ChCl:EG], [DAC:EG], [BTPC:EG], [MTPB:EG],

[TBAB:EG], [ChCl:DEG], [DAC:DEG], [BTPC:DEG], [MTPB:DEG], and [TBAB:DEG]. During and after the preparation of DESs, various kinds of phases were evident, such as solid, semi-solid, crystal, and liquid (Figure 3.3). The selected optimum molar ratio for each DES composition was the first molar ratio at which DES mixture was stable and homogeneous without any precipitate after several weeks of observation. Eventually, ten DESs were chosen for further characterization and application purposes.

3.2.1.3 DESs characterizations

The functional groups and freezing points of the ten selected DESs were measured using spectrum 400 FT-IR spectrometer and differential scanning calorimetry (DSC) METTLER TOLEDO respectively. A density meter (DM 40) METTLER TOLEDO, a Brookfield R/S Rheometer and an automated tensiometer Krüs K10ST classification B with Du Noüy ring method were utilized to determine densities, viscosities and surface tensions correspondingly. The conductivity of selected DESs was measured using Eutech Cyberscan Con 11 hand-held meter and the variation in the temperature range was controlled using an external water circulator (Techne-Tempette TE-8A). The standard uncertainties in measurements of each studied physical property are listed in Table 3.2.

Table 3.2: Standard uncertainties in measurements.

Measurements	Estimated uncertainties
Density ($g.cm^{-3}$)	± 0.0001
Viscosity (cP)	(3-5) %
Surface tension ($mN\ m^{-1}$)	± 0.1
Conductivity (µs/cm)	± 18
Freezing point (K)	± 0.01
pH	± 0.002

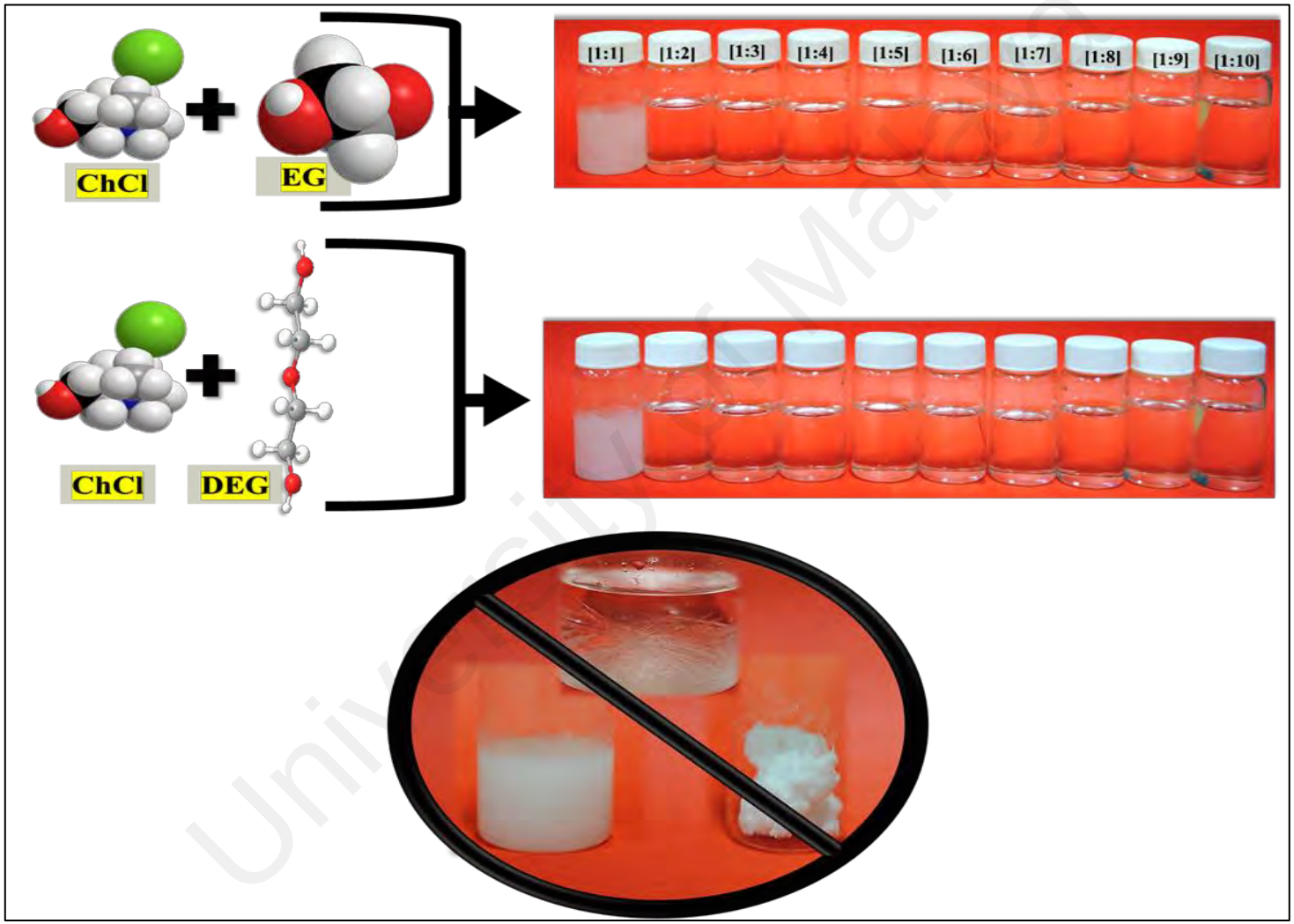

Figure 3.3: Resulted phases from the primary screening of DESs.

3.2.2 Functionalization of CNTs

Figure 3.4 summarizes all the procedures that are used to functionalize CNTs. Table 3.3 contains all functionalized CNTs along with their perspective abbreviations and functionalization method.

Table 3.3: Abbreviations and modification method of examined adsorbents.

No	Adsorbent abbreviation	Modification method
1	P-CNTs	Pristine
2	S-CNTs	Acidification with H_2SO_4
3	K-CNTs	Oxidation with $KMnO_4$
4	PChCl-CNTs	Pristine + sonication with [ChCl:EG]
5	Pn,n-CNTs	Pristine + sonication with [DAC:EG]
6	PTBAB-CNTs	Pristine + sonication with [TBAB:EG]
7	PBTPC-CNTs	Pristine + sonication with [BTPC:EG]
8	PMTPB-CNTs	Pristine + sonication with [MTPB:EG]
9	SChCl-CNTs	Acidification with H_2SO_4 + sonication with [ChCl:EG]
10	Sn,n-CNTs	Acidification with H_2SO_4 + sonication with [DAC:EG]
11	STBAB-CNTs	Acidification with H_2SO_4 + sonication with [TBAB:EG]
12	SBTPC-CNTs	Acidification with H_2SO_4 + sonication with [BTPC:EG]
13	SMTPB-CNTs	Acidification with H_2SO_4 + sonication with [MTPB:EG]
14	KChCl-CNTs	Oxidation with $KMnO_4$ + sonication with [ChCl:EG]
15	Kn,n-CNTs	Oxidation with $KMnO_4$ + sonication with [DAC:EG]
16	KTBAB-CNTs	Oxidation with $KMnO_4$ + sonication with [TBAB:EG]
17	KBTPC-CNTs	Oxidation with $KMnO_4$ + sonication with [BTPC:EG]
18	KMTPB-CNTs	Oxidation with $KMnO_4$ + sonication with [MTPB:EG]

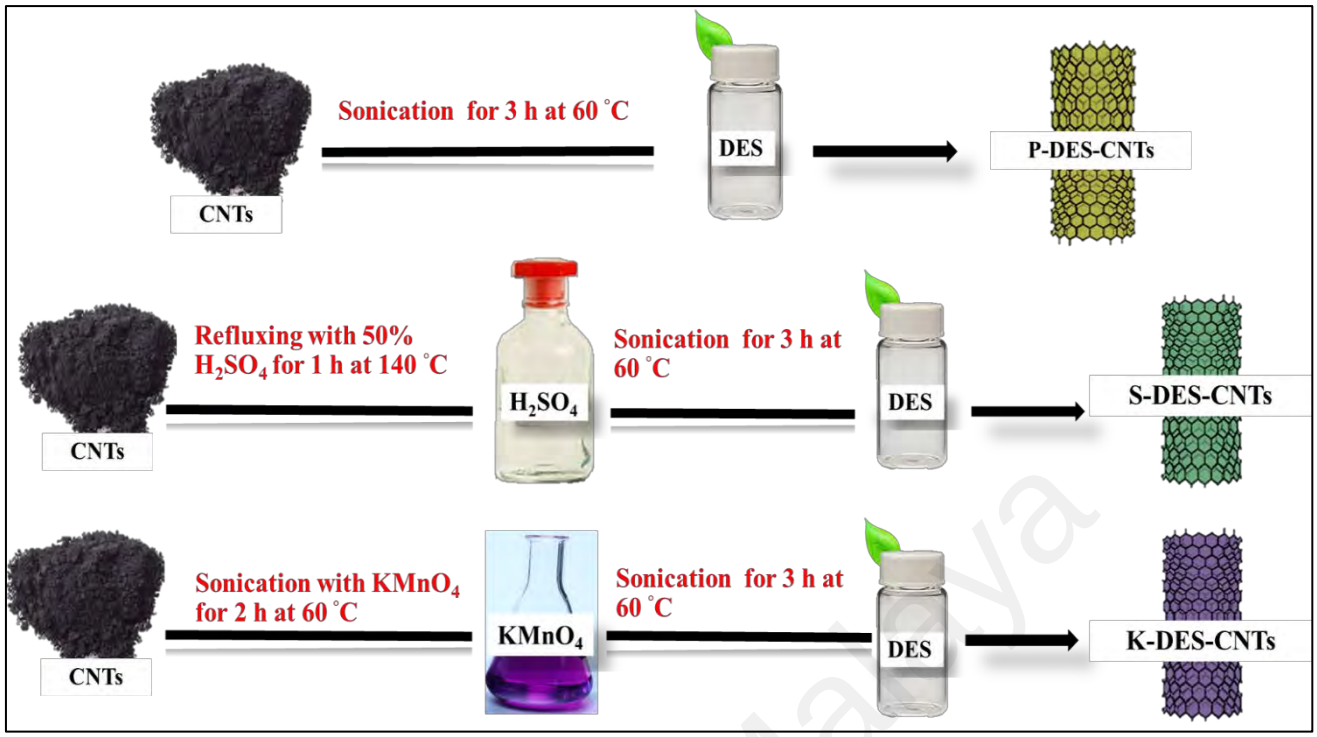

Figure 3.4: CNTs-functionalization methods

3.2.2.1 Acidification with sulfuric acids (H_2SO_4)

An amount of 500 mg of Pristine CNTs (P-CNTs) were dried overnight at 100 °C. Then the dried P-CNTs were refluxed with 50% H_2SO_4 for 1 h at 140 °C using reflux reaction apparatus to prepare S-CNTs. The mixture was then filtered using vacuum filtration system and washed with distilled water several times. The process repeated until the pH of the filtrate water became neutral. The filtered solid S-CNTs was dried and stored for further functionalization, adsorption and characterizations.

3.2.2.2 Oxidation with Potassium Permanganate ($KMnO_4$)

An amount of 200 mg of P-CNTs were dried overnight at 100 °C. The dried P-CNTs sample was then place in a glass vial (10 ml) containing 7 ml of $KMnO_4$ (1M) solution. An ultrasonic bath was used to sonicate the mixture of P-CNTs and $KMnO_4$ for 2 h at 60 °C to prepare K-CNTs. A vacuum filtration system was used to filter and wash the mixture with distilled water until the pH of the filtrate became 7. The filtered solid K-CNTs was dried and stored for further functionalization, adsorption and characterizations.

3.2.2.3 Functionalization with DES

Five DESs (EG based DESs) were used to functionalize three samples of CNTs (i.e. P-CNTs, S-CNTs and K-CNTs). A amount of 200 mg of each sample was sonicated separately with 7 ml of each selected DES in a glass vial for 3 h at 60 °C. The mixture was then filtered and washed using vacuum filtration system and dried under vacuum for 24 h at 60 °C. All produced DES-functionalized CNTs are listed in Table 3.3.

3.2.2.4 Characterization

Fourier transform infrared (FTIR) spectroscopy PerkinElmer® FTIR spectrometer was used to study the surface modification and the functional groups of CNTs after and before the functionalization process. Raman shift for all samples was obtained by Raman spectroscopy (Renishaw System 2000 Raman Spectrometer). The surface charge was evaluated by the zeta potential using Zetasizer (Malvern, UK). The thermal stability of all adsorbents was analyzed using thermogravimetric analysis (TGA) and differential thermogravimetry (DTG) by Thermal Analyzer (STA-6000, PerkinElmer®). FieldEmission Scanning Electron Microscope (JEOL Ltd., Japan. JSM-6700F) was used to obtain high resolution images to observe the morphology of all concerned adsorbents. The surface area for all examined samples was estimated using a fully Automated Gas Sorption System (micromeritics, TriStar II 3020, USA) based on the method of Brunauer-Emmett-Teller (BET).

3.2.3 Batch adsorption studies

Two organic pollutants namely, 2,4-dichlorophenol (2,4-DCP) and methyl orange (MO) were selected as samples to investigate the effectiveness of DES-CNTs combination as novel adsorbent. The adsorption processes for each pollutant went through four studies: screening, optimization, kinetic and isotherm studies. The

concentration of 2,4-DCP was determined using ultra high-performance chromatography (Waters ACQUITY UPLC System) at wavenumber of 285 nm (60 ACN: 40 MeOH). On the other hand, the concentration of MO was analyzed using a UV−visible spectrophotometer (Shimadzu UV-160A) at maximum wavelengths of 464 nm.

3.2.3.1 Screening of adsorbents for 2,4 DCP and MO

The primary adsorption screening was carried out to select the adsorbent with the highest removal efficiency for 2,4-DCP removal. A fixed dosage of each adsorbent (10 mg) was shaken at room temperature into 50 ml of 2, 4-DCP stock solution of 10 mg/L and into 50 ml of MO stock solution of 40 mg/L. The screening experiments for both pollutants were performed using a mechanical shaker at pH value of 6.5, contact time of 30 min and at a constant agitation speed of 180 rpm. Further characterization and studies were investigated for the adsorbents with the highest removal efficiency.

3.2.3.2 Optimization studies

Design expert software (version 7.0) was used to optimize the significant adsorption parameter for each adsorbent individually. The response surface was set as a type of study and the central composite design (CCD) was adopted to conduct the adsorption experiment. The optimum conditions for 2,4-DCP and MO adsorption was determined by setting removal efficiency (%) as responding model and by setting a range of three different parameters including, pH (2-10), dose (5-15 mg), and contact time (20-60 min). List of design of experiments runs is presented in Table 3.4.

Table 3.4: List of design of experiments runs and the actual values obtained from each response for all adsorbents

Run	Factors		
	A	B	C
1	2	5	20
2	6	15	40
3	2	5	60
4	10	5	20
5	10	10	40
6	10	15	20
7	2	15	60
8	6	10	40
9	10	15	60
10	6	10	60
11	6	10	20
12	10	5	60
13	2	15	20

A: pH, B: adsorbent dosage (mg) and C: contact time (min).

3.2.3.3 Adsorption kinetics

The adsorption kinetics experiment was conducted by employing the optimum conditions of each adsorbent suggested by design expert software. The initial concentration for 2,4-DCP and MO was 10 mg/L and 40 mg/L, respectively. The contact times used to define the most applicable kinetic model were (5 min, 10 min, 20 min, 30 min, 60 min, 120 min, 180 min and 24 h). Pseudo first order, pseudo second order and intraparticle diffusion models were applied on the experimental data.

(a) ***Pseudo-first order***

The kinetic process of the liquid/ solid adsorption system can be described by pseudo-first order equation which is developed by Lagergren in 1899. This equation is considered the primal model to describe the adsorption rate based on the adsorption capacity. The linearized form of Langergren equation can be presented as follow:

$$\ln(q_e - q_t) = \ln q_e - k_1 t \qquad (3.1)$$

where q_e and q_t (mg g^{-1}) are the amounts of the adsorbed solid at equilibrium and at time *t* (min), respectively, and k_1 is the adsorption rate constant (min^{-1}). The values of q_e and k_1 can be respectively acquired from the intercept and the slope of plots of $\ln(q_e - q_t)$ versus *t* (Figure 3.5). It is worth mentioning that this equation does not fit in most cases with all range of contact time, but it is generally applicable for short initial period of reaction.

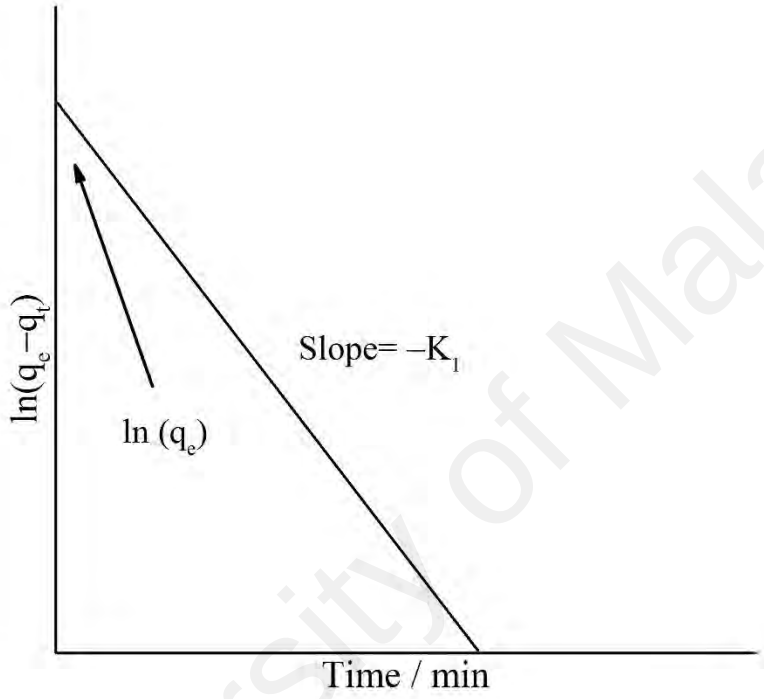

Figure 3.5: First-order kinetic model linear representation.

(b) ***Pseudo second order***

In 1995, Ho and Mckay suggested a pseudo-second order equation based on the amount of adsorbate adsorbed onto the adsorbent. The main assumption of this equation is that the adsorption process may be a second order process and the chemical adsorption can be the rate limiting step. It is well known that the chemical adsorption is usually involves the participation of valent forces in the adsorption process through sharing or the exchange of the electrons between the adsorbent and the adsorbate. The nonlinear form of pseudo-second order kinetic model is expressed as follow:

$$\frac{dq}{dt} = k_2(q_e - q_t)^2 \qquad (3.2)$$

where q_e (mg g^{-1}) is the amount of the adsorbed solid at equilibrium and k_2 (g mg^{-1} min^{-1}) is the rate constant of the second order adsorption. After integration of Eq (3.2), the linearized form of the pseudo-second order chemisorption kinetics rate equation can be obtained as follow:

$$\frac{t}{q_t} = \frac{1}{k_2 q_e^2} + \frac{t}{q_e} \qquad (3.2a)$$

The constants can be determined by plotting t/qt versus t (Figure 3.6), where the values of k_2 and q_e were obtained from the slope and the intercept of the plot, respectively.

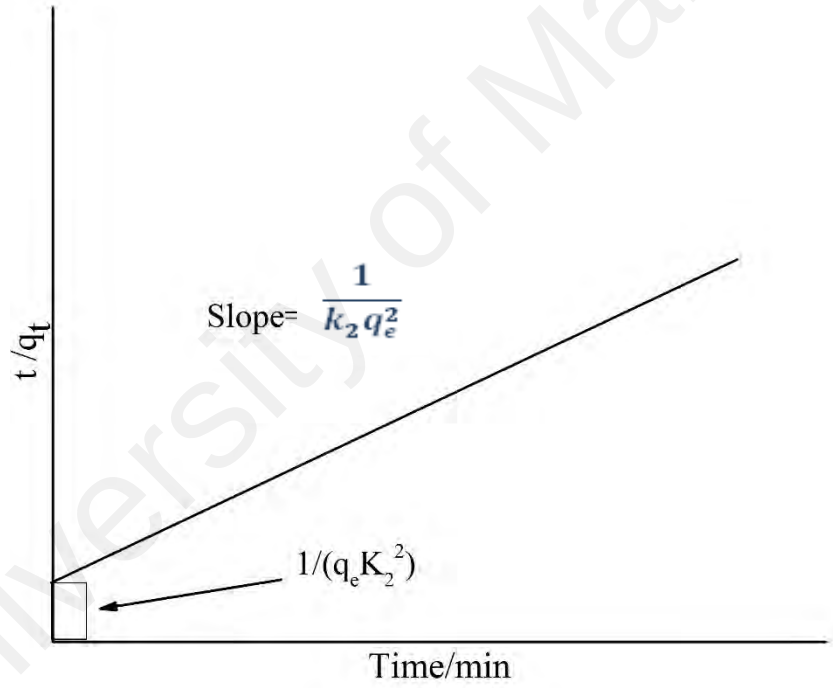

Figure 3.6: second-order kinetic model linear representation

(c) ***Intraparticle diffusion***

The involvement of the intraparticle diffusion (ID) in the adsorption mechanism can be tested by applying the Weber and Morris equation (2008) which proposes that in many adsorption cases, the adsorbate uptake change almost proportionally with $t^{0.5}$ rather than with contact time t:

$$q_t = K_d t^{0.5} + C \quad (3.3)$$

where q_t is the amount of pollutant adsorbed onto the adsorbents (mg g^{-1}) at time t (min), K_d is the initial rate coefficient of intraparticle diffusion (g mg^{-1} $min^{0.5}$) and C represents the initial value of q_t at time t=0. Both K_d and C can be obtained from the slope and the intercept of the plot of q_t versus $t^{0.5}$ (Figure 3.7).

According to Eq.(3.3), Intraparticle diffusion is the rate limiting step if the plot of q_t versus $t^{0.5}$ is a straight line. Moreover, for Weber and Morris model, intraparticle diffusion is the sole rate limiting step if the plot of q_t versus $t^{0.5}$ passes through the origin. However, in many adsorption cases the slope is not equal to zero which may be resulted from the simultaneous control of film diffusion and intraparticle diffusion on the adsorption kinetics (Qiu et al., 2009).

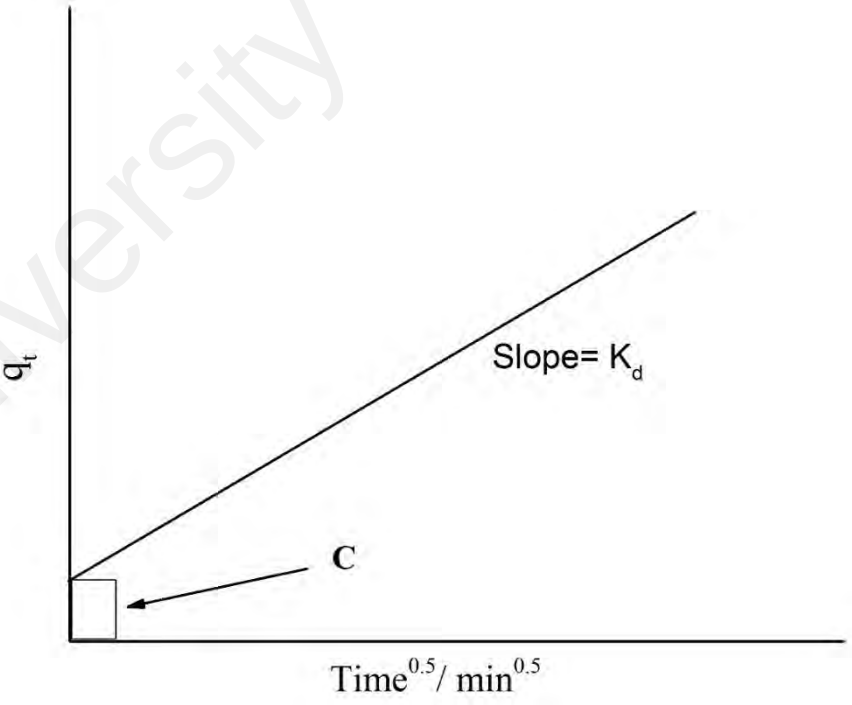

Figure 3.7: Intraparticle diffusion kinetic model.

3.2.3.4 Adsorption isotherms

Various initial concentration used for these experiments (5, 10, 20, 30, 40, 50, 60 and 80 mg/L) to achieve equilibrium conditions and the equilibrium concentration was recorded accordingly. The isotherm study covered the applicability of three isotherm models (e.g. Langmuir, Freundlich and Temkin isotherm models). The correlation coefficient (R^2) was calculated to determine the most appropriate isotherm model to describe the adsorption process.

(a) ***Langmuir isotherm***

The main assumption of Langmuir isotherm model is that a monolayer adsorption takes place at homogeneous sites onto adsorbent surface and when the molecule of adsorbate fills the site, saturation occurs and no further adsorption takes place at that site (Langmuir, 1918; Weber & Chakravorti, 1974). In addition, this model suggests that all the adsorption sites have equal adsorbate affinity and the that adsorption at one site does not influence adsorption at an adjacent site, the well-known linearized form of Langmuir equation is given as:

$$\frac{C_e}{q_e} = \frac{1}{K_L q_m} + \left(\frac{1}{q_m}\right) C_e \qquad (3.4)$$

where, c_e (mg L^{-1}) is the equilibrium concentration of adsorbate, q_e (mg g^{-1}) is the amount of adsorbate adsorbed per unit mass of the adsorbent. K_L and q_m are Langmuir constants related to adsorption equilibrium constant and maximum adsorption capacity, respectively. When C_e/q_e is plotted against C_e (Figure 3.8), the values of K_L and q_m can be evaluated correspondingly from the intercept and the slope of the linear line.

The value of the dimensionless constant equilibrium parameter (R_L) can be used to indicate the essential feature and the type of Langmuir isotherm: unfavorable ($R_L > 1$),

linear ($R_L = 1$), favorable ($0 < R_L < 1$) or irreversible ($R_L = 0$). The following equation is used to calculate R_L value:

$$R_L = \frac{1}{1+K_L C_i} \tag{3.5}$$

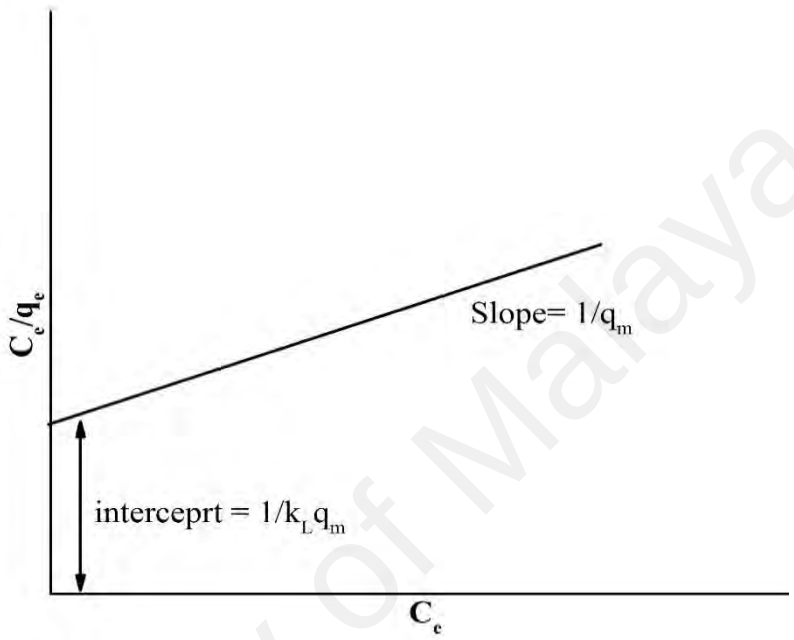

Figure 3.8: Langmuir adsorption isotherm model

(b) ***Freundlich isotherm***

Freundlich isotherm can be employed to describe heterogeneous systems by which the adsorption occurs onto surfaces supporting binding sites of diverse affinities (Freundlich, 1906). It is suggested that the adsorbate primarily occupies the stronger binding sites, and as the degree of site occupation increases the binding strength decreases (Tan, Ahmad, & Hameed, 2009). The Freundlich model is not limited to the formation of monolayers and it describes reversible adsorption process (Smith et al., 2016). The linearized Freundlich equation is expressed as below:

$$\ln q_e = \ln K_F + \frac{1}{n} \ln C_e \tag{3.6}$$

where, K_f and n are Freundlich isotherm constant and can be attained from the intercept and the slope of the linear line of the ln qe versus ln Ce plot (Figure 3.9). The distribution coefficient $K_{f,}$ represents the amount of adsorbate adsorbed onto adsorbent for a unit of equilibrium concentration (Haghseresht & Lu, 1998). While the heterogeneity factor 1/n defines the heterogeneity of the adsorbent surface (Hameed, Ahmad, & Aziz, 2007), and as its value gets closer to zero, the possibility of the adsorbent surface to become more heterogeneous increases (Haghseresht & Lu, 1998).

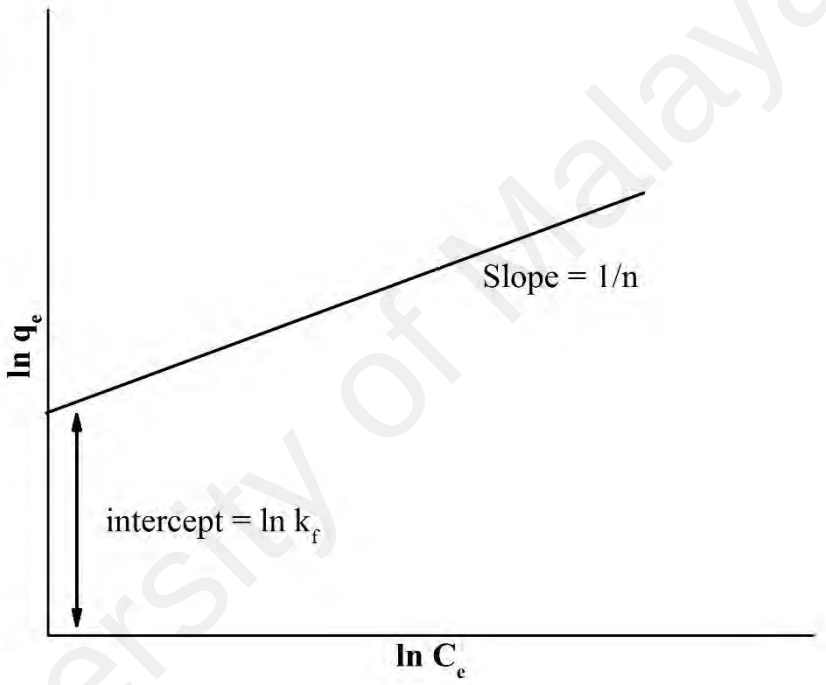

Figure 3.9: Freundlich adsorption kinetic model.

(c) ***Temkin***

The main theory of Temkin isotherm model considers the attraction between the adsorbent and adsorbate as the main reason that causes the heat of adsorption of all molecules in layer to decrease linearly rather than logarithmic with coverage (Dada et al., 2012). Also, the Temkin isotherm assumes that the adsorption is identified by a uniform distribution of the binding energies (up to some maximum binding energies) (Foo & Hameed, 2010). The Temkin model has generally been applied in the following linear form:

$$q_e = B_1 \ln k_t + B_1 \ln C_e \quad (3.7)$$

Where B_1 (dimensionless) = RT/b, b is the Temkin constant related to the heat of adsorption (J mol^{-1}), R the gas constant (8.314 J mol^{-1} K^{-1}), T the absolute temperature in kelvin (room temperature = 298.15 K), and k_t is the Temkin isotherm equilibrium binding constant (L mg^{-1}). If the adsorption obeys Temkin equation, its constants can be calculated from the slope and the intercept of the plot q_e versus ln C_e (Figure 3.10)

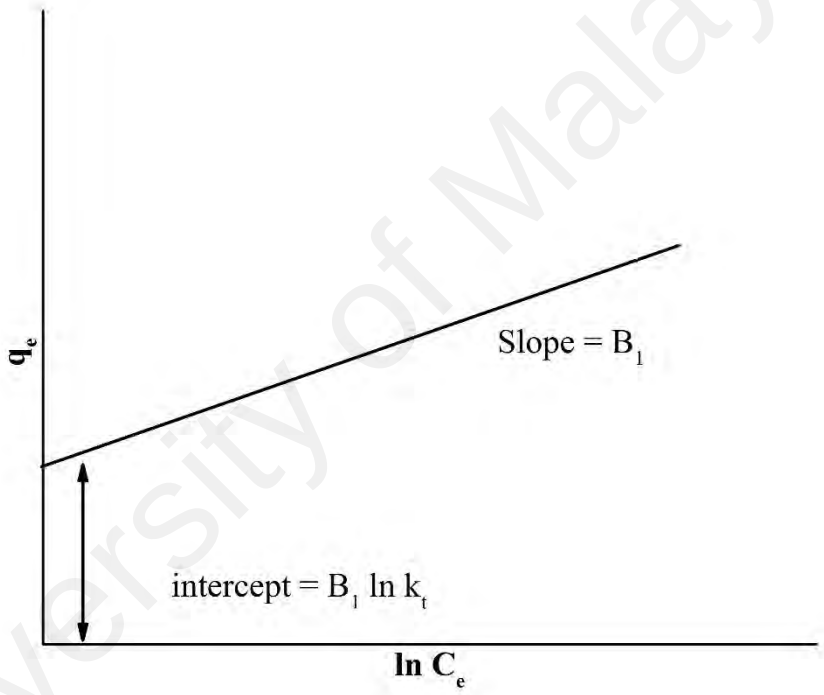

Figure 3.10: Temkin adsorption kinetic model.

CHAPTER 4: RESULTS AND DISCUSSION

4.1 DES preparation and characterization

4.1.1 Physical properties of system (1): EG based DESs

This system includes five DESs with EG as HBD and they are listed in Table 4.1 along with their abbreviations and calculated molecular weight.

4.1.1.1 Freezing point

As demonstrated by their definition, DESs have a freezing point lower than that of either their constituents (salt and the HDB) (Hayyan et al., 2010b) , and that was evident for the five DESs systems under consideration. The freezing points of the studied DESs are listed in Table 4.1, and as can be observed all the values are lower than that of EG (260.25 K), and lower than that of the five used salts (BTPC (610.15 K), MTPB (506.15 K), ChCl (578.15 K), TBAB (376.15 K), DAC (409.15 K)). The noteworthy depression of the freezing points is originated from the interaction between the anion of the salt and the HBD and it is affected by the type of interaction, the changes of entropy accompanying the liquid phase formation, and DESs lattice energies (Zhang, De Oliveira Vigier, et al., 2012b). The five studied DESs have promising potentials to be employed in separation and reaction applications due to their low recorded freezing points.

Table 4.1: Composition and abbreviations for the studied DESs.

Salt	HBD	Molar ratio	Abbreviation	Freezing point (T_f/K)
MTPB	**EG**	[1:3]	**[MTPB:EG]**	248.65
ChCl		[1:2]	**[ChCl:EG]**	236.89
DAC		[1:3]	**[DAC:EG]**	248.96
BTPC		[1:11]	**[BTPC:EG]**	248.43
TBAB		[1 :2]	**[TBAB:EG]**	248.22

4.1.1.2 FTIR

FTIR is a fingerprint analysis to identify the structure of unknown compounds as well as the amount of the components in a mixture. Figure 4.1, shows the spectral peaks of the

five DESs and it is noticeable that the spectrums of all the DESs are similar due to that the same HBD was used to synthesize all DES systems, which was asserted by the existence of O-H stretching bond between 3500-3200 cm^{-1} (Coates, 2000a; Stuart, 2004). The DESs spectra also show the peaks of alkanes stretching bands (C-H) of CH_2, CH_3 at 3200-2800 cm^{-1} and saturated ester stretching bands (O-C-C) at (1100-1030 cm^{-1}) (Smith, 1998). The effect of ammonium salts and phosphonium salts components on the structure of the examined DESs can be marked by the presence of N-H and P-H stretch, respectively, which may interlock with other fundamental stretching bands (O-H and C-H) of peaks at 3000–1700 cm^{-1} (Stuart, 2004; Weyer & Lo, 2006). In addition, peaks at 800-600 cm^{-1} are another proof of salts contribution to DESs structure, and these peaks represent the existence of halide ions (Br and Cl) (Coates, 2000a; Stuart, 2004). It is worth mention, that conducting the functional group analysis for DESs is a significant step to understand their structure to predict their applicability in a wide range of processes.

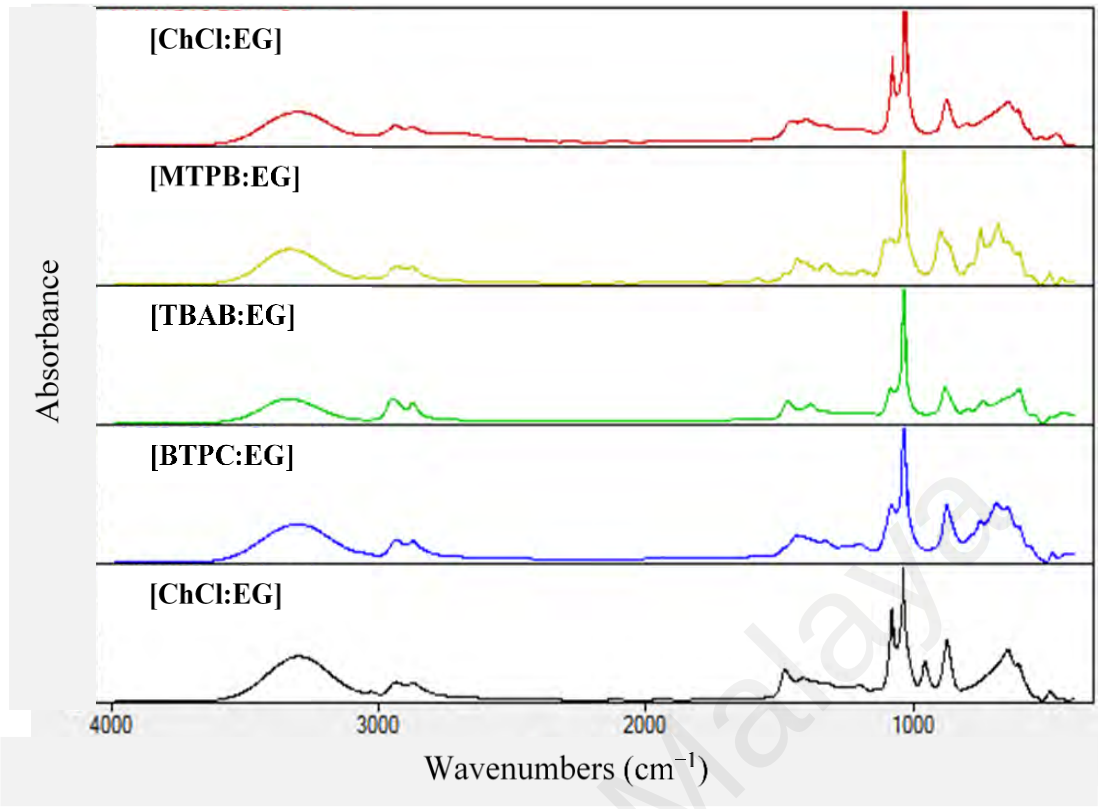

Figure 4.1: FTIR spectrums of EG-based DESs.

4.1.1.3 Density

Density is a substantial physical property to identify the nature of elements in environment and various industrial applications. The densities of the fives studied DESs were determined as functions of temperature. Figure 4.2 illustrates the temperature impacts on the densities of the synthesized DESs. As can be noticed, the highest density is that of [MTPB: EG] with a maximum density of 1.25 g.cm^{-3} at room temperature and a minimum density of 1.21 g.cm^{-3} at 353.15 K. The density of [ChCl:EG] was in the middle range as the maximum density was 1.12 g.cm^{-3} at room temperature and the minimum of 1.09 g.cm^{-3} at 353.15 K. The DES of [TBAB:EG] attained the lowest density with a maximum of 1.07 g.cm^{-3} at 293.15 K and a minimum of 1.03 g.cm^{-3} at the high temperature of 353.15 K . The recorded density of [ChCl: EG] at 293.15 K was obviously lower than that reported of DES synthesized from ChCl and malonic acid at molar ratio of 1:1 (1.37 g.cm^{-3} at 293.15 K) (Bahadori et al., 2013a). The density value of

[TBAB:EG] at 293.15 K was approximately similar to that of 1-butylimidazolium L-lactate (1.06 g.cm^{-3} at 293.15 K) (Pernak, Goc, & Mirska, 2004). For the full range of temperature, the densities of MTPB, BTPC and ChCl based DESs were higher than that of their HBD (EG); whereas the densities of DAC and TBAB based DES were lower than that of EG. Moreover, the densities of the studied DESs were highly affected by the volume of the molecular structure of both salts and HBD.

The density values of all studied DESs were decreased with increasing of temperature due to the additional thermal energy that earned by the molecules of DES and resulted in their vigorous mobility and lesser density. The relationship between the density and the temperature was extremely linear with a value of R^2 higher than 0.998 for all examined DESs. The following linear equation was fitted to the density-temperature relationship:

$$\rho = a + b\mathrm{T} \qquad (4.1)$$

where ρ is the density, T is temperature in centigrade, and *a* and *b* are constants (curve fit parameters, *a*: the intercept and *b*: the slope of the line), and their values are presented in Table 4.2.

Table 4.2: Density- temperature model parameters.

DES	*a*	*b*	R^2
[MTPB:EG]	1.45	-7×10^{-4}	0.99
[ChCl:EG]	1.27	-5×10^{-4}	0.99
[DAC:EG]	1.28	-6×10^{-4}	0.99
[BTPC:EG]	1.34	-7×10^{-4}	0.99
[TBAB:EG]	1.25	-6×10^{-4}	0.99

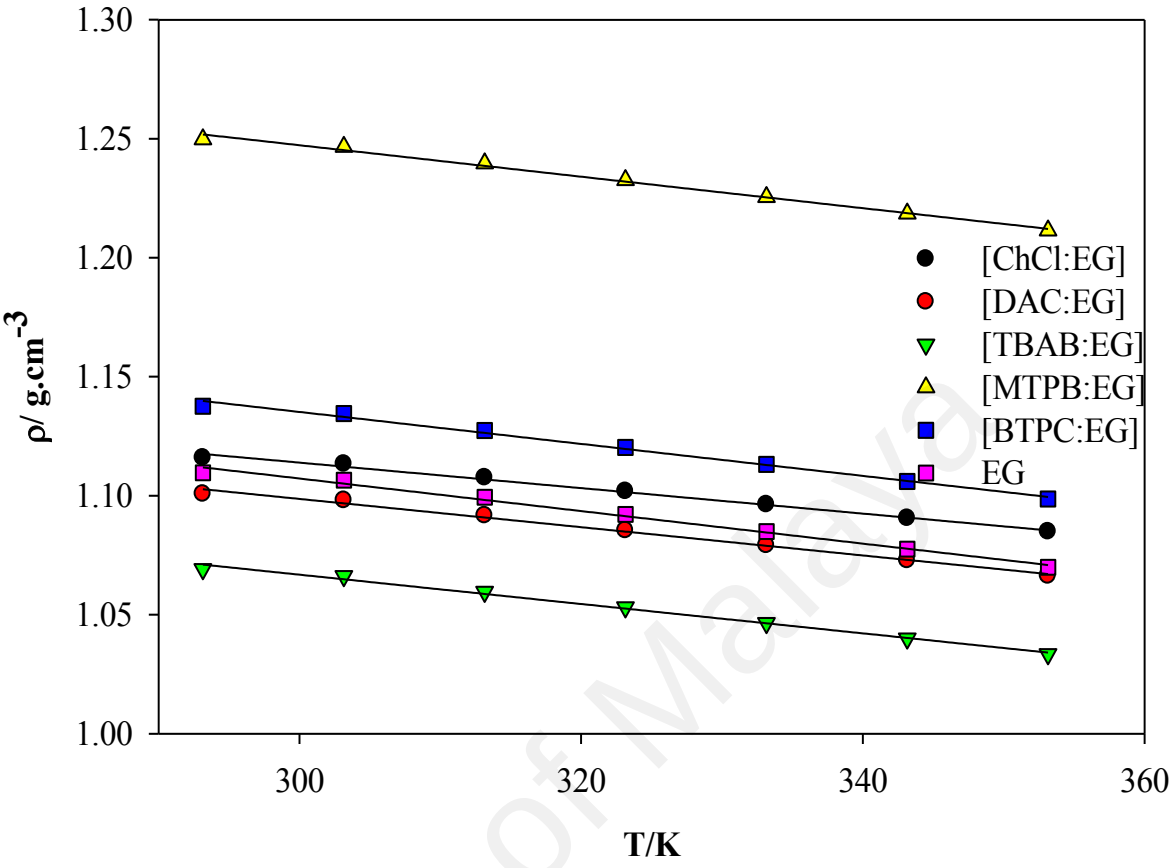

Figure 4.2: Densities for EG based DESs as a function of temperature.

4.1.1.4 Viscosity and conductivity

Conducting the viscosity analysis is of a significant concern to describe the fluidity of a solvent and its resistance to flowing. Furthermore, it is important to study the temperature effect on the viscosity of DESs to assess their applicability and predict the energy required for their processing.

Figure 4.3 depicts the viscosities of the five synthesized DESs as functions of temperature. It is obvious that all DESs viscosity values are much higher than that of EG, and they are obeying the following sequence: [TBAB:EG] > [MTPB:EG] > [BTPC:EG] > [ChCl:EG] > [DAC:EG]. At room temperature, the recorded viscosities of the considered DESs were similar to the reported viscosities of some of ILs; for example, the viscosity of [BTPC:EG] is same as that of 1,1-diallylpyrrolidinium

bis(trifluoromethanesulfonyl)imide (i.e. 57 cP at 293.15 K)(Yim et al., 2007); [TBAB:EG] and [MTPB:EG] viscosities data are almost similar to that of N-methoxyethyl-N-methyloxazolidinium (nonafluoro-n-butyl)trifluoroborate (i.e. 177 cP at 293.15 K)(Zhou, Matsumoto, & Tatsumi, 2006). In addition, the viscosities of [DAC:EG] and [ChCl:EG] were very low in comparison to DES prepared from DAC and malonic acid at ratio of (1:1) (541.1 cP at 298.15 K) (Bahadori et al., 2013a) and DES prepared from ChCl and urea at ratio of (1:2) (750 cP at 298 K)(Abbott, Harris, et al., 2011b), respectively. At 298 K, all DESs showed viscosity value extremely lower than that reported for [MTPB:Glycerol] (2775.9 cP) and then that of [ChCl:glycerol] (AlOmar, Hayyan, et al., 2016a). Based on this, it can be assumed that all concerned EG based DESs exhibit low viscosity in comparison to previously reported DESs.

It is well known that the viscosity of solvent is related to the free volume and the possibility of finding holes of proper dimensions which enable the movement of solvent molecules or ions (Klossek, Touraud, & Kunz, 2013; Schoettl et al., 2014). As a result, the viscosity value of DES is highly dependent on the nature of its components (the salt and HBD) (Zhang, De Oliveira Vigier, et al., 2012b), as well as on the size of DES cations and anions.

Temperature is considered one of the important factors that directly influence the viscosity behavior. Figure 4.3 shows that the viscosity is exponentially decreasing with the increase of temperature and this is similar to the trend of viscosity-temperature profile of some reported ILs (Ghatee et al., 2010). The temperature effects can be explained by the hole theory, which governs the mobility of species into the mixture (Abbott, 2004), when heating the DES mixture, the further energy added resulting in speeding up and spreading out the molecules (Hayyan et al., 2012a) leading to availability of large holes that permit the effortless movement of molecules passing each other and accordingly

decreasing the viscosity. The viscosity-temperature trend can be expressed by the following Arrhenius model (Giap, 2010a):

$$\mu = \mu_{\circ}\, e^{\left[\frac{E_{\mu}}{RT}\right]} \qquad (4.2)$$

where μ is the viscosity, $\mu_{\circ}$ is a preexponential factor, E_{μ} is the viscosity activation energy, R is the gas constant and T is temperature in centigrade. The values of Regression (R^2) are listed in Table 4.3.

Table 4.3: Viscosity- temperature model parameters.

DES	$\mu_{\circ}$	(E_{μ} R^{-1})	R^2
[MTPB:EG]	3×10^{-4}	3947.45	0.99
[ChCl:EG]	25×10^{-3}	2178.87	0.96
[DAC:EG]	25×10^{-3}	2144.94	0.98
[BTPC:EG]	3×10^{-3}	2906.31	0.99
[TBAB:EG]	7×10^{-4}	3663.59	0.97

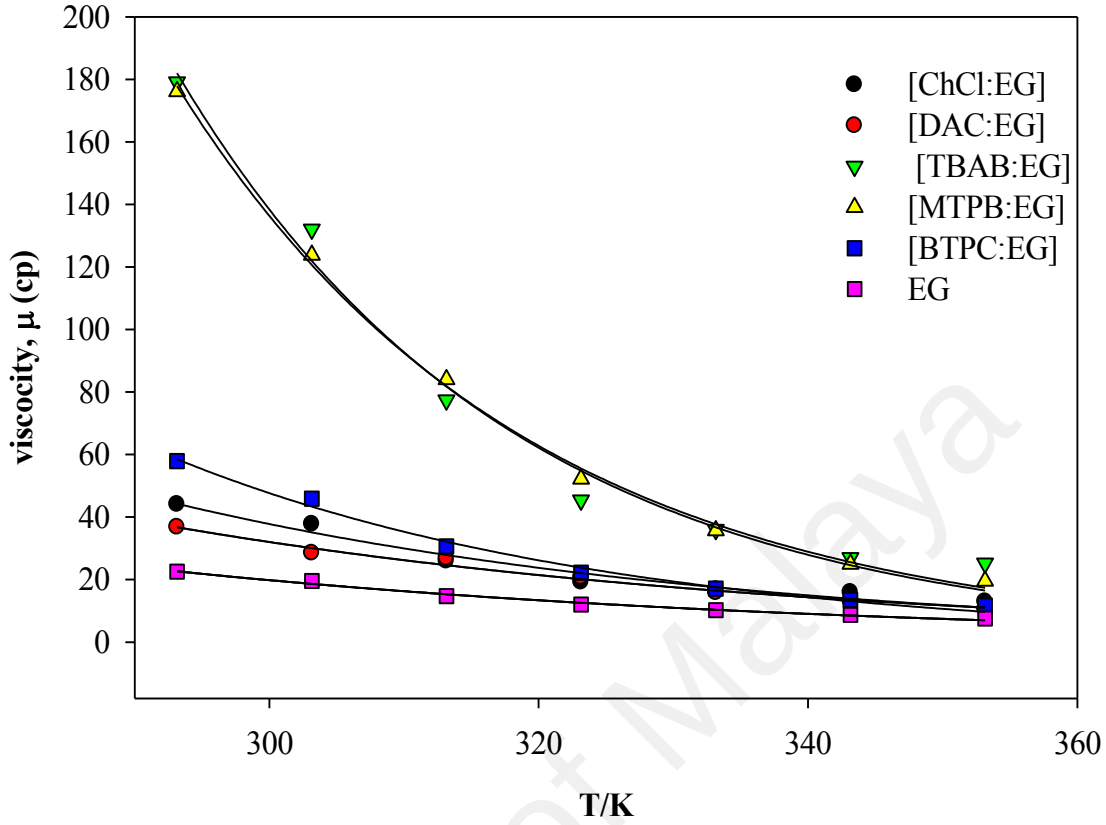

Figure 4.3: Viscosities for EG based DESs as a function of temperature.

On the other hand, the conductivity (S) measured values in Figure 4.4 show that the highly viscous DESs have the lower conductivity values which is proving the fact that the variation of conductivity values is inversely proportional to that of viscosity, for the simple reason that the motion level of the ionic species is governed by the consistency of the solvent. Moreover, high weight ratio of the salt in DESs structure contributes to higher conductivity and that can be noticed in Table 4.4, for example, [ChCl:EG] shows at room temperature, a higher conductivity (with a value of 7160 (μs/cm)) compared to [DAC:EG] (with conductivity value of 5270 (μs/cm)) due to the high salt ratio in its structure. However, [TBAB: EG] has the highest salt ratio amongst the five studied DESs, yet it attained the lowest conductivity value of 635 (μs/cm) at 293.15 K, due to its extremely high viscosity that restricts the transmission of the electrical currents.

The behavior of the conductivity at respect temperatures for the studied DESs was similar to that of viscosity but in the opposite direction, and it was fitted by the following Arrhenius equation (Vila et al., 2006a):

$$S = S_\circ \, e^{[\frac{-E_S}{RT}]} \qquad (4.3)$$

where S is the conductivity in (µs/cm), $S_\circ$ is pre-exponential factor, E_s is the activation energy of electrical conduction, R is the gas constant, and T is the temperature in K. Regression coefficient values for all five DESs are scheduled in Table 4.5.

Table 4.4: Salt ratio effect on DES conductivity.

DES	Salt ratio (g)	S (µs/cm)
[MTPB:EG]	65.73457	1133
[BTPC:EG]	36.28737	1399
[ChCl:EG]	52.9352	7160
[DAC:EG]	45.20979	5270
[TBAB:EG]	72.19759	635

Table 4.5: Conductivity- temperature model parameters.

DES	$S_\circ$	(E_sR^{-1})	R^2
[MTPB:EG]	2×10^6	-2176	0.99
[BTPC:EG]	2×10^6	-2038	0.96
[ChCl:EG]	1×10^6	-1464	0.98
[DAC:EG]	4×10^5	-1265	0.99
[TBAB:EG]	1×10^7	-2831	0.98

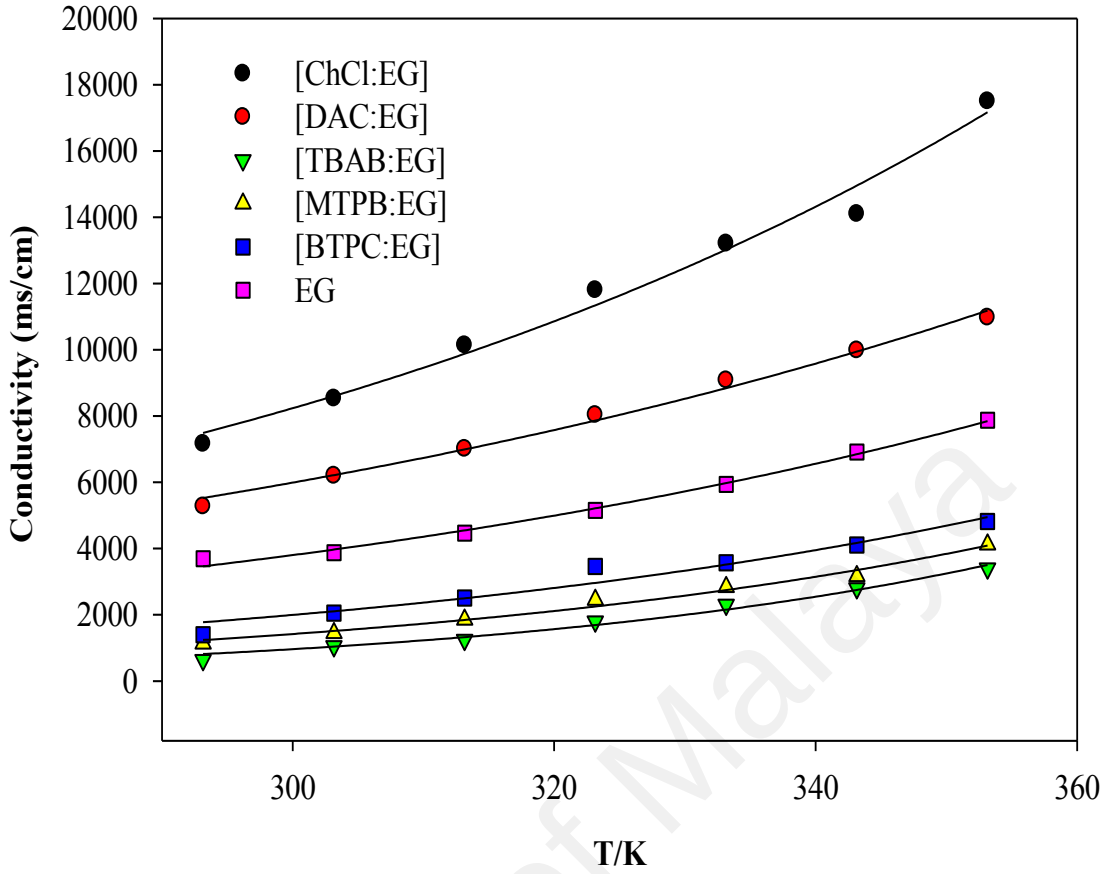

Figure 4.4: Conductivities for EG based DESs as a function of temperature.

4.1.1.5 Surface Tension

Determination of surface tension, can tremendously give an interpretation and understanding of the intermolecular forces intensity between the molecules in the mixture (Shahbaz, Mjalli, et al., 2012). It is a very essential physical factor to be encountered in different types of industrial and chemical applications and most commonly those that depend on their systems wettability (Karbowiak, Debeaufort, & Voilley, 2006).

At room temperature, the surface tension for the whole examined DESs, were higher than that of tetrabutylammonium chloride and EG based DES system (Mjalli et al., 2014a), with values of 58.74, 74.55, 53.31, 73.59, 66.93 mN m^{-1} for [ChCl:EG], [DAC:EG], [TBAB:EG], [MTPB:EG], [BTPC:EG] respectively. Some of the studied DESs have the same surface tension of ILs but at different temperature, for example, at (323.15 K) the surface tension value of [MTPB:EG] is similar to that of 1-amyl-3-

methylimidazolium tetrachloroaluminate at 288.15 K (with a value of 43.1 mN m^{-1}) (Tong et al., 2006), while at 343.15 K its surface tension is the same as that of 1-butyl-3-methylimidazolium bis trifluoromethylsulfonylimide at 298.15 K (a value of 37.5 mN m^{-1}) (Huddleston et al., 2001).

The variation of surface tension of the five studied DESs with the temperature is presented in Figure 4.5 The surface tension of DESs depended on the composition and thermal activity of DES mixture and this was obvious when the increase in temperature reduced the cohesive forces of surface tension, due to the increasing of the kinetic energy of the DESs molecules. Additionally, the decline in surface tension for [ChCl:EG] against temperature followed a trend of a lower slope in comparison with the other studies DESs and that can be ascribed to effect of choline chloride salt in thermally stabilizing the DES mixture. The trend of surface tension was linearly fitted according to the following relationship:

$$\sigma = a + b\mathrm{T} \qquad (4.4)$$

where σ is the surface tension, T is the temperature, and a and b are constants (curve fit parameters, a: the intercept and b: the slope of the line), and their values are shown in Table 4.6.

Table 4.6: Surface tension- temperature model parameters.

DES	a	b	R^2
[MTPB:EG]	252.09	-0.6216	0.95
[ChCl:EG]	158.75	-0.3508	0.95
[DAC:EG]	290.89	-0.7255	0.94
[BTPC:EG]	265.05	-0.6702	0.96
[TBAB:EG]	228.71	-0.5951	0.97

.

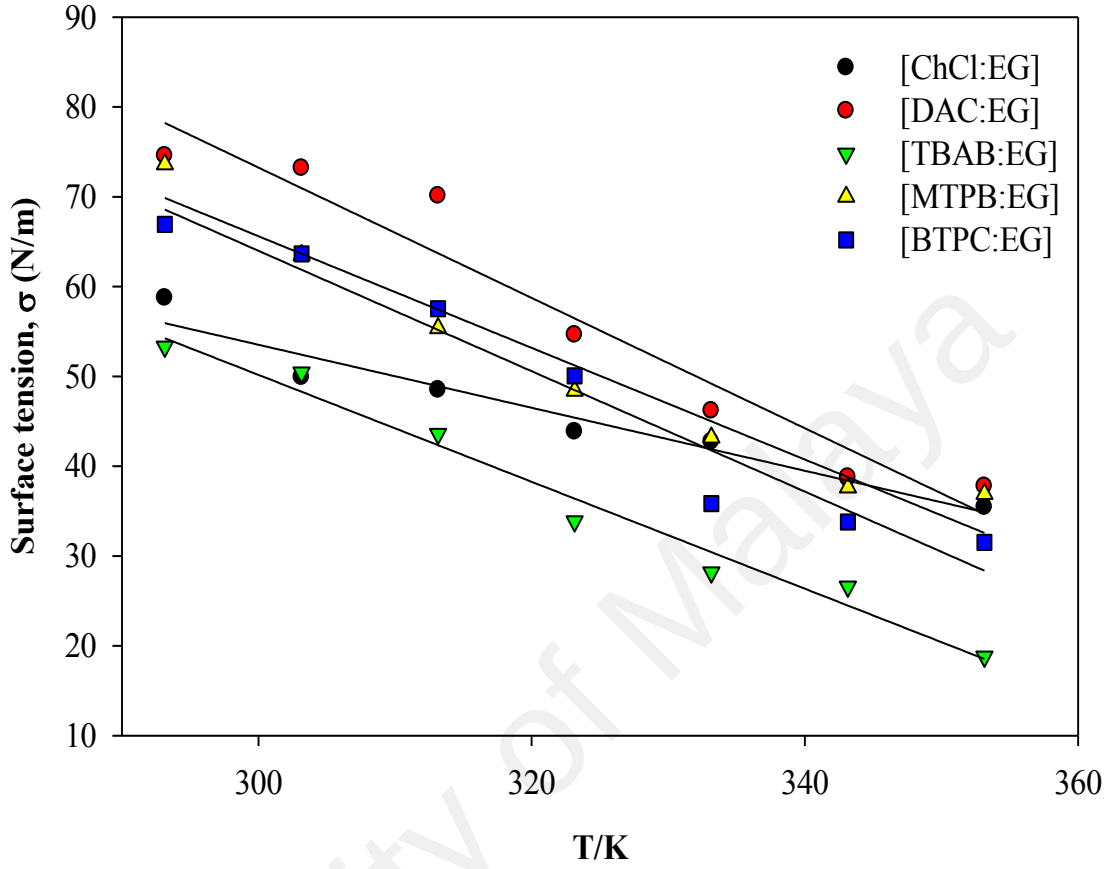

Figure 4.5: Surface tension of EG based DESs as function of temperature.

4.1.2 Physical properties of system (2): DEG based DESs

This system involves five DESs with DEG as HBD and they are listed in Table 4.7 along with their abbreviations and calculated molecular weight.

Table 4.7: Composition and abbreviations for the studied DESs

Salt	**Salt Molar ratio**	**HBD**	**HBD Molar ratio**	**DES Abbreviation**	**DES molecular weight**	**Freezing point.[a] (T_f/K)**
ChCl	1	DEG	2	[ChCl:DEG]	117.288	260.52
DAC	1		3	[DAC:DEG]	118.002	262.39
TBAB	1		2	[TBAB:DEG]	178.202	247.92
BTPC	1		7	[BTPC:DEG]	141.463	248.52
MTPB	1		4	[MTPB:DEG]	156.340	248.39

[a] Freezing point value represents the average point between the first crystal appearance and the last liquid drop disappearance. All freezing point data are reported at pressure of 0.1 MPa

4.1.2.1 Freezing point

The selected series of DESs are in liquid form under room-temperature conditions, which facilitate their exploitations in different industrial applications. The freezing point of DES can be partially measured by the melting points of the pure components parts, and it is dependent on the entropy changes, lattice energy and on the way of interaction between cation and anion components (Liu, Chen, & Xing, 2014). The melting points of the salts used in this study, i.e., BTPC, MTPB, ChCl, DAC, and TBAB, are 603.15, 507.15, 575.15, 409.15, and 376.15 K, while the freezing point of DEG is 264.15 k. Table 4.7 displays the freezing points of the five studied DESs. All the values are in agree with the general definition of DES that characterize the DES mixture with a lower freezing point than that of its individual constituents. As can be concluded from the data, the freezing points range between 247.92- 262.39 K, with the highest freezing point for [DAC: DEG] while the lowest freezing point for [TBAB:DEG]. All the recorded freezing points were below 323.15 K, and as reported by Zhang (Zhang, De Oliveira Vigier, et al., 2012a), DESs with freezing points lower than 323.15 K are more attractive to be employed as cheap and safe ambient temperature solvents in many different fields.

4.1.2.2 FTIR

The result of FTIR analysis is shown in Figure 4.6 indicates that the pure constituents of DESs (salt-HBD) have obvious effects on the structure of the DESs. The effect of DEG as HBD can be noticed in all DESs spectrums at peaks between 3500-3200 cm^{-1}, representing the O–H stretching bond (Coates, 2000b; Smith, 1998; Stuart, 2004). Moreover, due to the utilization of DEG as HBD in the current DESs synthesizing process, the spectral peaks of the examined DES systems are virtually alike. On the other hand, the effect of salts can be inferred from the existence of the P–H bonds in the structure of phosphonium based DESs, which could be overlapped with C–H bands at the region between 3000-2800 cm^{-1} (Smith, 1998; Stuart, 2004). In addition, the effect of salts on ammonium based DESs assimilated in the presence of ammonium structures between 3200-2400 cm^{-1}, mainly N–H stretch at 2870 cm^{-1} (Luo, Conrad, & Vankelecom, 2012; Roeges, 1994; Smith, 1998). For all examined DESs, the intense absorption bands at (800-700 cm^{-1}) and (700-600 cm^{-1}) were assigned to aliphatic organohalogen compounds with stretching bonds (C–Cl) and (C–Br) respectively (Coates, 2000b). Furthermore, the strong bonds ranging from (1200-1050 cm^{-1}), (1600-1800 cm^{-1}), and (1400-1340 cm^{-1}) are assigned to C–O, C=O and N–O correspondingly. The stretch PO_4^{-3} at (1100-1000 cm^{-1}) (Coates, 2000b; Smith, 1998) was strong and broad in [MTPB:DEG] and [BTPC:DEG] while peaks at (1310-1230 cm^{-1}) (Coates, 2000b; Smith, 1998) representing C–N stretch, were explicit in [ChCl:DEG], [DAC:DEG], and [TBAB:DEG].

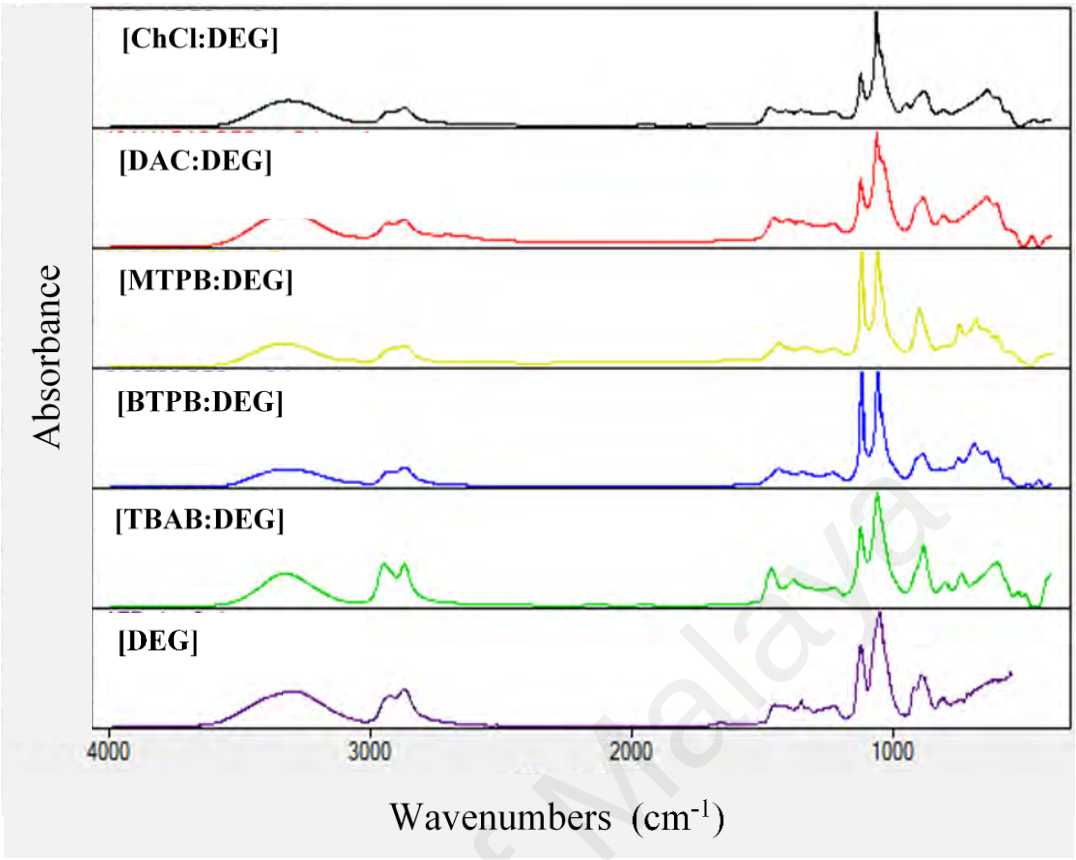

Figure 4.6: FTIR Spectra of DEG based DESs

4.1.2.3 Density

The density values of the five selected DESs as function of temperature are illustrated in Figure 4.7. At room temperature, [MTPB:DEG] attained the highest density of 1.209 g.cm^{-3}, whereas [TBAB:DEG] attained the lowest density of 1.078 g.cm^{-3}. At 293.15 K, the density of [ChCl:DEG] (1.1216 g.cm^{-3}) was found to be similar to that of [ChCl: EG] (1.12 g.cm^{-3}) (Abbott, Harris, et al., 2011b; Shahbaz, Baroutian, et al., 2012a),and lower than that of [ChCl:urea] (1.25 g.cm^{-3}) (Abbott et al., 2007a; Abbott, Capper, & Gray, 2006a). Additionally, [MTPB:DEG] had a density value of 1.209 g.cm^{-3} which was lower than the reported density for [MTPB:GL] (1.30 g.cm^{-3}) (Kareem et al., 2010b), and slightly higher than that reported for [MTPB: TEG] (1.19 g.cm^{-3}) (Shahbaz et al., 2011).

The calculated densities using the simple mixing rule (Eq. 4.5)(Williams, Svrcek, & Monnery, 2003) were found to be incompatible with the recorded experimental densities and that indicates the interaction of both components molecules and confirms the

hydrogen bonding formation which reduces the molecular distance between the salt and HBD.

$$\frac{1}{\rho_m} = \sum_i \frac{x_i}{\rho_i} \quad (4.5)$$

where ρ_m is the density of DES mixture (gm.cm^{-3}), x_i is mass fraction of component *i*, and ρ_i is the density of component *i* (gm.cm^{-3}).

Moreover, the densities of the examined DESs series decreased with the increase of temperature due to the effects of the increased internal energy on the mobility of DES molecule resulting in increasing the thermal expansion of DES volume (Mjalli et al., 2014b).

For all examined DESs, the density-temperature relationship was fitted linearly using the following equation with regression values R^2 of 0.99:

$$\rho = a + b\mathrm{T} \quad (4.6)$$

where ρ is the density, T is temperature in kelvin, and *a* and *b* are constants and their values are listed in Table 4.8.

Table 4.8: Density- temperature model parameters.

DES	*a*	*b*	R^2
[ChCl:DEG]	1.2932	-0.0006	0.99
[DAC:DEG]	1.2922	-0.0006	0.99
[TBAB:DEG]	1.2581	-0.0006	0.99
[BTPC:DEG]	1.3358	-0.0007	0.99
[MTPB:DEG]	1.4055	-0.0007	0.99

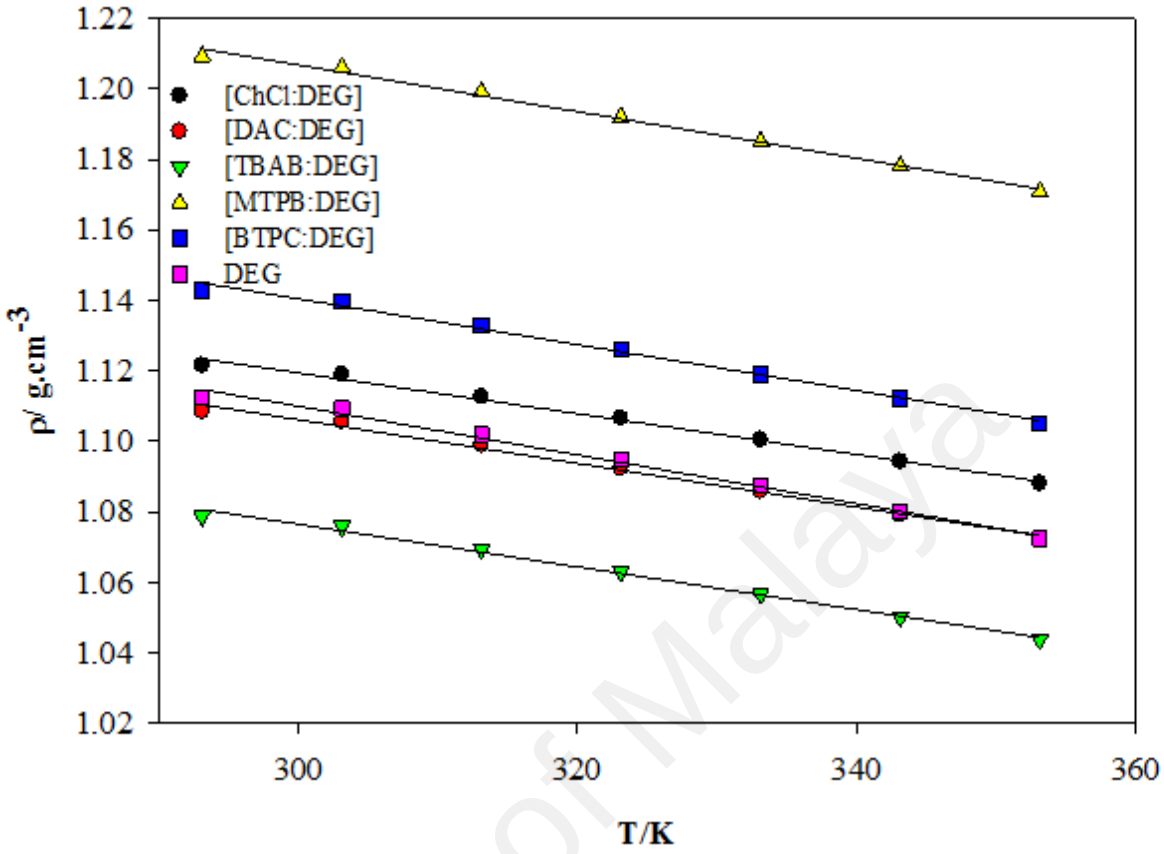

Figure 4.7: Densities for DEG based DESs as a function of temperature.

4.1.2.4 Viscosity and conductivity

The values of viscosity and conductivity are the prominent attributes of DESs to be utilized as significant candidates as an electrolyte in electrochemical applications such as batteries, electroplating, electrolysis, etc. Figure 4.8 and Figure 4.9 elucidate the effect of temperature on the viscosity and the electrical conductivity of the studied DESs, respectively. For all selected DESs, the noted values of viscosity and conductivity were determined at temperature range of (293.15-353.15 K), and both physical properties for DESs were higher than those for DEG. At room temperature, the deliberated DESs series had the following viscosity sequence: [TBAB:DEG] > [MTPB:DEG] > [BTPC:DEG] >

[DAC:DEG] > [ChCl:DEG]; while their conductivity order was as following: [ChCl:DEG] > [DAC:DEG] > [MTPB:DEG] > [BTPC:DEG] > [TBAB:DEG]. It is noticeable that DES with the highest viscosity, attained the lowest conductivity value due to the extreme high consistency of DES mixture that constrained the transmission of the electrical current through the mixture. Another significant factor that have a perceptible impact on the viscosity and conductivity values is the ratio of salt in the DES mixture. Table 4.9 depicts that although [MTPB:DEG] has a higher viscosity than that of [BTPC:DEG], it recorded a higher electrical transmission ability due to its high salt ratio content; moreover, it can be concluded from Table 4.9 that DES viscosity data is relatively proportional to the ratio of salt in DESs. It is noteworthy, that the temperature has an adverse influence on the viscosity because of the energetic motion gained by DESs molecules when the temperature increases, resulting in reducing the strength of intermolecular forces, decreasing the mixture viscosity and consequently increasing its conductivity. Comparing the current considered DESs systems with previous works, reveals that at 293.15 K, [ChCl:DEG] had a viscosity of 52.49 cP higher than that of [ChCl: ethylene glycol] (37.0 cP) (Abo-Hamad et al., 2015), lower than that of [TBAC:EG] (>200 cP) (Mjalli et al., 2014b) and extremely lower than that of [Chcl: zinc chloride] (85000 cP) (Abbott, Capper, et al., 2004a). Also, the viscosity of [MTPB:glycerol] was reported to be very high (2775.9 cP) at 298 K (AlOmar, Hayyan, et al., 2016b), while the viscosity of [MTPB:DEG] in this study was found to be comparatively low (141.3 cP) at 293.15 K. All the recorded viscosities of the concerned DESs at 353.15 K were much lower than the lowest viscosities values reported for triethylene glycol (TEG) based DESs (Hayyan, Abo-Hamad, et al., 2015a).

On the other hand, the conductivity of [DAC:DEG] (2040 $\mu S.cm^{-1}$) at 298.15 K was found to be higher than that of [DAC: malonic acid] (1130 $\mu S.cm^{-1}$) and much lower than that of [DAC: zinc nitrate] (7050 $\mu S.cm^{-1}$) (Bahadori et al., 2013b). The conductivity of

[ChCl:DEG] at 293.15 was found to be (2670 μS.cm^{-1}) which is higher than that of [ChCl: 1,4-butanediol] (1654 μS.cm^{-1}) (Abbott, Harris, & Ryder, 2007a) and that of [ChCl: triethanolamine] (650 μS.cm^{-1}) (Bahadori et al., 2013b). It is worth mentioning that in this study ChCl salt based DES had attained the lowest viscosities and the highest conductivities among all DESs and that was similar to the reported case of ChCl salt based DES with Glycerol (GLY) as HBD (AlOmar, Hayyan, et al., 2016b).

The trend of viscosity-temperature can be expressed with a regression value (R^2) higher than 0.97 for all DESs by the following Arrhenius-like equation (Giap, 2010b):

$$\mu = \mu_{\circ}\, e^{\left[\frac{E_{\mu}}{RT}\right]} \tag{4.7}$$

where μ is the viscosity, $\mu_{\circ}$ is a pre-exponential factor, E_{μ} is the viscosity activation energy, R is them gas constant and T is temperature in K. The model parameter values are listed in Table 4.10.

The trend of conductivity-temperature is similar to that of viscosity-temperature but in the opposite direction and it can also be fitted using the following Arrhenius model (eq 4) (Vila et al., 2006b):

$$S = S_{\circ}\, e^{\left[\frac{-E_S}{RT}\right]} \tag{4.8}$$

where S is the conductivity in (μs/cm), $S_{\circ}$ is pre-exponential factor, E_s is the activation energy of electrical conduction, R is the gas constant, and T is the temperature in K. The model parameter and the regression coefficient values for all five DESs are arranged in Table 4.11.

Table 4.9: Salt ratio effect on the viscosity and conductivity (At 293.15 K).

DES	Salt ratio	μ (cP)	S (μs/cm)
[ChCl:DEG]	30.49	52.49	2670
[DAC:DEG]	32.55	56.09	1940
[TBAB:DEG]	60.3	203.9	325
[BTPC:DEG]	34.36	124.8	466
[MTPB:DEG]	45.7	141.3	618

Table 4.10: Viscosity- temperature model parameters

DES	$\mu_\circ$	($E_\mu R^{-1}$)	R^2
[ChCl:DEG]	7×10^{-3}	2654.02	0.97
[DAC:DEG]	3×10^{-3}	2908.94	0.98
[TBAB:DEG]	4×10^{-4}	3892.81	0.99
[BTPC:DEG]	6×10^{-4}	3599.62	0.99
[MTPB:DEG]	3×10^{-4}	3784.48	0.98

Table 4.11: Conductivity- temperature model parameters.

DES	$S_\circ$	($E_S R^{-1}$)	R^2
[ChCl:DEG]	6×10^{5}	-1584.26	0.98
[DAC:DEG]	6×10^{5}	-1697.13	0.99
[TBAB:DEG]	1×10^{7}	-3010.37	0.99
[BTPC:DEG]	2×10^{6}	-2461.27	0.98
[MTPB:DEG]	2×10^{7}	-2960.37	0.98

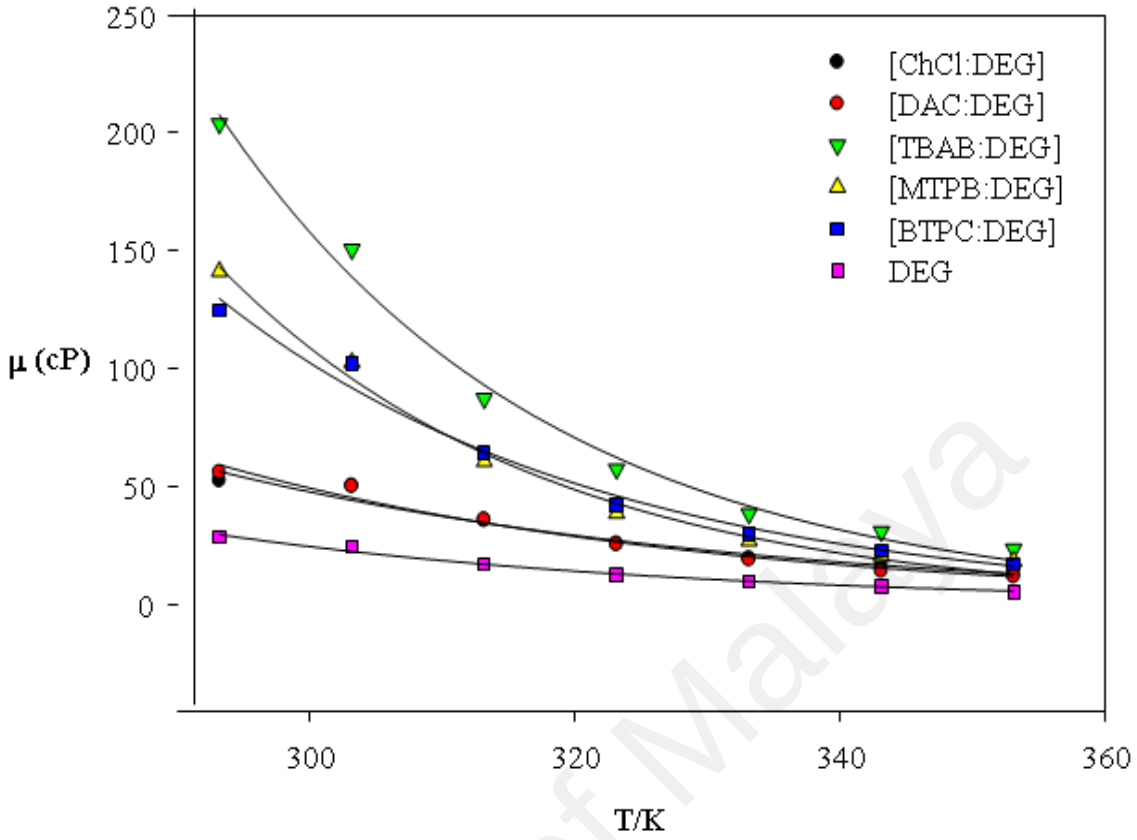

Figure 4.8:Viscosities for DEG based DESs as a function of temperature.

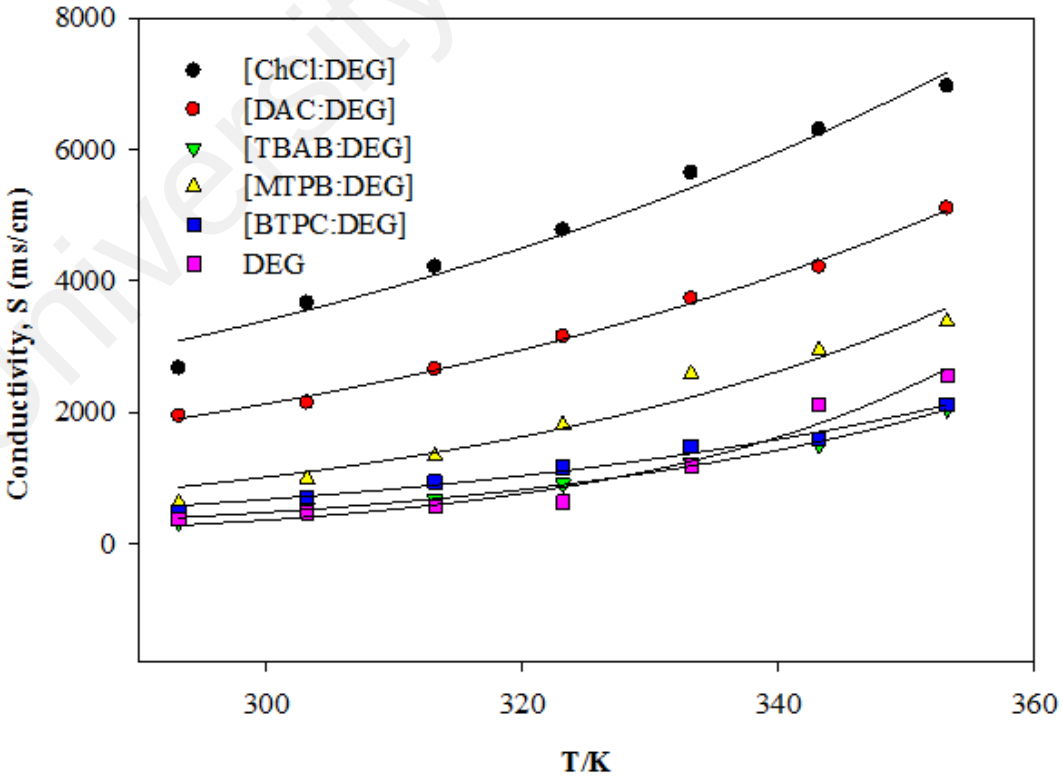

Figure 4.9: Conductivities for DEG based DESs as a function of temperature.

4.1.2.5 Surface tension

The surface tension is one of the important properties that affects the reactivity of DESs and it is one of the crucial liquid characterization that is required in many industries. Figure 4.10, represents the surface tension of the studied DESs as function of temperature. At 293.15 K, the highest surface tension value was 66.98 mN m^{-1} for [MTPB:DEG], while the lowest surface tension value was 48.49 mN m^{-1} for [ChCl:DEG]. At 353.15 K, the surface tension of [MTPB:DEG], [ChCl:DEG] and [DAC:DEG] were almost the same with a value of 33.0 mN m^{-1}. Comparatively, at 313.15 K, the surface tension of [ChCl:DEG] (42.82 mN m^{-1}) was higher than that of [ChCl: 2,2,2-trifluoroacetamide] (35.9 mN m^{-1}) (Abbott, Capper, & Gray, 2006a). Meanwhile, at room temperature [ChCl:DEG] had a surface tension value (48.49 mN m^{-1}) lower than that of [zinc chloride:ethylene glycol] (56.9 mN m^{-1}) (Zhang, De Oliveira Vigier, et al., 2012a) and that of [ChCl:malonic acid] (65.7 mN m^{-1})(Smith, Abbott, & Ryder, 2014b) .

As expected, the trend of the surface tension-temperature is similar to that of viscosity-temperature, since both of the properties are highly dependent on the strength of the molecular interaction that rules the formation of DES mixture (Zhang, De Oliveira Vigier, et al., 2012a). As can be simplified from Figure 4.10, when the temperature increases, the surface tension of DES decreases because of the reduced effects of the cohesive forces between the surface molecules which is resulted from the vibrant motion of molecules due to the thermal expansion (Mjalli et al., 2014b). The surface tension-temperature relationship was linearly fitted according to the following equation:

$$\sigma = a + b\mathrm{T} \qquad (4.9)$$

where σ is the surface tension, T is the temperature in K, and a and b are constants. The model parameters along with the regression coefficient values (R2) are shown in Table 4.12.

Table 4.12: Surface tension- temperature model parameters

DES	*a*	*b*	R^2
[ChCl:DEG]	115.0892	-0.2297	0.98
[DAC:DEG]	233.3722	-0.5631	0.94
[TBAB:DEG]	170.1202	-0.3932	0.95
[BTPC:DEG]	238.0510	-0.5840	0.95
[MTPB:DEG]	249.7380	-0.6098	0.95

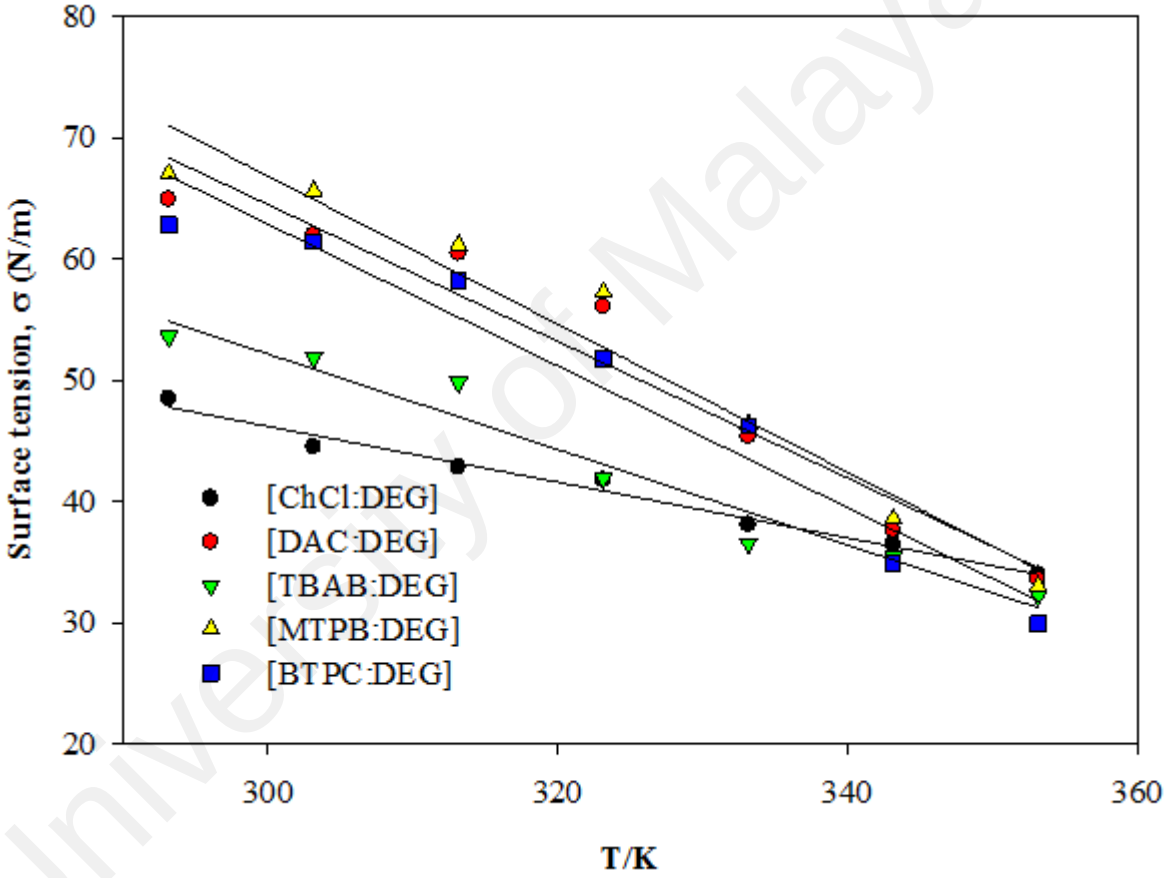

Figure 4.10: Surface tension for Di-ethylene glycol based deep eutectic solvents as a function of temperature.

4.2 Application of DESs-functionalized carbon nanotubes for organic pollutant removal from aqueous solution.

4.2.1 Characterization of DES-functionalized CNTs

4.2.1.1 Primary Screening

The characterization process was merely conducted for the adsorbents with the highest removal efficiencies. This was determined based on the results from a separate primary screening study which was carried out for the two examined pollutants (2,4-DCP and MO). The primary screening for 2,4-DCP was performed using 18 different adsorbents and the results is visualized by Figure 4.11. It is noticeable that all adsorbents treated with $KmnO_4$/ $KmnO_4$ + DESs exhibited the lowest removal efficiency for 2,4-DCP. Four adsorbents (i.e. P-CNTs, S-CNTs, PChCl-CNTs and SChCl-CNTs) recorded the highest removal efficiency for 2,4-DCP and they were selected for further characterization and adsorption studies.

Furthermore, Figure 4.12 represents the primary screening conducted for 12 different adsorbents to select the ones with the highest efficiency for the removal of MO from aqueous solution. It is also obvious that after modifying carbon nanotubes with KmnO4/ or KmnO4 + DESs, the removal of MO was shapely diminished which may be ascribed to the adsorbent surface charge. The adsorbents treated with [ChCl:EG] DES and [DAC:EG] DES showed the highest removal efficiency therefore, they were chosen for further characterization and adsorption studies.

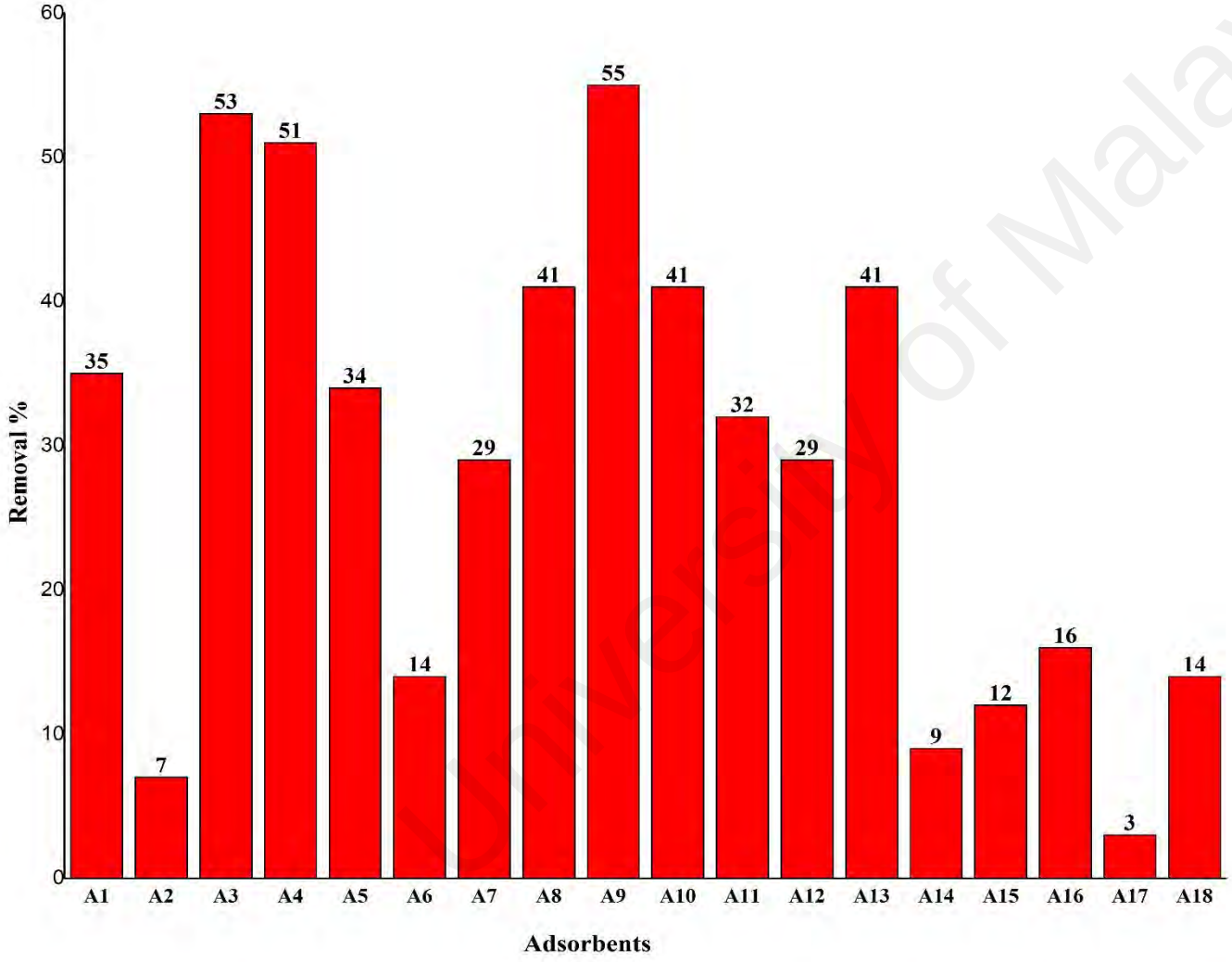

Figure 4.11: Primary screening of adsorbents for 2,4-DCP removal from water.

Adsorbents

A1	:	P-CNTs
A2	:	K-CNTs
A3	:	S-CNTs
A4	:	PChCl-CNTs
A5	:	Pn,n-CNTs
A6	:	PTBAB-CNTs
A7	:	PBTPC-CNTs
A8	:	PMTPB-CNTs
A9	:	SChCl-CNTs
A10	:	Sn,n-CNTs
A11	:	STBAB-CNTs
A12	:	SBTPC-CNTs
A13	:	SMTPB-CNTs
A14	:	KChCl-CNTs
A15	:	Kn,n-CNTs
A16	:	KTBAB-CNTs
A17	:	KBTPC-CNTs
A18	:	KMTPB-CNTs

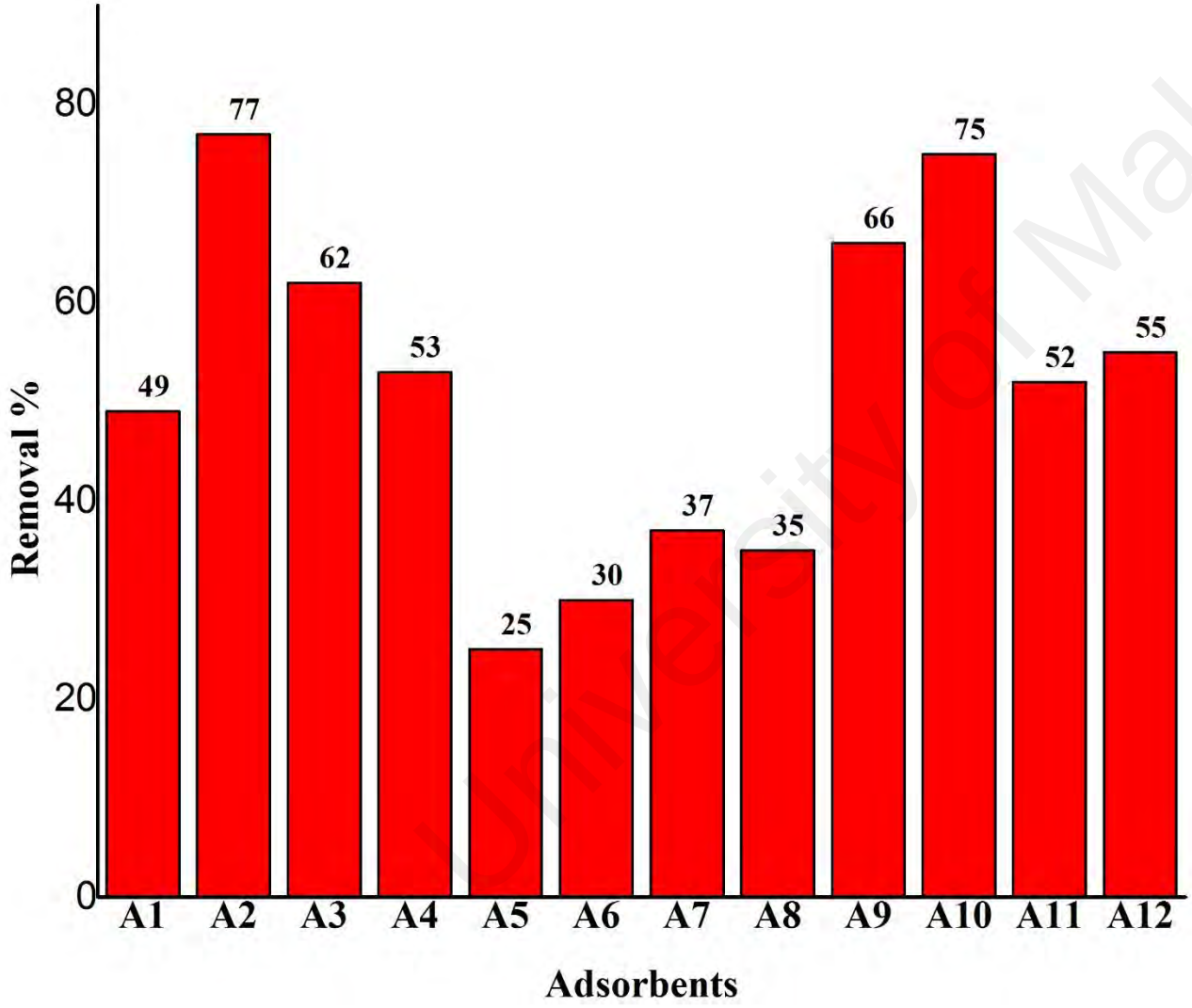

Figure 4.12: Primary screening of adsorbents for MO removal from water.

Adsorbents		
A1	:	P-CNTs
A2	:	PChCl-CNTs
A3	:	Pn,n-CNTs
A4	:	PMTPB-CNTs
A5	:	K-CNTS
A6	:	KChCl-CNTs
A7	:	Kn,n-CNTs
A8	:	KMTPB-CNTs
A9	:	S-CNTs
A10	:	SChCl-CNTs
A11	:	Sn,n-CNTs
A12	:	SMTPB-CNTs

4.2.1.2 Raman spectroscopy

Raman spectroscopy has valuably played a key role in the study and characterization of various carbon based nanostructures. Thus, in this study Raman spectroscopy was carried out to identify and compare the changes occurred in the structure of pristine CNTs after each treatment.

As can be noticed from Figure 4.13 that for all concerned samples there are two obvious sharp peaks detected at ~1350 and ~ 1590 cm^{-1} wavelength. The peak at 1300-1400 cm^{-1} is the D band which is a defect-induced mode caused by sp3-hybridized carbon atoms in the sidewall of CNT (Bahr et al., 2001; Ying et al., 2003) and is often attributed to the existence of amorphous and disordered carbon in the CNT samples (Datsyuk et al., 2008; Ferrari et al., 2006). While peaks at 1550-1680 cm^{-1} is the G band which is a common tangential mode to all sp2 carbon systems and it is raised from the stretching of C-C bond in graphitic materials (Dresselhaus et al., 2010). Moreover, D', is also a defect or disorder induced Raman feature presented by a weak shoulder of the G-band, can be clearly found in P-CNTs and PChCl-CNTs at 1609 cm^{-1} and 1612 cm^{-1} wavelength, respectively. Whereas for S-CNTs, SChCl-CNTs and Pn,n-CNts, D' cannot be detected demonstrating a better quality of these adsorbents . Another Raman feature is the radial breathing mode (RBM), which is considered important in identifying the tube diameter(Dresselhaus et al., 2010). However, RBM was too weak to be detected for all concerned CNTs adsorbents and that proves the large diameter of their tubes (Datsyuk et al., 2008).

Furthermore, Raman spectroscopy can be a symptomatic characterization of the degree of carbon-containing defects of adsorbents by calculating the ratio of D band to G band intensities (I_D/I_G) (Tsai & Chen, 2003). The values of I_D/I_G for all adsorbents are listed in Table 4.13. It is evident from the Table 4.13 that I_D/I_G for P-CNTs has been increased from 1.11 to 1.20 after treatment with [ChCl:EG] DES and that gives an

indication of new sp3-hybridized functional groups formation on the P-CNTs surface (AlOmar, Alsaadi, Hayyan, Akib, & Hashim, 2016). It is also apparent from Table 4.13 that the I_D/I_G value of P-CNTs has decreased after treatment with H_2SO_4 and [DAC:EG] which suggests that the modified adsorbents (S-CNTs and Pn,n-CNTs) has less carbon-containing defects and more graphitized structures (Lu et al., 2008). However, the value of I_D/I_G of S-CNTs has increased slightly after treatment with [ChCl:EG] which may be due to the increased level of covalent functionalization on the surface of SChCl-CNTs.

Table 4.13: Intensities and location of Raman spectroscopy bands.

Adsorbent	D band		G band		D' band		I_D/I_G
	Wave No.	Intensity	Wave No.	Intensity	Wave No.	Intensity	
P-CNTs	1349	1942	1589	1710	1609	1558	1.11
S-CNTs	1358	1114	1592	1056	———	———	1.05
PChCl-CNTs	1353	1023	1594	846	1612	741	1.2
SChCl-CNTs`	1353	1131	1588	1044	———	———	1.08
Pn,n-CNTs	1350	2085	1586	1888	———	———	1.10

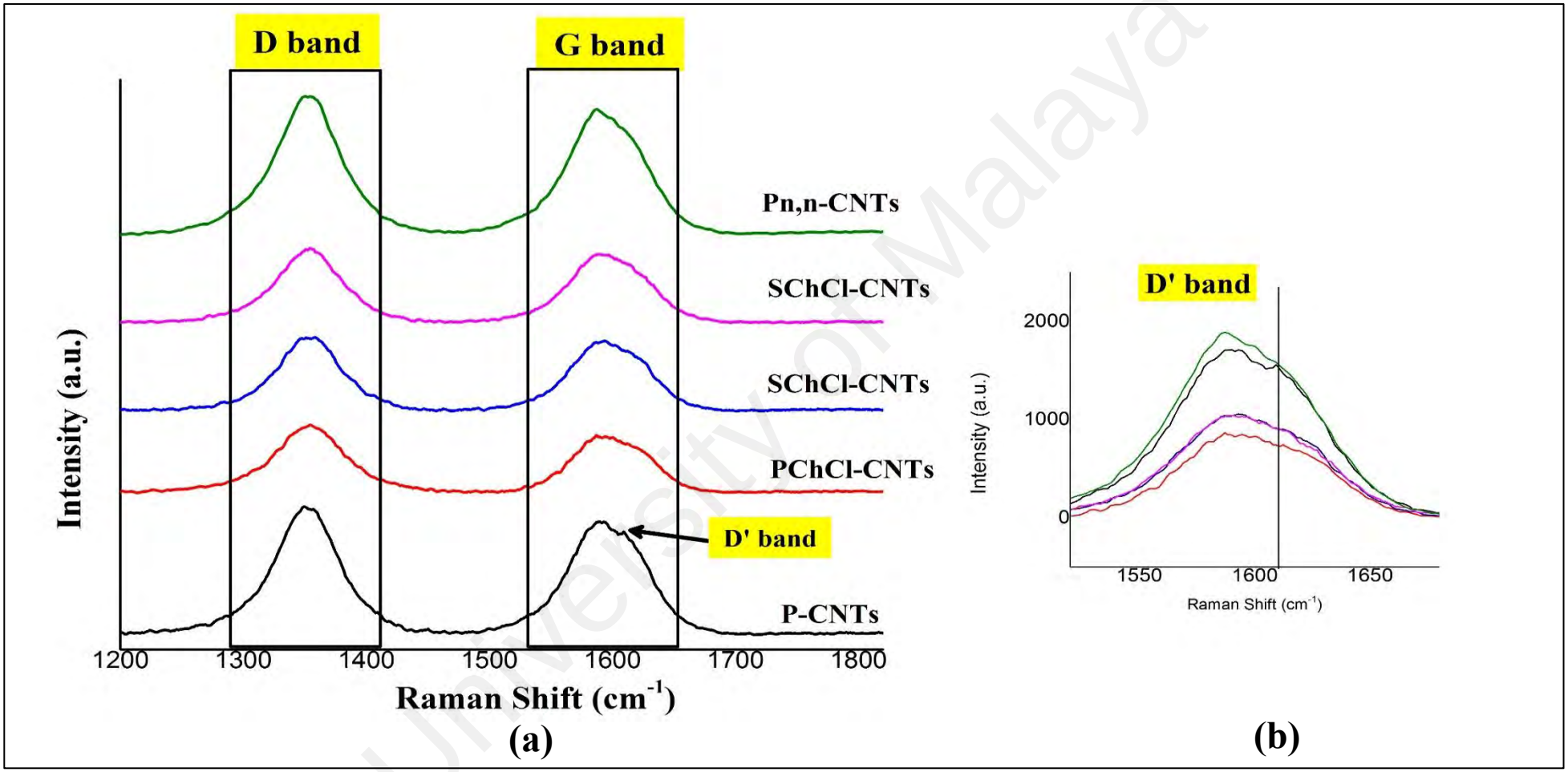

Figure 4.13: Raman spectroscopy for a) D band and G band and b) D' band shift.

4.2.1.3 Surface Chemistry analysis (FTIR)

Fourier transform infrared (FTIR) spectroscopy is a prevalent method to investigate the surface chemistry in term of functional groups. It is worth mentioning that the adsorption efficiency of any adsorbent depends on the chemical reactivity of its surface and the various forms of oxygen containing functional groups. Being that, FTIR was essentially used in this study to confirm the functionalization of CNTs by inspecting the formation of new functional groups. Figure 4.14 displays the FTIR spectra for all examined adsorbents. Obviously, there is a significant change in the spectrum of P-CNTs after treatment with acid and DESs which confirms their capability as functionalization agents of adding new and abundant functional groups onto the surface of P-CNTs. The strong absorbance peak at ~ 3460 cm^{-1} for all functionalized CNTs is assigned to O−H stretching bond (hydroxyl groups) (Coates, 2000a). However, O−H may overlap with N−H stretching bond in the region of (3500-3000) cm^{-1} (Das, Maiti, & Khatua, 2015). The emergence of peaks at ~ 3750 cm^{-1} after functionalization are assigned to C−H stretching bond. Furthermore, Asymmetric and symmetric stretching of CH_2 groups are highly detectable at ~ 2900 cm^{-1} and ~ 2800 cm^{-1} , respectively (Machado et al., 2011a). All adsorbents showed an obvious peak around 2350 cm^{-1} indicative of aromatic sp2 C−H stretching vibration (Maiti & Khatua, 2013). Moreover, the production of carbonyl groups (C=O) and carboxyl groups (–COOH) onto P-CNTs after functionalization is symbolized by the presence of peaks at ~ 1400 and ~ 1650 cm^{-1} (Sheng, Shao, et al., 2010). The increased intensity of these oxygen containing functional groups after treatment with DESs indicating their abundance onto the external and the internal surfaces of functionalized CNTs pores which provides more adsorption sites (Lu, Chung, & Chang, 2006) and thereby enhances the adsorption capacity of DESs functionalized CNTs. Additionally, the dispersion of functionalized CNTs in aqueous solution was improved due to the hydrophilic traits of the aforementioned functional groups (Yang et

al., 2009). Peaks in the region between (800-600) cm^{-1} are assigned to C-Cl bond for all [ChCl:EG] treated adsorbents (AlOmar, Alsaadi, Hayyan, Akib, Ibrahim, et al., 2016). The main source of $=CH_2$ and C−H functional groups onto DES functionalized CNTs could be the constituents of the used DESs, either from salt and/ or HBD (Abo-Hamad et al., 2017). Moreover, Functionalization of P-CNTs with H_2SO_4 produced different bonds containing sulfur such as C−S stretching (700-600) cm^{-1} and SO_2 symmetric stretching (1153) cm^{-1} (Stuart). Table 4.14 summarizes some of expected functional groups onto studied adsorbents.

Table 4.14: Some of the predicted functional groups on the surface of the studied adsorbents

Expected functional groups	Involving adsorbents
C−H stretching	ALL
C=O	ALL
C=C−C Aromatic ring stretch	ALL
S−S stretching	SChCl-CNTs, S-CNTs.
C-S stretching	SChCl-CNTs, S-CNTs.
SO_2 symmetric and asymmetric stretching	SChCl-CNTs, S-CNTs.
S=O stretching	SChCl-CNTs.
$O-CH_3$	P-CNTs, S-CNTs, SChCl-CNTs.
C−Cl	PChCl-CNTs, SChCl-CNTs.
N–H stretching Third overtone	PChCl-CNTs, SChCl-CNTs, Pn,n-CNTs.

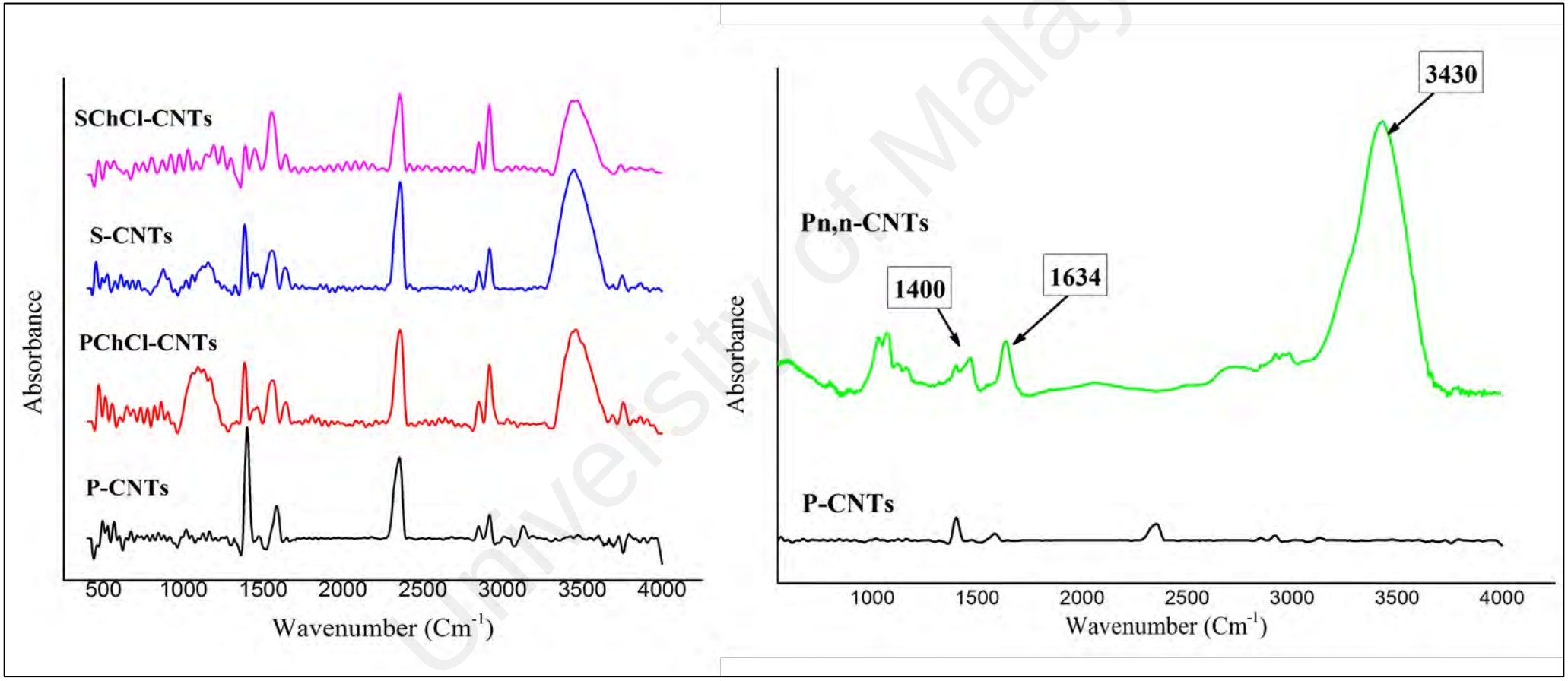

Figure 4.14: FTIR spectrums for pristine and functionalized CNTs

4.2.1.4 Thermogravimetric analyses (TGA)

To investigate the oxidation behavior of the studied adsorbents, thermal gravimetric analysis was performed under air flow rate of 50 mL/min at a temperature range of (25-800) °C with a heating rate of 10 °C/min. It is noteworthy that higher activation energies are required for oxidizing well graphitized carbons (Datsyuk et al., 2008). On the other hand more active sites are available on the amorphous or disordered carbons, consequently dropping off their activation energies for oxidation (Hou et al., 2001). Figure 4.15 shows the thermogravimetric analyses (TGA) curves for all adsorbents. The combustion profiles of all samples propose that P-CNTs possess the highest thermal stability and purity compare to the other functionalized CNTs. Furthermore, three regions can be observed for each adsorbent TGA curve. The first region is attributed to the loss of adsorbed water and it is remarked by the initial gradual weigh loss of 1% for P-CNTs, S-CNTs, SChCl-CNTs and PChCl-CNTs, and 7% for Pn,n-CNTs at around 150 °C. The weight of all samples declines constantly until the onset combustion temperature is reached at 526.6 °C, 510.06 °C, 530.28 °C, 516.9 °C and 403.8 °C for P-CNTs, PChCl-CNTs, S-CNTs, SChCl-CNTs and Pn,n-CNTs, respectively. Subsequently the second region starts where a steep drop occurs due to the decarboxylation of carboxylic functional groups and the elimination of hydroxyl functional groups onto the walls of CNTs (Grandi et al., 2006; Tang, Dou, & Sun, 2006). The final stage begins at temperature higher than 500 °C where the weight loss of the samples is caused by the thermal oxidation of the remaining amorphous carbon (Hou et al., 2001). It can be noticed from TGA profiles, that the combustion rate for DES-functionalized CNTs, especially for Pn,n-CNTs, was relatively higher than that for P-CNTs. This can be assigned to the role of the used DESs by adding new oxygen and carbon containing functional groups onto

P-CNTs as shown by FTIR analysis. The purity of all samples was affirmed by the zero percentage of residues left at the end of their thermal oxidation.

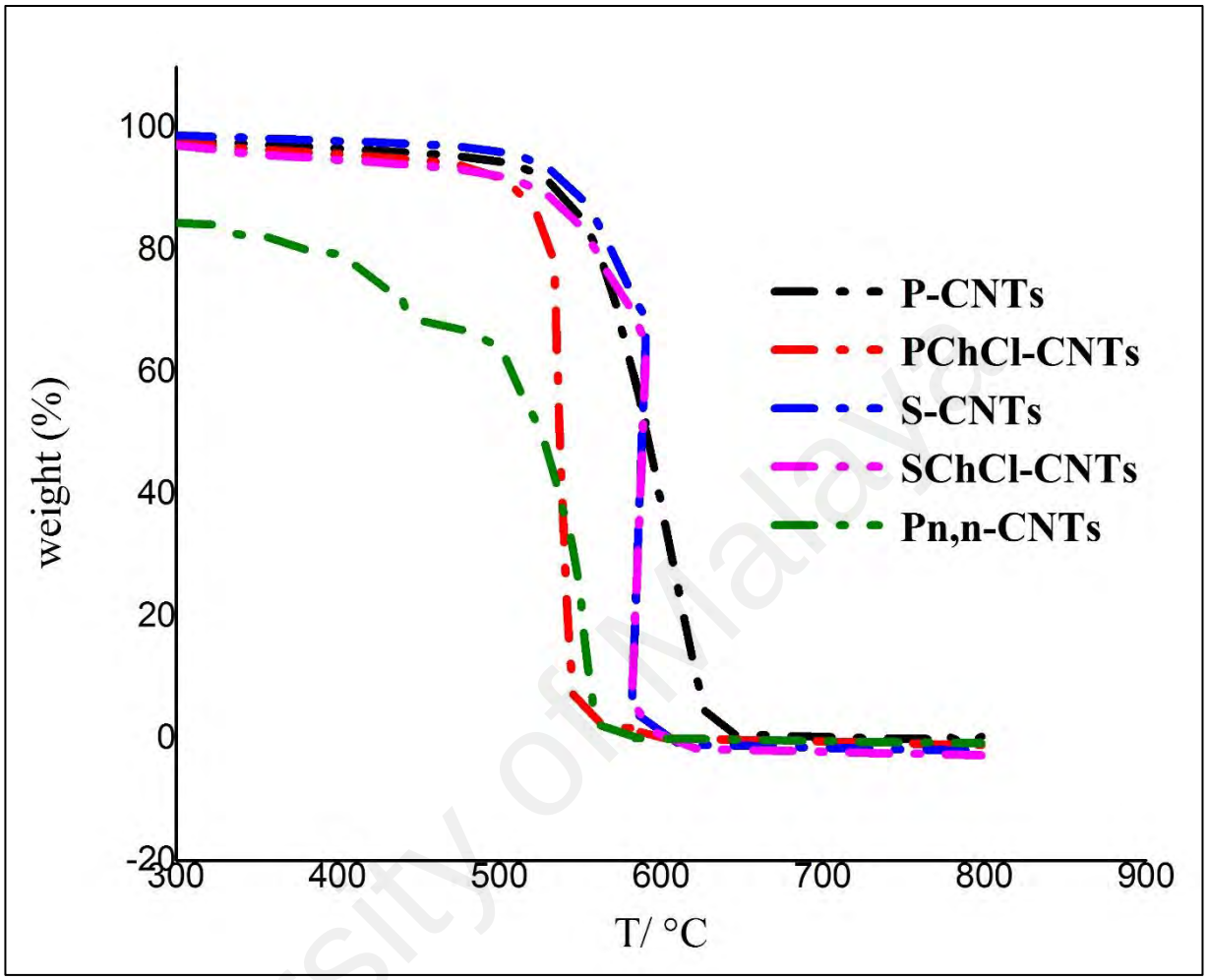

Figure 4.15: TGA curves for pristine and functionalized CNTs

4.2.1.5 Zeta potential

Zeta potential was measured by discrete dispersion of 2.5 mg of each adsorbent in 5 mL of deionized water. The arrangements of the results are presented in Figure 4.16. S-CNTs, PChCl-CNTs, SChCl-CNTs and Pn,n-CNTs possessed more negative surface charges than P-CNTs due to the presence of more oxygen-containing groups such as carbonyl, carboxyl and hydroxyl groups as revealed in FTIR spectra (Fan et al., 2012; Lu & Chiu, 2008). The significant variation in the absolute value of zeta potential for P-CNTs after functionalization depends on the influence of hydrophilicity or hydrophobicity properties of various kind of functional groups formed on the surface of

P-CNTs. The treatment of P-CNTs either with acid or DES has increased its zeta potential absolute value which enables the formation of a stable water suspension, and increases the functionality degree of the functionalized CNTs (Kharissova, Kharisov, & de Casas Ortiz, 2013), by offering an acceptable contact between the adsorbents and the adsorbates in the aqueous solution.

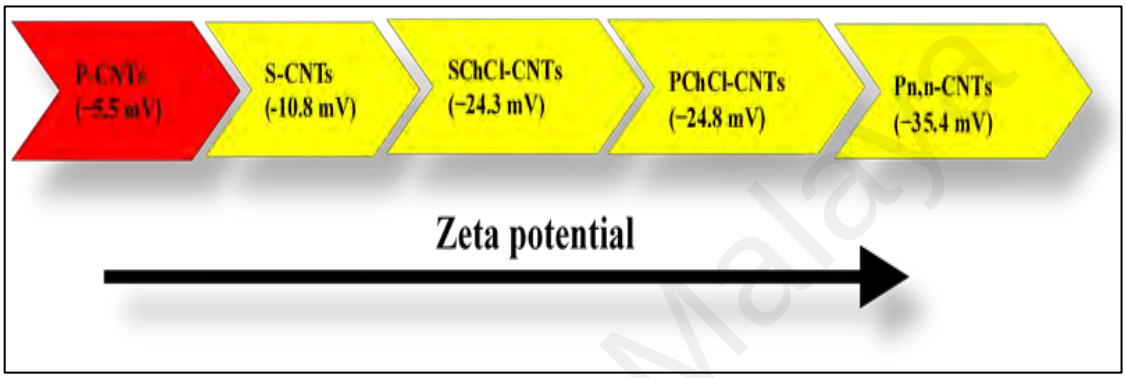

Figure 4.16: The order of zeta potential valus for pristine and functionalized CNTs

4.2.1.6 BET surface area

The surface area for all studied adsorbents were evaluated using BET method. Table 4.15 shows the surface area, pore volume and diameter for all adsorbents. It is noticeable that the surface area of P-CNTs has remarkably increased after functionalization with acid or/and DES. This significant increase in the surface area of Functionalized CNTs can be attributed to the removal of impurities on its surface by H_2SO_4 or by [ChCl:EG] and [DAC:EG]. As a result, the adsorption capacity for the functionalized CNTs was much higher than that of P-CNTs.

Table 4.15: BET surface area, pore volume and diameter of all adsorbents.

Property	P-CNTs	S-CNTs	PChCl-CNTs	SChCl-CNTs	Pn,n-CNTs
BET Surface Area (m^2/g)	123.54	226.11	197.8	193.10	169.7
Total pore volume (cm^3/g)	0.62	1.45	1.19	1.22	1.27
Average Pore Diameter (Å)	20.49	256.84	241.28	254.21	300.9

4.2.1.7 TEM and FESEM

Figure 4.17 and Figure 4.18 depict the TEM and FESEM images for pristine and functionalized CNTs. It is obvious that there is no significant destruction in the structure of CNTs, which proposes that the functionalization with DES is a non-destructive functionalization which ensures the electrical and the mechanical properties of CNTs and enhances the interfacial properties between CNTs and the pollutants. Furthermore, after acid treatment, more agglomeration-like behavior was observed and DES has a significant cleaning effect by removing the agglomeration produced by acid.

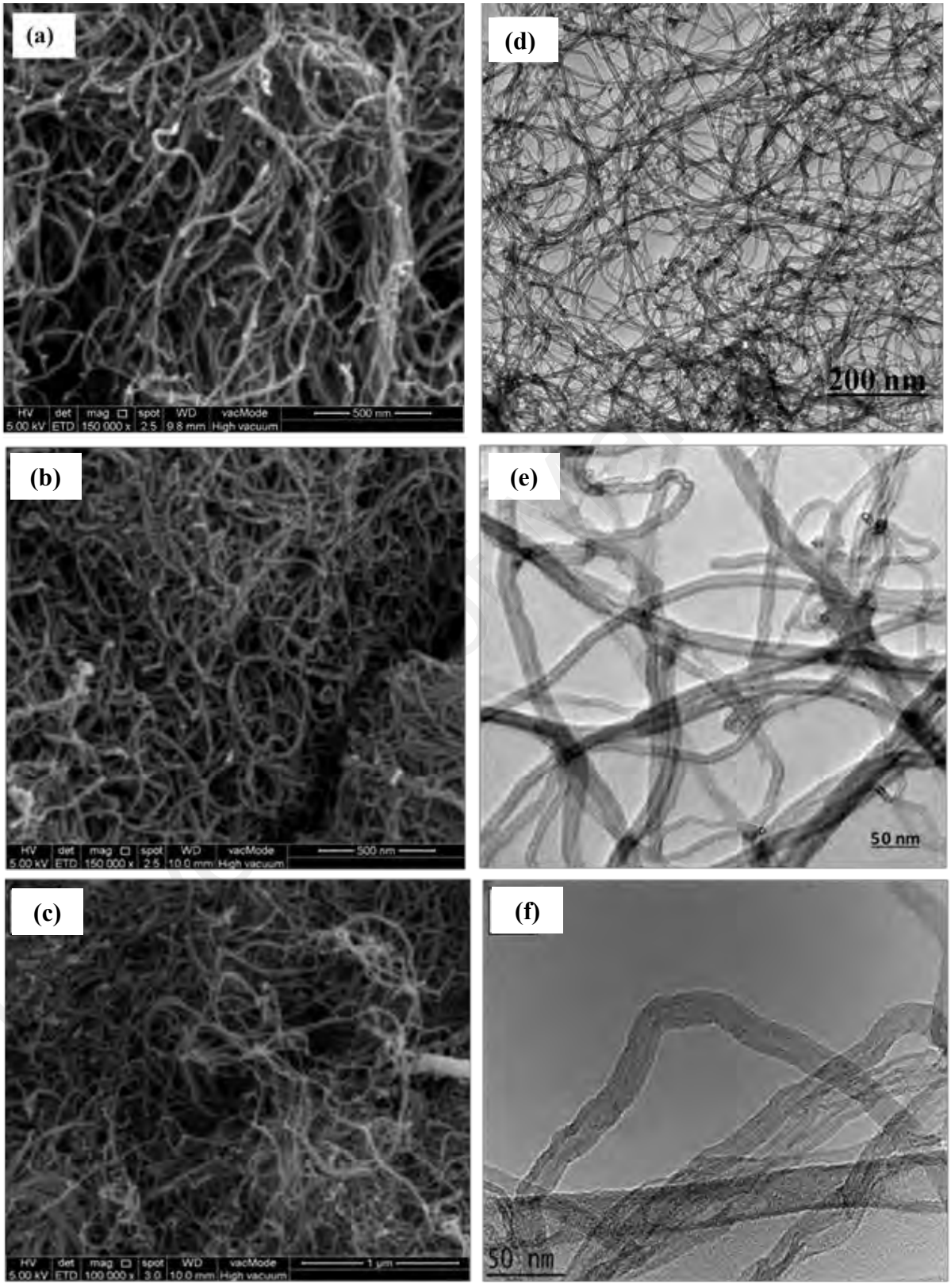

Figure 4.17: SEM images for: (a) P-CNTs, (b) PChCl-CNTs, and (c) Pn,n-CNTs; and TEM images for: (d) P-CNTs, (e) PChCl-CNTs, and (f) Pn,n-CNTs.

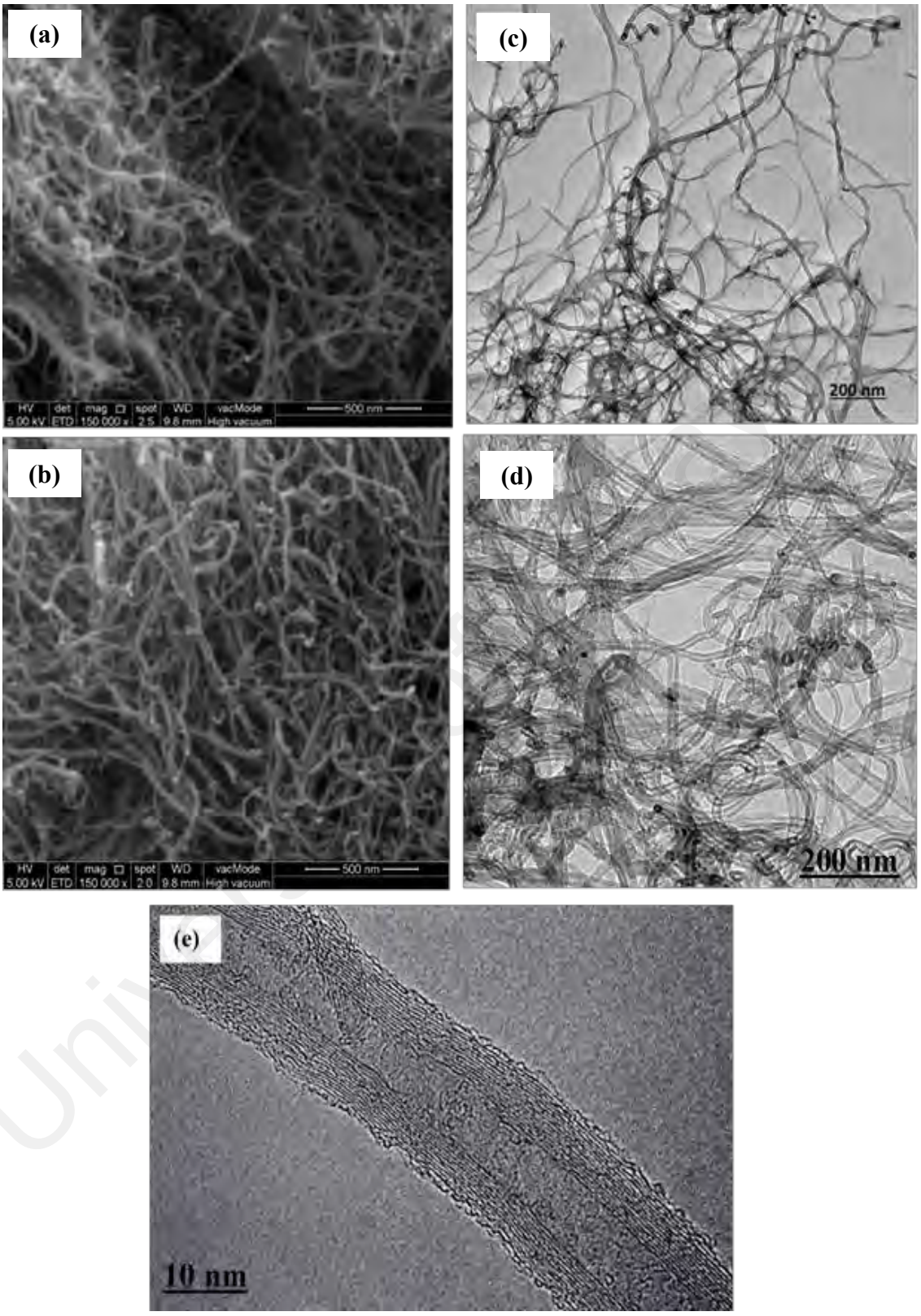

Figure 4.18: SEM images for: (a) S-CNTs and (b) SChCl-CNTs; and TEM images for: (c) S-CNTs, (d) and (e) SChCl-CNTs.

4.2.2 Adsorption of 2,4-DCP

The studies of 2,4-DCP adsorption was performed and compared on four different adsorbents which showed the highest removal efficiency in the primary screening studies, and they are : P-CNTs, PChCl-CNTs, S-CNTs and SChCl-CNTs.

4.2.2.1 Response surface methodology (RSM)

*(a) **Analysis of variance (ANOVA)***

The analysis of variance (ANOVA) was used to justify the adequacy of the models adopted for one response for all adsorbent which is the removal efficiency. A subset of the model with fewer terms was selected to ensure the significance of the models for a good representation of the experimental data (Wächter & Cordery, 1999). The reduced cubic model analysis (ANOVA) of removal efficiency % response for P-CNTs and for S-CNTs is listed in Table 4.16. Regarding PChCl-CNTs and SChCl-CNTs their reduced cubic model (ANOVA) of removal efficiency % is listed in Table 4.17. The models F-values for all absorbents confirmed that all models are statistically significant. There is only a 1.05%, 0.62%, chance that the a "Model F-value" can occur due to the noise for the removal efficiency response of PChCl-CNTs and SChCl-CNTs, respectively. The desirable value of signal to noise ratio should be greater than 4 and it is measured by the "Adeq Precision". Based on that, for all adsorbents, the models showed a ratio value greater than 4 which indicates an adequate signal.

The relatioship between the independent variables and the removal effeciency % for all adsorbents is expressed by the following quadratic equations:

$$\text{2,4-DCP R \% of P-CNTs} = 72.17 - 26.24A + 10.29B + 20C - 11.34AB - 2.47AC - 2.17BC - 29.21A^2 - 4.27B^2 - 10.11C^2 \quad (4.10)$$

$$\text{2,4-DCP R \% of S-CNTs} = 71.88 - 29.15A + 6.05B + 1.28C - 7.37AB + 1.14\ AC - 1.96BC - 29.95A^2 - 5.19B^2 - 11.33C^2 \quad (4.11)$$

$$\text{2,4-DCP R \% of PChCl-CNTs} = 66.23 - 25.61A + 7.72B - 0.37C - 9.90AB - 2.94AC - 2.03BC - 22.96A^2 - 6.04B^2 - 12.38C^2 \quad (4.12)$$

$$\text{2,4-DCP R \% of SChCl-CNTs} = 73.50 - 18.65A + 2.38B - 1.21C - 7.05AB + 2.00AC - 3.69BC - 26.66A^2 - 1.41B^2 - 16.37C^2 \quad (4.13)$$

where A, B, C represents pH, Dosage (mg) and contact time (min). The predicted values of removal effeciency % calculated from ANOVA model equations along with the actual values for all adsorbents are listed in Table 4.18.

Furthermore, the predicted values were plotted versus the experimental data for the examined adsorbents (Figure 4.19). It can be observed that the experimental data are close to the predicted data suggested by the apporved models. The correlation coefficient R^2 value for removal effeciency response for all studied adsorbents is greater than 0.98 and that confirms the competence of the models adopted for the studied adsorbents.

Table 4.16: Reduced cubic model analysis of variance (ANOVA) for 2,4-DCP removal (%) by P-CNTs and S-CNTs.

Source*	P-CNTs					S-CNTs				
	Sum of squares	df	Mean square	F-value	p-value prob > F	Sum of squares	df	Mean square	F-value	p-value prob > F
Model	12522.18	9	1391.35	80.02	0.0021	12863.17	9	1429.24	29.69	0.0089
A	5608.55	1	5608.55	322.58	0.0004	6922.20	1	6922.20	143.80	0.0012
B	863.48	1	863.48	49.66	0.0059	298.26	1	298.26	6.20	0.0886
C	0.42	1	0.42	0.024	0.8870	16.37	1	16.37	0.34	0.6008
AB	1028.32	1	1028.32	59.14	0.0046	434.54	1	434.54	9.03	0.0575
AC	48.88	1	48.88	2.81	0.1922	10.43	1	10.43	0.22	0.6733
BC	37.73	1	37.73	2.17	0.2371	30.80	1	30.80	0.64	0.4822
A^2	1211.23	1	1211.23	69.66	0.0036	1272.92	1	1272.92	26.44	0.0143
B^2	25.83	1	25.83	1.49	0.3100	38.23	1	38.23	0.79	0.4385
C^2	173.06	1	173.06	9.95	0.0511	224.89	1	224.89	4.67	0.1194
	Adj R-Squared 0.98**			**Pred R-Squared** 0.91**		**Adj R-Squared** 0.95**			**Pred R-Squared** 0.82**	
	C.V. % 10.43**			**Std. Dev** 4.17**		**C.V. %** 18.80**			**Std. Dev** 6.94**	

*A: pH, B: adsorbent dosage and C: contact time; ** The "Pred R-Squared" is in reasonable agreement with the "Adj R-Squared".

.Table 4.17: Reduced cubic model analysis of variance (ANOVA) for 2,4-DCP removal (%) by PChCl-CNTs and SChCl-CNTs.

Source*	PChCl-CNTs					SChCl-CNTs				
	Sum of squares	df	Mean square	F-value	p-value prob > F	Sum of squares	df	Mean square	F-value	p-value prob > F
Model	10503.64	9	1167.07	26.38	0.0105	7375.88	9	819.54	37.76	0.0062
A	5343.95	1	5343.95	120.79	0.0016	2834.06	1	2834.06	130.59	0.0014
B	485.38	1	485.38	10.97	0.0453	46.28	1	46.28	2.13	0.2403
C	1.40	1	1.40	0.032	0.8701	14.71	1	14.71	0.68	0.4706
AB	783.79	1	783.79	17.72	0.0245	397.44	1	397.44	18.31	0.0234
AC	69.06	1	69.06	1.56	0.3001	32.04	1	32.04	1.48	0.3112
BC	32.94	1	32.94	0.74	0.4517	108.77	1	108.77	5.01	0.1111
A^2	748.44	1	748.44	16.92	0.0260	1009.14	1	1009.14	46.50	0.0065
B^2	51.76	1	51.76	1.17	0.3586	2.84	1	2.84	0.13	0.7417
C^2	259.21	1	259.21	5.86	0.0941	453.44	1	453.44	20.89	0.0196
	Adj R-Squared 0.95**		**Pred R-Squared** 0.77**			**Adj R-Squared** 0.96**		**Pred R-Squared** 0.76**		
	C.V. % 18.78		**Std. Dev** 6.65			**C.V. %** 11.58		**Std. Dev** 4.66		

*A: pH, B: adsorbent dosage and C: contact time; ** The "Pred R-Squared" is in reasonable agreement with the "Adj R-Squared"

Table 4.18: List of the actual and predicted values for 2,4-DCP removal response.

Run order	P-CNTs		S-CNTs		PChCl-CNTs		SChCl-CNTs	
	Actual value	Predicted value	Actual value	Predicted value	Actual value	Predicted value	Actual value	Predicted value
1	29.36	28.34	38.53	38.84	28.44	28.25	39.45	37.8
2	1.85	3.48	-9.63	-7	-0.62	2.7	8.02	10.6
3	74.31	75.94	66.97	69.6	64.22	67.54	61.47	64.04
4	5.56	5.74	-7.41	-5.71	1.85	2.4	9.26	8.64
5	37.61	38.03	44.04	43.04	37.61	37.44	37.61	38.75
6	4.32	3.29	3.7	1.77	3.09	0.14	21.6	19.55
7	77.98	76.95	67.89	65.95	71.56	68.61	52.29	50.24
8	-4.76	-3.14	-5.19	-4.8	-8.84	-8.28	0.68	2.84
9	19.14	16.72	15.56	12.78	19.14	17.65	30.25	28.19
10	67.35	72.17	66.33	71.88	63.27	66.23	69.39	73.5
11	80.61	78.2	75.51	72.74	69.39	67.91	76.53	74.47
12	64.29	61.86	66.33	59.07	61.22	54.23	61.22	58.35
13	62.24	62.26	57.14	61.63	47.96	53.48	55.1	55.92

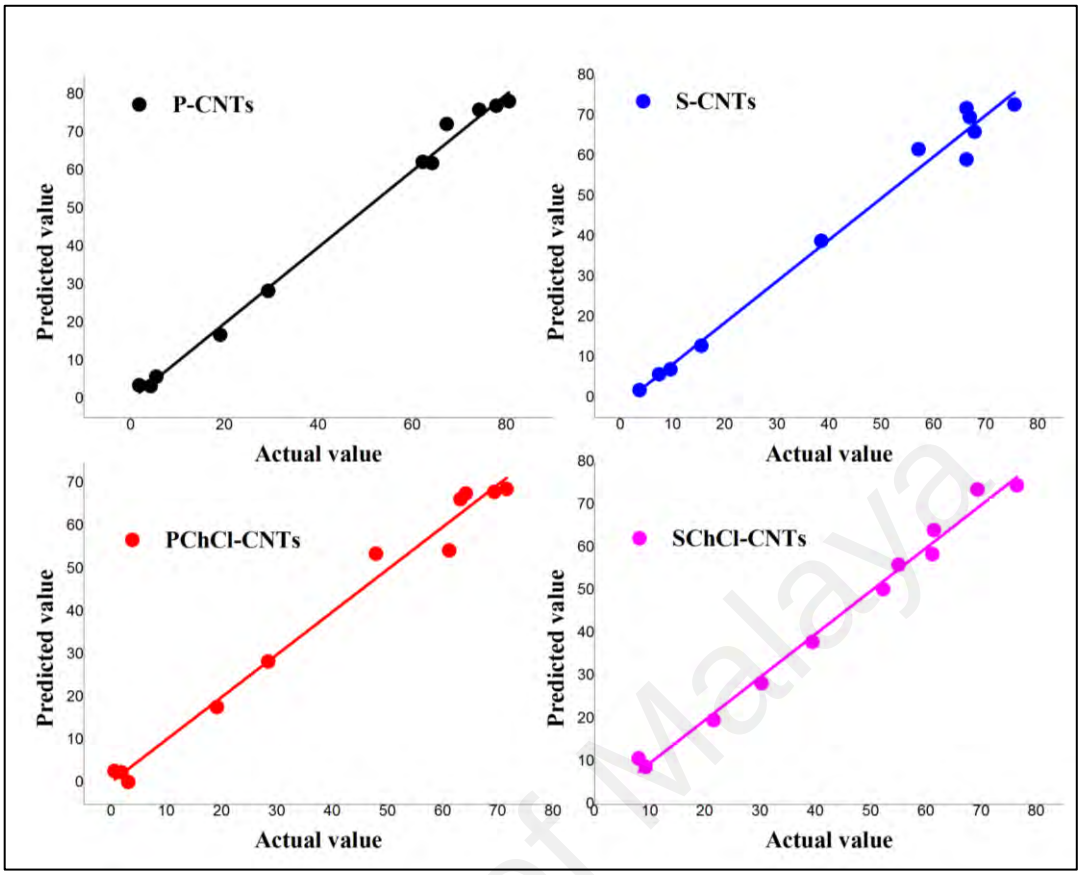

Figure 4.19: Predicted values vs actual values for 2,4-DCP removal response.

(b) ***The interactive effects of selected independent parameters on the adsorption of 2,4-DCP***

The removal efficiency % of all used adsorbents over different combinations of independent variables were presented by three-dimension view of response surface plot as a function of two independent parameters (Figure 4.20 and Figure 4.21). The initial concentration of 2,4-DCP was constant for all cases with a value of 10 mg/L. It is obvious that for all adsorbents, the removal efficiency (%) increased gradually with the increasing of contact time until the systems reached equilibrium. Table 4.19 shows some constrains and different importance levels which were set for optimization of four goals (i.e. contact time, pH, adsorbent dosage and R% of 2,4-DCP) to select the optimum conditions for 2,4-DCP adsorption onto the studied adsorbents. The effect of pH was remarkably

noticeable on the removal efficiency as it effects the properties of both adsorbate and adsorbents. Adsorption of 2,4-DCP was clearly weakened with increasing of pH. This can be explained by the deprotonation of some surface functional groups resulting in more negatively charged adsorbents surface (Gupta, Ali, & Saini, 2006). As well as, high pH leads to more dissociation of 2,4-DCP molecules into $C_6H_3Cl_2O^-$ form, subsequently increasing the electrostatic repulsion and lowering the adsorption capacity (Ma et al., 2010). Moreover, 2,4-DCP adsorption was enhanced with the decreasing of initial pH and the removal efficiency reached to a ma ximum at pH 3.87 and 5.14 for PChCl-CNTs and SChCl-CNTs, respectively (Table 4.20). This can be attributed to the presence of 2,4-DCP in non-dissociated form and the surface of the adsorbent is highly protonated at acidic pH value, leading to easy adsorption process by high electrostatic attraction between the adsorbent and the adsorbate (Darvishi Cheshmeh Soltani et al., 2015). Meanwhile, the dose of adsorbate has an obvious effect on 2,4-DCP removal efficiency. The figures exhibit that the removal efficiency increased along with the increasing of adsorbent dose which can be ascribed to the increase of surface area and the availability of more adsorptive sites for the removal of 2,4-DCP.

Table 4.19: Constraints for optimization process based on CCD for 2,4-DCP adsorption.

Name		Goal	Lower limit	Upper limit	Importance
A		In range	2	10	-
B		Minimize	5	15	1
C		In range	20	60	-
R%	P-CNTs	Maximize	1.8	80.6	5
	PChCl-CNTs		1.85	71.5	
	S-CNTs		3.7	75.5	
	SChCl-CNTs		0.68	76.53	

A: pH, B: adsorbent dosage (mg) and C: contact time (min)

Table 4.20: Optimum adsorption conditions suggested by DOE software for 2,4-DCP adsorption.

Adsorbent	pH	Dose (mg)	Contact time (min)	Predicted Removal (%)
P-CNTs	4.11	9.68	41.65	77.0919
S-CNTs	4.22	8.23	41.56	74.8842
PChCl-CNTs	3.87	9.35	41.42	71.5545
SChCl-CNTs	5.14	5.00	41.25	71.0324

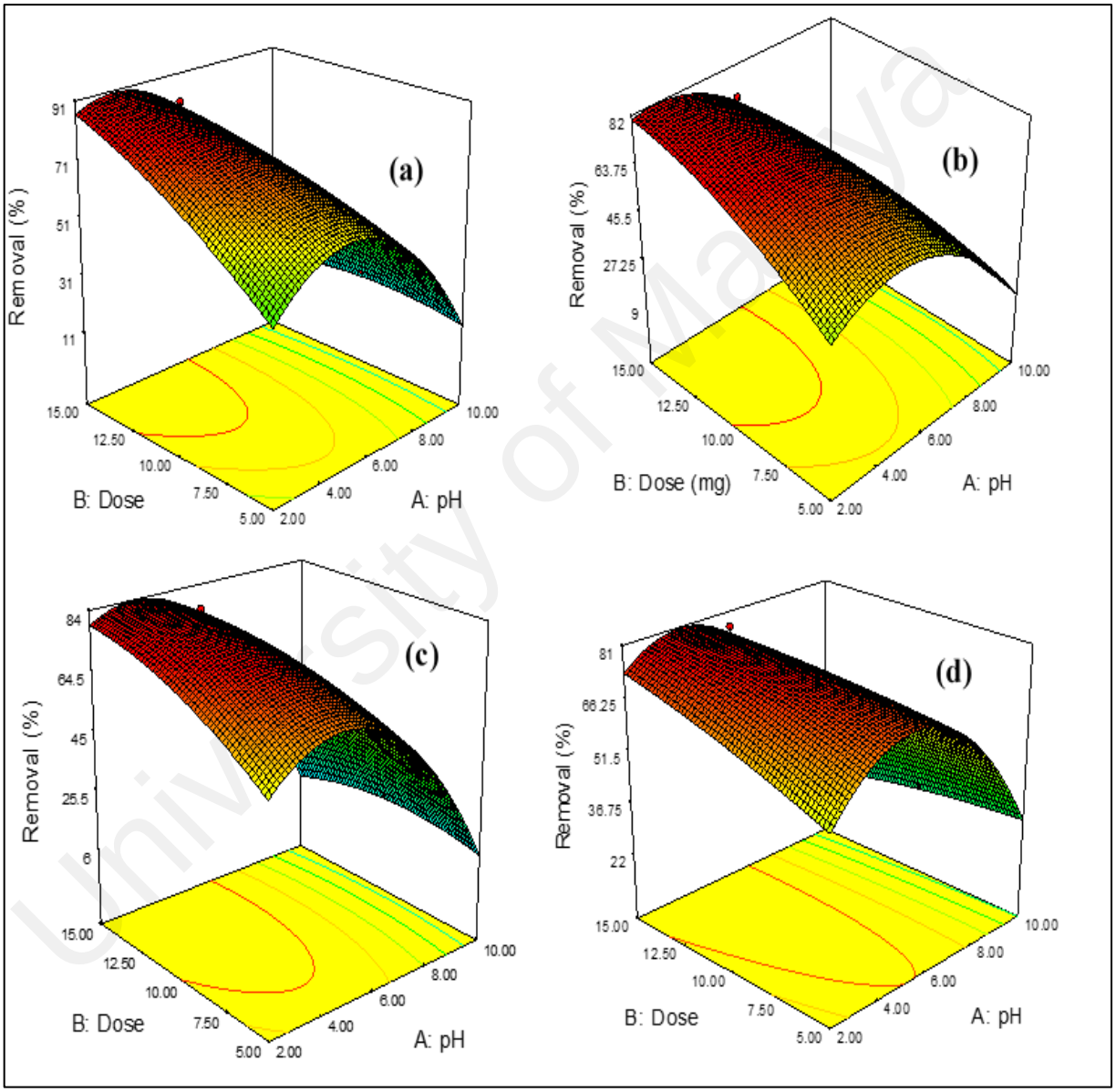

Figure 4.20: Surface response representation of removal (%) of 2,4-DCP interaction with adsorbent dose and pH by fixing contact time to the optimum value for: (a) P-CNTs, (b) PChCl-CNTs, (c) S-CNTs, and (d) SChCl-CNTs.

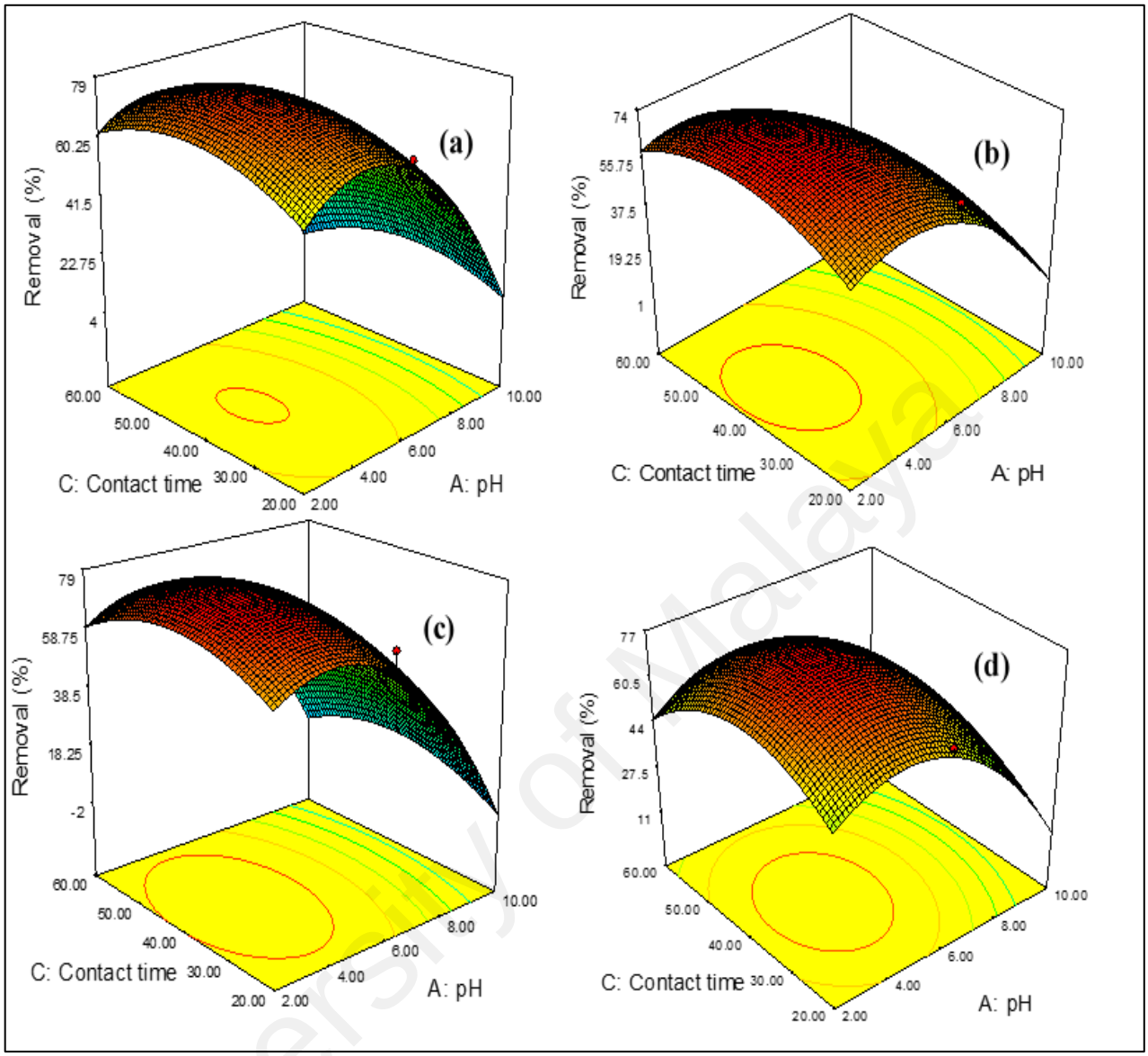

Figure 4.21: Surface response representation of removal (%) of 2,4-DCP interaction with contact time and pH by fixing adsorbent dosage to the optimum value for: (a) P-CNTs, (b) PChCl-CNTs, (c) S-CNTs, and (d) SChCl-CNTs.

4.2.2.2 Kinetics study

To analyze the adsorption equilibrium time and describe the uptake of 2,4-DCP on the concerned adsorbents, the adsorption kinetic was investigated. The amount of 2,4-DCP onto pristine / functionalized at time (t); q_t (mg g^{-1}) was calculated using the following means of expression:

$$q_t = \frac{(C_0 - C_t)V}{W} \qquad (4.14)$$

where C_0 and C_t are 2,4-DCP stock solution concentrations at initial and pre-determined time *t* (mg L^{-1}), respectively, V is the volume of the stock solution (L) and W is the dry weight of the added pristine / functionalized CNTs (g).

Two kinetics models, which are: Pseudo-first order kinetic model and Pseudo-second order kinetic model (Figure 4.22 and Figure 4.23), were applied to the experimental data. It is obvious from Table 4.21 that the calculated q_e values of Pseudo-first order kinetic did not agree with the experimental q_e values, while for Pseudo-second order kinetic the calculated values of q_e agree with the experimental q_e values. Not to mention, for all examined adsorbents the correlation coefficient (R^2) values of Pseudo-second order model was (0.99) which is much higher than that of Pseudo-first order model (0.69-0.80). Therefore, the adsorption of 2,4-DCP on pristine/ functionalized CNTs is not a first order reaction and it is ideally obeying the Pseudo-second order kinetic model. Similar kinetics were found to be well fitted for the adsorption of 2,4-DCP onto activated carbon fiber (Wang, Feng, & Yu, 2007), and onto Mn-modified activated carbon prepared from Polygonum orientale Linn (Wang et al., 2011). The applicability of Pseudo-second order kinetic model to describe the adsorption of 2,4-DCP in this study indicates that the adsorption process rate was controlled by chemisorption involving valence forces through exchange or sharing electrons (Vimonses et al., 2009) which suggests the possibility of adsorbate and adsorbent involvement in the adsorption mechanism (Pavan et al., 2008).

For further identification of adsorption mechanism, weber and Morris (Weber & Morris, 1962) proposed an empirically found functional relationship based on a theory by which the rate of uptake changes proportionally with $t^{1/2}$ rather than with contact time *t*, specifically called intraparticle diffusion (Tan, Ahmad, & Hameed, 2009) and it can be expressed as below :

$$q_t = K_d t^{\frac{1}{2}} + C \qquad (4.15)$$

Where C is the intercept and K_d (g mg^{-1} $min^{0.5}$) is the intraparticle diffusion rate constant and it can be obtained from the slope of q_t versus $t^{0.5}$ (Figure 4.24). The intraparticle diffusion model suggests three adsorption regions. The first region is the boundary layer diffusion where the adsorption occurs instanteneously from the bulk solution to the adsorbent external surface. The second one is the intraparticle diffusion region where the adsorption takes place gradually and the adsorbate difuses further on the adsorption sites. The third region exisits when the equillibrium stage starts when the adsorbate are adsorbed on the active sites and the intraparticle diffuion slows down due to the very low 2,4-DCP concentration left in the the solution (Cheung, Szeto, & McKay, 2007). The intraparticle diffusion is the only rate-controlling step if the regression of q_t versus $t^{0.5}$ passes through the origin. So as can be observed from Figure 4.24 the linear plot for all adsorbents did not pass through the origin which proposes that along with the intraparticle diffusion some other mechanisms are involved in the rate limiting process and the boundary layer diffusion dominated the adsorption process to some point. The increase in C value is an indication to the increased thickness and effect of the bounndry layer on the rate controlling step (Shaarani & Hameed, 2010; Tan, Ahmad, & Hameed, 2009). As can be seen from Table 4.21 SChCl-CNTs has the greatest intercept value among other adsorbents which suggests the more contribution of the adsorbent surface in 2,4-DCP adsorption process.

Table 4.21: linearized equations of all studied kinetics models and their parameters and correlation coefficients for 2,4-DCP adsorption.

Kinetics	Equations	Parameters	Adsorbents			
			P-CNTs	S-CNTs	PChCl-CNTs	SChCl-CNTs`
Pseudo-first order	$\ln(q_e - q_t) = \ln q_e - k_1 t$	**R^2**	0.69	0.80	0.69	0.79
		K_1	0.01	0.01	0.01	0.01
		q_e	9.34	13.23	16.13	22.96
Pseudo-Second order	$\frac{t}{q_t} = \frac{1}{k_2 q_e^2} + \frac{t}{q_e}$	R^2	0.99	0.99	0.99	0.99
		K_2	0.0065	0.0041	0.0023	0.002
		q_e	38.01	39.57	41.92	61.69
Intraparticle diffusion	$q_t = K_d t^{\frac{1}{2}} + C$	R^2	0.82	0.74	0.79	0.85
		Kd	0.796	1.114	1.69	1.92
		q_e	26.19	22.91	16.76	32.67
	q_e (experimental)		37.5	38.82	40.22	60

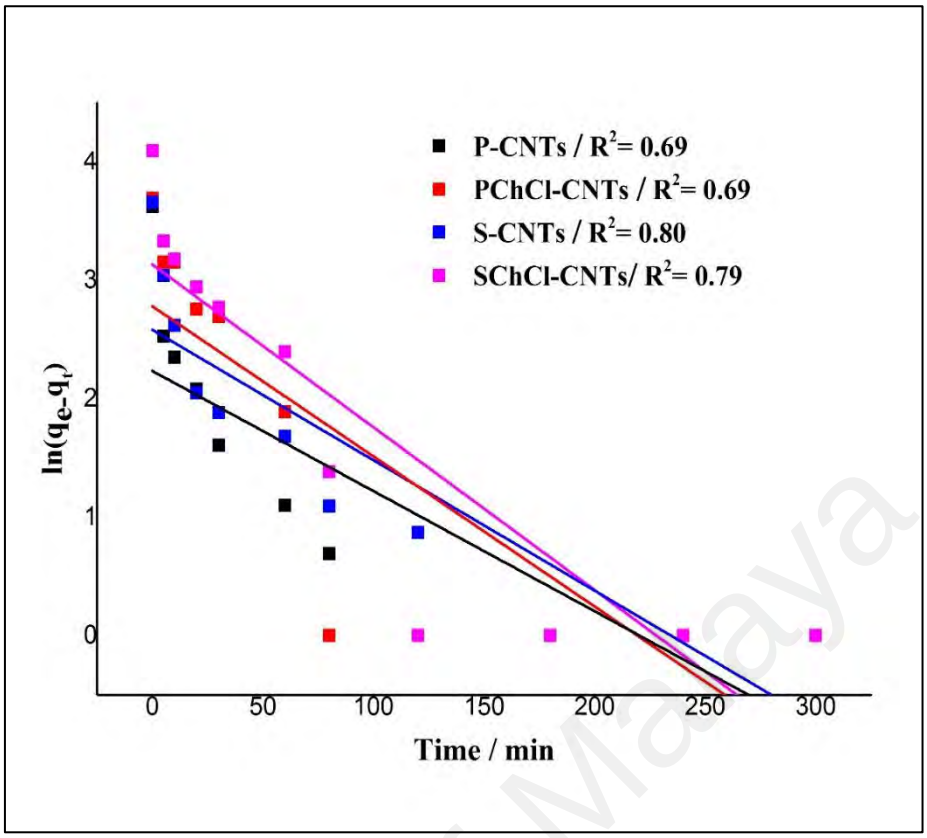

Figure 4.22: Pseudo-first order kinetic model for 2,4-DCP adsorption.

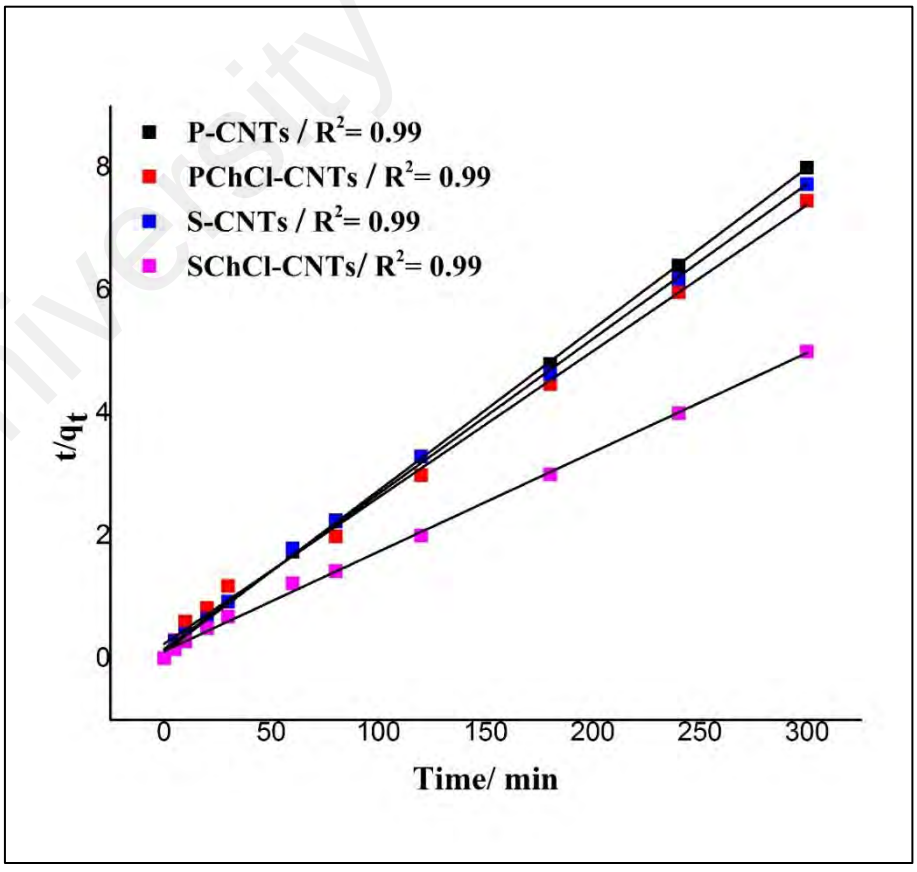

Figure 4.23: Pseudo-second order kinetic model for 2,4-DCP adsorption.

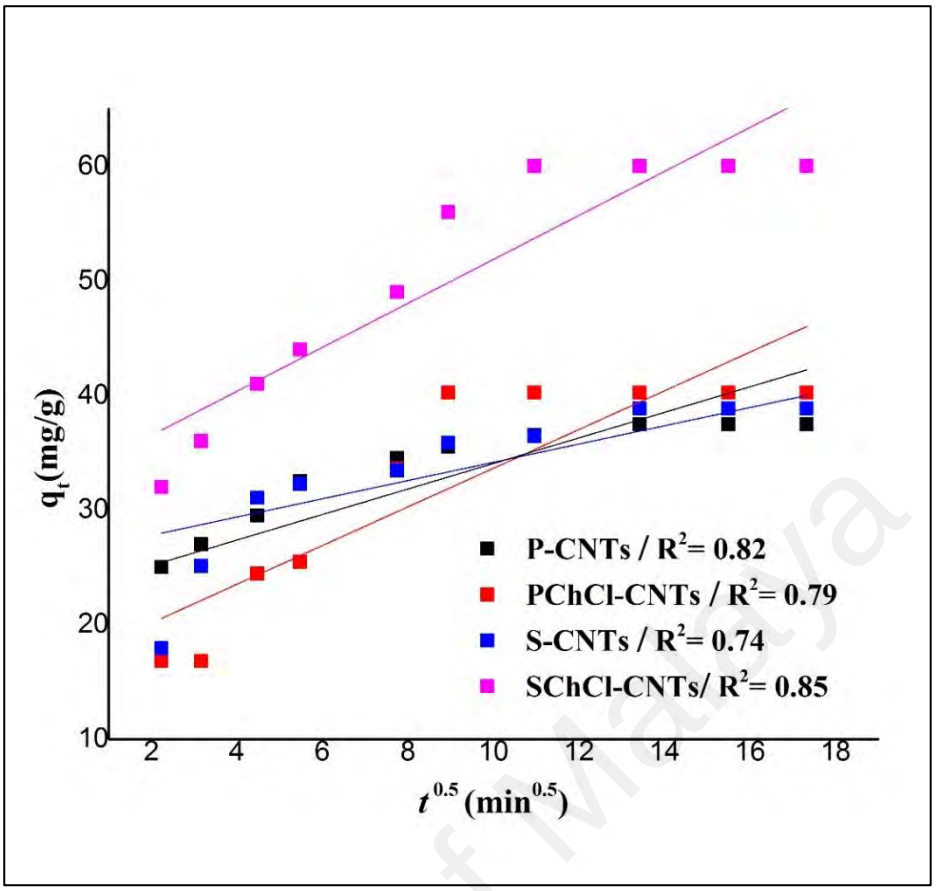

Figure 4.24: intraparticle diffusion kinetic model for 2,4-DCP adsorption.

4.2.2.3 Isotherms study

Three isotherm models (i.e. Langmuir, Freundlich and Temkin) were applied to all the studied adsorbents in order to investigate the interaction between the adsorbent and the adsorbate until the equilibrium point is reached (Zhang, Zhang, et al., 2010). The correlation coefficient R^2 was calculated to establish the most appropriate isotherm model to describe the adsorption process. The plot of each model is presented in Figure 4.25, Figure 4.26 and Figure 4.27. As well as the constants of all models and all correlation factors are summarized in Table 4.22. As can be observed, the values of R_L and n of Langmuir and Freundlich adsorption isotherms, respectively, confirmed the adsorption favorability of 2,4-DCP by all studied adsorbents under experimental conditions (Mahmoud et al., 2012; Namasivayam, Jeyakumar, & Yamuna, 1994). However, Langmuir isotherm yielded the better fit for all adsorbents with high correlation

coefficient R^2 ranged from 0.95 to 0.99, as compared to Freundlich isotherm. This is an indication of a monolayer adsorption of 2,4-DCP onto the homogeneous surface of the tested adsorbents. On the other hand, compared to the other adsorbents, the higher R^2 of Freundlich model for the two adsorbents of PChCl-CNTs and SChCl-CNTs suggests that different active sites with various affinities to 2,4-DCP molecules can cause the adsorption to take place onto the heterogeneous surface of these two adsorbents and according to n value (>1) the adsorptive behavior is dominated as a physical adsorption process (Özcan, Erdem, & Özcan, 2005). Furthermore, the value of R_L was found to be decreasing as the initial concentration of 2,4-DCP increased, proving again the applicability of Langmuir isotherm for the 2,4-DCP adsorption and the favorable adsorption of 2,4-DCP at higher initial concentration. Table 4.23 provides the comparisons of the adsorption isotherms and the maximum monolayer adsorption capacity of 2,4-DCP on several adsorbents. As compared to previous works, in this study the CNTs adsorbent modified with H_2SO_4 and [ChCl:EG] shown a significant maximum adsorption capacity of 390.35 mg g^{-1}.

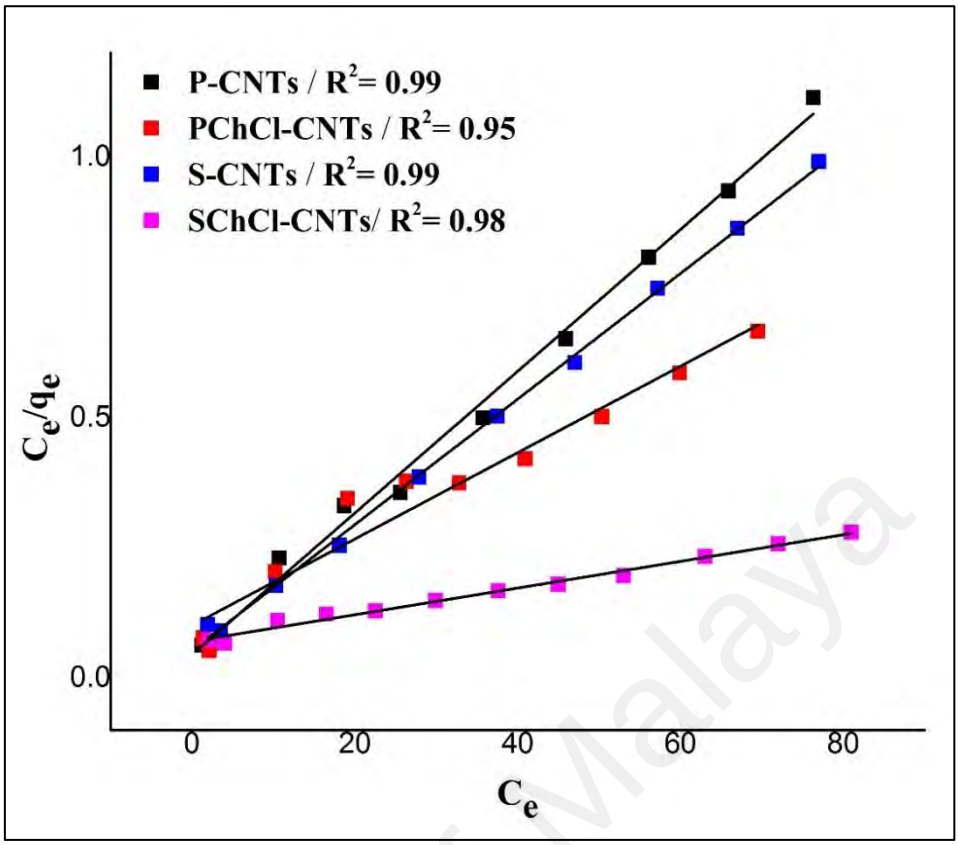

Figure 4.25: Langmuir isotherm model for 2,4-DCP adsorption.

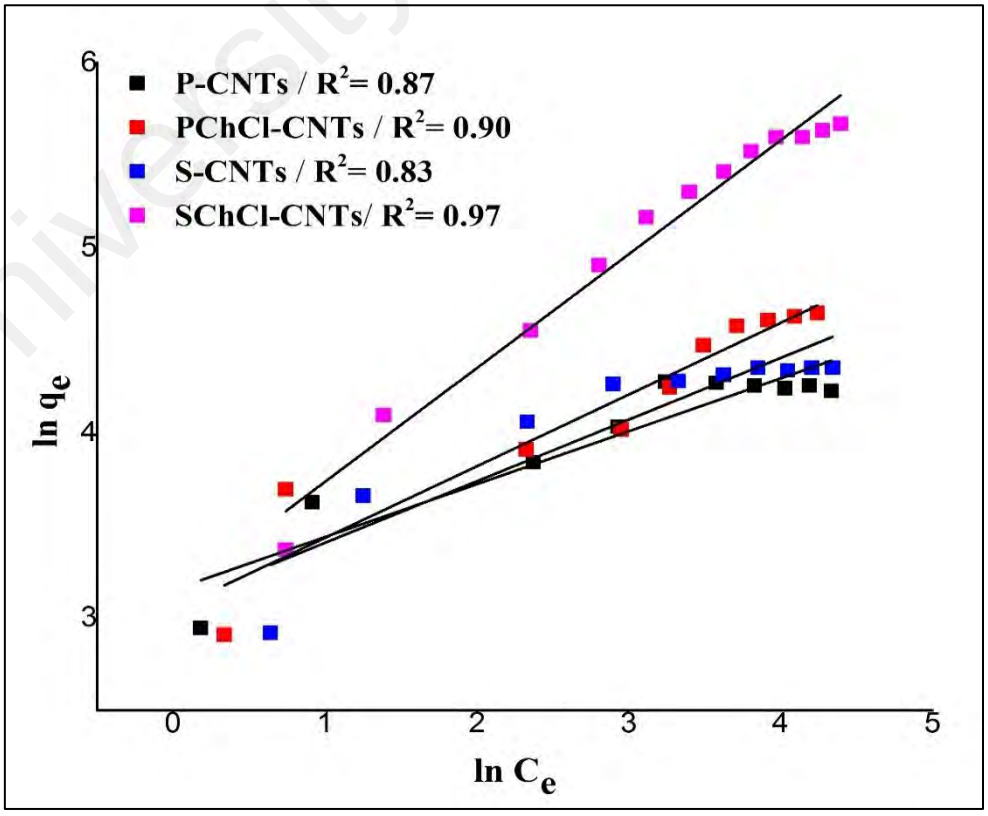

Figure 4.26: Freundlich isotherm model for 2,4-DCP adsorption.

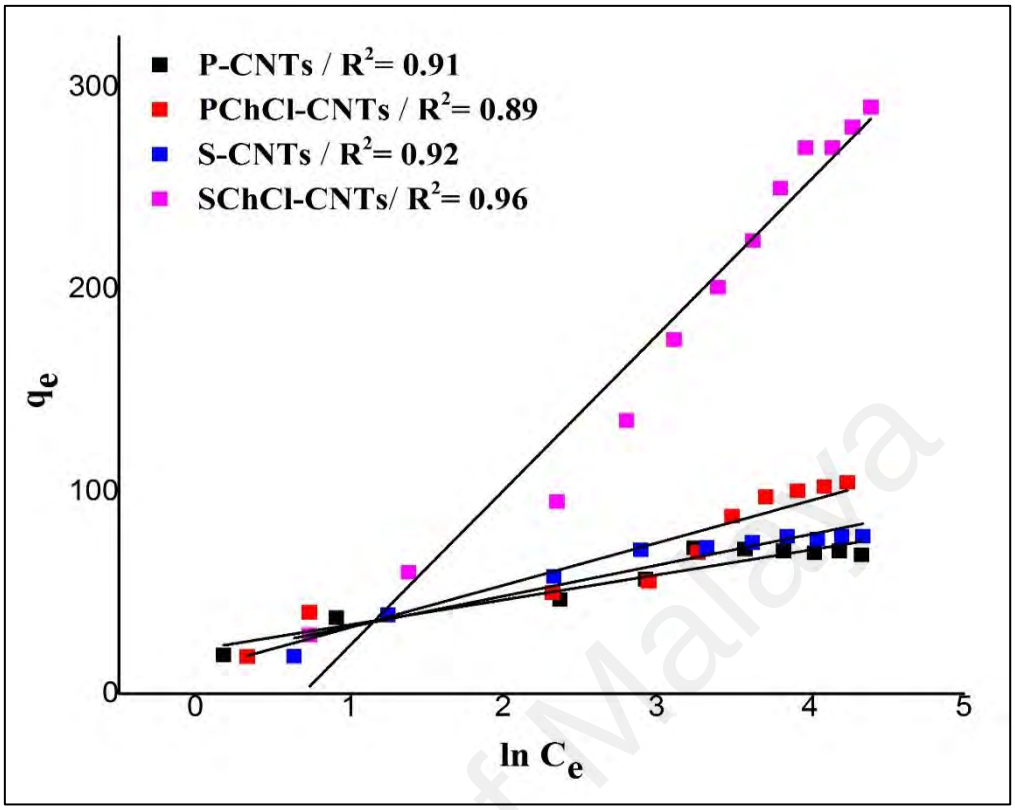

Figure 4.27: Temkin isotherm model for 2,4-DCP adsorption.

Table 4.22: linearized equations of all studied isotherm models and their parameters and correlation coefficients for 2,4-DCP adsorption.

Isotherms	Equations	Parameters	Adsorbents			
			P-CNTs	S-CNTs	PChCl-CNTs	SChCl-CNTs`
Langmuir	$\frac{C_e}{q_e} = \frac{1}{K_L Q_m} + \left(\frac{1}{Q_m}\right) C_e$	Q_m (mg g^{-1})	73.47	82.94	120.59	390.53
		K_L (L mg^{-1})	3.26	4.41	12.18	27.46
		R_L	0.057	0.043	0.016	0.007
		R^2	0.99	0.99	0.95	0.98
Freundlich	$\ln q_e = \ln K_F + \frac{1}{n} \ln C_e$	n	3.49	3.00	2.58	1.62
		K_F (L mg^{-1})	23.35	21.58	20.99	22.63
		R^2	0.87	0.83	0.90	0.97
Temkin	$q_e = B_1 \ln k_t + B_1 \ln C_e$	B_1	12.35	15.27	20.95	30.84
		k_t (L mg^{-1})	5.76	3.17	1.75	0.02
		R^2	0.91	0.92	0.89	0.96

Table 4.23: comparison between the maximum adsorption capacity of DES treated CNTs and some reported adsorbent for 2,4-DCP removal.

Adsorbent	Q_m (mg/g)	REF
SChCl-CNTs`	390.53	Present work
PChCl-CNTs	120.59	Present work
MWCNT	19.61	(Xu et al., 2012)
MWCNT–OH	20 .9	(Kusmierek, Sankowska, & Swiatkowski, 2013)
MWCNTs-Fe_3O_4-Fe	7.1	(Xu, Liu, et al., 2016)
CB-V carbon black	72.2	(Kuśmierek, Szala, & Świątkowski, 2016b)
Carbonaceous adsorbent	277.7	(Gupta, Ali, & Saini, 2006)
Commercial AC (Prolabo)	256 .4	(Hamdaoui & Naffrechoux, 2007a)
AC from banana stalk	196.3	(Salman, Njoku, & Hameed, 2011)
AC from apricot stone shells	339	(Daifullah & Girgis, 1998)
AC from date stones	238.10	(Hameed, Salman, & Ahmad, 2009)
Coconut coir pith carbon	19.12	(Namasivayam & Kavitha, 2005)
Palm pith carbon	19.16	(Sathishkumar et al., 2007)

4.2.2.4 Mechanisms

The adsorption of 2,4-DCP onto the studied adsorbents was highly dependent on the characteristics of the adsorbents, the operational conditions, as well as on the molecular properties of 2,4-DCP. The oxygen-containing groups on functionalized CNTs, played an important role in the adsorption of 2,4-DCP by enhancing the dispersion of CNTs in water and defining the interaction between 2,4-DCP and the adsorbents surface by acting as acids or bases, which can adsorb 2,4-DCP through donor-acceptor complex formation. The molecular size of 2,4-DCP and its pKa value influenced its affinity towards CNTs surface. The adsorption of 2,4-DCP onto CNTs might be achieved through π-π interaction which is resulted from the interaction between the electron in the aromatic rings of 2,4-DCP and the graphene layer of CNTs and it might encompass charge-transfer, polar electrostatic components and dispersive force (Jung et al., 2001). Not to mention, controlling solution pH proved to have a remarkable implication on the adsorption mechanism. Since the phenolic compounds behave as weak acids in aqueous solution (Demirak et al., 2011), the pH of the solution has a strong effect on the dissociation of

hydrogen ion from 2,4-DCP. The anionic form of 2,4-DCP is the predominant form when the solution pH is high, whereas the molecular form dominates in acidic solutions (Nadavala et al., 2009). For all cases of adsorbents used to remove 2,4-DCP from water, it was found that the optimum pH required to obtain the highest removal efficiency is less than the pKa value of 2,4-DCP, which approve that the adsorption mechanism was governed by the synergetic effects of π-π interaction (Luboch et al., 2005; Wang, Chen, et al., 2007).

4.2.3 Adsorption of methyl orange

According to the highest removal efficiency obtained from the primary screening for MO removal from water, the adsorption performance of three different adsorbents (i.e. P-CNTs, PChCl-CNTs and Pn,n-CNTs) is comprehensively examined in this section.

4.2.3.1 Response surface methodology (RSM)

*(a) **Analysis of variance (ANOVA)***

The regression and the graphical analysis of the acquired data were accomplished by the Design Expert (DE) V7.0. software. The conditions for MO removal were optimized using response surface methodology (RSM), and the adsorption experiments were conducted according to the central composite design (CCD) matrix selected by the software. The study involved the use of analysis of variance (ANOVA) to analyze the variation in one response variable, which is removal efficiency % (R %) measured under conditions defined by three discrete factors (pH (2-10), dose (5-15) mg, and contact time (20-60) min.

By the application of RSM, an empirical relationship between R% and the three input variables can be obtained and presented by the following regression equations for P-CNTs, PChCl-CNTs and Pn,n-CNTs, accordingly:

$$\boldsymbol{MO\ \ R\%\ of\ P-CNTs} = 58.85 - 10.30A + 24.19B + 5.25C + 1.17AB - 2.69AC + 0.71BC + 0.61A^2 - 2.55B^2 - 0.88C^2 \quad (4.16)$$

$$\boldsymbol{MO\ R\%\ of\ PChCl-CN} = 78.76 - 14.50A + 23.48B + 7.62C + 7.90AB - 1.10AC - 4.50BC\ + 4.12A^2 - 8.99B^2 - 7.66C^2 \quad (4.17)$$

$$\boldsymbol{MO\ R\%\ of\ Pn,n-CNTs} = (5.68 - 1.05A + 2.19B + 0.44C + 0.05AB - 0.16AC + 0.67A^2 - 0.73B^2)^{o.5} \quad (4.18)$$

where A, B, and C represents pH, contact time , and adsorbent dosage, respectively.

Table 4.24 shows the evaluation results of the R% regression model in term of ANOVA. The significance of ANOVA modelling for R% model of P-CNTs, PChCl-CNTs and Pn,n-CNTs was confirmed by the model F-values which were 173.99, 91.5 and 58.69 respectively. There is only 0.06%, 0.17% and 0.01 % chance that a "Model F-Value" of P-CNTs, PChCl-CNTs and Pn,n-CNTs could occur due to noise. The strength of the model and the sufficiency of its response prediction were determined by the value of the correlation coefficient (R^2). The R^2 value of the model for all studied adsorbents was higher than 0.98 which proved that the model was well fitted and explained most of the total variables. Moreover, for each adsorbent model, the value of the predicted R^2 was high and in reasonable agreement with the value of the adjusted R^2. This supports the good correlation between the values predicted by the model and the actual values observed from the experiments (Figure 4.28 and Table 4.25), consequently proving the adequacy of the regression model to explain the relationship between the R% response and the three defined variables (Garg et al., 2008). Furthermore, it can be seen from Table 4.24, the value of the coefficient of variation (CV) for all adsorbents was low indicating a good accuracy of the experiments (Amini et al., 2008) and confirming the reliability of the model to be used for further analysis.

Table 4.24: Reduced cubic model analysis of variance (ANOVA) for MO removal (%) by P-CNTs, PChCl-CNTs and Pn,n-CNTs.

Source*	P-CNTs					PChCl-CNTs					Pn,n-CNTs				
	Sum of squares	**df**	**Mean square**	**F-value**	**p-value prob > F**	**Sum of squares**	**df**	**Mean square**	**F-value**	**p-value prob > F**	**Sum of squares**	**df**	**Mean square**	**F-value**	**p-value prob > F**
Model	6493.46	9	721.50	173.99	0.0006	8077.90	9	897.54	91.50	0.0017	51.73	7	7.39	42.90	0.0004
A	864.43	1	864.43	208.46	0.0007	1712.26	1	1712.26	174.56	0.0009	9.24	1	9.24	53.63	0.0007
B	4767.08	1	4767.08	1149.57	< 0.0001	4490.73	1	4490.73	457.83	0.0002	40.31	1	40.31	234.07	< 0.0001
C	276.05	1	276.05	66.57	0.0039	580.80	1	580.80	59.21	0.0046	1.93	1	1.93	11.21	0.0204
AB	11.01	1	11.01	2.65	0.2017	499.28	1	499.28	50.90	0.0057	0.020	1	0.020	0.12	0.7482
AC	57.94	1	57.94	13.97	0.0334	9.77	1	9.77	1.00	0.3919	0.21	1	0.21	1.25	0.3148
BC	4.08	1	4.08	0.98	0.3944	162.18	1	162.18	16.53	0.0268					
A^2	0.54	1	0.54	0.13	0.7431	24.04	1	24.04	2.45	0.2154	0.66	1	0.66	3.83	0.1078
B^2	9.20	1	9.20	2.22	0.2331	114.63	1	114.63	11.69	0.0419	0.79	1	0.79	4.57	0.0857
C^2	1.30	1	1.30	0.31	0.6143	99.31	1	99.31	10.12	0.0500					
	Adj R-Squared 0.99		**Pred R-Squared 0.97**			**Adj R-Squared 0.98**		**Pred R-Squared 0.95**			**Adj R-Squared 0.96**		**Pred R-Squared 0.88**		
	C.V. % 3.52		**Std. Dev 2.04**			**C.V. % 4.46**		**Std. Dev 3.13**			**C.V. % 7.25**		**Std. Dev 0.42**		

*A: pH, B: adsorbent dosage and C: contact time; ** The "Pred R-Squared" is in reasonable agreement with the "Adj R-Squared".

Table 4.25: List of the actual and predicted values for MO removal response.

Run order	P-CNTs		PChCl-CNTs		Pn,n-CNTs*	
	Actual	Predicted	Actual	Predicted	Actual	Predicted
1	35.47	36.10	53.61	54.13	4.26	3.87
2	18.07	18.53	6.12	7.13	1.95	2.10
3	80.24	80.70	93.28	94.29	7.96	8.26
4	67.35	67.83	77.90	78.89	6.68	6.49
5	51.11	50.56	76.92	76.17	4.82	5.08
6	22.77	22.23	34.36	33.58	2.68	2.65
7	98.55	98.02	99.09	98.31	9.64	9.47
8	75.08	74.38	87.62	87.33	6.87	7.04
9	48.87	49.17	69.31	68.38	5.40	5.30
10	59.46	58.85	76.90	78.76	5.15	5.68
11	80.19	80.49	94.18	93.25	7.25	7.15
12	54.74	52.72	67.00	63.48	5.28	5.24
13	60.91	63.23	76.13	78.72	6.52	6.12

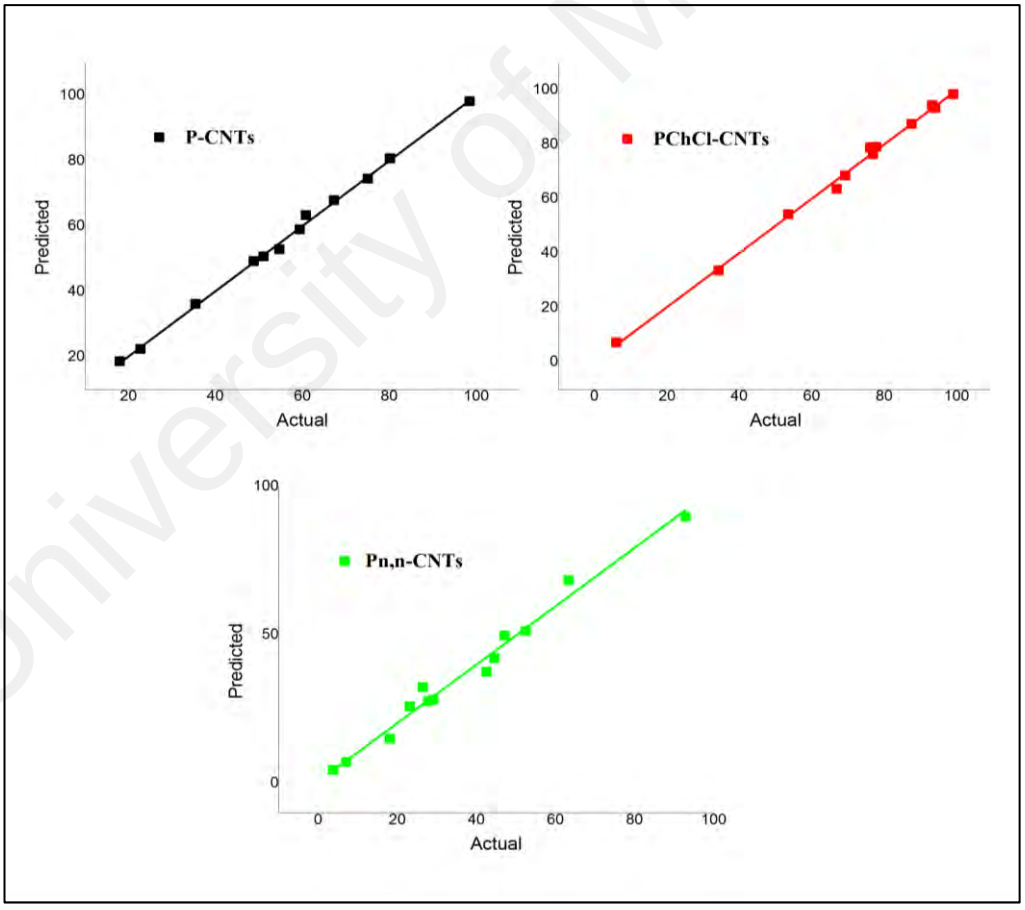

Figure 4.28: Predicted values vs actual values for MO removal response.

(b) ***The interactive effects of selected independent parameters on the adsorption of MO***

Figure 4.29 shows the interaction effects of pH and contact time on MO R% of all adsorbents at constant adsorbent dosage, while Figure 4.30 represents the interaction effects of pH and adsorbent dosage on MO R% of adsorbent at constant contact time. It is noticeable that the variation in the MO removal at different solution pH values reveals the importance of pH factor on the adsorption process. The adsorption of MO onto the used adsorbents increased as the pH value came close to acidic. This can be justified by two assumptions: (1) changes in the charge of the adsorbent surface , and (2) Dissociation/ ionization of the dye molecule (Yao et al., 2011). On the other hand, the R% increased along with the increase of contact time until the adsorption reached equilibrium. As well as, it is obvious that the R% of MO is influenced by the adsorbent dosage, as the dosage increased the R% increased due to the availability of more surface area of the adsorbent and in consequence, more adsorption sites are available to capture MO from water. (Wu, 2007; Yao et al., 2010). The optimum experiment conditions for MO% removal (Table 4.26) was selected by setting several constrains and different importance levels for optimization of four goals, namely the contact time, pH, adsorbent dosage and R% of MO as shown in Table 4.27.

Table 4.26:Optimum adsorption conditions suggested by DOE software for MO adsorption.

Adsorbent	pH	Dose (mg)	Contact time (min)	Predicted Removal (%)
P-CNTs	2	11.91	60.00	85.51
PChCl-CNTs	2	7.45	51.50	89.6
Pn,n-CNTs	2	9.77	60.00	62.34

Table 4.27: Constraints for optimization process based on CCD for MO adsorption.

Name		Goal	Lower limit	Upper limit	Importance
A		In range	2	10	-
B		Minimize	5	15	2
C		In range	20	60	-
R%	P-CNTs	Maximize	18.07	98.55	5
	PChCl-CNTs		6.12	99.09	
	Pn,n-CNTs		1.95	9.6	

A: pH, B: adsorbent dosage (mg) and C: contact time (min)

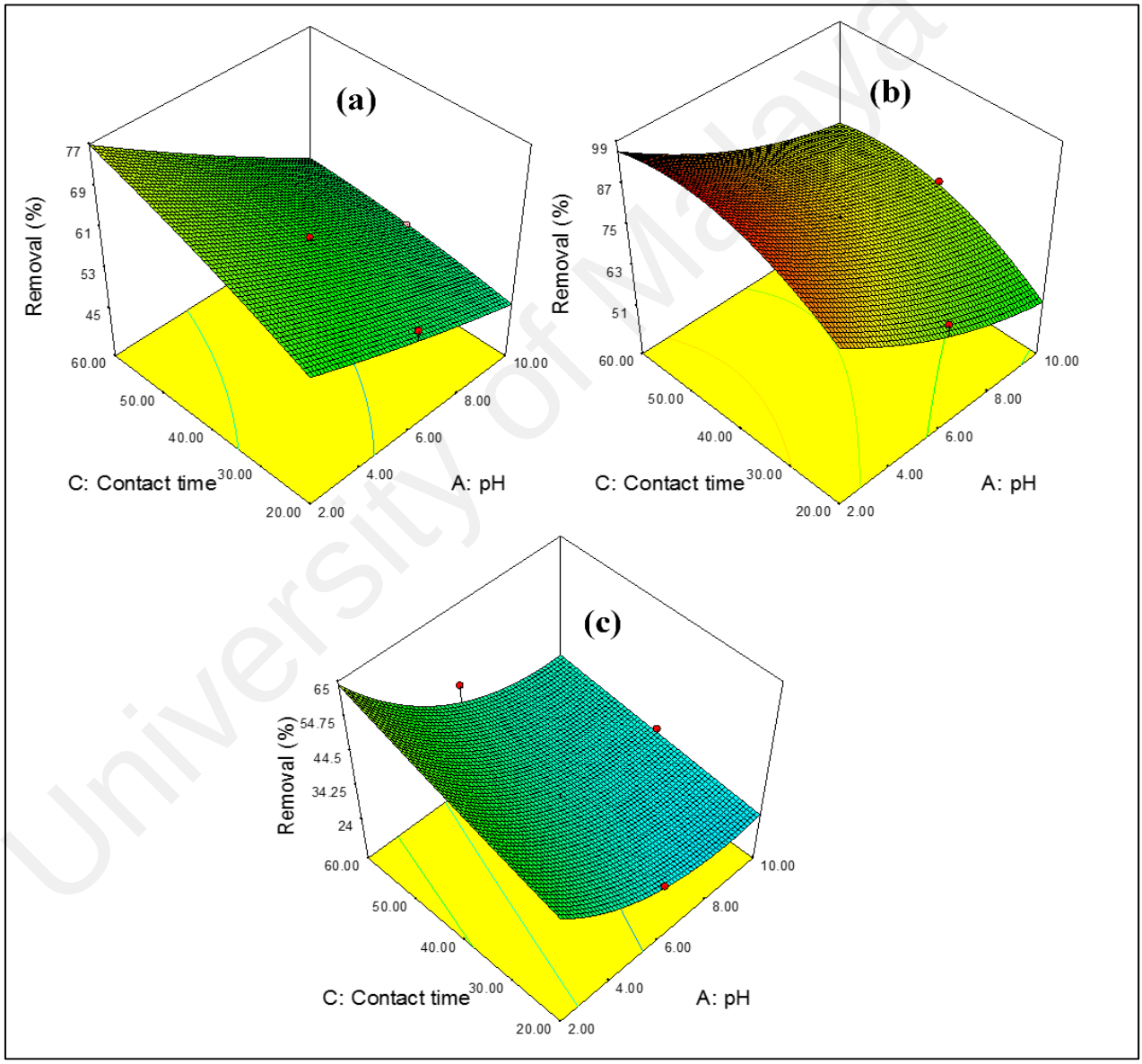

Figure 4.29: Surface response representation of MO removal (%) interaction with pH and contact time by fixing adsorbent dosage to the optimum value for a) P-CNTs, b) PChCl-CNTs and c) Pn,n-CNTs.

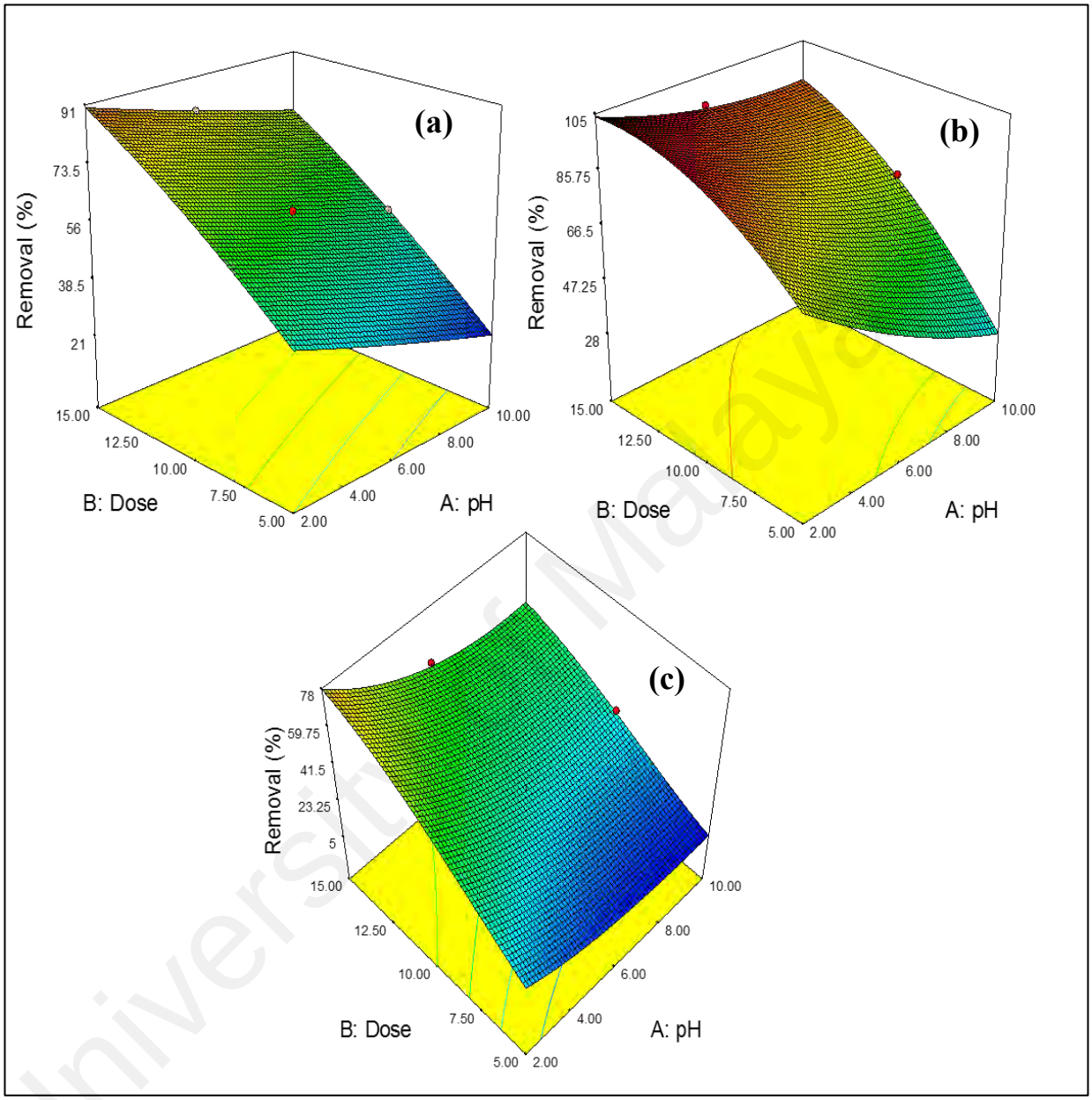

Figure 4.30: Surface response representation of MO removal (%) interaction with pH and adsorbent dosage by fixing contact time to the optimum value for a) P-CNTs, b) PChCl-CNTs and c) Pn,n-CNTs.

4.2.3.2 Kinetics studies

In order to acquire a better understanding of the adsorption kinetic behavior of MO onto PCNTs, PChCl-CNTs and Pn,n-CNTs, four of the well-known kinetic models were used to analyze the experimental data, i.e. pseudo-first order, pseudo-second order and intraparticle diffusion kinetic model. The kinetic experiments for each adsorbent were conducted at the optimum conditions selected by DOE, with agitation speed of 180 rpm and MO initial concentration of 40 mg/L. A contact time of 6 h was used to ensure that the adsorption process reached equilibrium

Figure 4.31, Figure 4.32 and Figure 4.33 show the plots of kinetic models for all examined adsorbents. All related equations and parameters are listed in Table 4.28. The value of the correlation coefficient (R^2) is an indication of the suitability of each model. It is obvious that the adsorption rate for all adsorbents can be well described by pseudo-second order with R^2 value (> 0.99) higher than that of Pseudo-first order. This suggests that the chemisorption is a significant rate-determining step and also suggests the involvement of the adsorbent and the adsorbate in the adsorption process through sharing of electrons or valence forces (Arshadi et al., 2016; Ho & McKay, 1999). Similar kinetic model fitting was observed for the adsorption behavior of different anionic dyes onto various kinds of adsorbents (Dulman & Cucu-Man, 2009; Porkodi & Kumar, 2007; Zhuannian et al., 2009). For further explanation of the adsorption kinetics, the intraparticle diffusion model (ID) was investigated to analyze the diffusion mechanism during the adsorption process. It is well known that the only condition that approves the involvement of ID in the adsorption process and confirms its role as a sole rate-controlling step is to obtain a linear plot of q_t versus $t^{1/2}$ passes through the origin (Ai, Zhang, & Meng, 2011; Arami, Limaee, & Mahmoodi, 2008). As seen from Figure 4.33 the ID plot of each adsorbent was not linear over whole time range and did not pass through the origin. This indicates the participation of ID in the adsorption process but it was not the

only rate controlling step, as well as the boundary layer diffusion, to some degree, is the dominant step in MO adsorption process (Cheung, Szeto, & McKay, 2007). It can be noticed from Figure 4.33 that all adsorbents showed linear film diffusion region followed by linear intraparticle diffusion region, proving that the adsorption process is influenced by more than one process (Uğurlu, 2009). The first region corresponds to the stage of rapid diffusion of MO molecules through the solution and their adsorption by the exterior surface of the adsorbents (Ahmad et al., 2017). Whereas the second linear section occurs when the first adsorption stage reaches saturation and the molecules of MO gradually diffuse through the pores of the adsorbents and adsorbed by the adsorbents interior surface (Ai, Zhang, & Meng, 2011). Moreover, the value of C is represented by the intercept and it refers to the thickness of the boundary layer. The increase in C value is a sign of a thicker boundary layer and its higher effect in the adsorption process (Mahmoud et al., 2012). Pn,n-CNTs adsorbent attained the highest C value, conforming the more involvement of the adsorbent surface in the adsorption of MO.

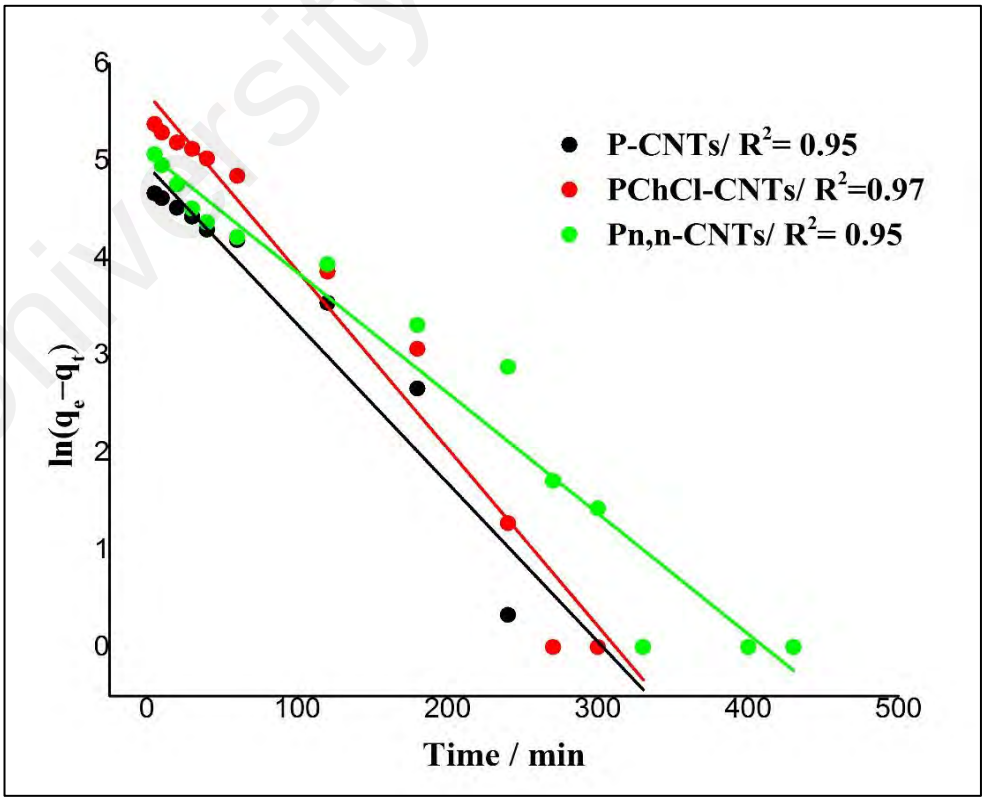

Figure 4.31: Pseudo-first order kinetic model for MO adsorption.

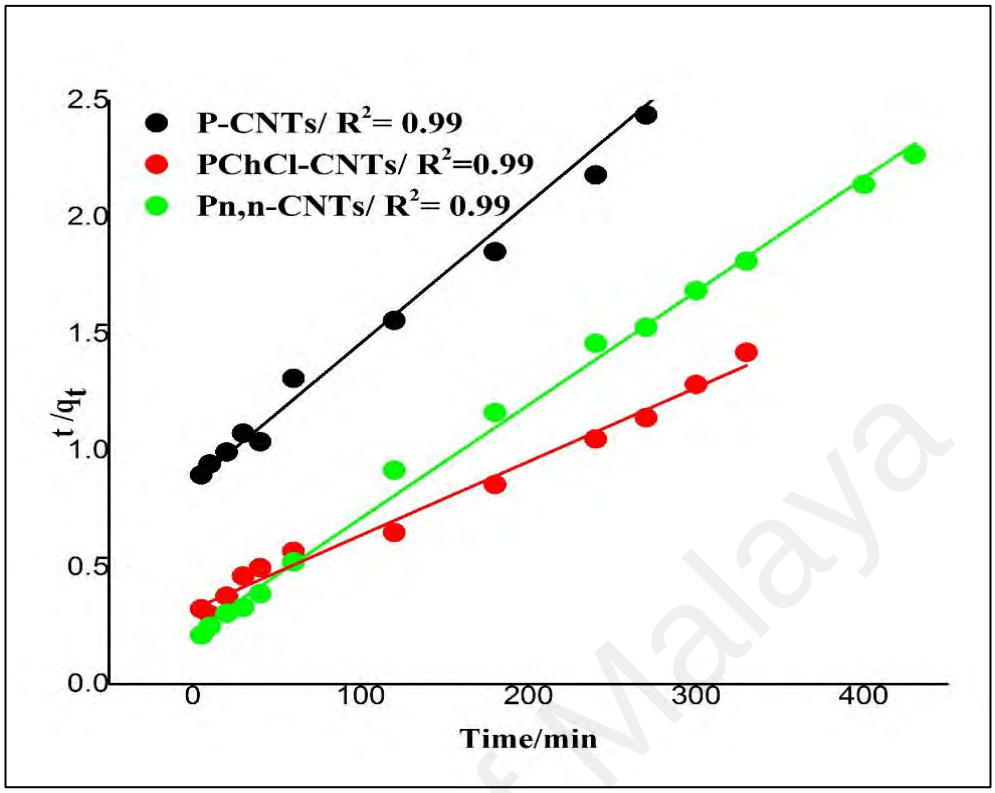

Figure 4.32: Pseudo-second order kinetic model for MO adsorption

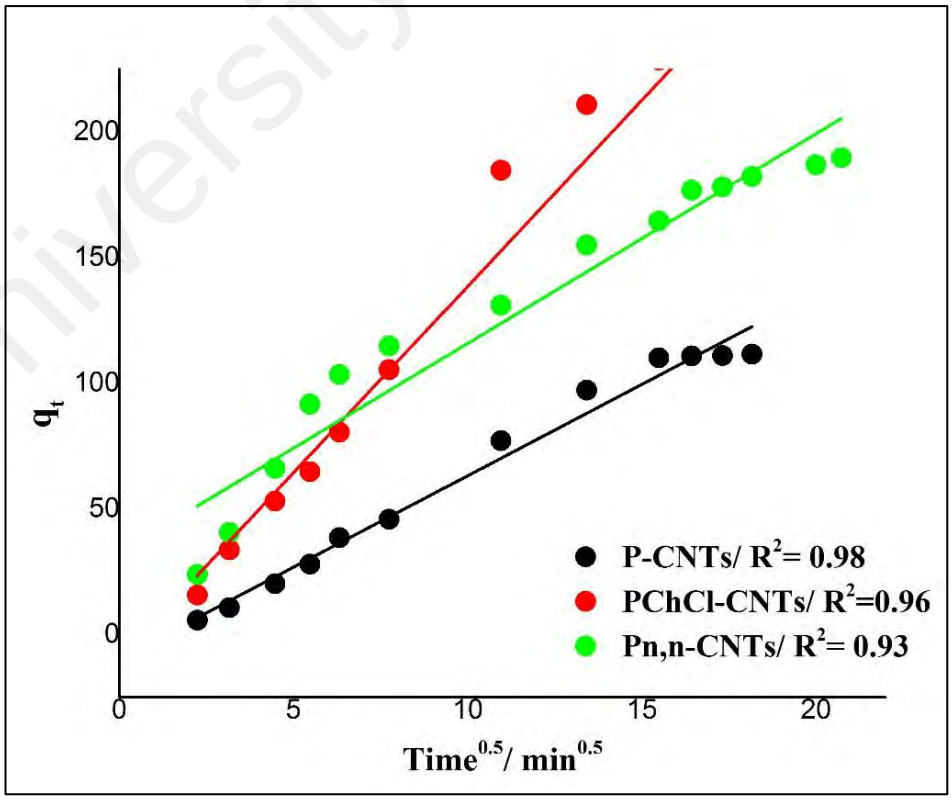

Figure 4.33: Intraparticle diffusion kinetic model for MO adsorption.

Table 4.28: linearized equations of all studied kinetics models and their parameters and correlation coefficients for MO adsorption.

Kinetics	Equations	Parameters	Adsorbents		
			P-CNTs	PChCl-CNTs	Pn,n-CNTs
Pseudo-first order	$\ln(q_e - q_t) = \ln q_e - k_1 t$	R^2	0.95	0.97	0.95
		K_1	0.016	0.018	0.0124
		q_e	142.59	298.12	162.967
Pseudo-Second order	$\frac{t}{q_t} = \frac{1}{k_2 q_e^2} + \frac{t}{q_e}$	R^2	0.99	0.99	0.99
		K_2	4.17×10^{-5}	3.1×10^{-5}	0.00011
		q_e	166.79	316.20	205.69
Intraparticle diffusion	$q_t = K_d t^{\frac{1}{2}} + C$	R^2	0.98	0.96	0.94
		K_d	7.27	14.82	8.33
		C	9.61	9.74	32.4
qe (experimental)			110.93	232.16	189.68

4.2.3.3 Isotherms studies

Three isotherm models (i.e. Langmuir, Freundlich and Temkin) were used to investigate the behavior of MO adsorption onto P-CNTs, PChCl-CNTs and Pn,n-CNTs. The linearized plots for the four studied isotherms are presented in Figure 4.34, figure 4.35 and Figure 4.36 and the linearized equations the models and related parameters are listed in Table 4.29. Although the correlation coefficient (R^2) value of both Freundlich and Temkin isotherm models, Langmuir isotherm model acquired the highest R^2 value with "a range of (0.97-099)" which confirms the reliability of this model to explain the adsorption behavior of MO on each adsorbent. This suggests the occurrence of a monolayer adsorption of MO at the homogeneous sites on the adsorbent surface, as well as, no more adsorption occurs when these sites are saturated with MO molecules. The value of the adsorption capacity (Q_m) is clearly increased after the functionalization of CNTs with DES to reach 310.2 (mg g^{-1}) for PChCl-CNTs. The dimensionless constant R_L is known as separation factor and considered a basic feature to determine the

favorability of Langmuir isotherm model. Table 4.29 reveals that Langmuir isotherm model is highly favorable with ($0 < R_L < 1$) for all adsorbents.

Regarding Freundlich isotherm model, R^2 value was higher than 0.9 for all adsorbents, which assumes the presence of non-equivalent binding sites in the heterogeneous surface energy system (Mahmoud et al., 2012). The value of the slope (1/n) decides the intensity of MO adsorption onto the heterogeneous surface and it was stated that the closer its value to zero, the more heterogeneous the system is (Yao et al., 2011). Whereas, n value determines the status of the adsorption chrematistics, and as it can be seen from Table 4.29, the n value for all adsorbents was greater than 1 which represents a suitable adsorption condition (Mahmoud et al., 2012).

On the other hand, Temkin isotherm was carried out to estimate the effect of adsorbent-adsorbate interactions on the adsorption process and it is characterized by the uniform distribution of binding energies (Ghaedi, Hassanzadeh, & Kokhdan, 2011). The value of B_1 represents the heat of adsorption while the value of K_t represents the equilibrium binding constant and they are listed in Table 4.29. In general, the interpretation of the experimental results showed that, Langmuir isotherm is the best model which can describe the adsorption of MO on all concerned adsorbent. Table 4.30 shows a comparison of maximum monolayer adsorption capacity of MO on different reported adsorbents.

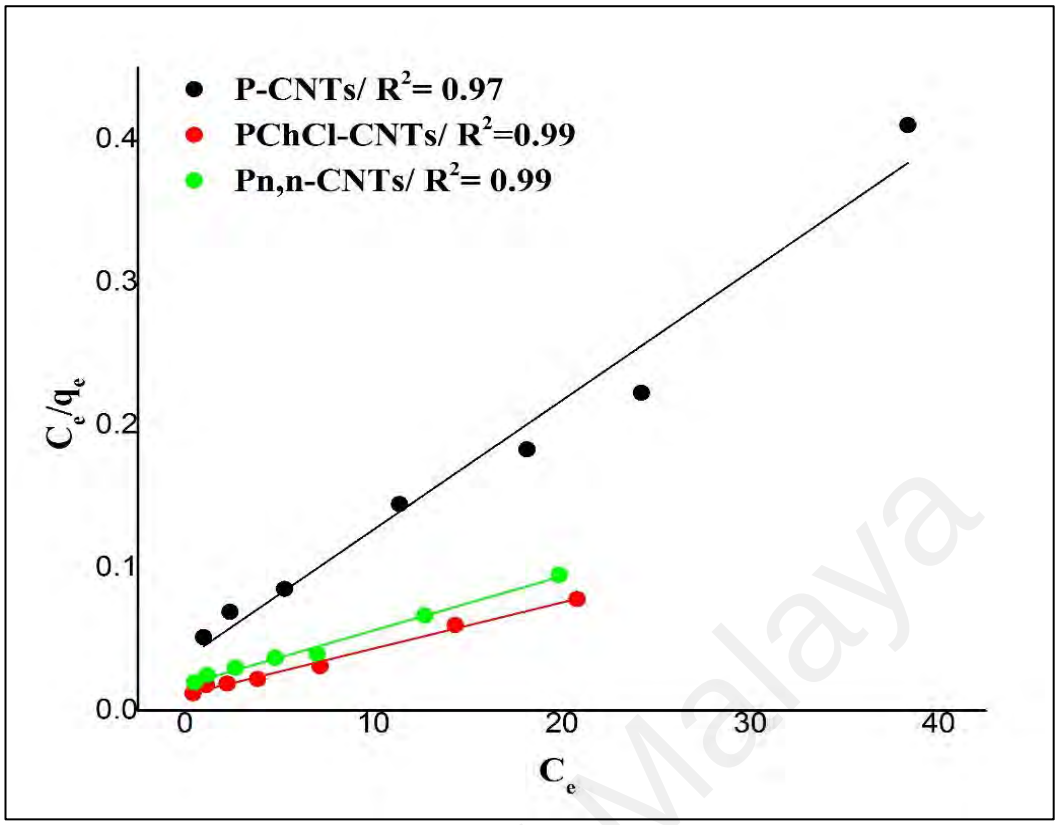

Figure 4.34: Langmuir isotherm model for MO adsorption.

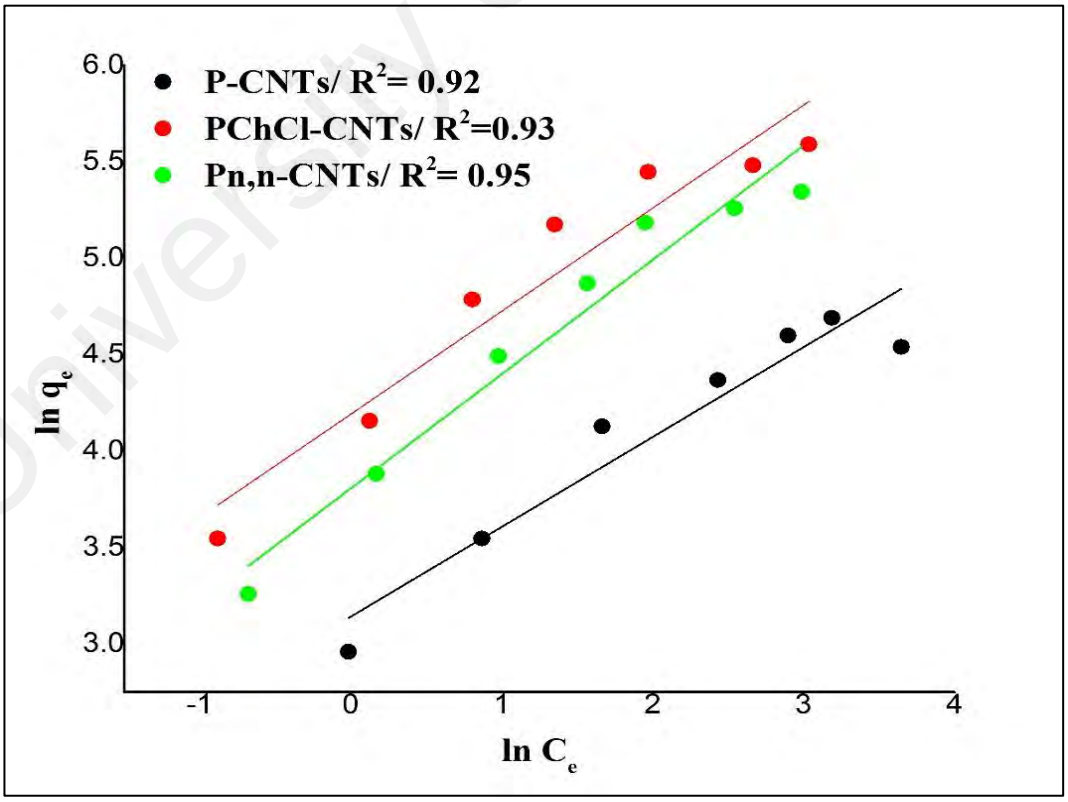

Figure 4.35: Freundlich isotherm model for MO adsorption.

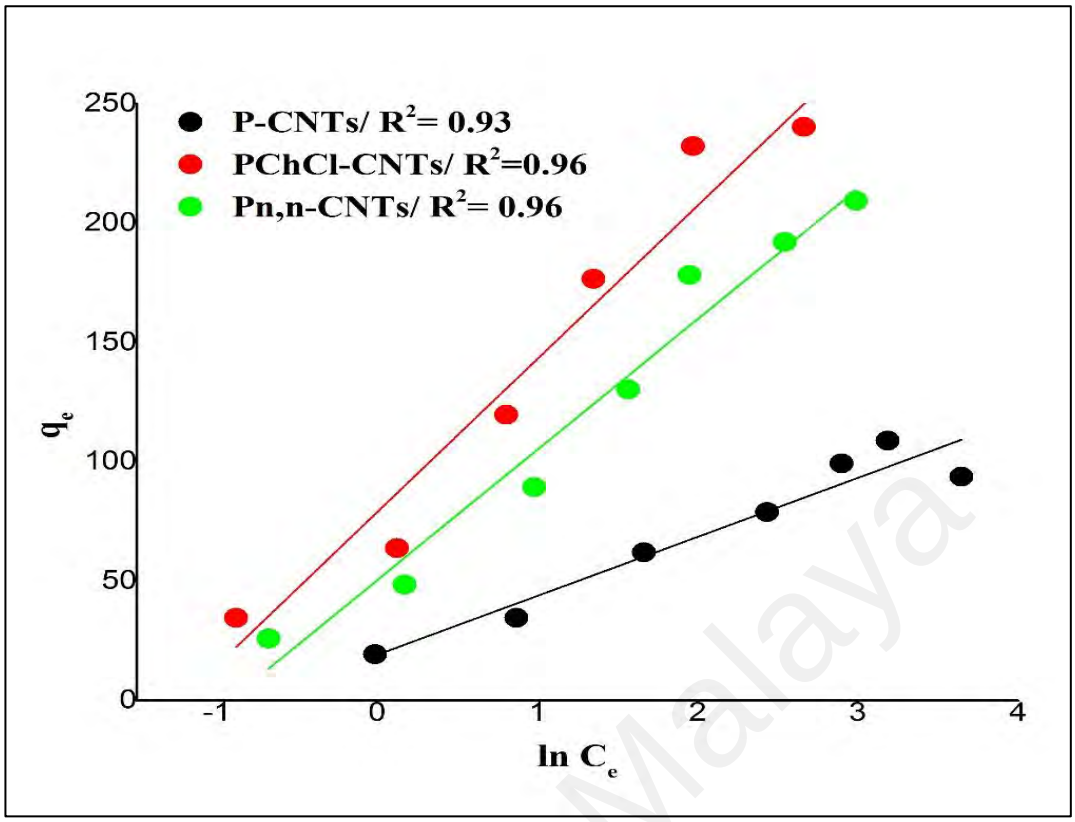

Figure 4.36: Temkin isotherm model for MO adsorption.

Table 4.29: linearized equations of the examined isotherm models along with their parameters and correlation coefficients.

Isotherms	Equations	Parameters	Adsorbents		
			P-CNTs	PChCl-CNTs	Pn,n-CNTs
Langmuir	$\frac{C_e}{q_e} = \frac{1}{K_L Q_m} + \left(\frac{1}{Q_m}\right) C_e$	R^2	0.97	0.99	0.99
		Q_m (mg g^{-1})	110.45	310.2	263.14
		K_L (L mg^{-1})	3.98	3.45	4.73
		R_L	0.043	0.049	0.036
Freundlich	$\ln q_e = \ln K_F + \frac{1}{n} \ln C_e$	R^2	0.92	0.93	0.95
		n	2.14	1.87	1.68
		K_F (L mg^{-1})	23.10	65.99	44.9
Temkin	$q_e = B_1 \ln k_t + B_1 \ln C_e$	R^2	0.93	0.96	0.96
		B_1	24.7	64.21	54.68
		k_t (L mg^{-1})	2.16	3.41	2.51

Table 4.30: comparison between the maximum adsorption capacity of DES treated CNTs and some reported adsorbents for MO removal.

Adsorbent	Q_{max} (mg/g)	Reference
P-CNTs	110.45	Present work
PChCl-CNTs	310.2	Present work
Pn,n-CNTs	263.14	Present work
De-oiled soya	16.7	(Mittal et al., 2007)
Banana peel	21	(Annadurai, Juang, & Lee, 2002)
Orange peel	20.5	(Annadurai, Juang, & Lee, 2002)
MWCNTs produced by CVD using the carbon from acetylene cracking	35.4–64.7	(Yao et al., 2011)
Silver nanoparticle loaded on activated carbon	55.54	(Karimi, Mousavi, & Sadeghian, 2012)
m-CS/ λ-Fe_2O_3/MWCNTs	66.09	(Zhu et al., 2010)
Hypercrosslinked polymeric adsorbent	70.9	(Huang, Huang, et al., 2008)
Iron(II) cross-linked chitin-based gel beads	107.5	(Li, Du, et al., 2010)
Calcined layered double hydroxides	200	(Ni et al., 2007)
Phragmites australis activated carbon	217	(Chen et al., 2010)
mesoporous carbon	294.1	(Mohammadi et al., 2011)
Lapindo volcanic mud	333.33	(Jalil et al., 2010)
Pinecone derived activated carbon	404.4	(Samarghandi et al., 2010)
λ-Fe_2O_3/SiO_2 nanocomposites	476	(Deligeer, Gao, & Asuha, 2011)

4.2.3.4 Mechanism

To understand and illustrate the mechanism of MO adsorption mechanism onto P-CNTs, PChCl-CNTs and Pn,n-CNTs, a simple glance was taken onto the role of solution pH and onto the assumption of ID kinetic model. It was clear that controlling the value of solution pH played a remarkable role in MO adsorption process through defining the interaction between the adsorbent and the adsorbate. It is worth mentioning that based on the value of solution pH, MO can be presented in two different chemical structure, expressed as (Chen et al., 2010):

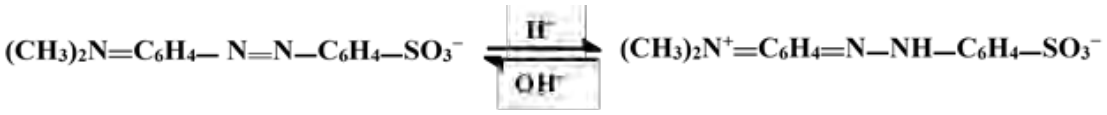

As already mentioned, the removal efficiency of the studied adsorbents was low at high pH value and it increased as pH value decreased until it reached its maximum value

at pH 2. Such phenomena may attribute to the number of negatively charged sites onto the surface of DES functionalized CNTs due to the added oxygen-containing groups. Under alkaline conditions, the decrease in MO removal is because of: (1) the competition between the abundant OH^- ions and anionic dye in the solution (Yao et al., 2011); (2) The electrostatic repulsion between MO anionic molecules and the adsorbent as the number of negatively charged sites are increased onto the adsorbent surface (Hamdaoui & Naffrechoux, 2007b; Jalil et al., 2010). Further, the higher MO adsorption under acidic condition may attribute to the electrostatic attraction between the anionic molecules of MO and the neutralized negatively charged sites resulted from the abundance of H^+ ions (Mittal et al., 2007) . On the other hand, ID model assumed that the adsorption of MO can involve two main steps: (1) film diffusion by which MO adsorption occurs onto the surface of the adsorbent; (2) intraparticle or pore diffusion by which MO molecules adsorbed onto the interior surface of the adsorbent. Moreover, the results revealed the involvement of other mechanisms in MO adsorption process along with intraparticle diffusion, as well as it was found that the boundary layer diffusion was the controlling step to some extent.

CHAPTER 5: CONCLUSION AND RECOMMENDATIONS

5.1 Conclusion

In this study five types of salts and two types of HBDs were used to prepare two new systems of DESs. Screening studies for salt to HBD ration was carried out to determine the most stable molar ration for each prepared DESs. A comprehensive investigation of the physical properties for the studied DESs were conducted including freezing point, density, viscosity, conductivity, surface tension and FTIR. Thereafter, the capability of DESs as novel functionalization agents was ascertained through the selection of two DESs to functionalize pristine CNTs (P-CNTs), primarily acidified CNTs with H_2SO_4 (S-CNTs) and oxidized CNTs with $KMnO_4$ (K-CNTs). Later, DES-functionalized CNTs were used as novel adsorbents for the removal of two organic pollutants from water (i.e 2,4-DCP and MO). An elementary screening for batch adsorption studies was conducted to select the adsorbent with the highest removal efficiency to proceed with further characterizations. The characterization for the selected adsorbents included BET surface area, Raman spectroscopy, FTIR, TGA, SEM, TEM, and zeta potential. The optimum removal conditions were detected through optimizations studies by using RSM-CCD experimental design. The removal efficiency was chosen as the only response and ANOVA was used to develop its empirical equation. Moreover, four kinetic models and four isotherm models were studied for each selected adsorbent. The key findings of this work can be summarized as following:

1. The synthesis process of each studied DES involved changing its compositions ratio by fixing the ratio of salt and changing the ratio of HBD from 1 to 10 as a result 100 DESs samples were produced. The first ratio by which DES is presented in stable and homogeneous liquid phase was selected to be the optimum ratio and based on that only ten DESs were chosen for further studies of their physical properties. The unsuccessful salt to HBD ratio resulted in the

formation of participates and crystals within DES mixture which led to the appearance of many phases, during synthesizing and storing of DESs such as solid and semi-solid phases. This phenomenon was explained by the insufficient amount of HBD to build a hydrogen bonding with the halide anion of the abundant salt concentration. All selected DESs were compatible with the general definition of DESs that describes DES of having a freezing point lower that of its individual constituents.

2. The Physical properties of the ten selected DESs were obtained at temperature range of (20-80) °C, then all data were simply correlated and fitted to adequate models. Both surface tension and density data decreased with the increase of temperature and their temperature trends were fitted linearly. The temperature trend for the conductivity and viscosity was exponential growth and exponential decay, respectively, and both trends were successfully fitted to Arhenius-like model. Additionally, the FTIR analysis revealed that the chemical structure of both salt and HBD has an explicit effect on the DESs structure. Furthermore, it was concluded that varying the temperature, or/and the DESs individual components, or/and the ratio of salt to HBD are of a considerable concern to obtain a eutectic mixture with adaptable physical characterizations to a specific type of application, which consequently contributes in widening the horizon of DESs employments as ILs alternatives.
3. EG based DESs were used as samples to study the possibility of using DESs as functionalization gent for CNTs. Three types of CNTs (i.e. P-CNTs, K-CNTs and S-CNTs) were simply sonicated with each of the selected DES and used as novel adsorbent for the removal of two organic pollutants, namely, 2,4-DCP and MO. The characterization studies for the new adsorbents were performed for the adsorbents that showed the highest removal efficiency for

both studied pollutants. The characterization studies proved the functionality of DESs as functionalization agents by significantly purifying CNTs, adding more oxygen containing groups, enhancing CNTs dispersion, and increasing CNTs surface area with conserving their unique structure.

4. Based on screening studies, four adsorbents (P-CNTs, S-CNTs, PChCl-CNTs and SChCl-CNTs) were found to have the highest removal efficiency for 2,4-DCP from water. The Optimization studies conducted by RSM-CCD experimental design revealed that the adsorption of 2,4-DCP was highly dependent on the pH solution, and on the surface charge of the adsorbents, the optimum pH for all adsorbents was found to be less than pka value of 2,4-DCP (>7.4). The 2,4-DCP adsorption kinetics for all examined adsorbents were well described by pseudo-second order model. The equilibrium adsorption data was best presented by Langmuir isotherm model indicating a monolayer adsorption on a homogeneous surface with a highest maximum adsorption capacity of 390.53 mg/g obtained for SChCl-CNTs.
5. Twelve DESs-CNTs combinations were applied as new adsorbents for MO removal from aqueous solution. Three adsorbents (P-CNTs, PChCl-CNTs and Pn,n-CNTs) showed the highest removal efficiency and their optimal removal conditions for MO removal were achieved at pH 2.0, adsorbent dosage > 10.0 mg and contact time > 60 min. Pseudo-second order perfectly explained MO adsorption system. The adsorption data were excellently fitted by Langmuir isotherm with the maximum adsorption capacity of 310.2 mg/g and 263.14 mg/g for PChCl-CNTs and Pn,n-CNTs respectively.

5.2 Recommendations

In summary, the result of this work is very promising and it is suggesting a prominent approach in CNTs functionalization area and in water remediation domain. Many recommendations can be concluded from the different steps of the experimental work which can lead to a better performance or future research work. These proposed recommendations can be summarized as following:

1. Further research is recommended to use metal salts or organic salts to synthesize new types of DESs and study their characteristics to encourage their applications on both laboratory and industrial scales.
2. The concept of using DESs as functionalization agents for MWCNTs can comprehend other types of nanomaterials such as SWCNTs, graphene, titanium dioxide, iron oxides, etc.
3. Due to the distinguished performance of the novel DESs-CNTs adsorbents in the removal of MO and 2,4-DCP, the investigation should cover the removal of other types of hazardous organic pollutants and bio-pollutants.
4. Adsorption processes can be further developed by: (a) Performing a column study to explore the breakthrough conditions, (b) Desorption study is necessary to determine the recyclability of the adsorbent composite, or/ and (c) A competitive study is required to analyze the behavior of each adsorbent in the presence of other organic pollutants or heavy metal ions.
5. In addition to adsorption processes, other techniques including membrane processes, photocatalysis and sensing systems can be used for further investigations of the applicability of the novel DES-CNTs combinations.

REFERENCES

Abbasizadeh, S., Keshtkar, A. R., & Mousavian, M. A. (2014). Sorption of heavy metal ions from aqueous solution by a novel cast PVA/TiO2 nanohybrid adsorbent functionalized with amine groups. Journal of Industrial and Engineering Chemistry, 20(4), 1656-1664.

Abbott, A. P. (2004). Application of hole theory to the viscosity of ionic and molecular liquidsChemPhysChem. 5(8), 1242-1246.

Abbott, A. P., Barron, J. C., Ryder, K. S., & Wilson, D. (2007a). Eutectic-Based Ionic Liquids with Metal-Containing Anions and Cations. Chem. - Eur. J., 13, 6495-6501.

Abbott, A. P., Barron, J. C., Ryder, K. S., & Wilson, D. (2007b). Eutectic-Based Ionic Liquids with Metal-Containing Anions and Cations. Chemistry – A European Journal, 13(22), 6495-6501.

Abbott, A. P., Boothby, D., Capper, G., Davies, D. L., & Rasheed, R. K. (2004). Deep eutectic solvents formed between choline chloride and carboxylic acids: versatile alternatives to ionic liquids. Journal of the American Chemical Society, 126(29), 9142-9147.

Abbott, A. P., Capper, G., Davies, D. L., Munro, H. L., Rasheed, R. K., & Tambyrajah, V. (2001). Preparation of novel, moisture-stable, Lewis-acidic ionic liquids containing quaternary ammonium salts with functional side chains. Chemical Communications(19), 2010-2011.

Abbott, A. P., Capper, G., Davies, D. L., & Rasheed, R. (2004a). Ionic Liquids Based upon Metal Halide/Substituted Quaternary Ammonium Salt Mixtures. J. Inorg. Chem., 43, 3447-3452.

Abbott, A. P., Capper, G., Davies, D. L., & Rasheed, R. (2004b). Ionic Liquids Based upon Metal Halide/Substituted Quaternary Ammonium Salt Mixtures. Inorganic Chemistry, 43(11), 3447-3452.

Abbott, A. P., Capper, G., Davies, D. L., Rasheed, R. K., & Tambyrajah, V. (2003). Novel solvent properties of choline chloride/urea mixtures. Chemical Communications(1), 70-71.

Abbott, A. P., Capper, G., & Gray, S. (2006a). Design of Improved Deep Eutectic Solvents Using Hole Theory. ChemPhysChem, 7, 803-806.

Abbott, A. P., Capper, G., & Gray, S. (2006b). Design of Improved Deep Eutectic Solvents Using Hole Theory. ChemPhysChem, 7(4), 803-806.

Abbott, A. P., Frisch, G., Hartley, J., & Ryder, K. S. (2011). Processing of metals and metal oxides using ionic liquids. Green Chemistry, 13(3), 471-481.

Abbott, A. P., Harris, R. C., & Ryder, K. S. (2007a). Application of hole theory to define ionic liquids by their transport properties. J. Phys. Chem. B, 111, 4910-4913.

Abbott, A. P., Harris, R. C., & Ryder, K. S. (2007b). Application of Hole Theory to Define Ionic Liquids by their Transport Properties†. The Journal of Physical Chemistry B, 111(18), 4910-4913.

Abbott, A. P., Harris, R. C., Ryder, K. S., D'Agostino, C., Gladden, L. F., & Mantle, M. D. (2011a). Glycerol eutectics as sustainable solvent systems. Green Chemistry, 13(1), 82-90.

Abbott, A. P., Harris, R. C., Ryder, K. S., D'Agostino, C., Gladden, L. F., & Mantle, M. D. (2011b). Glycerol eutectics as sustainable solvent systems. Green Chem., 13, 82-90.

Abbott, A. P., & McKenzie, K. J. (2006). Application of ionic liquids to the electrodeposition of metals. Physical Chemistry Chemical Physics, 8(37), 4265-4279.

Abbott, A. P., Ttaib, K. E., Frisch, G., Ryder, K. S., & Weston, D. (2012). The electrodeposition of silver composites using deep eutectic solvents. Physical Chemistry Chemical Physics, 14(7), 2443-2449.

Abdel-Ghani, N. T., El-Chaghaby, G. A., & Helal, F. S. (2014). Individual and competitive adsorption of phenol and nickel onto multiwalled carbon nanotubes. Journal of Advanced Research(0).

Abdel Salam, M., & Burk, R. C. (2008). Thermodynamics of pentachlorophenol adsorption from aqueous solutions by oxidized multi-walled carbon nanotubes. Applied Surface Science, 255(5, Part 1), 1975-1981.

Abo-Hamad, A., Hayyan, M., AlSaadi, M. A., & Hashim, M. A. (2015). Potential applications of deep eutectic solvents in nanotechnology. Chemical Engineering Journal, 273, 551-567.

Abo-Hamad, A., Hayyan, M., AlSaadi, M. A., Mirghani, M. E., & Hashim, M. A. (2017). Functionalization of carbon nanotubes using eutectic mixtures: A promising route for enhanced aqueous dispersibility and electrochemical activity. Chemical Engineering Journal, 311, 326-339.

Adams, L. K., Lyon, D. Y., & Alvarez, P. J. J. (2006). Comparative eco-toxicity of nanoscale TiO2, SiO2, and ZnO water suspensions. Water Research, 40(19), 3527-3532.

Afroz, R., Masud, M. M., Akhtar, R., & Duasa, J. B. (2014). Water pollution: Challenges and future direction for water resource management policies in Malaysia. Environment and urbanization ASIA, 5(1), 63-81.

Ahmad, A., Razali, M. H., Mamat, M., Mehamod, F. S. B., & Amin, K. A. M. (2017). Adsorption of methyl orange by synthesized and functionalized-CNTs with 3-aminopropyltriethoxysilane loaded TiO 2 nanocomposites. Chemosphere, 168, 474-482.

Ahmed, F., Santos, C. M., Mangadlao, J., Advincula, R., & Rodrigues, D. F. (2013). Antimicrobial PVK:SWNT nanocomposite coated membrane for water purification: Performance and toxicity testing. Water Research, 47(12), 3966-3975.

Ahmed, F., Santos, C. M., Vergara, R. A. M. V., Tria, M. C. R., Advincula, R., & Rodrigues, D. F. (2011). Antimicrobial Applications of Electroactive PVK-SWNT Nanocomposites. Environmental Science & Technology, 46(3), 1804-1810.

Ai, L., Zhang, C., Liao, F., Wang, Y., Li, M., Meng, L., & Jiang, J. (2011). Removal of methylene blue from aqueous solution with magnetite loaded multi-wall carbon nanotube: Kinetic, isotherm and mechanism analysis. Journal of Hazardous Materials, 198(0), 282-290.

Ai, L., Zhang, C., & Meng, L. (2011). Adsorption of methyl orange from aqueous solution on hydrothermal synthesized Mg–Al layered double hydroxide. Journal of Chemical & Engineering Data, 56(11), 4217-4225.

Ajji, Z., & Ali, A. M. (2007). Adsorption of methyl violet and brilliant blue onto poly(vinyl alcohol) membranes grafted with N-vinyl imidazole/acrylic acid. Nuclear Instruments and Methods in Physics Research Section B: Beam Interactions with Materials and Atoms, 265(1), 362-365.

Aksu, Z. (2005a). Application of biosorption for the removal of organic pollutants: a review. Process Biochemistry, 40(3–4), 997-1026.

Aksu, Z. (2005b). Application of biosorption for the removal of organic pollutants: a review. Process Biochemistry, 40(3), 997-1026.

Aksu, Z., & Yener, J. (2001). A comparative adsorption/biosorption study of mono-chlorinated phenols onto various sorbents. Waste management, 21(8), 695-702.

Al-Bastaki, N. (2004). Removal of methyl orange dye and Na 2 SO 4 salt from synthetic waste water using reverse osmosis. Chemical Engineering and Processing: Process Intensification, 43(12), 1561-1567.

Al-Hamdi, A. M., Sillanpää, M., & Dutta, J. (2015). Photocatalytic degradation of phenol by iodine doped tin oxide nanoparticles under UV and sunlight irradiation. Journal of Alloys and Compounds, 618(0), 366-371.

AlOmar, M. K., Alsaadi, M. A., Hayyan, M., Akib, S., & Hashim, M. A. (2016). Functionalization of CNTs surface with phosphonuim based deep eutectic solvents for arsenic removal from water. Applied Surface Science, 389, 216-226.

AlOmar, M. K., Alsaadi, M. A., Hayyan, M., Akib, S., Ibrahim, R. K., & Hashim, M. A. (2016). Lead removal from water by choline chloride based deep eutectic solvents functionalized carbon nanotubes. Journal of Molecular Liquids.

AlOmar, M. K., Hayyan, M., Alsaadi, M. A., Akib, S., Hayyan, A., & Hashim, M. A. (2016a). Glycerol-based deep eutectic solvents: Physical properties. Journal of Molecular Liquids, 215, 98-103.

AlOmar, M. K., Hayyan, M., Alsaadi, M. A., Akib, S., Hayyan, A., & Hashim, M. A. (2016b). Glycerol-based deep eutectic solvents: Physical properties. J. Mol. Liq., 215, 98-103.

Amini, M., Jahanshahi, M., & Rahimpour, A. (2013). Synthesis of novel thin film nanocomposite (TFN) forward osmosis membranes using functionalized multi-walled carbon nanotubes. Journal of Membrane Science, 435(0), 233-241.

Amini, M., Younesi, H., Bahramifar, N., Lorestani, A. A. Z., Ghorbani, F., Daneshi, A., & Sharifzadeh, M. (2008). Application of response surface methodology for optimization of lead biosorption in an aqueous solution by Aspergillus niger. Journal of Hazardous Materials, 154(1), 694-702.

Andreescu, S., Njagi, J., Ispas, C., & Ravalli, M. T. (2009). JEM Spotlight: Applications of advanced nanomaterials for environmental monitoring. Journal of environmental monitoring, 11(1), 27-40.

Annadurai, G., Juang, R.-S., & Lee, D.-J. (2002). Use of cellulose-based wastes for adsorption of dyes from aqueous solutions. Journal of hazardous materials, 92(3), 263-274.

Apul, O. G., & Karanfil, T. (2015). Adsorption of synthetic organic contaminants by carbon nanotubes: A critical review. Water Research, 68(0), 34-55.

Aquino, A., Chan, J., Giolma, K., & Loh, M. (2010). The effect of a fullerene water suspension on the growth, cell viability, and membrane integrity of Escherichia coli B23. J. Exp. Microbiol. Immunol, 14, 13-20.

Arahman, N., Maruyama, T., Sotani, T., & Matsuyama, H. (2009). Fouling reduction of a poly(ether sulfone) hollow-fiber membrane with a hydrophilic surfactant prepared via non-solvent-induced phase separation. Journal of Applied Polymer Science, 111(3), 1653-1658.

Arami, M., Limaee, N. Y., & Mahmoodi, N. M. (2008). Evaluation of the adsorption kinetics and equilibrium for the potential removal of acid dyes using a biosorbent. Chemical Engineering Journal, 139(1), 2-10.

Arias, L. R., & Yang, L. (2009). Inactivation of Bacterial Pathogens by Carbon Nanotubes in Suspensions. Langmuir, 25(5), 3003-3012.

Arshadi, M., Mousavinia, F., Amiri, M., & Faraji, A. (2016). Adsorption of methyl orange and salicylic acid on a nano-transition metal composite: Kinetics, thermodynamic and electrochemical studies. Journal of Colloid and Interface Science, 483, 118-131.

Aruoja, V., Dubourguier, H.-C., Kasemets, K., & Kahru, A. (2009). Toxicity of nanoparticles of CuO, ZnO and TiO2 to microalgae Pseudokirchneriella subcapitata. Science of The Total Environment, 407(4), 1461-1468.

Auffan, M., Rose, J., Proux, O., Borschneck, D., Masion, A., Chaurand, P., . . . Bottero, J.-Y. (2008). Enhanced Adsorption of Arsenic onto Maghemites Nanoparticles: As(III) as a Probe of the Surface Structure and Heterogeneity. Langmuir, 24(7), 3215-3222.

Augugliaro, V., Litter, M., Palmisano, L., & Soria, J. (2006). The combination of heterogeneous photocatalysis with chemical and physical operations: A tool for improving the photoprocess performance. Journal of Photochemistry and Photobiology C: Photochemistry Reviews, 7(4), 127-144.

Bae, T.-H., & Tak, T.-M. (2005). Effect of TiO2 nanoparticles on fouling mitigation of ultrafiltration membranes for activated sludge filtration. Journal of Membrane Science, 249(1–2), 1-8.

Bahadori, L., Chakrabarti, M. H., Mjalli, F. S., AlNashef, I. M., Manan, N. S. A., & Hashim, M. A. (2013a). Physicochemical properties of ammonium-based deep eutectic solvents and their electrochemical evaluation using organometallic reference redox systems. Electrochimica Acta, 113(0), 205-211.

Bahadori, L., Chakrabarti, M. H., Mjalli, F. S., AlNashef, I. M., Manan, N. S. A., & Hashim, M. A. (2013b). Physicochemical properties of ammonium-based deep eutectic solvents and their electrochemical evaluation using organometallic reference redox systems. Electrochim. Acta, 113, 205-211.

Bahr, J. L., Yang, J., Kosynkin, D. V., Bronikowski, M. J., Smalley, R. E., & Tour, J. M. (2001). Functionalization of Carbon Nanotubes by Electrochemical Reduction of Aryl Diazonium Salts: A Bucky Paper Electrode. Journal of the American Chemical Society, 123(27), 6536-6542.

Bailey, S. E., Olin, T. J., Bricka, R. M., & Adrian, D. D. (1999). A review of potentially low-cost sorbents for heavy metals. Water research, 33(11), 2469-2479.

Balamurugan, R., Sundarrajan, S., & Ramakrishna, S. (2011). Recent trends in nanofibrous membranes and their suitability for air and water filtrations. Membranes, 1(3), 232-248.

Balta, S., Sotto, A., Luis, P., Benea, L., Van der Bruggen, B., & Kim, J. (2012). A new outlook on membrane enhancement with nanoparticles: The alternative of ZnO. Journal of Membrane Science, 389(0), 155-161.

Bamba, T. (2014). High-throughput simultaneous analysis of pesticides by supercritical fluid chromatography coupled to high-resolution mass spectrometry. Journal of agricultural and food chemistry.

Banerjee, S., Pillai, S. C., Falaras, P., O'Shea, K. E., Byrne, J. A., & Dionysiou, D. D. (2014). New Insights into the Mechanism of Visible Light Photocatalysis. The Journal of Physical Chemistry Letters, 5(15), 2543-2554.

Baolong, Z., Baishun, C., Keyu, S., Shangjin, H., Xiaodong, L., Zongjie, D., & Kelian, Y. (2003). Preparation and characterization of nanocrystal grain TiO2 porous microspheres. Applied Catalysis B: Environmental, 40(4), 253-258.

Başar, C. A. (2006). Applicability of the various adsorption models of three dyes adsorption onto activated carbon prepared waste apricot. Journal of Hazardous Materials, 135(1), 232-241.

Berger, T., Diwald, O., Knözinger, E., Sterrer, M., & Yates Jr, J. T. (2006). UV induced local heating effects in TiO 2 nanocrystals. Physical Chemistry Chemical Physics, 8(15), 1822-1826.

Bernardo, P., Drioli, E., & Golemme, G. (2009). Membrane gas separation: a review/state of the art. Industrial & Engineering Chemistry Research, 48(10), 4638-4663.

Bhatt, J., Mondal, D., Devkar, R. V., & Prasad, K. (2016). Synthesis of functionalized N-doped graphene DNA hybrid material in a deep eutectic solvent. Green Chemistry.

Bhattacharya, S., & Banerjee, R. (2008). Laccase mediated biodegradation of 2, 4-dichlorophenol using response surface methodology. Chemosphere, 73(1), 81-85.

Bilgin Simsek, E., Aytas, B., Duranoglu, D., Beker, U., & Trochimczuk, A. W. (2016). A comparative study of 2-chlorophenol, 2,4-dichlorophenol, and 2,4,6-trichlorophenol adsorption onto polymeric, commercial, and carbonaceous adsorbents. Desalin. Water Treat., 57(21), 9940-9956.

Bird, R. B., Stewart, W. E., & Lightfoot, E. N. Transport Phenomena: John Wiley & Sons, Inc.

Bjørkøy, A., & Fiksdal, L. (2009). Characterization of biofouling on hollow fiber membranes using confocal laser scanning microcscopy and image analysis. Desalination, 245(1–3), 474-484.

Boulos, R. A., Eroglu, E., Chen, X., Scaffidi, A., Edwards, B. R., Toster, J., & Raston, C. L. (2013). Unravelling the structure and function of human hair. Green Chemistry, 15(5), 1268-1273.

Buonomenna, M. G. (2013). Membrane processes for a sustainable industrial growth. RSC Advances, 3(17), 5694-5740.

Bystrzejewski, M., & Pyrzyńska, K. (2011). Kinetics of copper ions sorption onto activated carbon, carbon nanotubes and carbon-encapsulated magnetic nanoparticles. Colloids and Surfaces A: Physicochemical and Engineering Aspects, 377(1–3), 402-408.

Bystrzejewski, M., Pyrzyńska, K., Huczko, A., & Lange, H. (2009). Carbon-encapsulated magnetic nanoparticles as separable and mobile sorbents of heavy metal ions from aqueous solutions. Carbon, 47(4), 1201-1204.

Cai, N., & Larese-Casanova, P. (2014). Sorption of carbamazepine by commercial graphene oxides: A comparative study with granular activated carbon and multiwalled carbon nanotubes. Journal of Colloid and Interface Science, 426(0), 152-161.

Calace, N., Nardi, E., Petronio, B., & Pietroletti, M. (2002). Adsorption of phenols by papermill sludges. Environmental Pollution, 118(3), 315-319.

Cao, X., Ma, J., Shi, X., & Ren, Z. (2006). Effect of TiO2 nanoparticle size on the performance of PVDF membrane. Applied Surface Science, 253(4), 2003-2010.

Caratto, V., Setti, L., Campodonico, S., Carnasciali, M., Botter, R., & Ferretti, M. (2012). Synthesis and characterization of nitrogen-doped TiO2 nanoparticles prepared by sol–gel method. Journal of sol-gel science and technology, 63(1), 16-22.

Chang, C.-F., Chang, C.-Y., & Hsu, T.-L. (2011). Removal of fluoride from aqueous solution with the superparamagnetic zirconia material. Desalination, 279(1–3), 375-382.

Chang, J.-S., Chou, C., Lin, Y.-C., Lin, P.-J., Ho, J.-Y., & Hu, T. L. (2001). Kinetic characteristics of bacterial azo-dye decolorization by Pseudomonas luteola. Water Research, 35(12), 2841-2850.

Chávez, F., Pérez-Sánchez, G. F., Goiz, O., Zaca-Morán, P., Peña-Sierra, R., Morales-Acevedo, A., . . . Soledad-Priego, M. (2013). Sensing performance of palladium-functionalized WO3 nanowires by a drop-casting method. Applied Surface Science, 275(0), 28-35.

Chen, C.-Y., Ozasa, K., Kitamura, F., Katsumata, K.-i., Maeda, M., Okada, K., & Matsushita, N. (2015). Self-organization of TiO2 Nanobamboos by Anodization with Deep Eutectic Solvent. Electrochimica Acta, 153, 409-415.

Chen, C., Hu, J., Shao, D., Li, J., & Wang, X. (2009). Adsorption behavior of multiwall carbon nanotube/iron oxide magnetic composites for Ni(II) and Sr(II). Journal of Hazardous Materials, 164(2–3), 923-928.

Chen, C., & Wang, X. (2006). Adsorption of Ni (II) from aqueous solution using oxidized multiwall carbon nanotubes. Ind. Eng. Chem. Res., 45(26), 9144-9149.

Chen, F., Xie, S., Zhang, J., & Liu, R. (2013). Synthesis of spherical Fe3O4 magnetic nanoparticles by co-precipitation in choline chloride/urea deep eutectic solvent. Materials Letters, 112, 177-179.

Chen, G.-C., Shan, X.-Q., Pei, Z.-G., Wang, H., Zheng, L.-R., Zhang, J., & Xie, Y.-N. (2011). Adsorption of diuron and dichlobenil on multiwalled carbon nanotubes as affected by lead. Journal of Hazardous Materials, 188(1–3), 156-163.

Chen, G.-C., Shan, X.-Q., Wang, Y.-S., Wen, B., Pei, Z.-G., Xie, Y.-N., . . . Pignatello, J. J. (2009). Adsorption of 2,4,6-trichlorophenol by multi-walled carbon nanotubes as affected by Cu(II). Water Research, 43(9), 2409-2418.

Chen, S., Kobayashi, K., Miyata, Y., Imazu, N., Saito, T., Kitaura, R., & Shinohara, H. (2009). Morphology and Melting Behavior of Ionic Liquids inside Single-Walled Carbon Nanotubes. Journal of the American Chemical Society, 131(41), 14850-14856.

Chen, S., Zhang, J., Zhang, C., Yue, Q., Li, Y., & Li, C. (2010). Equilibrium and kinetic studies of methyl orange and methyl violet adsorption on activated carbon derived from Phragmites australis. Desalination, 252(1), 149-156.

Chen, Y., Vedala, H., Kotchey, G. P., Audfray, A., Cecioni, S., Imberty, A., . . . Star, A. (2011). Electronic detection of lectins using carbohydrate-functionalized nanostructures: graphene versus carbon nanotubes. ACS nano, 6(1), 760-770.

Chen, Z., Pierre, D., He, H., Tan, S., Pham-Huy, C., Hong, H., & Huang, J. (2011). Adsorption behavior of epirubicin hydrochloride on carboxylated carbon nanotubes. International Journal of Pharmaceutics, 405(1–2), 153-161.

Cheung, W., Szeto, Y., & McKay, G. (2007). Intraparticle diffusion processes during acid dye adsorption onto chitosan. Bioresource technology, 98(15), 2897-2904.

Chin, S. S., Chiang, K., & Fane, A. G. (2006). The stability of polymeric membranes in a TiO2 photocatalysis process. Journal of Membrane Science, 275(1–2), 202-211.

Cho, H.-H., Huang, H., & Schwab, K. (2011). Effects of Solution Chemistry on the Adsorption of Ibuprofen and Triclosan onto Carbon Nanotubes. Langmuir, 27(21), 12960-12967.

Choi, H., Al-Abed, S. R., Dionysiou, D. D., Stathatos, E., & Lianos, P. (2010). Chapter 8 TiO2-Based Advanced Oxidation Nanotechnologies for Water Purification and Reuse. In C. E. Isabel & I. S. Andrea (Eds.), Sustainability Science and Engineering (Vol. Volume 2, pp. 229-254): Elsevier.

Choi, H., Stathatos, E., & Dionysiou, D. D. (2006). Sol–gel preparation of mesoporous photocatalytic TiO2 films and TiO2/Al2O3 composite membranes for environmental applications. Applied Catalysis B: Environmental, 63(1–2), 60-67.

Choi, H., Zakersalehi, A., Al-Abed, S. R., Han, C., & Dionysiou, D. D. (2014). Chapter 8 - Nanostructured Titanium Oxide Film- and Membrane-Based Photocatalysis for Water Treatment. In A. S. S. D. Savage (Ed.), Nanotechnology Applications for Clean Water (Second Edition) (pp. 123-132). Oxford: William Andrew Publishing.

Choi, J.-H., Jegal, J., & Kim, W.-N. (2006). Fabrication and characterization of multi-walled carbon nanotubes/polymer blend membranes. Journal of Membrane Science, 284(1–2), 406-415.

Chong MN, J. B., Chow CWK, Saint C. (2010). Recent developments in photocatalytic water treatment technology. Water Res., 44, 2997–3027.

Chong, M. N., Jin, B., Chow, C. W. K., & Saint, C. (2010). Recent developments in photocatalytic water treatment technology: A review. Water Research, 44(10), 2997-3027.

Chowdhury, S. R., & Yanful, E. K. (2013). Kinetics of cadmium(II) uptake by mixed maghemite-magnetite nanoparticles. Journal of Environmental Management, 129(0), 642-651.

Chronopoulos, D., Karousis, N., Zhao, S., Wang, Q., Shinohara, H., & Tagmatarchis, N. (2014). Photocatalytic application of nanosized CdS immobilized onto functionalized MWCNTs. Dalton Trans., 43(20), 7429-7434.

Chung, T.-S., Li, X., Ong, R. C., Ge, Q., Wang, H., & Han, G. (2012). Emerging forward osmosis (FO) technologies and challenges ahead for clean water and clean energy applications. Current Opinion in Chemical Engineering, 1(3), 246-257.

Ciston, S., Lueptow, R. M., & Gray, K. A. (2009). Controlling biofilm growth using reactive ceramic ultrafiltration membranes. Journal of Membrane Science, 342(1–2), 263-268.

Cloete, T. E. (2010). Nanotechnology in water treatment applications: Horizon Scientific Press.

Coates, J. (2000a). Interpretation of infrared spectra, a practical approach. Encyclopedia of analytical chemistry.

Coates, J. (2000b). Interpretation of Infrared Spectra, A Practical Approach Encyclopedia of Analytical Chemistry (pp. 10815–10837). New York, NY: John Wiley & Sons, Ltd.

Cornelissen, E., Harmsen, D., De Korte, K., Ruiken, C., Qin, J.-J., Oo, H., & Wessels, L. (2008). Membrane fouling and process performance of forward osmosis membranes on activated sludge. Journal of Membrane Science, 319(1), 158-168.

Crane, R. A., & Scott, T. B. (2012). Nanoscale zero-valent iron: Future prospects for an emerging water treatment technology. Journal of Hazardous Materials, 211, 112-125.

Cui, H., Li, Q., Gao, S., & Shang, J. K. (2012). Strong adsorption of arsenic species by amorphous zirconium oxide nanoparticles. Journal of Industrial and Engineering Chemistry, 18(4), 1418-1427.

Cui, Y., Kim, S. N., Naik, R. R., & McAlpine, M. C. (2012). Biomimetic peptide nanosensors. Accounts of chemical research, 45(5), 696-704.

Cvjetko Bubalo, M., Vidović, S., Radojčić Redovniković, I., & Jokić, S. (2015). Green solvents for green technologies. Journal of Chemical Technology & Biotechnology, 90(9), 1631-1639.

D'Agostino, C., Harris, R. C., Abbott, A. P., Gladden, L. F., & Mantle, M. D. (2011). Molecular motion and ion diffusion in choline chloride based deep eutectic solvents studied by 1H pulsed field gradient NMR spectroscopy. Physical Chemistry Chemical Physics, 13(48), 21383-21391.

Dada, A., Olalekan, A., Olatunya, A., & Dada, O. (2012). Langmuir, Freundlich, Temkin and Dubinin–Radushkevich isotherms studies of equilibrium sorption of Zn2+ unto phosphoric acid modified rice husk. IOSR Journal of Applied Chemistry, 3(1), 38-45.

Dai, Y., van Spronsen, J., Witkamp, G.-J., Verpoorte, R., & Choi, Y. H. (2013). Natural deep eutectic solvents as new potential media for green technology. Analytica Chimica Acta, 766, 61-68.

Daifullah, A. A. M., & Girgis, B. S. (1998). REMOVAL OF SOME SUBSTITUTED PHENOLS BY ACTIVATED CARBON OBTAINED FROM AGRICULTURAL WASTE. Water Research, 32(4), 1169-1177.

Daraei, P., Madaeni, S. S., Ghaemi, N., Khadivi, M. A., Astinchap, B., & Moradian, R. (2013). Enhancing antifouling capability of PES membrane via mixing with various types of polymer modified multi-walled carbon nanotube. Journal of Membrane Science, 444(0), 184-191.

Darvishi Cheshmeh Soltani, R., Khataee, A., Godini, H., Safari, M., Ghanadzadeh, M., & Rajaei, M. (2015). Response surface methodological evaluation of the adsorption of textile dye onto biosilica/alginate nanobiocomposite: thermodynamic, kinetic, and isotherm studies. Desalination and Water Treatment, 56(5), 1389-1402.

Das, A. K., Maiti, S., & Khatua, B. (2015). High performance electrode material prepared through in-situ polymerization of aniline in the presence of zinc acetate and

graphene nanoplatelets for supercapacitor application. Journal of Electroanalytical Chemistry, 739, 10-19.

Datsyuk, V., Kalyva, M., Papagelis, K., Parthenios, J., Tasis, D., Siokou, A., . . . Galiotis, C. (2008). Chemical oxidation of multiwalled carbon nanotubes. Carbon, 46(6), 833-840.

De Gusseme, B., Hennebel, T., Christiaens, E., Saveyn, H., Verbeken, K., Fitts, J. P., . . . Verstraete, W. (2011). Virus disinfection in water by biogenic silver immobilized in polyvinylidene fluoride membranes. Water Research, 45(4), 1856-1864.

De Laat, J., Le, G. T., & Legube, B. (2004). A comparative study of the effects of chloride, sulfate and nitrate ions on the rates of decomposition of H 2 O 2 and organic compounds by Fe (II)/H 2 O 2 and Fe (III)/H 2 O 2. Chemosphere, 55(5), 715-723.

de María, P. D., & Maugeri, Z. (2011). Ionic liquids in biotransformations: from proof-of-concept to emerging deep-eutectic-solvents. Current opinion in chemical biology, 15(2), 220-225.

Deligeer, W., Gao, Y. W., & Asuha, S. (2011). Adsorption of methyl orange on mesoporous γ-Fe2O3/SiO2 nanocomposites. Applied Surface Science, 257(8), 3524-3528.

Demirak, A., Dalman, Ö., Tilkan, E., Yıldız, D., Yavuz, E., & Gökçe, C. (2011). Biosorption of 2, 4 dichlorophenol (2, 4-DCP) onto Posidonia oceanica (L.) seagrass in a batch system: Equilibrium and kinetic modeling. Microchemical journal, 99(1), 97-102.

Deng, J., Shao, Y., Gao, N., Deng, Y., Tan, C., Zhou, S., & Hu, X. (2012). Multiwalled carbon nanotubes as adsorbents for removal of herbicide diuron from aqueous solution. Chemical Engineering Journal, 193–194(0), 339-347.

Deshmukh, R. R., Rajagopal, R., & Srinivasan, K. V. (2001). Ultrasound promoted C-C bond formation: Heck reaction at ambient conditions in room temperature ionic liquids. Chemical Communications(17), 1544-1545.

Di Francia, G., Alfano, B., & La Ferrara, V. (2009). Conductometric Gas Nanosensors. Journal of Sensors, 2009.

Dizaj, S. M., Lotfipour, F., Barzegar-Jalali, M., Zarrintan, M. H., & Adibkia, K. (2014). Antimicrobial activity of the metals and metal oxide nanoparticles. Materials Science and Engineering: C, 44(0), 278-284.

Dizaj, S. M., Mennati, A., Jafari, S., Khezri, K., & Adibkia, K. (2014). Antimicrobial Activity of Carbon-Based Nanoparticles. Advanced Pharmaceutical Bulletin.

Dong, F., Zhao, W., & Wu, Z. (2008). Characterization and photocatalytic activities of C, N and S co-doped TiO2 with 1D nanostructure prepared by the nano-confinement effect. Nanotechnology, 19(36), 365607.

Dresselhaus, M. S., Jorio, A., Hofmann, M., Dresselhaus, G., & Saito, R. (2010). Perspectives on carbon nanotubes and graphene Raman spectroscopy. Nano letters, 10(3), 751-758.

Dulman, V., & Cucu-Man, S. M. (2009). Sorption of some textile dyes by beech wood sawdust. Journal of hazardous materials, 162(2), 1457-1464.

Duncan, T. V. (2011). Applications of nanotechnology in food packaging and food safety: barrier materials, antimicrobials and sensors. Journal of colloid and interface science, 363(1), 1-24.

Durand, E., Lecomte, J., & Villeneuve, P. (2013). Deep eutectic solvents: Synthesis, application, and focus on lipase- catalyzed reactions. European Journal of Lipid Science and Technology, 115(4), 379-385.

Engates, K., & Shipley, H. (2011). Adsorption of Pb, Cd, Cu, Zn, and Ni to titanium dioxide nanoparticles: effect of particle size, solid concentration, and exhaustion. Environmental Science and Pollution Research, 18(3), 386-395.

Fagan, R., McCormack, D. E., Dionysiou, D. D., & Pillai, S. C. (2016). A review of solar and visible light active TiO2 photocatalysis for treating bacteria, cyanotoxins and contaminants of emerging concern. Materials Science in Semiconductor Processing, 42, Part 1, 2-14.

Fan, J., Shi, Z., Tian, M., Wang, J., & Yin, J. (2012). Unzipped multiwalled carbon nanotube oxide/multiwalled carbon nanotube hybrids for polymer reinforcement. ACS applied materials & interfaces, 4(11), 5956-5965.

Fan, L., Zhou, Y., Yang, W., Chen, G., & Yang, F. (2008). Electrochemical degradation of aqueous solution of Amaranth azo dye on ACF under potentiostatic model. Dyes and Pigments, 76(2), 440-446.

Fang, J., Lyon, D. Y., Wiesner, M. R., Dong, J., & Alvarez. (2007). Effect of a Fullerene Water Suspension on Bacterial Phospholipids and Membrane Phase Behavior. Environmental Science & Technology, 41(7), 2636-2642.

Fathizadeh, M., Aroujalian, A., & Raisi, A. (2011). Effect of added NaX nano-zeolite into polyamide as a top thin layer of membrane on water flux and salt rejection in a reverse osmosis process. Journal of Membrane Science, 375(1–2), 88-95.

Feng, L., Cao, M., Ma, X., Zhu, Y., & Hu, C. (2012). Superparamagnetic high-surface-area Fe3O4 nanoparticles as adsorbents for arsenic removal. Journal of Hazardous Materials, 217–218(0), 439-446.

Feng, L., Zhu, A., Wang, H., & Shi, H. (2014). A nanosensor based on quantum-dot haptens for rapid, on-site immunoassay of cyanotoxin in environmental water. Biosensors and Bioelectronics, 53, 1-4.

Ferey, G. (2008). Hybrid porous solids: past, present, future. Chemical Society Reviews, 37(1), 191-214.

Ferrari, A., Meyer, J., Scardaci, V., Casiraghi, C., Lazzeri, M., Mauri, F., . . . Roth, S. (2006). Raman spectrum of graphene and graphene layers. Physical review letters, 97(18), 187401.

Foo, K., & Hameed, B. (2010). Insights into the modeling of adsorption isotherm systems. Chemical Engineering Journal, 156(1), 2-10.

Fotiou, T., Triantis, T. M., Kaloudis, T., O'Shea, K. E., Dionysiou, D. D., & Hiskia, A. (2016). Assessment of the roles of reactive oxygen species in the UV and visible light photocatalytic degradation of cyanotoxins and water taste and odor compounds using C–TiO2. Water Research, 90, 52-61.

Francisco, M., van den Bruinhorst, A., & Kroon, M. C. (2013). Low-Transition-Temperature Mixtures (LTTMs): A New Generation of Designer Solvents. Angewandte Chemie International Edition, 52(11), 3074-3085.

Freundlich, H. (1906). Over the adsorption in solution. J. Phys. Chem, 57(385471), 1100-1107.

Fujishima, A., Zhang, X., & Tryk, D. A. (2008). TiO2 photocatalysis and related surface phenomena. Surface Science Reports, 63(12), 515-582.

Gao, H., Zhao, S., Cheng, X., Wang, X., & Zheng, L. (2013). Removal of anionic azo dyes from aqueous solution using magnetic polymer multi-wall carbon nanotube nanocomposite as adsorbent. Chemical Engineering Journal, 223(0), 84-90.

Garg, U. K., Kaur, M., Garg, V., & Sud, D. (2008). Removal of Nickel (II) from aqueous solution by adsorption on agricultural waste biomass using a response surface methodological approach. Bioresource technology, 99(5), 1325-1331.

Gaya, U. I., & Abdullah, A. H. (2008a). Heterogeneous photocatalytic degradation of organic contaminants over titanium dioxide: A review of fundamentals, progress and problems. Journal of Photochemistry and Photobiology C-Photochemistry Reviews, 9(1), 1-12.

Gaya, U. I., & Abdullah, A. H. (2008b). Heterogeneous photocatalytic degradation of organic contaminants over titanium dioxide: a review of fundamentals, progress and problems. Journal of Photochemistry and Photobiology C: Photochemistry Reviews, 9(1), 1-12.

Ge, F., Li, M.-M., Ye, H., & Zhao, B.-X. (2012). Effective removal of heavy metal ions Cd2+, Zn2+, Pb2+, Cu2+ from aqueous solution by polymer-modified magnetic nanoparticles. Journal of Hazardous Materials, 211–212(0), 366-372.

Ge, Q., Su, J., Chung, T.-S., & Amy, G. (2010). Hydrophilic Superparamagnetic Nanoparticles: Synthesis, Characterization, and Performance in Forward Osmosis Processes. Industrial & Engineering Chemistry Research, 50(1), 382-388.

Gerez, V., Rondano, K., & Pasquali, C. (2014). A simple manifold flow injection analysis for determining phosphorus in the presence of arsenate. Journal of Water Chemistry and Technology, 36(1), 19-24.

Geyikçi, F. (2013). Adsorption of Acid Blue 161 (AB 161) Dye from Water by Multi-walled Carbon Nanotubes. Fullerenes, Nanotubes and Carbon Nanostructures, 21(7), 579-593.

Ghaedi, M., Hassanzadeh, A., & Kokhdan, S. N. (2011). Multiwalled Carbon Nanotubes as Adsorbents for the Kinetic and Equilibrium Study of the Removal of Alizarin Red S and Morin. Journal of Chemical & Engineering Data, 56(5), 2511-2520.

Ghaedi, M., & Kokhdan, S. N. (2012). Oxidized multiwalled carbon nanotubes for the removal of methyl red (MR): kinetics and equilibrium study. Desalination and Water Treatment, 49(1-3), 317-325.

Ghatee, M. H., Zare, M., Moosavi, F., & Zolghadr, A. R. (2010). Temperature-dependent density and viscosity of the ionic liquids 1-alkyl-3-methylimidazolium iodides: experiment and molecular dynamics simulation. Journal of Chemical and Engineering Data, 55(9), 3084-3088.

Giap, S. G. E. (2010a). The hidden property of Arrhenius-type relationship: viscosity as a function of temperature.

Giap, S. G. E. (2010b). The hidden property of Arrhenius-type relationship: viscosity as a function of temperature. J. Phys. Sci., 21, 29-39.

Goi, A., & Trapido, M. (2002). Hydrogen peroxide photolysis, Fenton reagent and photo-Fenton for the degradation of nitrophenols: a comparative study. Chemosphere, 46(6), 913-922.

Gong, J.-L., Wang, B., Zeng, G.-M., Yang, C.-P., Niu, C.-G., Niu, Q.-Y., . . . Liang, Y. (2009). Removal of cationic dyes from aqueous solution using magnetic multi-wall carbon nanotube nanocomposite as adsorbent. Journal of Hazardous materials, 164(2–3), 1517-1522.

Gopal, R., Kaur, S., Feng, C. Y., Chan, C., Ramakrishna, S., Tabe, S., & Matsuura, T. (2007). Electrospun nanofibrous polysulfone membranes as pre-filters: particulate removal. Journal of membrane science, 289(1), 210-219.

Gopal, R., Kaur, S., Ma, Z., Chan, C., Ramakrishna, S., & Matsuura, T. (2006). Electrospun nanofibrous filtration membrane. Journal of Membrane Science, 281(1), 581-586.

Gordon, T., Perlstein, B., Houbara, O., Felner, I., Banin, E., & Margel, S. (2011). Synthesis and characterization of zinc/iron oxide composite nanoparticles and their antibacterial properties. Colloids and Surfaces a-Physicochemical and Engineering Aspects, 374(1-3), 1-8.

Gorke, J. T., Srienc, F., & Kazlauskas, R. J. (2008). Hydrolase-catalyzed biotransformations in deep eutectic solvents. Chemical Communications(10), 1235-1237.

Govindhan, M., Adhikari, B.-R., & Chen, A. (2014). Nanomaterials-based electrochemical detection of chemical contaminants. RSC Advances, 4(109), 63741-63760.

Grandi, S., Magistris, A., Mustarelli, P., Quartarone, E., Tomasi, C., & Meda, L. (2006). Synthesis and characterization of SiO 2–PEG hybrid materials. Journal of non-crystalline solids, 352(3), 273-280.

Gray, S. R., Ritchie, C. B., Tran, T., Bolto, B. A., Greenwood, P., Busetti, F., & Allpike, B. (2008). Effect of membrane character and solution chemistry on microfiltration performance. Water Research, 42(3), 743-753.

Greenlee, L. F., Lawler, D. F., Freeman, B. D., Marrot, B., & Moulin, P. (2009). Reverse osmosis desalination: Water sources, technology, and today's challenges. Water Research, 43(9), 2317-2348.

Gu, C.-D., & Tu, J.-P. (2011). Thermochromic behavior of chloro-nickel(II) in deep eutectic solvents and their application in thermochromic composite films. RSC Advances, 1(7), 1220-1227.

GU, C. D., MAI, Y. J., ZHOU, J. P., & TU, J. P. (2011). SnO2 NANOCRYSTALLITE: NOVEL SYNTHETIC ROUTE FROM DEEP EUTECTIC SOLVENT AND LITHIUM STORAGE PERFORMANCE. Functional Materials Letters, 04(04), 377-381.

Guettai, N., & Amar, H. A. (2005). Photocatalytic oxidation of methyl orange in presence of titanium dioxide in aqueous suspension. Part I: Parametric study. Desalination, 185(1), 427-437.

Guo, W., Hou, Y., Ren, S., Tian, S., & Wu, W. (2013). Formation of Deep Eutectic Solvents by Phenols and Choline Chloride and Their Physical Properties. Journal of Chemical & Engineering Data, 58(4), 866-872.

Guo, W., Hou, Y., Wu, W., Ren, S., Tian, S., & Marsh, K. N. (2013). Separation of phenol from model oils with quaternary ammonium salts via forming deep eutectic solvents. Green Chemistry, 15(1), 226-229.

Gupta, V. K., Agarwal, S., & Saleh, T. A. (2011). Chromium removal by combining the magnetic properties of iron oxide with adsorption properties of carbon nanotubes. Water Research, 45(6), 2207-2212.

Gupta, V. K., Ali, I., & Saini, V. K. (2006). Adsorption of 2, 4-D and carbofuran pesticides using fertilizer and steel industry wastes. Journal of Colloid and Interface Science, 299(2), 556-563.

Gupta, V. K., & Imran, A. (2004). Adsorbents for water treatment: development of low-cost alternatives to carbon. Encycl. Surf. Colloid Sci., 2004 Update Supplement, 5, 1.

Gupta, V. K., Kumar, R., Nayak, A., Saleh, T. A., & Barakat, M. A. (2013). Adsorptive removal of dyes from aqueous solution onto carbon nanotubes: A review. Advances in Colloid and Interface Science, 193–194(0), 24-34.

Gutiérrez, M. C., Carriazo, D., Tamayo, A., Jiménez, R., Picó, F., Rojo, J. M., . . . del Monte, F. (2011). Deep-Eutectic-Solvent-Assisted Synthesis of Hierarchical Carbon Electrodes Exhibiting Capacitance Retention at High Current Densities. Chemistry – A European Journal, 17(38), 10533-10537.

Gutiérrez, M. C., Ferrer, M. L., Mateo, C. R., & del Monte, F. (2009). Freeze-Drying of Aqueous Solutions of Deep Eutectic Solvents: A Suitable Approach to Deep Eutectic Suspensions of Self-Assembled Structures. Langmuir, 25(10), 5509-5515.

Haghseresht, F., & Lu, G. (1998). Adsorption characteristics of phenolic compounds onto coal-reject-derived adsorbents. Energy & Fuels, 12(6), 1100-1107.

Hahn, M. A., Tabb, J. S., & Krauss, T. D. (2005). Detection of single bacterial pathogens with semiconductor quantum dots. Analytical chemistry, 77(15), 4861-4869.

Hamdaoui, O., & Naffrechoux, E. (2007a). Modeling of adsorption isotherms of phenol and chlorophenols onto granular activated carbon: Part I. Two-parameter models and equations allowing determination of thermodynamic parameters. Journal of Hazardous Materials, 147(1–2), 381-394.

Hamdaoui, O., & Naffrechoux, E. (2007b). Modeling of adsorption isotherms of phenol and chlorophenols onto granular activated carbon: Part II. Models with more than two parameters. Journal of Hazardous Materials, 147(1–2), 401-411.

Hameed, B., Salman, J., & Ahmad, A. (2009). Adsorption isotherm and kinetic modeling of 2, 4-D pesticide on activated carbon derived from date stones. Journal of Hazardous Materials, 163(1), 121-126.

Hameed, B. H., Ahmad, A. A., & Aziz, N. (2007). Isotherms, kinetics and thermodynamics of acid dye adsorption on activated palm ash. Chemical Engineering Journal, 133(1–3), 195-203.

Han, R., Zou, W., Li, H., Li, Y., & Shi, J. (2006). Copper(II) and lead(II) removal from aqueous solution in fixed-bed columns by manganese oxide coated zeolite. Journal of Hazardous Materials, 137(2), 934-942.

Hao, Y.-M., Man, C., & Hu, Z.-B. (2010). Effective removal of Cu (II) ions from aqueous solution by amino-functionalized magnetic nanoparticles. Journal of Hazardous Materials, 184(1–3), 392-399.

Hayyan, A., Mjalli, F. S., AlNashef, I. M., Al-Wahaibi, T., Al-Wahaibi, Y. M., & Hashim, M. A. (2012a). Fruit sugar-based deep eutectic solvents and their physical properties. Thermochimica Acta, 541(0), 70-75.

Hayyan, A., Mjalli, F. S., AlNashef, I. M., Al-Wahaibi, T., Al-Wahaibi, Y. M., & Hashim, M. A. (2012b). Fruit sugar-based deep eutectic solvents and their physical properties. Thermochimica Acta, 541, 70-75.

Hayyan, A., Mjalli, F. S., AlNashef, I. M., Al-Wahaibi, Y. M., Al-Wahaibi, T., & Hashim, M. A. (2013). Glucose-based deep eutectic solvents: Physical properties. Journal of Molecular Liquids, 178, 137-141.

Hayyan, M., Abo-Hamad, A., AlSaadi, M. A., & Hashim, M. A. (2015a). Functionalization of graphene using deep eutectic solvents. Nanoscale Res. Lett., 10(1), 1.

Hayyan, M., Abo-Hamad, A., AlSaadi, M. A., & Hashim, M. A. (2015b). Functionalization of graphene using deep eutectic solvents. Nanoscale Research Letters, 10(1), 1-26.

Hayyan, M., Aissaoui, T., Hashim, M. A., AlSaadi, M. A., & Hayyan, A. (2015). Triethylene glycol based deep eutectic solvents and their physical properties. Journal of the Taiwan Institute of Chemical Engineers, 50, 24-30.

Hayyan, M., Hashim, M. A., Al-Saadi, M. A., Hayyan, A., AlNashef, I. M., & Mirghani, M. E. (2013a). Assessment of cytotoxicity and toxicity for phosphonium-based deep eutectic solvents. Chemosphere, 93(2), 455-459.

Hayyan, M., Hashim, M. A., Al-Saadi, M. A., Hayyan, A., AlNashef, I. M., & Mirghani, M. E. S. (2013b). Assessment of cytotoxicity and toxicity for phosphonium-based deep eutectic solvents. Chemosphere, 93(2), 455-459.

Hayyan, M., Hashim, M. A., Hayyan, A., Al-Saadi, M. A., AlNashef, I. M., Mirghani, M. E. S., & Saheed, O. K. (2013). Are deep eutectic solvents benign or toxic? Chemosphere, 90(7), 2193-2195.

Hayyan, M., Looi, C. Y., Hayyan, A., Wong, W. F., & Hashim, M. A. (2015). In Vitro and In Vivo Toxicity Profiling of Ammonium-Based Deep Eutectic Solvents. PloS One, 10(2).

Hayyan, M., Mjalli, F. S., Hashim, M. A., & AlNashef, I. M. (2010a). A novel technique for separating glycerine from palm oil-based biodiesel using ionic liquids. Fuel Process. Technol., 91, 116-120.

Hayyan, M., Mjalli, F. S., Hashim, M. A., & AlNashef, I. M. (2010b). A novel technique for separating glycerine from palm oil-based biodiesel using ionic liquids. Fuel Processing Technology, 91(1), 116-120.

He, X., Aker, W. G., Pelaez, M., Lin, Y., Dionysiou, D. D., & Hwang, H.-m. (2016). Assessment of nitrogen–fluorine-codoped TiO2 under visible light for degradation of BPA: Implication for field remediation. Journal of Photochemistry and Photobiology A: Chemistry, 314, 81-92.

Herzberg, M., & Elimelech, M. (2007). Biofouling of reverse osmosis membranes: Role of biofilm-enhanced osmotic pressure. Journal of Membrane Science, 295(1–2), 11-20.

Ho, Y.-S., & McKay, G. (1999). Pseudo-second order model for sorption processes. Process biochemistry, 34(5), 451-465.

Holappa, J., Hjálmarsdóttir, M., Másson, M., Rúnarsson, Ö., Asplund, T., Soininen, P., . . . Järvinen, T. (2006). Antimicrobial activity of chitosan N-betainates. Carbohydrate Polymers, 65(1), 114-118.

Holloway, R. W., Childress, A. E., Dennett, K. E., & Cath, T. Y. (2007). Forward osmosis for concentration of anaerobic digester centrate. Water Research, 41(17), 4005-4014.

Hossain, F., Perales-Perez, O. J., Hwang, S., & Román, F. (2014). Antimicrobial nanomaterials as water disinfectant: Applications, limitations and future perspectives. Science of The Total Environment, 466–467(0), 1047-1059.

Hotze, M., & Lowry, G. (2011). Nanotechnology for Sustainable Water Treatment Sustainable Water (pp. 138-164): The Royal Society of Chemistry.

Hou, P., Liu, C., Tong, Y., Xu, S., Liu, M., & Cheng, H. (2001). Purification of single-walled carbon nanotubes synthesized by the hydrogen arc-discharge method. Journal of Materials Research, 16(09), 2526-2529.

Houde, M., Muir, D. C. G., Kidd, K. A., Guildford, S., Drouillard, K., Evans, M. S., . . . Kling, H. (2008). Influence of lake characteristics on the biomagnification of persistent organic pollutants in lake trout food webs. Environmental Toxicology and Chemistry, 27(10), 2169-2178.

Hu, H., Yu, B., Ye, Q., Gu, Y., & Zhou, F. (2010). Modification of carbon nanotubes with a nanothin polydopamine layer and polydimethylamino-ethyl methacrylate brushes. Carbon, 48(8), 2347-2353.

Hu, J., & Shipley, H. J. (2012). Evaluation of desorption of Pb (II), Cu (II) and Zn (II) from titanium dioxide nanoparticles. Science of The Total Environment, 431(0), 209-220.

Huang, J.-H., Huang, K.-L., Liu, S.-Q., Wang, A.-T., & Yan, C. (2008). Adsorption of Rhodamine B and methyl orange on a hypercrosslinked polymeric adsorbent in aqueous solution. Colloids and Surfaces A: Physicochemical and Engineering Aspects, 330(1), 55-61.

Huang, J., Cao, Y., Liu, Z., Deng, Z., Tang, F., & Wang, W. (2012). Efficient removal of heavy metal ions from water system by titanate nanoflowers. Chemical Engineering Journal, 180(0), 75-80.

Huang, Y., Li, Y., Huang, Q., Cui, Z., Yu, D., Rajput, I. R., . . . Li, W. (2012). Effect of orally administered Enterococcus faecium EF1 on intestinal cytokines and chemokines production of suckling piglets. Pak Vet J, 32, 81-84.

Huang, Z., Maness, P.-C., Blake, D. M., Wolfrum, E. J., Smolinski, S. L., & Jacoby, W. A. (2000). Bactericidal mode of titanium dioxide photocatalysis. Journal of Photochemistry and Photobiology A: Chemistry, 130(2), 163-170.

Huang, Z., Zheng, X., Yan, D., Yin, G., Liao, X., Kang, Y., . . . Hao, B. (2008). Toxicological Effect of ZnO Nanoparticles Based on Bacteria. Langmuir, 24(8), 4140-4144.

Huddleston, J. G., Visser, A. E., Reichert, W. M., Willauer, H. D., Broker, G. A., & Rogers, R. D. (2001). Characterization and comparison of hydrophilic and hydrophobic room temperature ionic liquids incorporating the imidazolium cation. Green Chemistry, 3(4), 156-164.

Ibrahim, R. K., Hayyan, M., AlSaadi, M. A., Hayyan, A., & Ibrahim, S. (2016). Environmental application of nanotechnology: air, soil, and water. Environ. Sci. Pollut. Res., 1-35.

Igbinosa, E. O., Odjadjare, E. E., Chigor, V. N., Igbinosa, I. H., Emoghene, A. O., Ekhaise, F. O., . . . Idemudia, O. G. (2013). Toxicological profile of chlorophenols and their derivatives in the environment: the public health perspective. Sci. World J., 2013.

Iijima, S. (1991). Helical microtubules of graphitic carbon. Nature, 354, 56–58.

J. Liu, A. G. R., H.J. Dai, J.H. Hafner, R.K. Bradley, P.J. Boul, A. Lu. (1998). Fullerene pipes. Science, 280, 1253–1256.

Jafari, M., & Aghamiri, S. (2011). Evaluation of carbon nanotubes as solid-phase extraction sorbent for the removal of cephalexin from aqueous solution. Desalination and Water Treatment, 28(1-3), 55-58.

Jalil, A. A., Triwahyono, S., Adam, S. H., Rahim, N. D., Aziz, M. A. A., Hairom, N. H. H., . . . Mohamadiah, M. K. A. (2010). Adsorption of methyl orange from aqueous solution onto calcined Lapindo volcanic mud. Journal of Hazardous Materials, 181(1–3), 755-762.

Jeong, B.-H., Hoek, E. M. V., Yan, Y., Subramani, A., Huang, X., Hurwitz, G., . . . Jawor, A. (2007). Interfacial polymerization of thin film nanocomposites: A new concept for reverse osmosis membranes. Journal of Membrane Science, 294(1–2), 1-7.

Ji, L., Chen, W., Bi, J., Zheng, S., Xu, Z., Zhu, D., & Alvarez, P. J. (2010). Adsorption of tetracycline on single-walled and multi-walled carbon nanotubes as affected by aqueous solution chemistry. Environmental Toxicology and Chemistry, 29(12), 2713-2719.

Ji, L., Chen, W., Duan, L., & Zhu, D. (2009). Mechanisms for strong adsorption of tetracycline to carbon nanotubes: A comparative study using activated carbon and graphite as adsorbents. Environmental Science & Technology, 43(7), 2322-2327.

Jibril, B., Mjalli, F., Naser, J., & Gano, Z. (2014). New tetrapropylammonium bromide-based deep eutectic solvents: Synthesis and characterizations. Journal of Molecular Liquids, 199, 462-469.

Jin, L. M., Yu, S. L., Shi, W. X., Yi, X. S., Sun, N., Ge, Y. L., & Ma, C. (2012). Synthesis of a novel composite nanofiltration membrane incorporated SiO2 nanoparticles for oily wastewater desalination. Polymer, 53(23), 5295-5303.

Jin, T., & He, Y. (2011). Antibacterial activities of magnesium oxide (MgO) nanoparticles against foodborne pathogens. Journal of Nanoparticle Research, 13(12), 6877-6885.

Jin, Z., Zhang, S. H., & Jian, X. G. (2007). Removal of 2, 4-dichlorophenol from wasterwater by vacuum membrane distillation using hydrophobic PPESK hollow hiber membrane. Chinese Chemical Letters, 18(12), 1543-1547.

Jing, Y., Li, L., Zhang, Q., Lu, P., Liu, P., & Lü, X. (2011). Photocatalytic ozonation of dimethyl phthalate with TiO 2 prepared by a hydrothermal method. Journal of Hazardous Materials, 189(1), 40-47.

Jones, N., Ray, B., Ranjit, K. T., & Manna, A. C. (2008). Antibacterial activity of ZnO nanoparticle suspensions on a broad spectrum of microorganisms. FEMS Microbiology Letters, 279(1), 71-76.

Joo, J. B., Lee, I., Dahl, M., Moon, G. D., Zaera, F., & Yin, Y. (2013). Controllable synthesis of mesoporous TiO2 hollow shells: toward an efficient photocatalyst. Advanced Functional Materials, 23(34), 4246-4254.

Jung, M.-W., Ahn, K.-H., Lee, Y., Kim, K.-P., Rhee, J.-S., Park, J. T., & Paeng, K.-J. (2001). Adsorption characteristics of phenol and chlorophenols on granular activated carbons (GAC). Microchemical Journal, 70(2), 123-131.

Jung, M. S., Hyeon- Lee, J., Lee, J. H., Park, J. J., Jung, I. S., & Kim, J. M. (2008). Photosensitive Carbon Nanotube Paste Based on Acrylated Single- Walled Carbon Nanotubes. Advanced Functional Materials, 18(3), 449-454.

Kaegi, R., Voegelin, A., Sinnet, B., Zuleeg, S., Hagendorfer, H., Burkhardt, M., & Siegrist, H. (2011). Behavior of Metallic Silver Nanoparticles in a Pilot Wastewater Treatment Plant. Environmental Science & Technology, 45(9), 3902-3908.

Kanade, K., Kale, B., Baeg, J.-O., Lee, S. M., Lee, C. W., Moon, S.-J., & Chang, H. (2007). Self-assembled aligned Cu doped ZnO nanoparticles for photocatalytic hydrogen production under visible light irradiation. Materials Chemistry and Physics, 102(1), 98-104.

Kang, S., Mauter, M. S., & Elimelech, M. (2009). Microbial Cytotoxicity of Carbon-Based Nanomaterials: Implications for River Water and Wastewater Effluent. Environmental Science & Technology, 43(7), 2648-2653.

Karbowiak, T., Debeaufort, F., & Voilley, A. (2006). Importance of surface tension characterization for food, pharmaceutical and packaging products: a review. Critical Reviews in Food Science and Nutrition, 46(5), 391-407.

Karci, A. (2014). Degradation of chlorophenols and alkylphenol ethoxylates, two representative textile chemicals, in water by advanced oxidation processes: The state of the art on transformation products and toxicity. Chemosphere, 99(0), 1-18.

Kareem, M. A., Mjalli, F. S., Hashim, M. A., & AlNashef, I. M. (2010a). Phosphonium-Based Ionic Liquids Analogues and Their Physical Properties. Journal of Chemical & Engineering Data, 55(11), 4632-4637.

Kareem, M. A., Mjalli, F. S., Hashim, M. A., & AlNashef, I. M. (2010b). Phosphonium-Based Ionic Liquids Analogues and Their Physical Properties. J. Chem. Eng. Data, 55, 4632-4637.

Karimi, H., Mousavi, S., & Sadeghian, B. (2012). Silver nanoparticle loaded on activated carbon as efficient adsorbent for removal of methyl orange. Indian Journal of Science and Technology, 5(3), 2346-2353.

Karimi, M., Eshraghi, M. J., & Jahangir, V. (2016). A facile and green synthetic approach based on deep eutectic solvents toward synthesis of CZTS nanoparticles. Materials Letters, 171, 100-103.

Karn, B., Kuiken, T., & Otto, M. (2009). Nanotechnology and in situ remediation: a review of the benefits and potential risks. Environmental Health Perspectives, 1823-1831.

Kaur, J., & Singhal, S. (2014). Facile synthesis of ZnO and transition metal doped ZnO nanoparticles for the photocatalytic degradation of Methyl Orange. Ceramics International, 40(5), 7417-7424.

KAUR, S., KOTAKI, M., MA, Z., GOPAL, R., RAMAKRISHNA, S., & NG, S. C. (2006). OLIGOSACCHARIDE FUNCTIONALIZED NANOFIBROUS MEMBRANE. International Journal of Nanoscience, 05(01), 1-11.

Khan, T. A., Nazir, M., Ali, I., & Kumar, A. Removal of Chromium(VI) from aqueous solution using guar gum–nano zinc oxide biocomposite adsorbent. Arabian Journal of Chemistry(0).

Kharissova, O. V., Kharisov, B. I., & de Casas Ortiz, E. G. (2013). Dispersion of carbon nanotubes in water and non-aqueous solvents. Rsc Advances, 3(47), 24812-24852.

Kilianová, M., Prucek, R., Filip, J., Kolařík, J., Kvítek, L., Panáček, A., . . . Zbořil, R. (2013). Remarkable efficiency of ultrafine superparamagnetic iron(III) oxide nanoparticles toward arsenate removal from aqueous environment. Chemosphere, 93(11), 2690-2697.

Kim, J., Cho, I., Kim, I., Kim, C., Heo, N. H., & Suh, S. (2006). Manufacturing of anti-viral inorganic materials from colloidal silver and titanium oxide. Revue Roumaine De Chimie, 51(11), 1121.

Klossek, M. L., Touraud, D., & Kunz, W. (2013). Eco-solvents–cluster-formation, surfactantless microemulsions and facilitated hydrotropy. Physical Chemistry Chemical Physics, 15(26), 10971-10977.

Koneswaran, M., & Narayanaswamy, R. (2009). l-Cysteine-capped ZnS quantum dots based fluorescence sensor for Cu2+ ion. Sensors and Actuators B: Chemical, 139(1), 104-109.

Kong, M., Chen, X. G., Xing, K., & Park, H. J. (2010). Antimicrobial properties of chitosan and mode of action: A state of the art review. International Journal of Food Microbiology, 144(1), 51-63.

Kosa, S. A., Al-Zhrani, G., & Abdel Salam, M. (2012). Removal of heavy metals from aqueous solutions by multi-walled carbon nanotubes modified with 8-hydroxyquinoline. Chemical Engineering Journal, 181–182(0), 159-168.

Koziol, K., Vilatela, J., Moisala, A., Motta, M., Cunniff, P., Sennett, M., & Windle, A. (2007). High-Performance Carbon Nanotube Fiber. Science, 318(5858), 1892-1895.

Küçükosmanoğlu, M., Gezici, O., & Ayar, A. (2006). The adsorption behaviors of methylene blue and methyl orange in a diaminoethane sporopollenin-mediated column system. Separation and purification technology, 52(2), 280-287.

Kuo, C.-Y., Wu, C.-H., & Wu, J.-Y. (2008). Adsorption of direct dyes from aqueous solutions by carbon nanotubes: Determination of equilibrium, kinetics and thermodynamics parameters. Journal of Colloid and Interface Science, 327(2), 308-315.

Kurniawan TA, S. M., Sillanpää M. (2011). Nanoadsorbents for remediation of aquatic environment: local and practical solutions for global water pollution problems. Crit Rev. Env Sci Technol, 42, 1233–1295.

Kusmierek, K., Sankowska, M., & Swiatkowski, A. (2013). Adsorption of dichlorophenols from aqueous solutions onto multi-walled carbon nanotubes. Przemysl Chemiczny, 92(7), 1257-1260.

Kuśmierek, K., Szala, M., & Świątkowski, A. (2016a). Adsorption of 2,4-dichlorophenol and 2,4-dichlorophenoxyacetic acid from aqueous solutions on carbonaceous materials obtained by combustion synthesis. J. Taiwan Inst. Chem. Eng., 63, 371-378.

Kuśmierek, K., Szala, M., & Świątkowski, A. (2016b). Adsorption of 2, 4-dichlorophenol and 2, 4-dichlorophenoxyacetic acid from aqueous solutions on carbonaceous materials obtained by combustion synthesis. Journal of the Taiwan Institute of Chemical Engineers, 63, 371-378.

Langmuir, I. (1918). The adsorption of gases on plane surfaces of glass, mica and platinum. Journal of the American Chemical Society, 40(9), 1361-1403.

Lee, K. P., Arnot, T. C., & Mattia, D. (2011). A review of reverse osmosis membrane materials for desalination—development to date and future potential. Journal of Membrane Science, 370(1), 1-22.

Lee, S. Y., Kim, H. J., Patel, R., Im, S. J., Kim, J. H., & Min, B. R. (2007). Silver nanoparticles immobilized on thin film composite polyamide membrane: characterization, nanofiltration, antifouling properties. Polymers for Advanced Technologies, 18(7), 562-568.

Li, G., Du, Y., Tao, Y., Deng, H., Luo, X., & Yang, J. (2010). Iron(II) cross-linked chitin-based gel beads: Preparation, magnetic property and adsorption of methyl orange. Carbohydrate Polymers, 82(3), 706-713.

Li, H., Zhang, D., Han, X., & Xing, B. (2014). Adsorption of antibiotic ciprofloxacin on carbon nanotubes: pH dependence and thermodynamics. Chemosphere, 95, 150-155.

Li, J.-h., Hong, R.-y., Luo, G.-h., Zheng, Y., Li, H.-z., & Wei, D.-g. (2010). An easy approach to encapsulating Fe3O4 nanoparticles in multiwalled carbon nanotubes. New Carbon Materials, 25(3), 192-198.

Li, Q., Mahendra, S., Lyon, D. Y., Brunet, L., Liga, M. V., Li, D., & Alvarez, P. J. J. (2008). Antimicrobial nanomaterials for water disinfection and microbial control: Potential applications and implications. Water Research, 42(18), 4591-4602.

Li, R., Chu, Q., & Liang, J. (2015). Electrodeposition and characterization of Ni-SiC composite coatings from deep eutectic solvent. RSC Advances, 5(56), 44933-44942.

Li, R., Hou, Y., & Liang, J. (2016). Electro-codeposition of Ni-SiO2 nanocomposite coatings from deep eutectic solvent with improved corrosion resistance. Applied Surface Science, 367, 449-458.

Li, T., Shi, L., Wang, E., & Dong, S. (2009). Multifunctional G- Quadruplex Aptamers and Their Application to Protein Detection. Chemistry-A European Journal, 15(4), 1036-1042.

Li, X., Fang, X., Pang, R., Li, J., Sun, X., Shen, J., . . . Wang, L. (2014). Self-assembly of TiO2 nanoparticles around the pores of PES ultrafiltration membrane for mitigating organic fouling. Journal of Membrane Science, 467(0), 226-235.

Li, X., Hou, M., Han, B., Wang, X., & Zou, L. (2008a). Solubility of CO2 in a Choline Chloride + Urea Eutectic Mixture. Journal of Chemical & Engineering Data, 53(2), 548-550.

Li, X., Hou, M., Han, B., Wang, X., & Zou, L. (2008b). Solubility of CO2 in a choline chloride+ urea eutectic mixture. Journal of Chemical and Engineering Data, 53(2), 548-550.

Li, X., Zhang, C., Zhao, R., Lu, X., Xu, X., Jia, X., . . . Li, L. (2013). Efficient adsorption of gold ions from aqueous systems with thioamide-group chelating nanofiber membranes. Chemical Engineering Journal, 229(0), 420-428.

Li, Y.-H., Ding, J., Luan, Z., Di, Z., Zhu, Y., Xu, C., . . . Wei, B. (2003). Competitive adsorption of Pb2+, Cu2+ and Cd2+ ions from aqueous solutions by multiwalled carbon nanotubes. Carbon, 41(14), 2787-2792.

Li, Y.-H., Wang, S., Luan, Z., Ding, J., Xu, C., & Wu, D. (2003). Adsorption of cadmium(II) from aqueous solution by surface oxidized carbon nanotubes. Carbon, 41(5), 1057-1062.

Li, Y.-H., Wang, S., Wei, J., Zhang, X., Xu, C., Luan, Z., . . . Wei, B. (2002). Lead adsorption on carbon nanotubes. Chemical Physics Letters, 357(3), 263-266.

Li, Y., Li, X., Li, Y., Qi, J., Bian, J., & Yuan, Y. (2009). Selective removal of 2,4-dichlorophenol from contaminated water using non-covalent imprinted microspheres. Environmental Pollution, 157(6), 1879-1885.

Liau, S. Y., Read, D. C., Pugh, W. J., Furr, J. R., & Russell, A. D. (1997). Interaction of silver nitrate with readily identifiable groups: relationship to the

antibacterialaction of silver ions. Letters in Applied Microbiology, 25(4), 279-283.

Likodimos, V., Han, C., Pelaez, M., Kontos, A. G., Liu, G., Zhu, D., . . . Falaras, P. (2013). Anion-Doped TiO2 Nanocatalysts for Water Purification under Visible Light. Industrial & Engineering Chemistry Research, 52(39), 13957-13964.

Lin, D., & Xing, B. (2008). Adsorption of phenolic compounds by carbon nanotubes: role of aromaticity and substitution of hydroxyl groups. Environmental science & technology, 42(19), 7254-7259.

Lin, Y.-H., Tseng, T.-K., & Chu, H. (2014). Photo-catalytic degradation of dimethyl disulfide on S and metal-ions co-doped TiO2 under visible-light irradiation. Applied Catalysis a-General, 469, 221-228.

Lind, M. L., Ghosh, A. K., Jawor, A., Huang, X., Hou, W., Yang, Y., & Hoek, E. M. V. (2009). Influence of Zeolite Crystal Size on Zeolite-Polyamide Thin Film Nanocomposite Membranes. Langmuir, 25(17), 10139-10145.

Liu, G., Han, J. F., Zhou, X., Huang, L., Zhang, F. X., Wang, X. L., . . . Li, C. (2013). Enhancement of visible-light-driven O-2 evolution from water oxidation on WO3 treated with hydrogen. Journal of catalysis, 307, 148-152.

Liu, Q.-S., Zheng, T., Wang, P., Jiang, J.-P., & Li, N. (2010). Adsorption isotherm, kinetic and mechanism studies of some substituted phenols on activated carbon fibers. Chemical Engineering Journal, 157(2–3), 348-356.

Liu, R., & Zhao, D. (2013). Synthesis and characterization of a new class of stabilized apatite nanoparticles and applying the particles to in situ Pb immobilization in a fire-range soil. Chemosphere, 91(5), 594-601.

Liu, S., Wei, L., Hao, L., Fang, N., Chang, M. W., Xu, R., . . . Chen, Y. (2009). Sharper and Faster "Nano Darts" Kill More Bacteria: A Study of Antibacterial Activity of Individually Dispersed Pristine Single-Walled Carbon Nanotube. ACS Nano, 3(12), 3891-3902.

Liu, W., Wang, T., Borthwick, A. G. L., Wang, Y., Yin, X., Li, X., & Ni, J. (2013). Adsorption of Pb2+, Cd2+, Cu2+ and Cr3+ onto titanate nanotubes: Competition and effect of inorganic ions. Science of The Total Environment, 456–457(0), 171-180.

Liu, X., Su, D. S., & Schlögl, R. (2008). Oxidative dehydrogenation of 1-butene to butadiene over carbon nanotube catalysts. Carbon, 46(3), 547-549.

Liu, Y.-T., Chen, Y.-A., & Xing, Y.-J. (2014). Synthesis and characterization of novel ternary deep eutectic solvents. Chin. Chem. Lett., 25, 104-106.

Liu, Y., Wang, Z., Wang, W., & Huang, W. (2014). Engineering highly active TiO2 photocatalysts via the surface-phase junction strategy employing a titanate nanotube precursor. Journal of catalysis, 310, 16-23.

Liu, Z., Bai, H., Lee, J., & Sun, D. D. (2011). A low-energy forward osmosis process to produce drinking water. Energy & Environmental Science, 4(7), 2582-2585.

López-Salas, N., Jardim, E. O., Silvestre-Albero, A., Gutiérrez, M. C., Ferrer, M. L., Rodríguez-Reinoso, F., . . . del Monte, F. (2014). Use of Eutectic Mixtures for Preparation of Monolithic Carbons with CO2-Adsorption and Gas-Separation Capabilities. Langmuir, 30(41), 12220-12228.

Lu, C., Bai, H., Wu, B., Su, F., & Hwang, J. F. (2008). Comparative study of CO2 capture by carbon nanotubes, activated carbons, and zeolites. Energy & Fuels, 22(5), 3050-3056.

Lu, C., & Chiu, H. (2006). Adsorption of zinc(II) from water with purified carbon nanotubes. Chemical Engineering Science, 61(4), 1138-1145.

Lu, C., & Chiu, H. (2008). Chemical modification of multiwalled carbon nanotubes for sorption of Zn 2+ from aqueous solution. Chemical Engineering Journal, 139(3), 462-468.

Lu, C., Chiu, H., & Liu, C. (2006). Removal of Zinc(II) from Aqueous Solution by Purified Carbon Nanotubes: Kinetics and Equilibrium Studies. Industrial & Engineering Chemistry Research, 45(8), 2850-2855.

Lu, C., Chung, Y.-L., & Chang, K.-F. (2006). Adsorption thermodynamic and kinetic studies of trihalomethanes on multiwalled carbon nanotubes. Journal of hazardous materials, 138(2), 304-310.

Lu, C., & Liu, C. (2006). Removal of nickel(II) from aqueous solution by carbon nanotubes. Journal of Chemical Technology & Biotechnology, 81(12), 1932-1940.

Luboch, E., Wagner-Wysiecka, E., Poleska-Muchlado, Z., & Kravtsov, V. C. (2005). Synthesis and properties of azobenzocrown ethers with π-electron donor, or π-electron donor and π-electron acceptor group (s) on benzene ring (s). Tetrahedron, 61(45), 10738-10747.

Lunge, S., Singh, S., & Sinha, A. (2014). Magnetic iron oxide (Fe3O4) nanoparticles from tea waste for arsenic removal. Journal of Magnetism and Magnetic Materials, 356(0), 21-31.

Luo, C., Wei, R., Guo, D., Zhang, S., & Yan, S. (2013). Adsorption behavior of MnO2 functionalized multi-walled carbon nanotubes for the removal of cadmium from aqueous solutions. Chemical Engineering Journal, 225(0), 406-415.

Luo, J., Conrad, O., & Vankelecom, I. F. (2012). Physicochemical properties of phosphonium-based and ammonium-based protic ionic liquids. J. Mater. Chem., 22, 20574-20579.

Luo, X., Wang, C., Wang, L., Deng, F., Luo, S., Tu, X., & Au, C. (2013). Nanocomposites of graphene oxide-hydrated zirconium oxide for simultaneous removal of As(III) and As(V) from water. Chemical Engineering Journal, 220(0), 98-106.

Lv, X., Xu, J., Jiang, G., & Xu, X. (2011). Removal of chromium(VI) from wastewater by nanoscale zero-valent iron particles supported on multiwalled carbon nanotubes. Chemosphere, 85(7), 1204-1209.

Lyon, D. Y., & Alvarez, P. J. J. (2008). Fullerene Water Suspension (nC60) Exerts Antibacterial Effects via ROS-Independent Protein Oxidation. Environmental Science & Technology, 42(21), 8127-8132.

Ma, J.-W., Wang, H., Wang, F.-Y., & Huang, Z.-H. (2010). Adsorption of 2, 4-dichlorophenol from Aqueous Solution by a New Low-Cost Adsorbent–Activated Bamboo Charcoal. Separation Science and Technology, 45(16), 2329-2336.

Ma, Q., Cui, H., & Su, X. (2009). Highly sensitive gaseous formaldehyde sensor with CdTe quantum dots multilayer films. Biosensors and Bioelectronics, 25(4), 839-844.

Ma, Z., Kotaki, M., & Ramakrishna, S. (2005). Electrospun cellulose nanofiber as affinity membrane. Journal of Membrane Science, 265(1–2), 115-123.

Machado, F. M., Bergmann, C. P., Fernandes, T. H., Lima, E. C., Royer, B., Calvete, T., & Fagan, S. B. (2011a). Adsorption of Reactive Red M-2BE dye from water solutions by multi-walled carbon nanotubes and activated carbon. Journal of hazardous materials, 192(3), 1122-1131.

Machado, F. M., Bergmann, C. P., Fernandes, T. H. M., Lima, E. C., Royer, B., Calvete, T., & Fagan, S. B. (2011b). Adsorption of Reactive Red M-2BE dye from water solutions by multi-walled carbon nanotubes and activated carbon. Journal of Hazardous Materials, 192(3), 1122-1131.

Machado, F. M., Bergmann, C. P., Lima, E. C., Royer, B., de Souza, F. E., Jauris, I. M., . . . Fagan, S. B. (2012). Adsorption of Reactive Blue 4 dye from water solutions by carbon nanotubes: experiment and theory. Physical Chemistry Chemical Physics, 14(31), 11139-11153.

Madrakian, T., Afkhami, A., & Ahmadi, M. (2013). Simple in situ functionalizing magnetite nanoparticles by reactive blue-19 and their application to the effective removal of Pb2+ ions from water samples. Chemosphere, 90(2), 542-547.

Madrakian, T., Afkhami, A., Ahmadi, M., & Bagheri, H. (2011). Removal of some cationic dyes from aqueous solutions using magnetic-modified multi-walled carbon nanotubes. Journal of Hazardous Materials, 196(0), 109-114.

Maggini, L., Raquez, J.-M., Marega, R., Jensen Ahrens, J., Pineux, F., Meyer, F., . . . Bonifazi, D. (2013). Magnetic Poly(vinylpyridine)-Coated Carbon Nanotubes: An Efficient Supramolecular Tool for Wastewater Purification. ChemSusChem, 6(2), 367-373.

Mahapatra, A., Mishra, B. G., & Hota, G. (2013). Electrospun Fe2O3–Al2O3 nanocomposite fibers as efficient adsorbent for removal of heavy metal ions from aqueous solution. Journal of Hazardous Materials, 258–259(0), 116-123.

Mahendra, S., Li, Q., Lyon, D. Y., Brunet, L., & Alvarez, P. J. J. (2014). Chapter 20 - Nanotechnology-Enabled Water Disinfection and Microbial Control: Merits and Limitations. In A. Street, R. Sustich, J. Duncan, & N. Savage (Eds.), Nanotechnology Applications for Clean Water (Second Edition) (pp. 319-327). Oxford: William Andrew Publishing.

Mahmoud, D. K., Salleh, M. A. M., Karim, W. A. W. A., Idris, A., & Abidin, Z. Z. (2012). Batch adsorption of basic dye using acid treated kenaf fibre char: equilibrium, kinetic and thermodynamic studies. Chemical Engineering Journal, 181, 449-457.

Maiti, S., & Khatua, B. B. (2013). Electrochemical and electrical performances of cobalt chloride (CoCl2) doped polyaniline (PANI)/graphene nanoplate (GNP) composite. RSC Advances, 3(31), 12874-12885.

Mąka, H., Spychaj, T., & Kowalczyk, K. (2014). Imidazolium and deep eutectic ionic liquids as epoxy resin crosslinkers and graphite nanoplatelets dispersants. Journal of Applied Polymer Science, 131(12), n/a-n/a.

Malato, S., Fernandez-Ibanez, P., Maldonado, M. I., Blanco, J., & Gernjak, W. (2009). Decontamination and disinfection of water by solar photocatalysis: Recent overview and trends. Catalysis Today, 147(1), 1-59.

Malato, S., Fernández-Ibáñez, P., Maldonado, M. I., & Oller, I. (2013). Chapter 15 - Solar Photocatalytic Processes: Water Decontamination and Disinfection. In S. L. Suib (Ed.), New and Future Developments in Catalysis (pp. 371-393). Amsterdam: Elsevier.

Martis, P., Dilimon, V. S., Delhalle, J., & Mekhalif, Z. (2010). Electro-generated nickel/carbon nanotube composites in ionic liquid. Electrochimica Acta, 55(19), 5407-5410.

Maugeri, Z., & Dominguez de Maria, P. (2012). Novel choline-chloride-based deep-eutectic-solvents with renewable hydrogen bond donors: levulinic acid and sugar-based polyols. RSC Advances, 2(2), 421-425.

Mauter, M. S., Wang, Y., Okemgbo, K. C., Osuji, C. O., Giannelis, E. P., & Elimelech, M. (2011). Antifouling Ultrafiltration Membranes via Post-Fabrication Grafting of Biocidal Nanomaterials. ACS Applied Materials & Interfaces, 3(8), 2861-2868.

Maximous, N., Nakhla, G., Wong, K., & Wan, W. (2010). Optimization of Al2O3/PES membranes for wastewater filtration. Separation and Purification Technology, 73(2), 294-301.

Mayer, B. K., Daugherty, E., & Abbaszadegan, M. (2014). Disinfection byproduct formation resulting from settled, filtered, and finished water treated by titanium dioxide photocatalysis. Chemosphere, 117(0), 72-78.

McCutcheon, J. R., & Elimelech, M. (2008). Influence of membrane support layer hydrophobicity on water flux in osmotically driven membrane processes. Journal of Membrane Science, 318(1), 458-466.

Meng, F., Chae, S.-R., Drews, A., Kraume, M., Shin, H.-S., & Yang, F. (2009). Recent advances in membrane bioreactors (MBRs): Membrane fouling and membrane material. Water Research, 43(6), 1489-1512.

Mittal, A., & Gupta, V. K. (2010). Adsorptive removal and recovery of the azo dye Eriochrome Black T. Toxicological and Environ Chemistry, 92(10), 1813-1823.

Mittal, A., Malviya, A., Kaur, D., Mittal, J., & Kurup, L. (2007). Studies on the adsorption kinetics and isotherms for the removal and recovery of Methyl Orange from wastewaters using waste materials. Journal of Hazardous Materials, 148(1), 229-240.

Mittal, A., Thakur, V., & Gajbe, V. (2013). Adsorptive removal of toxic azo dye Amido Black 10B by hen feather. Environmental Science and Pollution Research, 20(1), 260-269.

Mjalli, F. S., Naser, J., Jibril, B., Alizadeh, V., & Gano, Z. (2014a). Tetrabutylammonium Chloride Based Ionic Liquid Analogues and Their Physical Properties. Journal of Chemical and Engineering Data, 59(7), 2242-2251.

Mjalli, F. S., Naser, J., Jibril, B., Alizadeh, V., & Gano, Z. (2014b). Tetrabutylammonium Chloride Based Ionic Liquid Analogues and Their Physical Properties. J. Chem. Eng. Data, 59, 2242-2251.

Mohammadi, N., Khani, H., Gupta, V. K., Amereh, E., & Agarwal, S. (2011). Adsorption process of methyl orange dye onto mesoporous carbon material–kinetic and thermodynamic studies. Journal of colloid and interface science, 362(2), 457-462.

Monárrez-Cordero, B., Amézaga-Madrid, P., Antúnez-Flores, W., Leyva-Porras, C., Pizá-Ruiz, P., & Miki-Yoshida, M. (2014). Highly efficient removal of arsenic metal ions with high superficial area hollow magnetite nanoparticles synthetized by AACVD method. Journal of Alloys and Compounds, 586, Supplement 1(0), S520-S525.

Mondal, D., Sharma, M., Wang, C.-H., Lin, Y.-C., Huang, H.-C., Saha, A., . . . Prasad, K. (2016). Deep eutectic solvent promoted one step sustainable conversion of

fresh seaweed biomass to functionalized graphene as a potential electrocatalyst. Green Chemistry, 18(9), 2819-2826.

Moon, G. D., Joo, J. B., Dahl, M., Jung, H., & Yin, Y. (2014). Nitridation and Layered Assembly of Hollow TiO2 Shells for Electrochemical Energy Storage. Advanced Functional Materials, 24(6), 848-856.

Moradi, O. (2013). Adsorption Behavior of Basic Red 46 by Single-Walled Carbon Nanotubes Surfaces. Fullerenes, Nanotubes and Carbon Nanostructures, 21(4), 286-301.

Morrison, H. G., Sun, C. C., & Neervannan, S. (2009). Characterization of thermal behavior of deep eutectic solvents and their potential as drug solubilization vehicles. International Journal of Pharmaceutics, 378(1), 136-139.

Mota-Morales, J. D., Gutierrez, M. C., Ferrer, M. L., Jimenez, R., Santiago, P., Sanchez, I. C., . . . Luna-Barcenas, G. (2013). Synthesis of macroporous poly(acrylic acid)-carbon nanotube composites by frontal polymerization in deep-eutectic solvents. Journal of Materials Chemistry A, 1(12), 3970-3976.

Mubarak, N. M., Alicia, R. F., Abdullah, E. C., Sahu, J. N., Haslija, A. B. A., & Tan, J. (2013). Statistical optimization and kinetic studies on removal of Zn2+ using functionalized carbon nanotubes and magnetic biochar. Journal of Environmental Chemical Engineering, 1(3), 486-495.

Müller, B., Zumbuehl, A., Walter, M. A., Pfohl, T., Cattin, P. C., Huwyler, J., & Hieber, S. E. (2015). Translational Medicine: Nanoscience and Nanotechnology to Improve Patient Care. The Nano-Micro Interface: Bridging the Micro and Nano Worlds.

Nadavala, S. K., Swayampakula, K., Boddu, V. M., & Abburi, K. (2009). Biosorption of phenol and o-chlorophenol from aqueous solutions on to chitosan–calcium alginate blended beads. Journal of Hazardous Materials, 162(1), 482-489.

Namasivayam, C., Jeyakumar, R., & Yamuna, R. (1994). Dye removal from wastewater by adsorption on 'waste'Fe (III)/Cr (III) hydroxide. Waste management, 14(7), 643-648.

Namasivayam, C., & Kavitha, D. (2005). Adsorptive removal of 2, 4- dichlorophenol from aqueous solution by low- cost carbon from an agricultural solid waste: coconut coir pith. Separation science and technology, 39(6), 1407-1425.

Nassar, N. N. (2010). Rapid removal and recovery of Pb(II) from wastewater by magnetic nanoadsorbents. Journal of Hazardous Materials, 184(1–3), 538-546.

Ni, Z.-M., Xia, S.-J., Wang, L.-G., Xing, F.-F., & Pan, G.-X. (2007). Treatment of methyl orange by calcined layered double hydroxides in aqueous solution: adsorption property and kinetic studies. Journal of Colloid and Interface Science, 316(2), 284-291.

Niksefat, N., Jahanshahi, M., & Rahimpour, A. (2014). The effect of SiO2 nanoparticles on morphology and performance of thin film composite membranes for forward osmosis application. Desalination, 343(0), 140-146.

Obalová, L., Reli, M., Lang, J., Matějka, V., Kukutschová, J., Lacný, Z., & Kočí, K. (2013). Photocatalytic decomposition of nitrous oxide using TiO2 and Ag-TiO2 nanocomposite thin films. Catalysis Today, 209(0), 170-175.

Ofomaja, A. E., & Ho, Y.-S. (2008). Effect of temperatures and pH on methyl violet biosorption by Mansonia wood sawdust. Bioresource Technology, 99(13), 5411-5417.

Oh, J.-H., & Lee, J.-S. (2014). Synthesis of Gold Microstructures with Surface Nanoroughness Using a Deep Eutectic Solvent for Catalytic and Diagnostic Applications. Journal of Nanoscience and Nanotechnology, 14(5), 3753-3757.

Ohama, Y., & Van Gemert, D. (2011). Application of Titanium Dioxide Photocatalysis to Construction Materials: State-of-the-art Report of the RILEM Technical Committee 194-TDP (Vol. 5): Springer Science & Business Media.

Oseguera-Galindo, D. O., Machorro-Mejia, R., Bogdanchikova, N., & Mota-Morales, J. D. (2016). Silver nanoparticles synthesized by laser ablation confined in urea choline chloride deep-eutectic solvent. Colloids and Interface Science Communications, 12, 1-4.

Özcan, A. S., Erdem, B., & Özcan, A. (2005). Adsorption of Acid Blue 193 from aqueous solutions onto BTMA-bentonite. Colloids and Surfaces A: Physicochemical and Engineering Aspects, 266(1), 73-81.

Pacholczyk, A., Terzyk, A. P., Wiśniewski, M., Gauden, P. A., Wesołowski, R. P., Furmaniak, S., . . . Kruszka, B. (2011). Phenol adsorption on closed carbon nanotubes. Journal of Colloid and Interface Science, 361(1), 288-292.

Page, K., Palgrave, R. G., Parkin, I. P., Wilson, M., Savin, S. L. P., & Chadwick, A. V. (2007). Titania and silver-titania composite films on glass-potent antimicrobial coatings. Journal of Materials Chemistry, 17(1), 95-104.

Paiva, A., Craveiro, R., Aroso, I., Martins, M., Reis, R. L., & Duarte, A. R. C. (2014). Natural Deep Eutectic Solvents – Solvents for the 21st Century. ACS Sustain Chem Eng, 2(5), 1063-1071.

Pan, B., Lin, D., Mashayekhi, H., & Xing, B. (2008). Adsorption and Hysteresis of Bisphenol A and 17α-Ethinyl Estradiol on Carbon Nanomaterials. Environmental Science & Technology, 42(15), 5480-5485.

Pan, B., & Xing, B. (2008). Adsorption mechanisms of organic chemicals on carbon nanotubes. Environmental science & technology, 42(24), 9005-9013.

Pan, L., Wang, S., Zou, J.-J., Huang, Z.-F., Wang, L., & Zhang, X. (2014). Ti3+-defected and V-doped TiO2 quantum dots loaded on MCM-41. Chemical Communications, 50(8), 988-990.

Pan, L., Zou, J.-J., Wang, S., Huang, Z.-F., Yu, A., Wang, L., & Zhang, X. (2013). Quantum dot self-decorated TiO2 nanosheets. Chem. Commun., 49(59), 6593-6595.

Pang, R., Li, X., Li, J., Lu, Z., Sun, X., & Wang, L. (2014). Preparation and characterization of ZrO2/PES hybrid ultrafiltration membrane with uniform ZrO2 nanoparticles. Desalination, 332(1), 60-66.

Park, S., Park, S., Jung, J., Hong, T., Lee, S., Kim, H. W., & Lee, C. (2014). H2S gas sensing properties of CuO-functionalized WO3 nanowires. Ceramics International, 40(7, Part B), 11051-11056.

Patel, D. D., & Lee, J. M. (2012). Applications of ionic liquids. Chemical Record (New York, N.Y.), 12(3), 329-355.

Paul, D. (2004). Reformulation of the solution-diffusion theory of reverse osmosis. Journal of Membrane Science, 241(2), 371-386.

Pavan, F. A., Dias, S. L., Lima, E. C., & Benvenutti, E. V. (2008). Removal of Congo red from aqueous solution by anilinepropylsilica xerogel. Dyes and Pigments, 76(1), 64-69.

Pedersen, K. S., Lund, T., & Fredenslund, A. Surface Tension Of Petroleum Mixtures.

Pena- Pereira, F., & Namieśnik, J. (2014). Ionic Liquids and Deep Eutectic Mixtures: Sustainable Solvents for Extraction Processes. ChemSusChem.

Pendergast, M. M., & Hoek, E. M. (2011). A review of water treatment membrane nanotechnologies. Energy & Environmental Science, 4(6), 1946-1971.

Pendergast, M. T. M., Nygaard, J. M., Ghosh, A. K., & Hoek, E. M. V. (2010). Using nanocomposite materials technology to understand and control reverse osmosis membrane compaction. Desalination, 261(3), 255-263.

Peng, H., Feng, S., Zhang, X., Li, Y., & Zhang, X. (2012). Adsorption of norfloxacin onto titanium oxide: Effect of drug carrier and dissolved humic acid. Science of The Total Environment, 438(0), 66-71.

Peng, H., Pan, B., Wu, M., Liu, R., Zhang, D., Wu, D., & Xing, B. (2012). Adsorption of ofloxacin on carbon nanotubes: Solubility, pH and cosolvent effects. Journal of Hazardous Materials, 211–212(0), 342-348.

Peng, X., Li, Y., Luan, Z., Di, Z., Wang, H., Tian, B., & Jia, Z. (2003a). Adsorption of 1,2-dichlorobenzene from water to carbon nanotubes. Chemical Physics Letters, 376(1–2), 154-158.

Peng, X., Li, Y., Luan, Z., Di, Z., Wang, H., Tian, B., & Jia, Z. (2003b). Adsorption of 1, 2-dichlorobenzene from water to carbon nanotubes. Chemical Physics Letters, 376(1), 154-158.

Peng, X., Luan, Z., Di, Z., Zhang, Z., & Zhu, C. (2005). Carbon nanotubes-iron oxides magnetic composites as adsorbent for removal of Pb(II) and Cu(II) from water. Carbon, 43(4), 880-883.

Pera-Titus, M., García-Molina, V., Baños, M. A., Giménez, J., & Esplugas, S. (2004). Degradation of chlorophenols by means of advanced oxidation processes: a general review. Applied Catalysis B: Environmental, 47(4), 219-256.

Perez-Aguilar, N. V., Diaz-Flores, P. E., & Rangel-Mendez, J. R. (2011). The adsorption kinetics of cadmium by three different types of carbon nanotubes. Journal of Colloid and Interface Science, 364(2), 279-287.

Pernak, J., Goc, I., & Mirska, I. (2004). Anti-microbial activities of protic ionic liquids with lactate anion. Green Chemistry, 6(7), 323-329.

Phadtare, S. B., & Shankarling, G. S. (2010). Halogenation reactions in biodegradable solvent: Efficient bromination of substituted 1-aminoanthra-9,10-quinone in deep eutectic solvent (choline chloride : urea). Green Chemistry, 12(3), 458-462.

Porkodi, K., & Kumar, K. V. (2007). Equilibrium, kinetics and mechanism modeling and simulation of basic and acid dyes sorption onto jute fiber carbon: Eosin yellow, malachite green and crystal violet single component systems. Journal of hazardous materials, 143(1), 311-327.

Poursaberi, T., Hassanisadi, M., Torkestani, K., & Zare, M. (2012). Development of zirconium (IV)-metalloporphyrin grafted Fe3O4 nanoparticles for efficient fluoride removal. Chemical Engineering Journal, 189–190(0), 117-125.

Pratap Reddy, M., Venugopal, A., & Subrahmanyam, M. (2007). Hydroxyapatite-supported Ag–TiO2 as Escherichia coli disinfection photocatalyst. Water Research, 41(2), 379-386.

Pu, Y.-C., Ling, Y., Chang, K.-D., Liu, C.-M., Zhang, J. Z., Hsu, Y.-J., & Li, Y. (2014). Surface Passivation of TiO2 Nanowires Using a Facile Precursor-Treatment Approach for Photoelectrochemical Water Oxidation. The Journal of Physical Chemistry C, 118(27), 15086-15094.

Pyrzyńska, K., & Bystrzejewski, M. (2010). Comparative study of heavy metal ions sorption onto activated carbon, carbon nanotubes, and carbon-encapsulated magnetic nanoparticles. Colloids and Surfaces A: Physicochemical and Engineering Aspects, 362(1–3), 102-109.

Qi, L., Xu, Z., Jiang, X., Hu, C., & Zou, X. (2004). Preparation and antibacterial activity of chitosan nanoparticles. Carbohydrate Research, 339(16), 2693-2700.

Qiu, H., Lv, L., Pan, B.-c., Zhang, Q.-j., Zhang, W.-m., & Zhang, Q.-x. (2009). Critical review in adsorption kinetic models. Journal of Zhejiang University-Science A, 10(5), 716-724.

Qu, S., Huang, F., Yu, S., Chen, G., & Kong, J. (2008). Magnetic removal of dyes from aqueous solution using multi-walled carbon nanotubes filled with Fe2O3 particles. Journal of Hazardous Materials, 160(2–3), 643-647.

Qu, X., Alvarez, P. J. J., & Li, Q. (2013). Applications of nanotechnology in water and wastewater treatment. Water Research, 47(12), 3931-3946.

Qu, X., Brame, J., Li, Q., & Alvarez, P. J. J. (2013). Nanotechnology for a Safe and Sustainable Water Supply: Enabling Integrated Water Treatment and Reuse. Accounts of Chemical Research, 46(3), 834-843.

Rafiq, Z., Nazir, R., Durr e, S., Shah, M. R., & Ali, S. (2014). Utilization of magnesium and zinc oxide nano-adsorbents as potential materials for treatment of copper electroplating industry wastewater. Journal of Environmental Chemical Engineering, 2(1), 642-651.

Rahimpour, A. (2011). UV photo-grafting of hydrophilic monomers onto the surface of nano-porous PES membranes for improving surface properties. Desalination, 265(1–3), 93-101.

Rahimpour, A., & Madaeni, S. S. (2007). Polyethersulfone (PES)/cellulose acetate phthalate (CAP) blend ultrafiltration membranes: Preparation, morphology, performance and antifouling properties. Journal of Membrane Science, 305(1–2), 299-312.

Ramakrishna, S., Fujihara, K., Teo, W.-E., Yong, T., Ma, Z., & Ramaseshan, R. (2006). Electrospun nanofibers: solving global issues. Materials Today, 9(3), 40-50.

Ramsden, J. (2009). Essentials of nanotechnology: BookBoon.

Rao, G. P., Lu, C., & Su, F. (2007). Sorption of divalent metal ions from aqueous solution by carbon nanotubes: A review. Separation and Purification Technology, 58(1), 224-231.

Raymundo-Piñero, E., Azaïs, P., Cacciaguerra, T., Cazorla-Amorós, D., Linares-Solano, A., & Béguin, F. (2005). KOH and NaOH activation mechanisms of multiwalled carbon nanotubes with different structural organisation. Carbon, 43(4), 786-795.

Razmjou, A., Mansouri, J., & Chen, V. (2011). The effects of mechanical and chemical modification of TiO2 nanoparticles on the surface chemistry, structure and fouling performance of PES ultrafiltration membranes. Journal of Membrane Science, 378(1–2), 73-84.

Razmjou, A., Mansouri, J., Chen, V., Lim, M., & Amal, R. (2011). Titania nanocomposite polyethersulfone ultrafiltration membranes fabricated using a low temperature hydrothermal coating process. Journal of Membrane Science, 380(1–2), 98-113.

Razmjou, A., Resosudarmo, A., Holmes, R. L., Li, H., Mansouri, J., & Chen, V. (2012). The effect of modified TiO2 nanoparticles on the polyethersulfone ultrafiltration hollow fiber membranes. Desalination, 287(0), 271-280.

Recillas, S., García, A., González, E., Casals, E., Puntes, V., Sánchez, A., & Font, X. (2011). Use of CeO2, TiO2 and Fe3O4 nanoparticles for the removal of lead from water: Toxicity of nanoparticles and derived compounds. Desalination, 277(1–3), 213-220.

Ren, X., Chen, C., Nagatsu, M., & Wang, X. (2011). Carbon nanotubes as adsorbents in environmental pollution management: a review. Chemical Engineering Journal, 170(2), 395-410.

Richardson, S. D., Plewa, M. J., Wagner, E. D., Schoeny, R., & DeMarini, D. M. (2007). Occurrence, genotoxicity, and carcinogenicity of regulated and emerging disinfection by-products in drinking water: a review and roadmap for research. Mutation Research/Reviews in Mutation Research, 636(1), 178-242.

Roeges, N. P. (1994). A guide to the complete interpretation of infrared spectra of organic structures. Chichester : New York: Wiley.

Ru, & Konig, B. (2012). Low melting mixtures in organic synthesis - an alternative to ionic liquids? Green Chemistry, 14(11), 2969-2982.

Rutala, W. A., Weber, D. J., & Control, C. f. D. (2008). Guideline for disinfection and sterilization in healthcare facilities, 2008: Centers for Disease Control (US).

Saha, K., Agasti, S. S., Kim, C., Li, X., & Rotello, V. M. (2012). Gold Nanoparticles in Chemical and Biological Sensing. Chemical Reviews, 112(5), 2739-2779.

Salah, N. H., Jenkins, D., & Handy, R. (2014). Graphene and its Influence in the Improvement of Surface Plasmon Resonance (SPR) Based Sensors: a Review.

Salam, M. A. (2013). Coating carbon nanotubes with crystalline manganese dioxide nanoparticles and their application for lead ions removal from model and real water. Colloids and Surfaces A: Physicochemical and Engineering Aspects, 419(0), 69-79.

Salam, M. A., Makki, M. S. I., & Abdelaal, M. Y. A. (2011). Preparation and characterization of multi-walled carbon nanotubes/chitosan nanocomposite and its application for the removal of heavy metals from aqueous solution. Journal of Alloys and Compounds, 509(5), 2582-2587.

Saleh, T. A., & Gupta, V. K. (2012). Photo-catalyzed degradation of hazardous dye methyl orange by use of a composite catalyst consisting of multi-walled carbon

nanotubes and titanium dioxide. Journal of Colloid and Interface Science, 371, 101-106.

Salman, J., Njoku, V., & Hameed, B. (2011). Adsorption of pesticides from aqueous solution onto banana stalk activated carbon. Chemical Engineering Journal, 174(1), 41-48.

Samarghandi, M., Hadi, M., Moayedi, S., & Barjasteh Askari, F. (2010). Two-parameter isotherms of methyl orange sorption by pinecone derived activated carbon.

Sánchez-Hernández, L., Hernández-Domínguez, D., Bernal, J., Neusüß, C., Martín, M. T., & Bernal, J. L. (2014). Capillary electrophoresis–mass spectrometry as a new approach to analyze neonicotinoid insecticides. Journal of Chromatography A, 1359, 317-324.

Sathish, M., Viswanath, R., & Gopinath, C. S. (2009). N, S-Co-doped TiO2 nanophotocatalyst: Synthesis, electronic structure and photocatalysis. Journal of nanoscience and nanotechnology, 9(1), 423-432.

Sathishkumar, M., Binupriya, A., Kavitha, D., & Yun, S. (2007). Kinetic and isothermal studies on liquid-phase adsorption of 2, 4-dichlorophenol by palm pith carbon. Bioresource Technology, 98(4), 866-873.

Savage, N., & Diallo, M. S. (2005). Nanomaterials and water purification: opportunities and challenges. Journal of Nanoparticle Research, 7(4-5), 331-342.

Savichtcheva, O., & Okabe, S. (2006). Alternative indicators of fecal pollution: relations with pathogens and conventional indicators, current methodologies for direct pathogen monitoring and future application perspectives. Water Research, 40(13), 2463-2476.

Sawada, I., Fachrul, R., Ito, T., Ohmukai, Y., Maruyama, T., & Matsuyama, H. (2012). Development of a hydrophilic polymer membrane containing silver nanoparticles with both organic antifouling and antibacterial properties. Journal of Membrane Science, 387–388(0), 1-6.

Sawai, J., & Yoshikawa, T. (2004). Quantitative evaluation of antifungal activity of metallic oxide powders (MgO, CaO and ZnO) by an indirect conductimetric assay. Journal of Applied Microbiology, 96(4), 803-809.

Scanlon, D. O., Dunnill, C. W., Buckeridge, J., Shevlin, S. A., Logsdail, A. J., Woodley, S. M., . . . Parkin, I. P. (2013). Band alignment of rutile and anatase TiO2. Nature materials, 12(9), 798-801.

Schoettl, S., Marcus, J., Diat, O., Touraud, D., Kunz, W., Zemb, T., & Horinek, D. (2014). Emergence of surfactant-free micelles from ternary solutions. Chemical Science, 5(8), 2949-2954.

Shaarani, F. W., & Hameed, B. H. (2010). Batch adsorption of 2,4-dichlorophenol onto activated carbon derived from agricultural waste. Desalination, 255(1–3), 159-164.

Shahbaz, K., Baroutian, S., Mjalli, F. S., Hashim, M. A., & AlNashef, I. M. (2012a). Densities of ammonium and phosphonium based deep eutectic solvents: Prediction using artificial intelligence and group contribution techniques. Thermochim. Acta, 527, 59-66.

Shahbaz, K., Baroutian, S., Mjalli, F. S., Hashim, M. A., & AlNashef, I. M. (2012b). Densities of ammonium and phosphonium based deep eutectic solvents: Prediction using artificial intelligence and group contribution techniques. Thermochimica Acta, 527, 59-66.

Shahbaz, K., Mjalli, F. S., Hashim, M. A., & AlNashef, I. M. (2011). Using Deep Eutectic Solvents Based on Methyl Triphenyl Phosphunium Bromide for the Removal of Glycerol from Palm-Oil-Based Biodiesel. Energy Fuels, 25, 2671-2678.

Shahbaz, K., Mjalli, F. S., Hashim, M. A., & AlNashef, I. M. (2012). Prediction of the surface tension of deep eutectic solvents. Fluid Phase Equilibria, 319(0), 48-54.

Shahidi, F., & Synowiecki, J. (1991). Isolation and characterization of nutrients and value-added products from snow crab (Chionoecetes opilio) and shrimp (Pandalus borealis) processing discards. Journal of Agricultural and Food Chemistry, 39(8), 1527-1532.

Shahidi, S., Iranpour, S., Iranpour, P., Alavi, A. A., Mahyari, F. A., Tohidi, M., & Safavi, A. (2015). A new X-ray contrast agent based on highly stable gum arabic-gold nanoparticles synthesised in deep eutectic solvent. Journal of Experimental Nanoscience, 10(12), 911-924.

Shankaran, D. R., Gobi, K. V., & Miura, N. (2007). Recent advancements in surface plasmon resonance immunosensors for detection of small molecules of biomedical, food and environmental interest. Sensors and Actuators B: Chemical, 121(1), 158-177.

Sheela, T., & Nayaka, Y. A. (2012). Kinetics and thermodynamics of cadmium and lead ions adsorption on NiO nanoparticles. Chemical Engineering Journal, 191(0), 123-131.

Shen, J.-n., Ruan, H.-m., Wu, L.-g., & Gao, C.-j. (2011). Preparation and characterization of PES–SiO2 organic–inorganic composite ultrafiltration membrane for raw water pretreatment. Chemical Engineering Journal, 168(3), 1272-1278.

Sheng, G., Li, J., Shao, D., Hu, J., Chen, C., Chen, Y., & Wang, X. (2010). Adsorption of copper(II) on multiwalled carbon nanotubes in the absence and presence of humic or fulvic acids. Journal of Hazardous Materials, 178(1–3), 333-340.

Sheng, G. D., Shao, D. D., Ren, X. M., Wang, X. Q., Li, J. X., Chen, Y. X., & Wang, X. K. (2010). Kinetics and thermodynamics of adsorption of ionizable aromatic compounds from aqueous solutions by as-prepared and oxidized multiwalled carbon nanotubes. Journal of Hazardous Materials, 178(1–3), 505-516.

Shintani, H. (2014). Toxic Compounds Analysis With High Performance Liquid Chromatography Detected By Electro Chemi-cal Detector (Ecd). Int J Clin Pharmacol Toxicol, 3(3), 121-127.

Shu, H.-Y., & Huang, C.-R. (1995). Degradation of commercial azo dyes in water using ozonation and UV enhanced ozonation process. Chemosphere, 31(8), 3813-3825.

Singh, B., Lobo, H., & Shankarling, G. (2011). Selective N-Alkylation of Aromatic Primary Amines Catalyzed by Bio-catalyst or Deep Eutectic Solvent. Catalysis Letters, 141(1), 178-182.

Singh, M., Thanh, D. N., Ulbrich, P., Strnadová, N., & Štěpánek, F. (2010). Synthesis, characterization and study of arsenate adsorption from aqueous solution by α- and δ-phase manganese dioxide nanoadsorbents. Journal of Solid State Chemistry, 183(12), 2979-2986.

Smart, S., Cassady, A., Lu, G., & Martin, D. (2006). The biocompatibility of carbon nanotubes. Carbon, 44(6), 1034-1047.

Smical, A.-I., Hotea, V., Oros, V., Juhasz, J., & Pop, E. (2008). Studies on transfer and bioaccumulation of heavy metals from soil into lettuce. Environmental Engineering and Management Journal, 7(5), 609-615.

Smith, B. C. (1998). Infrared spectral interpretation: a systematic approach: CRC press.

Smith, E. L., Abbott, A. P., & Ryder, K. S. (2014a). Deep Eutectic Solvents (DESs) and Their Applications. Chemical Reviews, 114(21), 11060-11082.

Smith, E. L., Abbott, A. P., & Ryder, K. S. (2014b). Deep Eutectic Solvents (DESs) and Their Applications. Chem. Rev., 114, 11060-11082.

Smith, Y. R., Bhattacharyya, D., Willhard, T., & Misra, M. (2016). Adsorption of aqueous rare earth elements using carbon black derived from recycled tires. Chemical Engineering Journal, 296, 102-111.

Song, K., Kim, W., Suh, C.-Y., Shin, D., Ko, K.-S., & Ha, K. (2013). Magnetic iron oxide nanoparticles prepared by electrical wire explosion for arsenic removal. Powder Technology, 246(0), 572-574.

Srivastava, V. C., Mall, I. D., & Mishra, I. M. (2006). Characterization of mesoporous rice husk ash (RHA) and adsorption kinetics of metal ions from aqueous solution onto RHA. Journal of hazardous materials, 134(1), 257-267.

Stafiej, A., & Pyrzynska, K. (2007). Adsorption of heavy metal ions with carbon nanotubes. Separation and Purification Technology, 58(1), 49-52.

Stuart, B. (2004). Infrared Spectroscopy: Fundamentals and Applications John Wiley & Sons, Ltd.

Stuart, B. H. Infrared Spectroscopy: Fundamentals and Applications/H. Barbara Stuart: Wiley, 2004, 224 p.

Su, F., Lu, C., & Hu, S. (2010). Adsorption of benzene, toluene, ethylbenzene and p-xylene by NaOCl-oxidized carbon nanotubes. Colloids and Surfaces A: Physicochemical and Engineering Aspects, 353(1), 83-91.

Su, S., Wu, W., Gao, J., Lu, J., & Fan, C. (2012). Nanomaterials-based sensors for applications in environmental monitoring. Journal of Materials Chemistry, 22(35), 18101-18110.

Su, W. C., Wong, D. S. H., & Li, M. H. (2009). Effect of water on solubility of carbon dioxide in (aminomethanamide+ 2-hydroxy-N, N, N-trimethylethanaminium chloride). Journal of Chemical and Engineering Data, 54(6), 1951-1955.

Su, Y., Cui, H., Li, Q., Gao, S., & Shang, J. K. (2013). Strong adsorption of phosphate by amorphous zirconium oxide nanoparticles. Water Research, 47(14), 5018-5026.

Sun, K., Zhang, Z., Gao, B., Wang, Z., Xu, D., Jin, J., & Liu, X. (2012). Adsorption of diuron, fluridone and norflurazon on single-walled and multi-walled carbon nanotubes. Science of The Total Environment, 439(0), 1-7.

Sun, M., Su, Y., Mu, C., & Jiang, Z. (2009). Improved Antifouling Property of PES Ultrafiltration Membranes Using Additive of Silica−PVP Nanocomposite. Industrial & Engineering Chemistry Research, 49(2), 790-796.

Sun, W., Li, Q., Gao, S., & Shang, J. K. (2012). Exceptional arsenic adsorption performance of hydrous cerium oxide nanoparticles: Part B. Integration with silica monoliths and dynamic treatment. Chemical Engineering Journal, 185–186(0), 136-143.

Suri, R. P., Thornton, H. M., & Muruganandham, M. (2012). Disinfection of water using Pt-and Ag-doped TiO2 photocatalysts. Environmental technology, 33(14), 1651-1659.

Tan, I., Ahmad, A., & Hameed, B. (2009). Adsorption isotherms, kinetics, thermodynamics and desorption studies of 2, 4, 6-trichlorophenol on oil palm empty fruit bunch-based activated carbon. Journal of Hazardous materials, 164(2), 473-482.

Tan, I. A. W., Ahmad, A. L., & Hameed, B. H. (2008). Preparation of activated carbon from coconut husk: Optimization study on removal of 2,4,6-trichlorophenol using

response surface methodology. Journal of Hazardous Materials, 153(1–2), 709-717.

Tan, K. A., Morad, N., Teng, T. T., Norli, I., & Panneerselvam, P. (2012). Removal of Cationic Dye by Magnetic Nanoparticle (Fe3O4) Impregnated onto Activated Maize Cob Powder and Kinetic Study of Dye Waste Adsorption. APCBEE Procedia, 1(0), 83-89.

Tang, B., & Row, K. (2013). Recent developments in deep eutectic solvents in chemical sciences. Monatsh. Chem., 144(10), 1427-1454.

Tang, C. Y., She, Q., Lay, W. C., Wang, R., & Fane, A. G. (2010). Coupled effects of internal concentration polarization and fouling on flux behavior of forward osmosis membranes during humic acid filtration. Journal of Membrane Science, 354(1), 123-133.

Tang, M., Dou, H., & Sun, K. (2006). One-step synthesis of dextran-based stable nanoparticles assisted by self-assembly. Polymer, 47(2), 728-734.

Tang, W.-W., Zeng, G.-M., Gong, J.-L., Liu, Y., Wang, X.-Y., Liu, Y.-Y., . . . Tu, D.-Z. (2012). Simultaneous adsorption of atrazine and Cu (II) from wastewater by magnetic multi-walled carbon nanotube. Chemical Engineering Journal, 211–212(0), 470-478.

Tarboush, B. J. A., Rana, D., Matsuura, T., Arafat, H. A., & Narbaitz, R. M. (2008). Preparation of thin-film-composite polyamide membranes for desalination using novel hydrophilic surface modifying macromolecules. Journal of Membrane Science, 325(1), 166-175.

Tasis, D., Tagmatarchis, N., Bianco, A., & Prato, M. (2006). Chemistry of Carbon Nanotubes. Chemical Reviews, 106(3), 1105-1136.

Theron, J., Eugene Cloete, T., & de Kwaadsteniet, M. (2010). Current molecular and emerging nanobiotechnology approaches for the detection of microbial pathogens. Critical reviews in microbiology, 36(4), 318-339.

Tiraferri, A., Vecitis, C. D., & Elimelech, M. (2011). Covalent Binding of Single-Walled Carbon Nanotubes to Polyamide Membranes for Antimicrobial Surface Properties. ACS Applied Materials & Interfaces, 3(8), 2869-2877.

Tohidi, M., Mahyari, F. A., & Safavi, A. (2015). A seed-less method for synthesis of ultra-thin gold nanosheets by using a deep eutectic solvent and gum arabic and their electrocatalytic application. RSC Advances, 5(41), 32744-32754.

Tong, J., Hong, M., Guan, W., Li, J.-B., & Yang, J.-Z. (2006). Studies on the thermodynamic properties of new ionic liquids: 1-Methyl-3-pentylimidazolium salts containing metal of group III. The Journal of Chemical Thermodynamics, 38(11), 1416-1421.

Tranchida, P. Q., Franchina, F. A., Dugo, P., & Mondello, L. (2014). Comprehensive two- dimensional gas chromatography- mass spectrometry: Recent evolution and current trends. Mass spectrometry reviews.

Tsai, C., & Chen, C. (2003). Characterization of bias-controlled carbon nanotubes. Diamond and Related Materials, 12(9), 1615-1620.

Uğurlu, M. (2009). Adsorption of a textile dye onto activated sepiolite. Microporous and Mesoporous Materials, 119(1), 276-283.

Vandevivere, P. C., Bianchi, R., & Verstraete, W. (1998). Review: Treatment and reuse of wastewater from the textile wet- processing industry: Review of emerging technologies. Journal of Chemical Technology and Biotechnology, 72(4), 289-302.

Vargas-Reus, M. A., Memarzadeh, K., Huang, J., Ren, G. G., & Allaker, R. P. (2012). Antimicrobial activity of nanoparticulate metal oxides against peri-implantitis pathogens. International Journal of Antimicrobial Agents, 40(2), 135-139.

Vatanpour, V., Madaeni, S. S., Khataee, A. R., Salehi, E., Zinadini, S., & Monfared, H. A. (2012). TiO2 embedded mixed matrix PES nanocomposite membranes: Influence of different sizes and types of nanoparticles on antifouling and performance. Desalination, 292(0), 19-29.

Vecitis, C. D., Zodrow, K. R., Kang, S., & Elimelech, M. (2010). Electronic-Structure-Dependent Bacterial Cytotoxicity of Single-Walled Carbon Nanotubes. ACS Nano, 4(9), 5471-5479.

Venkata Ramana, D. K., Yu, J. S., & Seshaiah, K. (2013). Silver nanoparticles deposited multiwalled carbon nanotubes for removal of Cu(II) and Cd(II) from water: Surface, kinetic, equilibrium, and thermal adsorption properties. Chemical Engineering Journal, 223(0), 806-815.

Venkatesham, V., Madhu, G. M., Satyanarayana, S. V., & Preetham, H. S. (2013). Adsorption of Lead on Gel Combustion Derived Nano ZnO. Procedia Engineering, 51(0), 308-313.

Vikesland, P. J., & Wigginton, K. R. (2010). Nanomaterial enabled biosensors for pathogen monitoring-a review. Environmental science & technology, 44(10), 3656-3669.

Vila, J., Ginés, P., Pico, J. M., Franjo, C., Jiménez, E., Varela, L. M., & Cabeza, O. (2006a). Temperature dependence of the electrical conductivity in EMIM-based ionic liquids: Evidence of Vogel–Tamman–Fulcher behavior. Fluid Phase Equilibria, 242(2), 141-146.

Vila, J., Ginés, P., Pico, J. M., Franjo, C., Jiménez, E., Varela, L. M., & Cabeza, O. (2006b). Temperature dependence of the electrical conductivity in EMIM-based

ionic liquids: Evidence of Vogel–Tamman–Fulcher behavior. Fluid Phase Equilib., 242, 141-146.

Vimonses, V., Lei, S., Jin, B., Chow, C. W., & Saint, C. (2009). Kinetic study and equilibrium isotherm analysis of Congo Red adsorption by clay materials. Chemical Engineering Journal, 148(2), 354-364.

Volkert, A. A., & Haes, A. J. (2014). Advancements in nanosensors using plastic antibodies. Analyst, 139(1), 21-31.

Vuković, G. D., Marinković, A. D., Čolić, M., Ristić, M. Đ., Aleksić, R., Perić-Grujić, A. A., & Uskoković, P. S. (2010). Removal of cadmium from aqueous solutions by oxidized and ethylenediamine-functionalized multi-walled carbon nanotubes. Chemical Engineering Journal, 157(1), 238-248.

Vuković, G. D., Marinković, A. D., Škapin, S. D., Ristić, M. Đ., Aleksić, R., Perić-Grujić, A. A., & Uskoković, P. S. (2011). Removal of lead from water by amino modified multi-walled carbon nanotubes. Chemical Engineering Journal, 173(3), 855-865.

Vuković, G. D., Tomić, S. Z., Marinković, A. D., Radmilović, V., Uskoković, P. S., & Čolić, M. (2010). The response of peritoneal macrophages to dapsone covalently attached on the surface of carbon nanotubes. Carbon, 48(11), 3066-3078.

Wächter, R., & Cordery, A. (1999). Response surface methodology modelling of diamond-like carbon film deposition. Carbon, 37(10), 1529-1537.

Wang, A., & Jing, H. (2014). Tunable catalytic activities and selectivities of metal ion doped TiO 2 nanoparticles–oxidation of organic compounds. Dalton Transactions, 43(3), 1011-1018.

Wang, H., Zhou, A., Peng, F., Yu, H., & Yang, J. (2007). Mechanism study on adsorption of acidified multiwalled carbon nanotubes to Pb(II). Journal of Colloid and Interface Science, 316(2), 277-283.

Wang, H. J., Zhou, A. L., Peng, F., Yu, H., & Chen, L. F. (2007). Adsorption characteristic of acidified carbon nanotubes for heavy metal Pb(II) in aqueous solution. Materials Science and Engineering: A, 466(1–2), 201-206.

Wang, J.-P., Chen, Y.-Z., Feng, H.-M., Zhang, S.-J., & Yu, H.-Q. (2007). Removal of 2, 4-dichlorophenol from aqueous solution by static-air-activated carbon fibers. Journal of colloid and interface science, 313(1), 80-85.

Wang, J.-P., Feng, H.-M., & Yu, H.-Q. (2007). Analysis of adsorption characteristics of 2, 4-dichlorophenol from aqueous solutions by activated carbon fiber. Journal of hazardous materials, 144(1), 200-207.

Wang, J., Li, Z., Li, S., Qi, W., Liu, P., Liu, F., . . . Wu, W. (2013). Adsorption of Cu(II) on Oxidized Multi-Walled Carbon Nanotubes in the Presence of Hydroxylated and Carboxylated Fullerenes. PLoS ONE, 8(8), e72475.

Wang, J. L., & Xu, L. J. (2012). Advanced oxidation processes for wastewater treatment: formation of hydroxyl radical and application. Critical reviews in environmental science and technology, 42(3), 251-325.

Wang, L., Ma, W., Xu, L., Chen, W., Zhu, Y., Xu, C., & Kotov, N. A. (2010). Nanoparticle-based environmental sensors. Materials Science and Engineering: R: Reports, 70(3–6), 265-274.

Wang, L., Zhang, J., Zhao, R., Zhang, C., Li, C., & Li, Y. (2011). Adsorption of 2,4-dichlorophenol on Mn-modified activated carbon prepared from Polygonum orientale Linn. Desalination, 266(1–3), 175-181.

Wang, S.-G., Gong, W.-X., Liu, X.-W., Yao, Y.-W., Gao, B.-Y., & Yue, Q.-Y. (2007). Removal of lead(II) from aqueous solution by adsorption onto manganese oxide-coated carbon nanotubes. Separation and Purification Technology, 58(1), 17-23.

Wang, W. D., Serp, P., Kalck, P., Silva, C. G., & Faria, J. L. (2008). Preparation and characterization of nanostructured MWCNT-TiO2 composite materials for photocatalytic water treatment applications. Materials Research Bulletin, 43(4), 958-967.

Wang, X., Chen, C., Liu, H., & Ma, J. (2008). Preparation and characterization of PAA/PVDF membrane-immobilized Pd/Fe nanoparticles for dechlorination of trichloroacetic acid. Water Research, 42(18), 4656-4664.

Wang, X., Yang, J., Zhu, M., & Li, F. (2013). Characterization and regeneration of Pd/Fe nanoparticles immobilized in modified PVDF membrane. Journal of the Taiwan Institute of Chemical Engineers, 44(3), 386-392.

Wang, Z., Yu, X., Pan, B., & Xing, B. (2010). Norfloxacin Sorption and Its Thermodynamics on Surface-Modified Carbon Nanotubes. Environmental Science & Technology, 44(3), 978-984.

Weber, T. W., & Chakravorti, R. K. (1974). Pore and solid diffusion models for fixed-bed adsorbers. AIChE Journal, 20(2), 228-238.

Weber, W., & Morris, J. (1962). Advances in water pollution research. Paper presented at the Proceedings of the First International Conference on Water Pollution Research.

Wei, L., Fan, Y.-J., Wang, H.-H., Tian, N., Zhou, Z.-Y., & Sun, S.-G. (2012). Electrochemically shape-controlled synthesis in deep eutectic solvents of Pt nanoflowers with enhanced activity for ethanol oxidation. Electrochimica Acta, 76, 468-474.

Weyer, L. G., & Lo, S. C. (2006). Spectra– Structure Correlations in the Near-Infrared Handbook of Vibrational Spectroscopy: John Wiley & Sons, Ltd.

WHO. (2012). Progress on Drinking Water and Sanitation.

Wildgoose, G. G., Banks, C. E., Leventis, H. C., & Compton, R. G. (2006). Chemically Modified Carbon Nanotubes for Use in Electroanalysis. Microchimica Acta, 152(3-4), 187-214.

Williams, J. D., Svrcek, W., & Monnery, W. (2003). The prediction of viscosity for mixtures using a modified square well intermolecular potential model. Dev Chem Eng Miner Process, 11, 267-285.

Wu, C.-H. (2007). Adsorption of reactive dye onto carbon nanotubes: equilibrium, kinetics and thermodynamics. Journal of Hazardous Materials, 144(1), 93-100.

Wu, C.-S., Khaing Oo, M. K., & Fan, X. (2010). Highly Sensitive Multiplexed Heavy Metal Detection Using Quantum-Dot-Labeled DNAzymes. ACS Nano, 4(10), 5897-5904.

Wu, G., Gan, S., Cui, L., & Xu, Y. (2008). Preparation and characterization of PES/TiO2 composite membranes. Applied Surface Science, 254(21), 7080-7086.

Wu, L., & Ritchie, S. M. C. (2008). Enhanced dechlorination of trichloroethylene by membrane-supported Pd-coated iron nanoparticles. Environmental Progress, 27(2), 218-224.

Wu, L., Shamsuzzoha, M., & Ritchie, S. M. C. (2005). Preparation of Cellulose Acetate Supported Zero-Valent Iron Nanoparticles for the Dechlorination of Trichloroethylene in Water. Journal of Nanoparticle Research, 7(4-5), 469-476.

Xiao, J., Xie, Y., & Cao, H. (2015). Organic pollutants removal in wastewater by heterogeneous photocatalytic ozonation. Chemosphere, 121(0), 1-17.

Xin, X., Wei, Q., Yang, J., Yan, L., Feng, R., Chen, G., . . . Li, H. (2012). Highly efficient removal of heavy metal ions by amine-functionalized mesoporous Fe3O4 nanoparticles. Chemical Engineering Journal, 184(0), 132-140.

Xing, Z., Asiri, A. M., Obaid, A. Y., Sun, X., & Ge, X. (2014). Carbon nanofiber-templated mesoporous TiO 2 nanotubes as a high-capacity anode material for lithium-ion batteries. RSC Advances, 4(18), 9061-9063.

Xiu, Z.-m., Zhang, Q.-b., Puppala, H. L., Colvin, V. L., & Alvarez, P. J. J. (2012). Negligible Particle-Specific Antibacterial Activity of Silver Nanoparticles. Nano Letters, 12(8), 4271-4275.

Xu, D., Tan, X., Chen, C., & Wang, X. (2008). Removal of Pb(II) from aqueous solution by oxidized multiwalled carbon nanotubes. Journal of Hazardous Materials, 154(1–3), 407-416.

Xu, J., Liu, X., Lowry, G. V., Cao, Z., Zhao, H., Zhou, J. L., & Xu, X. (2016). Dechlorination mechanism of 2, 4-dichlorophenol by magnetic MWCNTs supported Pd/Fe nanohybrids: rapid adsorption, gradual dechlorination, and desorption of phenol. ACS applied materials & interfaces, 8(11), 7333-7342.

Xu, J., Lv, X., Li, J., Li, Y., Shen, L., Zhou, H., & Xu, X. (2012). Simultaneous adsorption and dechlorination of 2,4-dichlorophenol by Pd/Fe nanoparticles with multi-walled carbon nanotube support. Journal of Hazardous Materials, 225–226, 36-45.

Xu, K., Wang, Y., Ding, X., Huang, Y., Li, N., & Wen, Q. (2016). Magnetic solid-phase extraction of protein with deep eutectic solvent immobilized magnetic graphene oxide nanoparticles. Talanta, 148, 153-162.

Xu, Y.-j., Rosa, A., Liu, X., & Su, D.-s. (2011). Characterization and use of functionalized carbon nanotubes for the adsorption of heavy metal anions. New Carbon Materials, 26(1), 57-62.

Yadav, A., Trivedi, S., Rai, R., & Pandey, S. (2014). Densities and dynamic viscosities of (choline chloride+ glycerol) deep eutectic solvent and its aqueous mixtures in the temperature range (283.15–363.15) K. Fluid Phase Equilibria, 367, 135-142.

Yamamoto, O. (2001). Influence of particle size on the antibacterial activity of zinc oxide. International Journal of Inorganic Materials, 3(7), 643-646.

Yan, H., Gong, A., He, H., Zhou, J., Wei, Y., & Lv, L. (2006). Adsorption of microcystins by carbon nanotubes. Chemosphere, 62(1), 142-148.

Yan, X. M., Shi, B. Y., Lu, J. J., Feng, C. H., Wang, D. S., & Tang, H. X. (2008). Adsorption and desorption of atrazine on carbon nanotubes. Journal of Colloid and Interface Science, 321(1), 30-38.

Yang, C., Mamouni, J., Tang, Y., & Yang, L. (2010). Antimicrobial Activity of Single-Walled Carbon Nanotubes: Length Effect. Langmuir, 26(20), 16013-16019.

Yang, D., Hou, M., Ning, H., Zhang, J., Ma, J., Yang, G., & Han, B. (2013a). Efficient SO2 absorption by renewable choline chloride-glycerol deep eutectic solvents. Green Chemistry, 15(8), 2261-2265.

Yang, D., Hou, M., Ning, H., Zhang, J., Ma, J., Yang, G., & Han, B. (2013b). Efficient SO 2 absorption by renewable choline chloride–glycerol deep eutectic solvents. Green Chemistry, 15(8), 2261-2265.

Yang, H.-L., Lin, J. C.-T., & Huang, C. (2009). Application of nanosilver surface modification to RO membrane and spacer for mitigating biofouling in seawater desalination. Water Research, 43(15), 3777-3786.

Yang, K., Wu, W., Jing, Q., Jiang, W., & Xing, B. (2010a). Competitive Adsorption of Naphthalene with 2,4-Dichlorophenol and 4-Chloroaniline on Multiwalled Carbon Nanotubes. Environmental Science and Technology, 44(8), 3021-3027.

Yang, K., Wu, W., Jing, Q., Jiang, W., & Xing, B. (2010b). Competitive Adsorption of Naphthalene with 2,4-Dichlorophenol and 4-Chloroaniline on Multiwalled Carbon Nanotubes. Environmental Science & Technology, 44(8), 3021-3027.

Yang, K., Wu, W., Jing, Q., & Zhu, L. (2008). Aqueous Adsorption of Aniline, Phenol, and their Substitutes by Multi-Walled Carbon Nanotubes. Environmental Science & Technology, 42(21), 7931-7936.

Yang, K., & Xing, B. (2009). Adsorption of fulvic acid by carbon nanotubes from water. Environmental Pollution, 157(4), 1095-1100.

Yang, K., & Xing, B. (2010). Adsorption of Organic Compounds by Carbon Nanomaterials in Aqueous Phase: Polanyi Theory and Its Application. Chemical Reviews, 110(10), 5989-6008.

Yang, N., Liu, Y., Wen, H., Tang, Z., Zhao, H., Li, Y., & Wang, D. (2013). Photocatalytic properties of graphdiyne and graphene modified TiO2: from theory to experiment. ACS nano, 7(2), 1504-1512.

Yang, S., Li, J., Shao, D., Hu, J., & Wang, X. (2009). Adsorption of Ni (II) on oxidized multi-walled carbon nanotubes: effect of contact time, pH, foreign ions and PAA. Journal of hazardous materials, 166(1), 109-116.

Yang, W., Ding, P., Zhou, L., Yu, J., Chen, X., & Jiao, F. (2013). Preparation of diamine modified mesoporous silica on multi-walled carbon nanotubes for the adsorption of heavy metals in aqueous solution. Applied Surface Science, 282(0), 38-45.

Yao, Y., Bing, H., Feifei, X., & Xiaofeng, C. (2011). Equilibrium and kinetic studies of methyl orange adsorption on multiwalled carbon nanotubes. Chemical Engineering Journal, 170(1), 82-89.

Yao, Y., Xu, F., Chen, M., Xu, Z., & Zhu, Z. (2010). Adsorption of cationic methyl violet and methylene blue dyes onto carbon nanotubes. Paper presented at the Nano/Micro Engineered and Molecular Systems (NEMS), 2010 5th IEEE International Conference on.

Yim, T., Lee, H. Y., Kim, H.-J., Mun, J., Kim, S., Oh, S. M., & Kim, Y. G. (2007). Synthesis and properties of pyrrolidinium and piperidinium bis (trifluoromethanesulfonyl) imide ionic liquids with allyl substituents.

Ying, Y., Saini, R. K., Liang, F., Sadana, A. K., & Billups, W. (2003). Functionalization of carbon nanotubes by free radicals. Organic letters, 5(9), 1471-1473.

You, Y., Han, J., Chiu, P. C., & Jin, Y. (2005). Removal and Inactivation of Waterborne Viruses Using Zerovalent Iron. Environmental Science & Technology, 39(23), 9263-9269.

Yu, B., Zhou, F., Liu, G., Liang, Y., Huck, W. T., & Liu, W. (2006). The electrolyte switchable solubility of multi-walled carbon nanotube/ionic liquid (MWCNT/IL) hybrids. Chemical communications(22), 2356-2358.

Yu, H., Zhang, X., Zhang, Y., Liu, J., & Zhang, H. (2013). Development of a hydrophilic PES ultrafiltration membrane containing SiO2@N-Halamine nanoparticles with both organic antifouling and antibacterial properties. Desalination, 326(0), 69-76.

Yu, J.-G., Zhao, X.-H., Yang, H., Chen, X.-H., Yang, Q., Yu, L.-Y., . . . Chen, X.-Q. (2014). Aqueous adsorption and removal of organic contaminants by carbon nanotubes. Science of The Total Environment, 482–483(0), 241-251.

Zang, L. (2011). Energy Efficiency and Renewable Energy Through Nanotechnology: Springer.

Zhang, C., Sui, J., Li, J., Tang, Y., & Cai, W. (2012). Efficient removal of heavy metal ions by thiol-functionalized superparamagnetic carbon nanotubes. Chemical Engineering Journal, 210(0), 45-52.

Zhang, D., Pan, B., Zhang, H., Ning, P., & Xing, B. (2010). Contribution of Different Sulfamethoxazole Species to Their Overall Adsorption on Functionalized Carbon Nanotubes. Environmental Science & Technology, 44(10), 3806-3811.

Zhang, D., Qiu, R., Song, L., Eric, B., Mo, Y., & Huang, X. (2009). Role of oxygen active species in the photocatalytic degradation of phenol using polymer sensitized TiO2 under visible light irradiation. Journal of Hazardous Materials, 163(2–3), 843-847.

Zhang, G., Zhang, Y. C., Nadagouda, M., Han, C., O'Shea, K., El-Sheikh, S. M., . . . Dionysiou, D. D. (2014). Visible light-sensitized S, N and C co-doped polymorphic TiO2 for photocatalytic destruction of microcystin-LR. Applied Catalysis B: Environmental, 144, 614-621.

Zhang, J., Wu, T., Chen, S., Feng, P., & Bu, X. (2009). Versatile Structure-Directing Roles of Deep-Eutectic Solvents and Their Implication in the Generation of Porosity and Open Metal Sites for Gas Storage. Angewandte Chemie International Edition, 48(19), 3486-3490.

Zhang, L., Song, X., Liu, X., Yang, L., Pan, F., & Lv, J. (2011). Studies on the removal of tetracycline by multi-walled carbon nanotubes. Chemical Engineering Journal, 178(0), 26-33.

Zhang, L., Xu, T., Liu, X., Zhang, Y., & Jin, H. (2011). Adsorption behavior of multi-walled carbon nanotubes for the removal of olaquindox from aqueous solutions. Journal of Hazardous Materials, 197(0), 389-396.

Zhang, Q., De Oliveira Vigier, K., Royer, S., & Jerome, F. (2012a). Deep eutectic solvents: syntheses, properties and applications. Chem. Soc. Rev., 41, 7108-7146.

Zhang, Q., De Oliveira Vigier, K., Royer, S., & Jerome, F. (2012b). Deep eutectic solvents: syntheses, properties and applications. Chemical Society Reviews, 41(21), 7108-7146.

Zhang, Q., Zhang, S., & Deng, Y. (2011). Recent advances in ionic liquid catalysis. Green Chemistry, 13(10), 2619-2637.

Zhang, Q. B., Abbott, A. P., & Yang, C. (2015). Electrochemical fabrication of nanoporous copper films in choline chloride-urea deep eutectic solvent. Physical Chemistry Chemical Physics, 17(22), 14702-14709.

Zhang, Z., Zhang, Z., Fernández, Y., Menéndez, J., Niu, H., Peng, J., . . . Guo, S. (2010). Adsorption isotherms and kinetics of methylene blue on a low-cost adsorbent recovered from a spent catalyst of vinyl acetate synthesis. Applied Surface Science, 256(8), 2569-2576.

Zhao, H., Baker, G. A., & Holmes, S. (2011). Protease activation in glycerol-based deep eutectic solvents. Journal of Molecular Catalysis B: Enzymatic, 72(3–4), 163-167.

Zhao, S., Zou, L., Tang, C. Y., & Mulcahy, D. (2012). Recent developments in forward osmosis: opportunities and challenges. Journal of Membrane Science, 396, 1-21.

Zhao, X., Wang, J., Wu, F., Wang, T., Cai, Y., Shi, Y., & Jiang, G. (2010). Removal of fluoride from aqueous media by Fe3O4@Al(OH)3 magnetic nanoparticles. Journal of Hazardous Materials, 173(1–3), 102-109.

Zheng, Y., Ye, L., Yan, L., & Gao, Y. (2014). The electrochemical behavior and determination of quercetin in choline chloride/urea deep eutectic solvent electrolyte based on abrasively immobilized multi-wall carbon nanotubes modified electrode. Int. J. Electrochem. Sci, 9, 238-248.

Zhou, Z. B., Matsumoto, H., & Tatsumi, K. (2006). Cyclic quaternary ammonium ionic liquids with perfluoroalkyltrifluoroborates: synthesis, characterization, and properties. Chemistry- A European Journal, 12(8), 2196-2212.

Zhu, H. Y., Jiang, R., Xiao, L., & Zeng, G. M. (2010). Preparation, characterization, adsorption kinetics and thermodynamics of novel magnetic chitosan enwrapping nanosized γ-Fe2O3 and multi-walled carbon nanotubes with enhanced adsorption properties for methyl orange. Bioresource Technology, 101(14), 5063-5069.

Zhuannian, L., Anning, Z., Guirong, W., & Xiaoguang, Z. (2009). Adsorption behavior of methyl orange onto modified ultrafine coal powder. Chinese Journal of Chemical Engineering, 17(6), 942-948.

Zodrow, K., Brunet, L., Mahendra, S., Li, D., Zhang, A., Li, Q., & Alvarez, P. J. J. (2009). Polysulfone ultrafiltration membranes impregnated with silver nanoparticles show improved biofouling resistance and virus removal. Water Research, 43(3), 715-723.

LIST OF PUBLICATIONS AND PAPERS PRESENTED

Published Papers

1. **Ibrahim, R. K.**, Hayyan, M., AlSaadi, M. A., Hayyan, A., & Ibrahim, S. (2016). Environmental application of nanotechnology: air, soil, and water. *Environmental Science and Pollution Research*, *23*(14), 13754-13788. ***ISI-Cited publication.***

2. **Ibrahim, R. K**., Hayyan, M., AlSaadi, M. A., Hayyan, A., & Ibrahim, S. (2017). Diethylene glycol based deep eutectic solvents and their physical properties. STUDIA UBB CHEMIA, LXII, 4, Tom II, 2017 (p. 433-450), DOI: 10.24193/subbchem.2017.4.37. ***ISI-Cited publication.***

Submitted papers (under review)

1. **Ibrahim, R. K**., Hayyan, M., AlSaadi, M. A., Hayyan, A., & Ibrahim, S. Physical properties of ethylene glycol based deep eutectic solvents. Journal of molecular liquids, Under review. **ISI-Cited publication**.

2. **Ibrahim, R. K**., Hayyan, M., AlSaadi, M. A., Hayyan, A., & Ibrahim, S. physical properties of diethylene glycol based deep eutectic solvents. Journal of chemical and engineering data, Under review. **ISI-Cited publication.**

3. **Ibrahim, R. K**., AlSaadi, M. A., & Ibrahim, S. Deep eutectic solvent functionalized carbon nanotubes for the removal of 2,4-dichlorophenol from water: characterization, optimization, kinetics and isotherms studies. Journal of hazardous materials, Under review. **ISI-Cited publication.**

4. **Ibrahim, R. K**., AlSaadi, M. A., & Ibrahim, S. Ethylene glycol based deep eutectic solvents as CNTs functionalization agents: Preparation, phesiochemical characterization, and application of methyl orange removal from water. Journal of Molecular Liquids, Submitted. **ISI-Cited publication.**

Conference Papers (Presenter)

1. **Rusul Khaleel Ibrahim**, Mohammed Abdulhakim AlSaadi, Maan Hayyan, Shatirah Mohamed Akib, Mohd Ali Hashim, (2014) *[Ethylene Glycol based Deep Eutectic Solvents: pH Study]*. Design for Scientific Renaissance DSR. Non Scopus-non ISI